POLYMERS FOR QUORUM SENSE INTERFERENCE

Xuan Xue, MSc

Thesis submitted to the School of Pharmacy,

University of Nottingham for the degree of

Doctor of Philosophy

July 2012

Abstract

The synthetic polymers reported in this thesis are able to bind the small molecule autoinducer-2 (AI-2) in the Quorum Sense (QS) pathways of the marine organism with high affinity, and some of the polymers are also able to sequester rapidly the same bacteria from suspension. Specifically, the Alizarin Red S (AR-S) assay was used to compare binding interactions of boric and boronic acid with diol species, and interactions were further probed by ^{11}B-NMR spectroscopy and Mass spectrometry. Dopamine was considered as a potential AI-2 scavenger for polymeric QS control owing to the high binding affinities for boron. Therefore, poly{N-(3,4-dihydroxyphenethyl) methacrylamide-co-N-[3-(dimethylamino)propyl] methacrylamide} [p(DMAm-*c*-DMAPMAm)] and poly(3,4-dihydroxy-L-phenylalanine methacrylamide) [p(L-DMAm)] were prepared via Reversible Addition Fragmentation Chain Transfer (RAFT) polymerization and characterized by ^{1}H-NMR spectroscopy. The activities of these catechol polymers and carbohydrate-based poly(β-D-glucosyloxyethyl methacrylate) (p(GlcEMA)) in QS interference was demonstrated by bioluminescence assays with the *Vibrio harveyi* MM32 strain and by bacterial aggregation experiments.

Polymersomes were then investigated as artificial protocells, with a view to establishing polymer vesicle containers as both reservoirs of QS mediated molecules, and of binding QS agents and bacteria. Hydrophobic monomers N-(2-Ethylhexyl) acrylamide [p(2-EHAm)] and N-phenylacrylamide [p(PAm)] were therefore polymerized into block copolymers from p(L-DMAm)-RAFT agents. The membrane permeability of polymersomes was measured via encapsulation and release of dyes, while the morphologies were examined with

Dynamic Light Scattering (DLS) and Transmission Electron Microscopy (TEM). Polymersomes were also investigated for potency in QS quenching via the bioluminescence assay and bacterial aggregation experiments. Initial studies of a communication feedback loop between bacteria and polymersome-encapsulated QS agents were performed again via bioluminescence assays. The results reveal that the investigated polymersomes exhibit potent activities in QS quenching, and further development might act as components of a synthetic biology approach to combating microbial pathogenicity.

Acknowledgments

I am heartily thankful and truly indebted to my supervisor Professor Cameron Alexander for all his guidance, motivation and support during my studies. I would like to gratefully thank Professor Steven Howdle for helpful discussions and assistance. I particularly acknowledge Dr. Francisco Fernandez-Trillo for all the helpful discussion, support and collaboration. I would like to thank Dr. Nigel Halliday for sharing his knowledge and help with bacterial assays. I gratefully thank Dr. Klaus Winzer for his helpful discussions and assistance with bacterial quorum sensing network. I would like to thank Professor Natalio Krasnogor and Dr. Leung Lui for helpful discussions. I acknowledge Professor Benjamin G. Davis (Department of Chemistry, University of Oxford) for giving support on bacterial bioluminescence and biofilm formation studies and helpful discussions. I thank Professor Bonnie Bassler (Department of Molecular Biology, Princeton University) for the gift of *Vibrio harveyi* strain MM32.

Many thanks go to Mrs. Christy Grainger-Boultry for giving technical aid and assistance with every day lab problems. I would like to thank Dr. Sebastian Spain for helping out with GPC analysis.

I acknowledge my coworkers in the advanced drug delivery group especially Dr. Johannes Magnusson, Dr. Felicity Heath, Dr. Giuseppe Mantovani, Dr. Aram Omer, Peter Maggenis and Teresa Matini for their useful discussions and company.

I would like to thank Oversea Research Scholarship for financial support.

Most important I would like to thank my parents for all their love and support.

Table of Contents

List of Abbreviations

AB – Assay broth

ACP – Acyl carrier protein

AFM – Atomic force microscopy

AHL – N-acylated homoserine lactone

AI – Autoinducer

AIBN – Azobisisobutyronitrile

AIP – Autoinducer peptides

AMC – Activated methyl cycle

Amino-PDO – 2-Amino-1,3-propanediol

AON – Antisense oligonucleotides

AR-S – Alizarin red S

CF – Carboxyfluorescein

CHELL – Chemical cell

Cryo – Cryogenic

CTA – Chain transfer agent

CTP – 4-Cyano-4-(phenylcarbonothioylthio)pentanoic acid

DCM – Dichloromethane

DDMAT – S-dodecyl-S-(a,a-dimethyl-a-acetic acid) trithiocarbonate

DLS – Dynamic light scattering

DLSM – Confocal laser scanning microscopy

DLVO – Derjaguin landau verwey overbeek

DMAm – N-dopamine methacrylamide

DMAPMAm – N-[3-(dimethylamino)propyl]methacrylamide

DMF – N, N-dimethylformamide

DMSO – Dimethyl sulfoxide

DOPC – 1,2-Dioleoyl-sn-glycero-3-phosphocholine

DOPG – 1,2-Dioleoyl-sn-glycero-3-phospho-rac-(1-glycerol) sodium salt

DP – Degree of polymerization

DPD – 4,5-Dihydroxy-2,3-pentanedione

GAS – Group a *streptococcus pyogenes*

GI – Gastrointestinal

GPC – Gel permeation chromatography

HAI-1 – 3OHC4-homoserine lactone

HEPES – 4-(2-Hydroxyethyl) piperazine-1-ethanesulfonic acid

HPLC – High performance liquid chromatography

HSL – Homoserine lactone

IM – Inner membrane

IND – Indomethacin

IR – Infrared spectroscopy

LB – Luria Bertani

LC – Loading content

LCST – Lower critical solution temperature

L-DMAm – 3,4-Dihydroxy-L-phenylamanine methacrylamide

L-DOPA – 3,4-Dihydroxy-L-phenylamanine

LE – Loading efficiency

LRP – Living radical polymerization

MDR - Multidrug resistance

Me-PDO – 2-Methyl-1,3-propanediol

MeO-β-Gal – MeO-β-galactopyranoside

MeO-β-Glc – MeO-β-glucopyranoside

MeO-PDO – 3-Methoxy-1,2-propanediol

MIP – Molecularly imprinted polymer

MS – Mass spectra

MWCO – Molecular weight cut off

NMR – Nuclear magnetic resonance

OD – Optical density

OM – Outer membrane

P(AAc-co-DSA) – Poly(acrylic acid-co-distearin acrylate)

PAPMAH – Poly(N-(3-aminopropyl) methacrylamide hydrochloride)

PB – Poly(butadiene)

PBA – Phenylboronic acid

PBS – Phosphate-buffered saline

PCL – Poly(caprolactone)

PDEGMA – Poly(diethyleneglycol methacrylate)

PDI – Polydispersity index

PDMAEMA – Poly(2-(dimethylamino)ethyl methacrylate)

PDO – Propanediol

PEG – Poly(ethylene glycol)

PEO – Poly(ethylene oxide)

PEO-*b*-p(DEA-*s*-TMSPMA) – Poly(ethylene oxide)-*block*-poly[2-(diethylamino)ethyl methacrylate-*stat*-3-(trimethoxy-silyl)propyl methacrylate]

Pfs – S-adenosylhomocysteine nucleosidase

P(GA) – Poly(glutamic acid)

PGEMA – Poly(2-glucosyloxyethylmethacrylate)

P(GlcEMA) – Poly(β-D-glucosyloxyethyl methacrylate)

PLA – Poly(lactide)

PNIPAAM – Poly(N-isopropylacrylamide)

P(PAm) – Poly(N-phenylacrylamide)

PVA – Poly(vinyl alcohol)

QS – Quorum sensing

RAFT – Reversible addition fragmentation chain transfer

Rh – Hydrodynamic radius

RI – Refractive index

RT – Room temperature

R-THMF – (2R,4S)-2-methyl-2,3,3,4-tetrahydroxytetrahydrofuran

SAH – S-adenosylhomocysteine

SAM – S-adenosyl-methionine

SfbI – Streptococcal fibronectin-binding protein I

SOD – Superoxide dismutase

SRH – S-ribosylhomosysteine

S-THMF – (2S,4S)-2-methyl-2,3,3,4-tetrahydroxytetra-hydrofuran-bonate

TEM – Transmission electron microscopy

THF – Tetrahydrofuran

UCST – Upper critical solution temperature

UV/Vis – Ultra violet/visual spectroscopy

2-EHAm – N-(2-ethylhexyl) acrylamide

2-EHMAm – N-(2-Ethylhexyl) methacrylamide

3-Oxo-C_6-AHL – N-(β-ketocaproyl)-L-homoserine lactone

3-Oxo-C_{12}-AHL - N-(3-oxododecanoyl)-L-homoserine lactone

4-ABA – 4-Aminobutanoic acid

4-AmBA – 4-Acrylamidobutanoic acid

Chapter 1. Introduction

The overall aim of the work reported in this thesis was to generate polymers that could interfere with bacterial communication systems, as a potential route to novel anti-bacterial therapeutics. A secondary objective was to introduce additional functionality into the polymers, such that they might form supramolecular mimics of biological cells, enabling them to contain and release anti-bacterial signals. Accordingly, the key concepts underlying bacterial communication, inhibition of bacterial signaling by small molecules and polymers, and the formation of polymeric containers for encapsulation and release of antibacterial compounds, are covered in this Introduction.

1.1 Bacterial chemical communication-Quorum Sensing (QS)

Over the last few decades, studies have shown that bacteria can signal to each other to regulate community behavior, and can do this as multicellular organisms rather than behave as individuals.[1] For example, activities such as biofilm formation,[2] infection,[3] virulence production,[4] bioluminescence,[5] sporulation,[6] swarming motility[7] and exchange of DNA[8] have all been shown to involve bacterial signaling. Most recently, cell-to-cell communication has been implicated in the mechanisms by which bacteria infect host organisms. Intervention in communication systems has therefore been considered as a potential approach to counter bacterial infections. Apart from direct cell-to-cell contact, bacterial communication is mediated via the secretion and detection of small signal molecules, known as autoinducers (AI). Once autoinducers reach a threshold concentration, bacteria are able to alter gene expression and correspondingly their behaviors in response. The overall system of coordinated

cell-to-cell behavior at a population level is generally termed quorum sensing.[1a] Bacterial signaling is one component amongst several strategies (e.g. response to temperature, pH, osmolarity, oxidative stress, nutrient derivation) by which cells can optimize their survival and growth.[1c] A number of different chemical 'languages' underlying the signaling mechanisms have now been identified. Considered together, these 'languages' form a comprehensive system for cell-to-cell 'cross-talk' that enables coordination across many bacterial species.

1.1.1 Mechanisms of bacterial Quorum Sensing networks

In terms of signaling mechanisms, most AI molecules are specific to particular bacterial species (*Figure 1-1*). In general bacteria detect and respond to different extracellular signaling molecules and subsequently mediate distinct population behaviors. In Gram-negative bacteria, N-acylated homoserine lactones (AHL, AI-1) are common signals, while in Gram-positive bacteria oligopeptides (autoinducer peptides, AIP) usually act as autoinducers.[1b, 1c] Rather than using one single type of autoinducer to control community cooperation, bacteria prefer to coordinate one behavior with multiple signals.[5c] Autoinducer-2 (AI-2) has been recognized as a key signal found across a remarkable wide variety of both Gram-negative and Gram-positive bacteria and accordingly this molecule has been described as a 'universal' signal for interspecies communication.[1, 9]

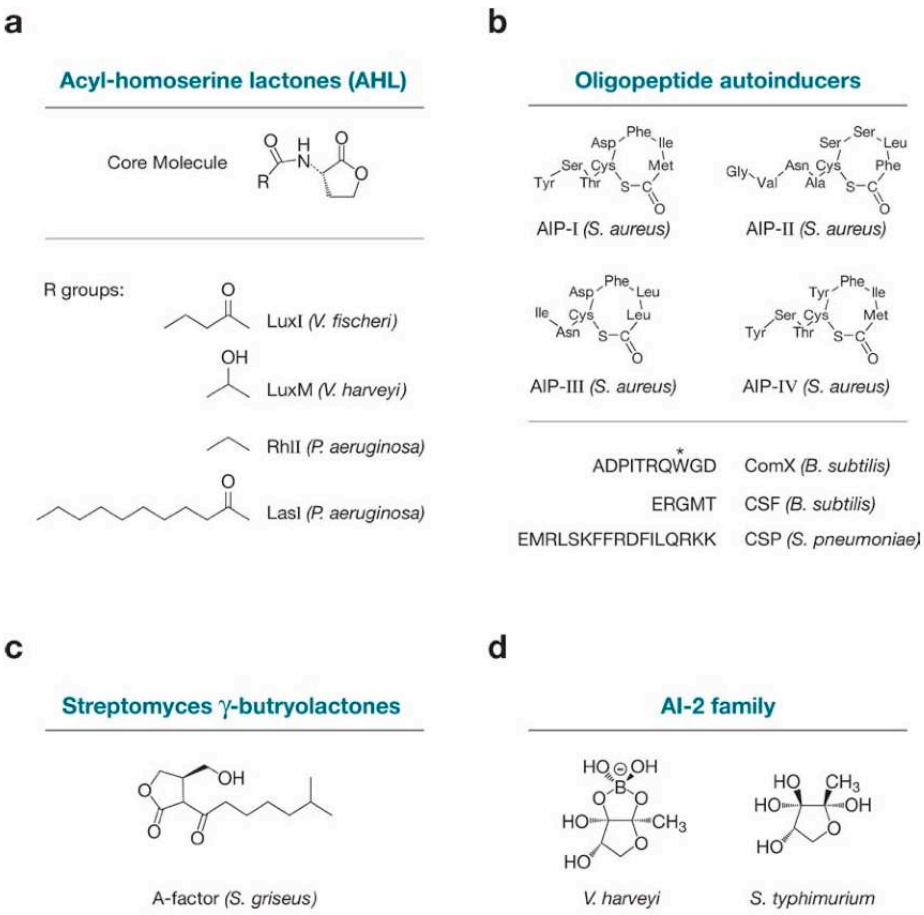

Figure 1-1. Classification of autoinducers found in different bacterial species. Taken from Ref.[1b]

The QS system of the Gram-negative, bioluminescent marine bacterium *Vibrio harveyi* was amongst the first to be characterized with multiple QS signals. There are three AI molecules and three cognate receptors in the *V. harveyi* QS system working in a parallel way to coordinate bioluminescence.[5c] One of the three AI molecules is the acyl homoserine lactone, 3OHC4-homoserine lactone (HAI-1), which is a common signal in Gram-negative bacteria. This compound is biosynthesized by the synthase enzyme LuxM in *V. harveyi*, and binds to a membrane-bound sensor histidine kinase, LuxN.[5b] The second signal in *V. harveyi* is CAI-1, produced by the CqsA enzyme, which interacts with another

membrane-bound sensor histidine kinase, CqsS.[10] The third signal is the 'universal' AI-2, which is a product of the LuxS enzyme.[11] In *V. harveyi*, AI-2 is bound in the periplasm by the protein LuxP to form a LuxP-AI-2 complex that interacts with another membrane-bound sensor histidine kinase, LuxQ.[5c] The detailed mechanism of such QS controlled behavior was explained in *Figure 1*-2, where arrows indicate the direction of phosphate flow in the low-cell-density state, OM/IM means outer/inner membrane. When there is a lack of AI molecules, accompanied by low local cell density, by using these three sensors as kinases, phosphate is transferred to the cytoplasmic protein LuxU and then to the DNA-binding response regulator protein LuxO. The phospho-LuxO induces the expression of the small RNAs responsible for destabilizing mRNA encoding the transcriptional activator, LuxR. When LuxR is degraded and does not activate transcription of the luciferase operon *lux*CDABE, the bacteria do not express the pathways leading to bioluminescence. In contrary, at high cell density and when AI molecules reach their threshold concentrations, interactions between AIs and their cognate membrane-bound sensor kinase will block the phosphate flow and thus 'switch on QS'.

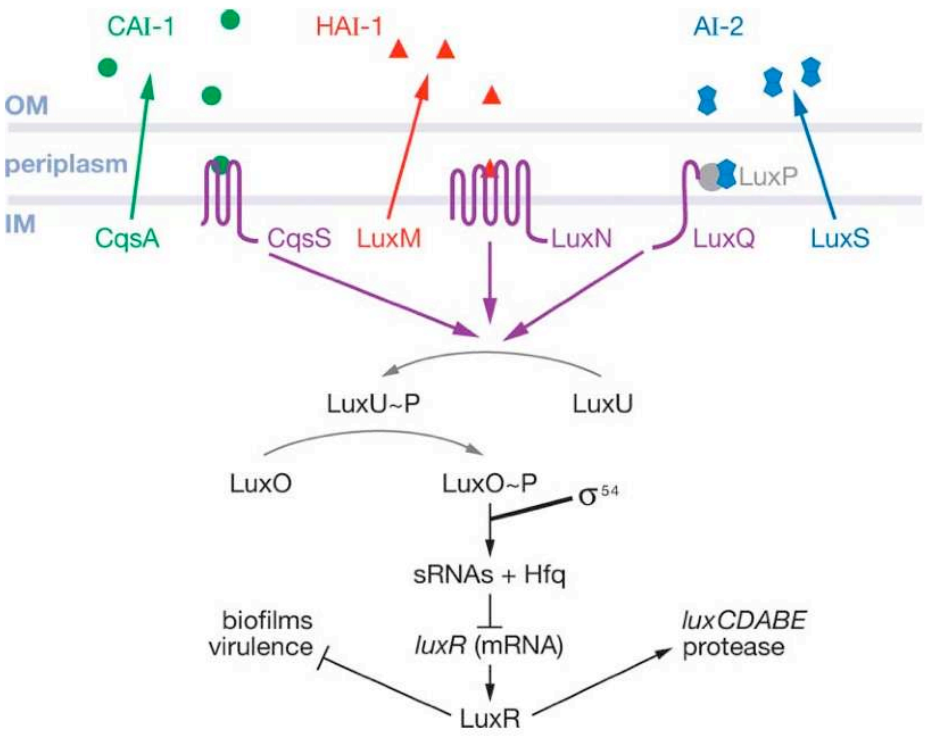

Figure 1-2. Scheme of *V. harveyi* bioluminescence mechanism, taken from Ref.[1b]

1.1.1.1 AI-2-based signaling system

The LuxS enzyme is responsible for metabolizing S-adenosyl-methionine (SAM) the major cellular methyl donor in the activated methyl cycle (AMC). By transferring the methyl groups provided by SAM, the toxic byproduct S-adenosylhomocysteine (SAH) is produced. Then SAH is hydrolyzed to adenosine, S-ribosylhomocysteine (SRH) by the nucleosidase enzyme 5' methylthioadenosine/S-adenosylhomocysteine nucleosidase (Pfs). SRH subsequently is metabolized with LuxS as a catalyst to 4,5-dihydroxy-2,3-pentanedione (DPD) and homocysteine[12] (*Figure 1-3*). Different bacteria generate distinct DPD derivatives that are generically termed as AI-2. In fact, luxS encoding the AI-2 synthase exists in almost half of all bacterial genomes. Polymerase chain reaction (PCR), combined with AI-2 activity assays, for

LuxS mutants of most of these bacteria have not identified any available genome sequences. Hence, LuxS enzyme is the prerequisite for bacteria to produce AI-2 molecules, and a lack of which eliminates AI-2 production.

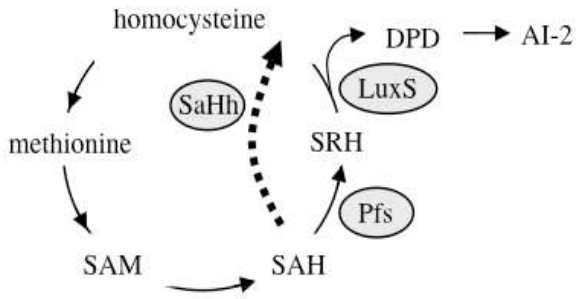

Figure 1-3. Process of LuxS biosynthesis of AI-2, taken from Ref.[1c]

The key AI-2 precursor DPD exists in several chemical forms in equilibrium in solution. The classical view of the active AI-2 signaling in *V. harveyi* is (2S,4S)-2-methyl-2,3,3,4-tetrahydroxytetra-hydrofuran-bonate (S-THMF, borate), a novel furanosyl borate diester with no similarity to other autoinducers.[13] Chen *et al*.[9] demonstrated (by crystallizing its binding complex) that the active form of AI-2 which binds LuxP (primary receptor of AI-2 in *V. harveyi*), is the furanosyl borate diester. It is surprising that a single boron atom exists in the AI-2 structure because few other examples exist of boron utilized in biological systems in this way.

However, this is not the only bacterial signaling molecule derived from DPD. Miller *et al.*[14] demonstrated that two different forms of autoinducers both derived from DPD were recognized by two different species of bacteria as communication signals (*Figure 1-4*). In *Salmonella typhimurium* with LuxS enzyme to biosynthesize DPD, LsrB protein, a periplasmic binding protein, was shown to bind a distinct DPD derivative (2R,4S)-2-methyl-2,3,3,4-tetrahydroxytetrahydrofuran (R-THMF) in the absence of boron, using

crystallography and ^{11}B-NMR to identify the structure of the LsrB ligand R-THMF complex. Considering the real biological environment, it is perhaps not surprising that at least two AI-2 signaling systems have been characterized. In a marine environment the natural concentration of boron (as boric acid/borates) reaches as high as 0.4 mM compared with a much lower concentration in terrestrial waters. Accordingly, boric acid enhances AI-2 signaling in *V. harveyi* but inhibits AI-2 signaling in *S. typhimurium* due to the structural exchange between the inactive and active forms of AI-2 molecules of each bacterial types, reflecting their different native environments. These results reveal that the molecule generically titled 'AI-2' is in fact a mixture of interconvertable molecules acting as interspecies signals.

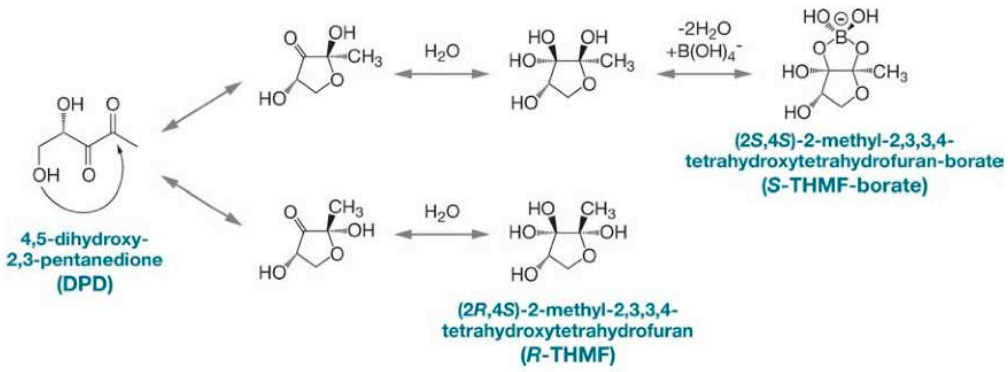

Figure 1-4. Structures of DPD and derivatives, taken from Ref. [1b, 9, 14]

As mentioned, AI-2 has been widely demonstrated as a signal that both Gram-negative and Gram-positive bacteria use as a common 'language' to 'talk' with each other, in a way to effectively regulate their community-scale behaviors and finally survive and develop their populations. Among the numerous bacterial species, the role of AI-2 in *V. harveyi* was the first discovered and well established.[5c] However, it is not readily understood the signaling functionality of AI-2 in the other bacteria.[15] Since AI-2 always works together

with other regulators, there is inevitably difficulty for identification of its exact function. DNA microarray techniques have been used to show that AI-2 controls numerous gene regulation behaviors including cell division, morphogenesis, and cell surface architecture.[16]

In *S. typhimurium* bacteria, Xavier *et al*.[17] identified that lsrK and glpD were functional in activating transcription of the lsr operon in response to AI-2. In both mutants, lsr could not actively express in the absence of phosphor-AI-2 (due to lsrK deficient) and cyclic AMP-catabolite activator protein-dependent activation (due to glpD deficient), and therefore AI-2 dependent QS was quenched. Hence, this study gave sort of mechanism explanation of AI-2 involved QS.

AI-2 has been reported to control biofilm formation in *Escherichia Coli* through enhancing the cell motility.[18] Three different *E. coli* strains (ATCC 25404, DH5α the LuxS deficient strain and K12 wild strain) were selected in this report and in all cases results demonstrated that AI-2 enhanced the biofilm formation, in terms of both mass and thickness through B3022, an uncharacterized protein termed the motility QS regulator gene (the mqsR gene). Some recent work revealed the pleiotropic roles of Lux S and AI-2 in *Actinobacillus pleuropneumoniae* virulence features.[19] From the microarray, significant differences in gene expression could be observed between the LuxS mutant and its parental strain. Results indicated that the LuxS mutant presented enhanced biofilm formation but reduced adhesion ability not because of absence of AI-2. In fact, both activities could be increased in the presence of exogenous AI-2. It is therefore possible to conclude that AI-2 can play a role in QS networks independent of its biosynthesis enzyme LuxS.

Significantly however, some reports challenged the role of AI-2 as a signal in QS network.[20] As a signal molecule, AI-2 must not only be released from an individual cells and internalized into a neighbouring cell, but also evolve their own production in response to alternation of the receiver's gene expression and such behavior should benefit both the producer and receiver. However, AI-2 was demonstrated to be the metabolic by-product and not responsible for activating any specific genes directly.[1c] In this case, AI-2 was more accurately defined as an environmental cue to regulate gene expression rather than a signal, since the AI-2 producing cells was not evolved by the receiver's response. This definition of the role of AI-2 in QS interspecies communication is important for researchers to explain the mechanisms of some phenomenon in their experimental studies.

1.1.1.2 Other signaling systems

The interspecies signaling molecule AI-2-based QS communication system has been discussed above. As mentioned, specific signals exist in two major catalogues of bacteria (Gram-negative bacteria with both inner (plasma) and outer cell membranes, and Gram-positive bacteria only with an inner (plasma) membrane). AHLs are found to be associated with most of the Gram-negative proteobacteria acting for intraspecies communications (*Figure 1-1*). There are similarities of this AHL-based system to AI-2-dependant QS network (*Figure 1-5*), as two major proteins are involved: LuxI the autoinducer synthase responsible for AHLs biosynthesis and LuxR the cytoplasmic autoinducer receptor/DNA-binding transcriptional activator. The product (AHL) of LuxI diffuses and thus releases to the surrounding environment consequently

increasing its concentration in proportion to cell population. When the AHL concentration reaches a threshold, it is bound to its receptor protein LuxR to be uptaken into cells. The LuxR-AHL complex subsequently activates the transcription of the operon encoding luciferase (*luxICDABE*) and thus induces LuxI expression encoded in the luciferase operon so that AHLs also control their own biosynthesis.[21]

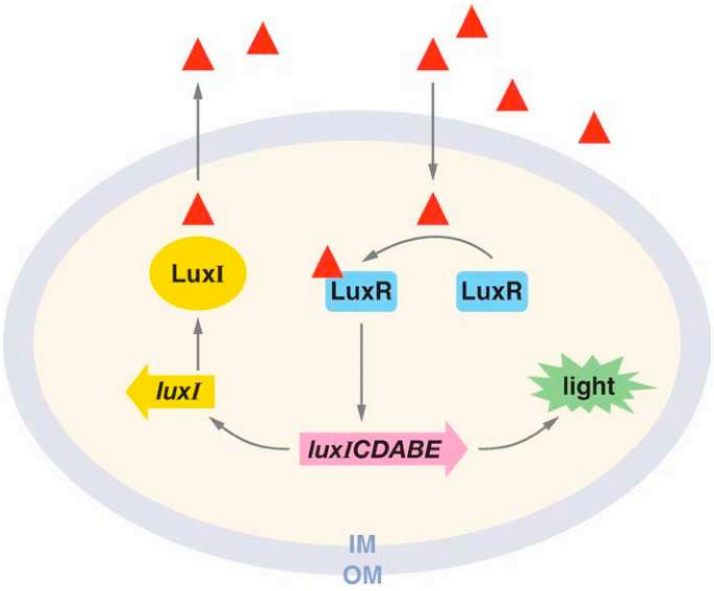

Figure 1-5. AHLs-based QS progress in *Vibrio fischeri*. AI molecules (red triangles) produced by LuxR protein and detected by LuxI. IM: inner membrane and OM: outer membrane of cells. Taken from Ref.[1b]

In fact, many bacterial species regulate their behaviors with multiple LuxR/LuxI families and even AHL.[1c] AHLs are synthesized from S-adenosyl-methionine (from SAM) and fatty acyl chains carried on acyl-acyl carrier protein (acyl-ACP) in the presence of LuxI protein catalyst.[22] In most cases, AHL is identified as a homoserine lactone (HSL) ring N-acylated with a fatty acyl group at α-position.[1b, 1c] Importantly, the fatty acyl group varies in chain length, backbone saturation and side-chain substitutions as specific LuxI

proteins only producing their cognate AHLs and binding to specific LuxR receptors.[23] The structures and mechanisms are distinct from those of AI-2-based systems, as AHLs are specific signals only to their corresponding bacteria species even in the environment of multiple AHLs produced by mixed bacteria.

Significantly however, the adaptability and flexibility of bacteria enables them to choose the best way to survive and develop, and thus it is understandable that one type of bacterium can respond to an AHL signal that is produced by another type of bacterium.[24] In most cases, the overall condition of the bacterial culture is crucial to the adaptability. In certain specific cultures, a given bacterium could adapt by producing several different types of AHLs that are detected as signals by another type of bacterium. Also the variability of its receptor protein LuxR homologues shows an alternative pathway for the bacterium to sense in response to exogenous AHLs (from other type of bacteria).[24]

Another signaling system based predominately in Gram-positive bacteria has to be mentioned here (*Figure 1-1*). Since my PhD project is using Gram-negative bacteria (*V. harveyi* and *E. coli*) as bacterial models and its main aim is to interfere in QS-controlled bacteria behaviors via modulating AI-2 concentrations in bacterial media, there will only give a brief introduction on autoinducing peptide (AIP) based communication. Gram-positive bacteria employ post-translationally modified oligopeptides (5-34 amino acids) as QS signal molecules, termed as AIPs. There are different AIP families and are naturally cataloged by their modified groups (lactone, thiolactone rings, lanthionines and isoprenyl groups). These specific AIP structures lead the

gram-positive bacteria to have similar mechanisms that Gram-negative bacteria use to regulate QS with AHL-LuxI/LuxR system. In this case, AIPs apparently confer specificity in intraspecies communication just as in the AHL-based QS circuits. The membrane bound receptors for AIP in gram-positive bacteria are involved in a two-component system (eg. AgrC and AgrA in *Staphylococcus aureus*[1b, 1c]). As peptide signals are macromolecules that are not able to diffuse across cell membranes, a third protein (eg. AgrB[1b, 1c]) is therefore responsible for processing and modification of signals in order to export signals to the extracellular environment. Similarly, there are several QS coordination behaviors in Gram-positive bacteria being modulated via multiple peptides together with other types of signals.

1.1.2 Therapeutics of Quorum Sensing-related bacterial infection

As mentioned above, some pathologically relevant events such as biofilm formation and bacterial virulence are under QS control,[5a] and therefore development of QS mediators has the potential to be used in antibiotic therapy. Among a great deal of efforts on this area, the investigation of QS inhibitors has attracted most attentions.[25] While initial research focused on QS inhibitors for AI-1 or AIP, more recent efforts have considered blocking AI-2 QS pathways.[26]

All of the references mentioned in the above paragraph are about design and characterization of small molecules as QS inhibitors. However, much less efforts have been made to develop macromolecular QS quenching systems until very recently. Amara *et al*.[27] reviewed research efforts on macromolecular inhibition of QS covering three aspect of proteins: enzymes,

antibodies and decoy receptors. A number of the proteins mentioned in this review displayed promising potency to inhibit QS, but not all of them were clearly understood as regards to their quenching mechanisms. In this case, this review also highlighted the issues that need to be considered for future studies: 1) selection pressure and resistance invoked in bacteria by antibiotics, 2) efficacy and rate of protein-mediated hydrolysis of autoinducers. Thus, the possibilities of using synthetic macromolecules as QS-quenchers or QS-interference systems have not been explored to any great extent to date.

Initial efforts in this direction have investigated polymeric materials that can be considered analogous to protein-based macromolecular QS inhibitors such as Molecularly Imprinted Polymers (MIPs). The group of Piletsky has developed some polymeric materials that were demonstrated to attenuate effectively some QS-controlled phenotypes. Polymers developed with the aid of molecular receptor-docking software were screened for their ability to specifically bind the signal molecule N-(β-ketocaproyl)-L-homoserine lactone (3-oxo-C_6-AHL) of the marine bacteria *V. fischeri* and thus quench its QS-controlled bioluminescence without damaging the cells.[28] Thereafter, a series of related molecular imprinted polymers that could bind the QS signal N-(3-oxododecanoyl)-L-homoserine lactone (3-oxo-C_{12}-AHL) in *Pseudomonas aeruginosa* pathogen and consequently attenuate its biofilm formation, were reported from their group based on the same strategy of specific QS signal sequestration.[29] However, imprinted polymers in general suffer from problems of poor scalability and difficult characterization, therefore, soluble polymers that could bind multiple QS signals are more widely considered to provide potent anti-infective activity. Interestingly, instead of targeting QS

signals to inhibit QS-controlled phenotypes, Janda's group reported their efforts on investigation of multivalent dendrimers as Lsr-type AI-2 receptor probes.[30] Accordingly, a series of DPD conjugating dendrimers (*Figure 1-6*) were demonstrated to inhibit QS in *S. typhimurium*. As described above, AI-2 signal in this species is R-RHMF form of DPD and thus the cognate receptor protein on the cell surfaces would be blocked if in the presence of such DPD conjugating dendrimers. These specific QS targeting dendrimers, which exhibited the advantage of multivalency not only acted as probes for specific AI-2 binding receptors in *S. typhimurium* but were also demonstrated to be potent as inhibitors for Lsr-type QS systems.

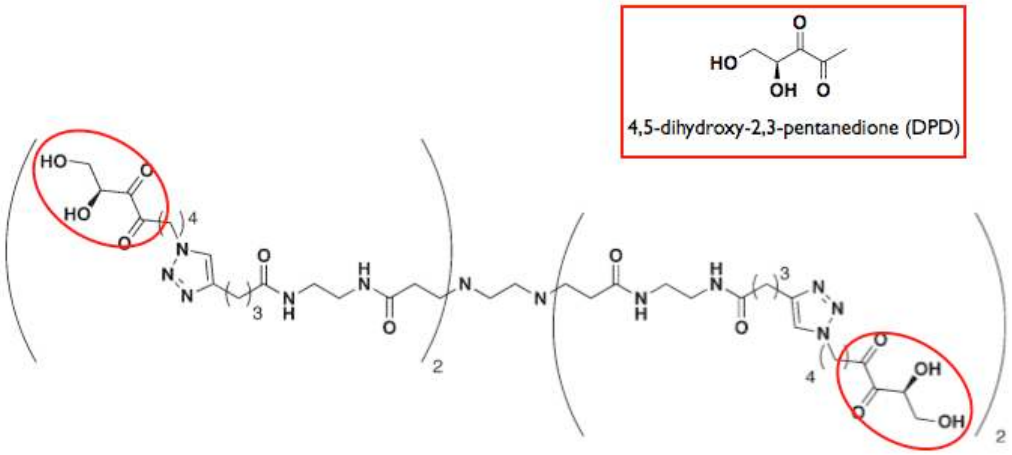

Figure 1-6. Structure of DPD conjugating dendrimer, adapted from Ref.[30]

In recent years, considerable effort has been expended in developing more active or responsive therapeutic and anti-infective materials. Of particular interest have been polymers with dynamic properties, especially those that involve self-assembly and triggered release. Accordingly, some significant examples of responsive systems, controlled release polymer micelles and polymersomes, and release mechanisms are reviewed, as these provide an

important background for some potential novel means by which interference in QS could be achieved.

1.2 Polymeric vesicles (polymersomes)

Polymeric vesicles, commonly called polymersomes, are hollow, lamellar spherical shell structures that enclose a volume with a membrane made of amphiphilic block copolymers in which there is both a hydrophobic and a hydrophilic block. The hydrophobic groups have high affinity for non-polar solvents and hence tend to self-assemble in water-like polar solvents, while the more hydrophilic fragments prefer to face the selective polar (aqueous) medium. Polymersome resemble liposomes, which are vesicles prepared from natural cell-membrane phospholipids, in their gross architecture, but in general are tougher and more stable. This is due to the thicker vesicle wall, which is composed of high molecular weight block copolymers rather than phospholipids. In addition, through appropriate functional group chemistry, polymeric vesicles can exhibit more favourable biological properties, such as long blood circulation times.[31]

The synthesis of block copolymers and polymersomes has become much more accessible through advances in controlled free radical polymerization chemistries. These enable many possibilities for preparing block copolymers with a much broader range of functional groups than those previously synthesized under living cationic or anionic polymerization.[32] It is now possible to assemble monomers with side-chains of very different functionalities into polymers, which allows the resulting materials to have the superior properties of each individual component. On the other hand, by

changing monomer types and molecular weight of each fragment, a series of polymersomes with various membrane thicknesses and permeabilities are available.[33] This advance in the precision of synthesis opens new opportunities for the use of polymers in applications such as encapsulation of therapeutic molecules, for example, proteins (enzymes), DNA/RNA fragments and both hydrophilic and hydrophobic drugs.[34]

1.2.1 Formation of polymersomes

Amphiphilic block copolymers are commonly composed of more than one type of monomer, typically one hydrophobic and one hydrophilic, so that the resulting molecules process regions that exhibit opposite affinities for an aqueous solvent. In aqueous solutions, amphiphilic molecules tend to achieve a state of minimum free energy by removing the hydrophobic blocks from the aqueous media. Depending on the system, amphiphilic block copolymers can yield different self-assembled superstructures with various morphologies, such as spherical micelles, cylindrical micelles or vesicles. Several factors including chemical constitution, the length of each individual block, the properties of the solvent and the environmental conditions of the solution such as pH, temperature, ions and concentration can control the size and shape of the aggregates.[35] Theoretically, these varying morphologies are basically a result of the inherent molecular curvature (*Figure 1-7*).[36] Based on the **Eq. 1**, a dimensionless 'packing parameter', 'p', of a presented molecule shows its most likely self-assembled morphology. When $p \leq 1/3$, spherical micelles are formed, when $1/3 \leq p \leq 1/2$, cylindrical micelles and polymersomes when $1/2 \leq p \leq 1$.

Equation 1

$$p = \frac{\gamma}{\alpha \cdot l}$$

In the equation, 'γ' represents the volume of the hydrophobic chains, 'α' is the optimal area of the head group, and 'l' means the length of the hydrophobic tail. The studies of polymersomes, the size of which can range from 100 nm to 1000 nm due to the factors mentioned above, have been focused more recently in experimental papers compared to the prior theoretical work concerning vesicular assembles from block copolymers. Hence, no generally applied computational model has been presented yet. In spite of this limitation in theory, polymersomes can be made in dilute solution from variety of amphiphilic systems, not only in aqueous media but also in organic environment, such as in N, N-dimethylformamide (DMF), tetrahydrofuran (THF), methanol or mixture solvents.

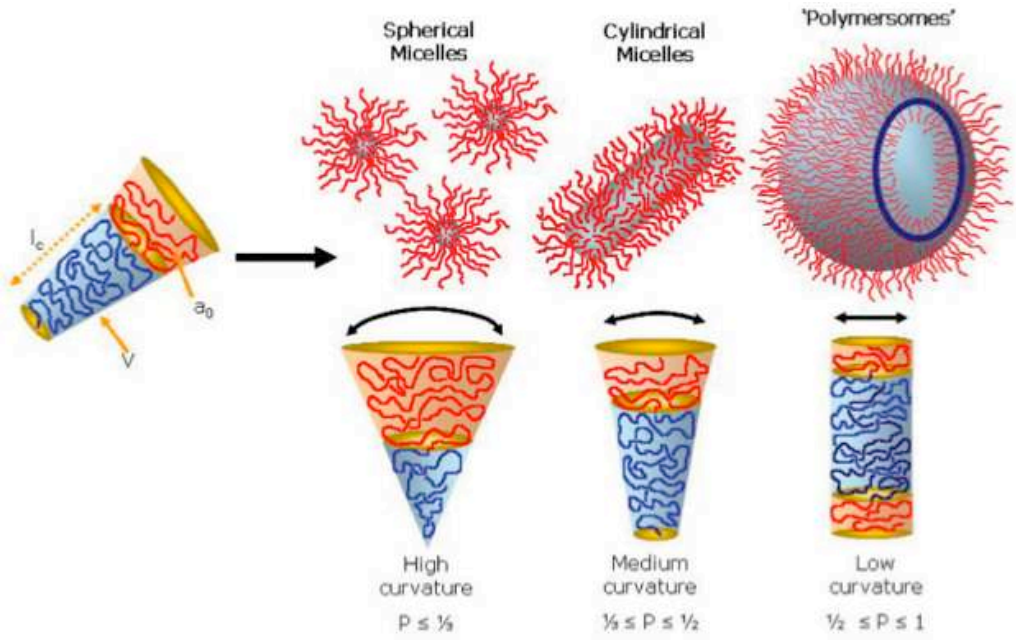

Figure 1-7. The relation between the inherent curvature of the amphiphilic block copolymers and their self-assembled structures, taken from Ref.[37]

Two typical and commonly used methods to make polymersomes are film rehydration and solvent-exchange techniques.[38] Specifically, polymersomes can be prepared via a film rehydration technique by dissolving the copolymers in a volatile organic solvent in which both hydrophilic and hydrophobic fragments are properly dissolved, through evaporating the solvent to form a thin film and rehydrating it in the aqueous phase to yield submicron vesicles with a relatively broad size distribution. The polymersomes prepared this way therefore need to be separated based on size by sequential extrusion.[39]

Another strategy is based on the solvent exchanging system. Similarly, a good volatile solvent for both hydrophilic and hydrophobic components is employed to dissolve the copolymers. Instead of forming a film, polymersomes can be prepared either by slowly adding this organic phase with copolymers to an aqueous phase or dropping aqueous solution into organic mixture. This way, the hydrophobic blocks are insoluble leading to the self-assembly and the precipitated structures remain stable after a few days of dialysis in water.[40]

Except for the intrinsic properties of polymer compositions, the factors that influence the formation of polymersomes are varied from preparation methods, polymer concentrations, the type of organic solvent, the volume ratio of organic phase and aqueous phase, and even the solvent removing rate.[41] In this case, the key to obtain well-defined polymersomes formed from newly investigated amphiphilic copolymers is selection of proper preparation methods and optimization of the preparation conditions.

1.2.2 Stimuli-responsive polymersomes

Once formed, polymersomes have fluid-filled cores with walls made of amphiphilic block copolymers, isolating the core from the outside solution. Furthermore, when compared to micelles, which can only encapsulate hydrophobic molecules, polymersomes can be the container of both hydrophilic compounds within the aqueous interior and also capture hydrophobic molecules within the membrane. However, for many practical applications, such as controlled encapsulation and release applications, one might require a polymersome to have a dynamic or 'switchable' structure, such that molecules, drugs or chemical signals can flow in and out of the vesicle center domain or polymer bilayer membrane.

Recently, the development of intelligent polymersomes responding to internal or external stimuli, especially pH, temperature, redox and light, has been attracting attention. To enhance the bioavailability of drugs, for example, and reduce any unwanted side effects, drug carriers should combine the properties of high incorporation of the therapeutic transit in the body, but rapid release at the target site. Polymersomes with stimuli-responsive groups might enable encapsulation and release of antibiotics or QS agents in a controlled manner. In this section, therefore, the issue of controlled release in stimuli-response polymersomes is considered.

Due to the variation of pH in the body, for example, along the gastrointestinal (GI) tract the change in pH from acidic in the stomach (pH 2) to more basic in the intestine (pH 5-8),[42] a pH-responsive polymersome is an obvious candidate as a carrier for controlled drug delivery. Moreover, the mildly acidic pH encountered in tumour and inflammatory tissues (pH 6.8) as well as in the

endosomal and lysosomal compartments of cells (pH 5-6), provides a potential trigger for the release of systemically administered drugs from a pH-sensitive carrier, since blood and normal tissues have a pH of 7.4.[42-43]

A pH-responsive polymersome design allows for either polyacid or polybase blocks in their structures, so that their solubility in water can be changed by a pH variation. Armes' group[44] have described polymersomes formed by the self-assembly of a pH-responsive, hydrolytically self-cross-linkable copolymer, poly(ethylene oxide)-*block*-poly[2-(diethylamino)ethyl methacrylate-*stat*-3-(trimethoxy-silyl)propyl methacrylate], [PEO-*b*-p(DEA-*s*-TMSPMA)] in THF/water mix solvent (*Figure 1-8*). In this research, the basic DEA in the polymer structure acts as the catalyst of TMSPMA hydrolysis. The hydrolysis of $–Si(OCH_3)_3$ to $–Si(OH)_3$ enables the formation of siloxane cross-links. DEA exists as a weak cationic polyelectrolyte at low pH, but deprotonates when the solution is above pH 7, this property remains when replacing DEA residues with TMSPMA up to 50 mol %. And presumably, the permeability of polymersome membrane was demonstrated to be sensitive to pH change by DLS and fluorescence studies. These pH-responsive polymersomes are of particular interest because of the novel idea of self-catalysis.

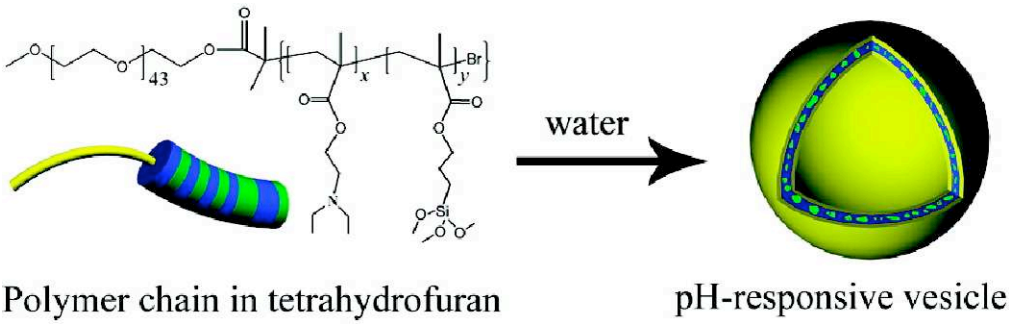

Figure 1-8. Schematic presentation of the formation of PEO-*b*-p(DEA-*s*-TMSPMA) polymersomes, taken from Ref.[44]

Borsali and coworkers[45] reported pH-responsive block copolymer vesicles could be conjugated to the hydrophobic nonsteroidal anti-inflammatory agent indomethacin (IND) via an ester bond. This system was also proven to be able to stabilize, transport and deliver physically encapsulated free-IND (F-IND). At neutral pH, F-IND was released in diffusing manner, because the ester bond between drug and the amphiphilic polymer was stable. At low pH, the bound IND could be released in a sustained way, due to the hydrolysis of the ester bonds. Thus, a controlled release system of IND was established in a pH dependent manner. Frechet's group[46] have used linear poly(amidoamine)s as pH-sensitive polymer materials with a pH-sensitive bond in the backbone. This family of acid-degradable poly(amidoamine)s (*Figure 1-9*) were designed to remain stable at the physiological pH of 7.4 but degrade more quickly into many small molecules in the pH 5.0-6.0 environment of lysosomes, endosomes, or tumor tissues. Thus, on the basis of Frechet's results, systems with these linear pH-sensitive polymer materials could be applicable in controlled drug delivery.

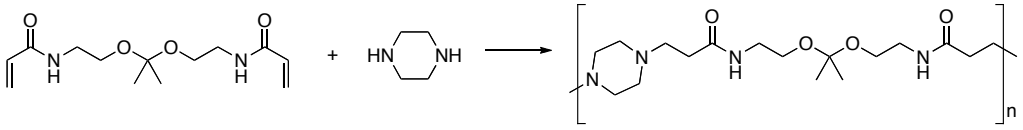

Figure 1-9. Preparation of poly(amidoamine)s pH-responsive polymers, adapted from Ref.[46]

The pH-responsive polymersomes have also been used as gene delivery systems, as reported by Song *et al.*[47] In this research, a novel acid-labile pH-responsive block copolymer composed of poly(ethylene glycol) (PEG) and poly(2-(dimethylamino)ethyl methacrylate) (PDMAEMA) segments connected

through a cyclic ortho ester linkage (PEG-*acid*-PDMAEMA) with a pH-sensitive PEG shield was prepared. More recently, 'smart' polymeric vesicles of poly[2-(dimethylamino)ethyl methacrylate]-*block*-poly(glutamic acid) [p(DMAEMA)-*b*-p(GA)] with multiresponsive function have been obtained from self-assembly of double hydrophilic block copolymers, providing facile, tunable and durable ways to develop biological applications.[48]

Additionally, studies in developing temperature responsive polymersomes are also of interest for many research groups. Temperature responsive polymersomes are commonly made from polymers those exhibit a phase transition at a certain temperature. Those polymers which exhibit a non-linear decrease in solubility upon heating are described as having a lower critical solution temperature (LCST), while those which become more soluble via a non-linear increase on heating have an upper critical solution temperature (UCST)[49]. Polymersomes composed of the temperature responsive poly(N-isopropylacrylamide) (PNIPAAM) have a phase transitions close to body temperature and thus have been extensively investigated. PNIPAAM undergoes a reversible coil-to-globule transition at ~ 32 °C. Below LCST, the polymer is extended and soluble in water; above this temperature, it is in a water-insoluble conformation and forms more hydrophobic aggregates. When block copolymers composed of PNIPAAM and PEG were made to be the carrier material, vesicles were formed at temperatures above the LCST, which was demonstrated by encapsulation and release of fluorescent dye recorded by fluorescent microscopy and data information from DLS. When the temperature was decreased below the LCST, the PNIPAAm block became soluble and the vesicle disassembles. Therefore, encapsulated drugs were released from the

vesicle when the temperature decreases below the LCST.[50] Leroux and coworkers[51] reported that poly(organophosphazenes) with varying ratios of ethylene oxide and alkyl chains for thermosensitivity and free acid units for pH sensitivity, had a pH-dependent LCST ranging from 32 to 44°C. Such copolymers were complexed to liposomes for the first time and released their contents upon a change in temperature and pH. McCormick's group[52] focused their attention on the controlled polymerization of hydrophilic methacrylamide monomers and subsequent vesicle formation from self-assembly of amphiphilic block copolymers in aqueous solutions by variation of solution temperature. The diblock copolymer poly(N-(3-aminopropyl) methacrylamide hydrochloride)-*block*-poly(N-isopropylacrylamide) (PAPMAH-*b*-PNIPAM) was synthesized by the reversible addition fragmentation chain transfer (RAFT) polymerization method. The LCST can be tuned to a desired value by changing the composition of the block copolymer. The LCST of the block could be lower in longer NIPAM block. However if the NIPAM block length were kept constant, increasing the AMPA block length led to an increase in the LCST. These block copolymers exist as unimers in aqueous solution at room temperature, and self-assemble into vesicles above LCST. Interestingly, such vesicles can be structurally locked via adding an oppositely charged polyelectrolyte. Temperature responsive polymersomes with LCST phenomena have been the most investigated for drug delivery[49, 53] but polymers with UCST behavior are also of potential in this application.

The controlled release from polymersomes can be triggered with other stimuli other than temperature and pH. For example, the extracellular fluids and certain pathophysiological inflamed or tumor tissues exhibit oxidative

environments while other cellular environments can be reducing. Based on this, redox responsive triggers have been used for the release of entrapped drugs from the polymer carriers.[54] In addition, polymersomes can be prepared to be photosensitive, so that the release of encapsulated cargo can be rapidly triggered at a selective time and targeted site via exposure to light. Azobenzene derivatives are the most extensively studied photochemical groups, as they can be reversible isomerized from *trans* to *cis* configurations by UV/Vis light and vice versa. Liu and Jiang[55] demonstrated the transition between the interpolymer complexes and micelles can be achieved via reversible optical switching of self-assembly with the aid of hydrogen-bonding interaction between carboxylic acid and pyridine. Additionally, the formed micelles can response to light irradiation to further cross-link with 1,4-diiodobutene accompanied with morphological changes and become hollow spheres in a reversible manner (*Figure 1-10*).

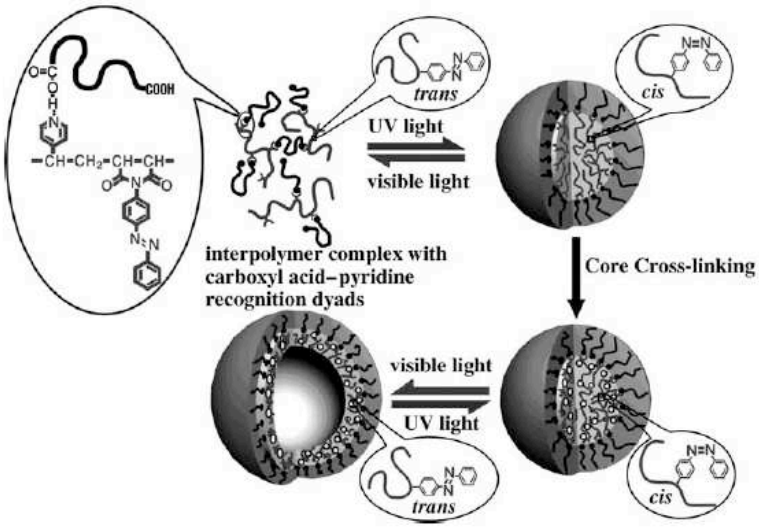

Figure 1-10. Illustration of the reversible photo-induced micellization and micelle-hollow-sphere transition of hydrogen-bonded polymers, taken from Ref.[55b]

1.2.3 'Evolved' smart polymers and polymersomes in applications ranging from controlled release to synthetic biology

Polymersomes composed of a variety of amphiphilic block copolymers can be modified by changing the structures of their component monomers, so that materials with a range of desirable properties can be obtained via chemical approaches. Additionally, polymersomes provide higher stability in the circulation than liposomes[56] and also are capable of loading both hydrophilic molecules in the aqueous core and hydrophobic compounds in the bilayer membrane, which make polymersomes much more suitable than liposomes for biomedical applications.[57] Obviously, most biomedical applications of block copolymers require biocompatible and biodegradable components.[58] Palmer's group[58b] developed biocompatible and biodegradable polymersomes from amphiphilic block copolymers composed of hydrophilic poly(ethylene oxide) (PEO) and hydrophobic block either poly(caprolactone) (PCL) or poly(lactide) (PLA). They successfully encapsulated hemoglobin in poly(ethylene oxide)-poly(caprolactone) (PEO-PCL) or poly(ethylene oxide)-poly(lactide) (PEO-PLA) polymersomes, without affecting oxygen binding properties of hemoglobin while retaining good release profiles. The anti-cancer drug paclitaxel has been encapsulated in self-assembled poly(butadiene)-*block*-poly(ethylene oxide) (PB-*block*-PEO) polymersomes and worm-like micelles for inhibiting proliferation of MCF-7 human breast cancer cells.[58f] The result of *in vivo* cytotoxicity assays indicated that the enhanced ability of paclitaxel-loaded polymersomes inhibiting proliferation of MCF-7 human breast cancer cells was a consequence of the increase of paclitaxel loading concentration. Kim *et al.*[58g] reported that loading and functional delivery of siRNA into

cancer cells *in vitro* and antisense oligonucleotides (AON) into muscle *in vivo* with non-ionic, nano-transforming polymersomes were developed. A series of copolymers were prepared into vesicles and quantitation of their loading efficiency was evaluated with fluorescent labeled complexes by using spectrofluorimetry. The advantage of such investigation was allowing delivery of negative changed complex in an exposed positive charged milieu.

Potential applications of polymersomes are strongly biased towards carriers for drug/gene delivery, but there have been a number of more recent studies of potentially new functions. For example, the internal space of polymersomes can be considered as a biomimetic nanoreactor if a protein can be encapsulated and remain active in situ.[59] Axthelm and his coworkers[59a] developed nanovesicles from amphiphilic block copolymers composed of poly(2-methyloxazoline)-poly(dimethylsiloxane)-poly(2-methyloxazoline) entrapped Cu, Zn superoxide dismutase (SOD) as antioxidant nanoreactors. To obtain the nanovesicles, the dissolved triblock copolymer in ethanol at 17% (w/w) was dropped slowly to the solution of SOD in phosphate-buffered saline (PBS) at room temperature. This shielding of SOD enabled biocompatibility and low non-specific protein binding ability. The resulting nanoreactor has the potential application in protecting compounds having antioxidant properties.

Additionally, surface modification of polymersomes, for example by attaching targeting moieties, is very important for drug/gene delivery systems, especially for targeted/sustained delivery systems. Polymersomes used in biomedical applications are generally self-assembled amphiphilic block copolymers composed of biocompatible, biodegradable hydrophobic polymer blocks (e.g. PCL, PLA) covalently bonded to a biocompatible hydrophilic block, typically

PEG.[60] It is generally known that PEG has the ability to prolong circulation time of nanoparticles and its high biocompatibility and hydrophilicity are also crucial properties for biomedical applications. Meng *et al.*[61] prepared polymersomes of amphiphilic block copolymers based on PEG and biodegradable polyesters or polycarbonate as the carriers for biofunctional compounds (model: carboxyfluorescein, CF). By using a PEG spacer, antibodies can be attached onto a polymersome with control of local steric crowding, by coupling the distal end of PEG chain specifically. The developed polymersome could thus be considered as a membrane-controlled reservoir system, in effect a simple 'artificial cell' mimic containing biofunctional compounds. Polymersomes made from double hydrophilic block copolymers with pendant glycofunctionality have been shown to transfer dyes across their membranes when bound to bacteria, which may offer a new approach to target planktonic bacteria, which in turn may be a promising route for prevention of infectivity, treatment of disease, and to control of new tissue formation.[62] In these systems poly(2-glucosyloxyethylmethacrylate) (PGEMA) and poly(diethyleneglycol methacrylate) (PDEGMA) were incorporated to form block copolymers which self-assembled into vesicles. Such containers with combined surface activity and biorecognition have the potential capability of transferring cargo to biological cells either via surface interaction, or via the release of the vesicle contents.

1.3 Aims and objectives of the project

From consideration of the prior examples of polymers in biomedical applications, the project was conceived to develop in two phases. The first phase was to establish efficacy of polymers as agents to interfere in QS of bacteria, as a potential new anti-infective strategy. The second phase was to consider self-assembled polymersomes as both binding agents and containers for QS components, such that a controllable interference with bacterial communication could be addressed. The latter stages of the project envisaged whether these polymersomes might even act as simple artificial mimics of a cell, in order to form 'intelligent' biomimetic materials.

1.3.1 Polymers for interference in bacterial Quorum Sensing (1st Phase)

In order to develop polymers for anti-infective strategies, a brief discussion of the infection mechanisms employed by bacteria is included. Based on the typical strategies used to survive and infect host cells, bacteria can be roughly categorized into two groups. The first group, including pathogens such as *Mycobacterium* and *Leishmania,* passively enter the intracellular milieu via phagocytosis. These cells are able to subvert the host's immune response and gain an intracellular niche as the consequence of altering phagosome maturation (*Figure 1-11*).[63] In this way, the bacteria protect themselves from the innate immune response and can act as parasites in the host-cells, leading to subsequent diseases.[63-64]

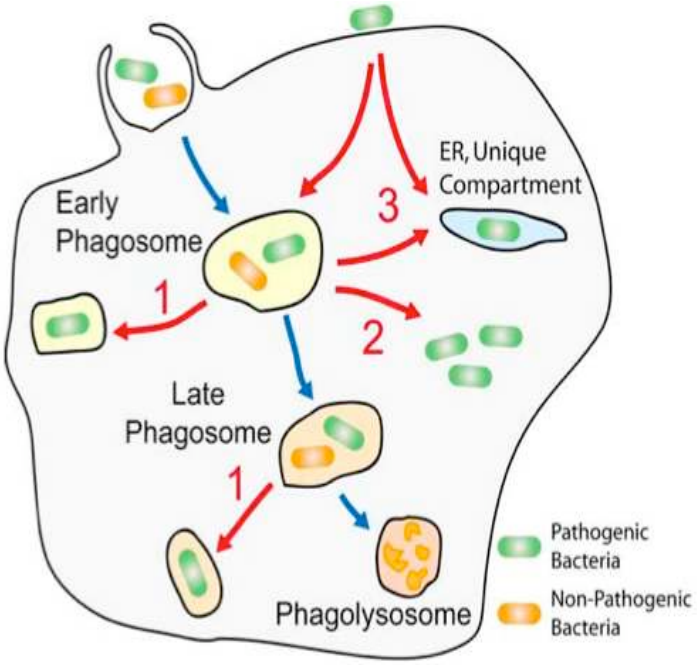

Figure 1-11. Schematic explanation of typical phagosome maturation and strategies of intracellular pathogen survival, taken from Ref.[63]

A second class of bacteria gain access to the host's intracellular environment actively by invasion, using multiple processes to promote their own internalization in cells that are normally non phagocytic.[63, 65] Invasive bacterial entry mechanisms (e.g. 'Zipper' and 'Secretory System' mechanisms), and their consequences have been reviewed elsewhere.[65-66] However, an understanding of invasion and colonization of host cells by bacteria is of importance to the work in this thesis, as this might inform the design of synthetic materials for bacterial infective therapeutics through targeting the 'contact and adherence' step involved in the entry mechanisms.

Significantly, although the entry mechanisms may vary in the successive steps depending on the bacterial species, invasive bacterial adhesion is the initial step in colonization[65] and the formation of resistant biofilms[67]. The most widely accepted mechanism of initial bacterial attachment is based on

Derjaguin Landau Verwey Overbeek (DLVO) colloid theory.[68] DLVO theory quantifies the roles of van der Waals and Coulomb force in the interaction of a colloidal particle with a surface. In principle, particles irreversibly attach on a surface when the two objects are close enough to allow van der Waals attractive forces to be dominant. In biological systems, adhesion of a charged particle on surfaces is also strongly related to ionic strength in the aqueous media.[68-69] According to DLVO theory, the repulsive electrostatic energy between the electric bilayers of bacterial cells and the surfaces decrease as the ionic strength of media increases due to enhanced shielding of the surface charges by the ions in the electrical bilayers. Moreover, the thermodynamic approach based on the surface free energy theory helps to explain and extend DLVO theory such that hydrophobic/hydrophilic and osmotic interactions are also considered besides Lifshitz-van der Waals and electrostastic bilayer interactions.[70] Lifshitz-van der Waals and electrostatic interactions are usually non-specific adhesion forces defined as a consequence of macroscopic, physicochemical surface properties over large separation distances between cells and surfaces, whereas hydrophobic force and directional interactions (e.g. H-bonding) are dominant at a small distance. The latter forces are more specific to particular cell surface interactions and are the predominant cause of strong and irreversible cell attachment.[71]

On the other hand, from a biomedical point of view, although the general strategies of bacterial attachment to surfaces may vary in different species, bacteria with particular structures/components capable of binding host cell receptors represent a large group of specific interactions that might be disrupted to prevent infection. For instance, numerous bacterial species have

evolved machinery to attach to and eventually internalize into host cells, for example by expressing fimbriae that can bind carbohydrates present on the host cells.[72] Also, it has been noted that many bacteria evolve and exploit more than one mechanism for invasion, allowing them to adhere to and subsequently enter into host cells to invoke infections. One example is that of Group A *Streptococcus pyogenes* (GAS), which utilizes the surface protein streptococcal fibronectin-binding protein I (SfbI) and its allelic variant F1 as the specific components to bind the fibronectin of the host's extracellular matrix, but which also can exploit other cell entry routes.[73] A recent review has provided an important overview of bacterial adhesion mechanisms covering physicochemical and cellular structural and chemical aspects, and also some novel technologies developed to address these adhesion mechanisms.[67]

Synthetic polymers that interfere with bacteria-host interactions are therefore a potentially useful approach for controlling infectious diseases, because their affinities with cell surface receptors can be tailored through multivalent ligand display. In fact, the specific recognition of bacterial surface adhesion protein to tissue (host)-secreted carbohydrates is inherently multivalent binding in nature,[74] and thus is an obvious candidate for 'polymer interference'. Carbohydrate-protein interactions are based on weak individual links when a single carbohydrate binds to a protein site, however, the progressive build-up of multivalent interactions for oligosaccharides involved in recognition processes enables much stronger binding to occur. For example, the exploited multivalent carbohydrates occupied the binding sites on the tissue surfaces prior to the adhesion protein on bacterium, and thus prevented bacterial from host invasion (*Figure 1-12*). Therefore, multivalency is an important design

factor for bacterial adhesion inhibitors. Since monovalent adhesion inhibitors always present limited affinities for target lectins, multivalent materials are good potential alternatives for therapeutic strategies against bacterial infection. A number of examples have been reported where multivalent ligands have been used advantageously compared to monovalent inhibitor.[74b, 75] The polymers those could easily be modified with various functionalities are believed to have high flexibility combined with mutivalency effect by using polymer chemistry.

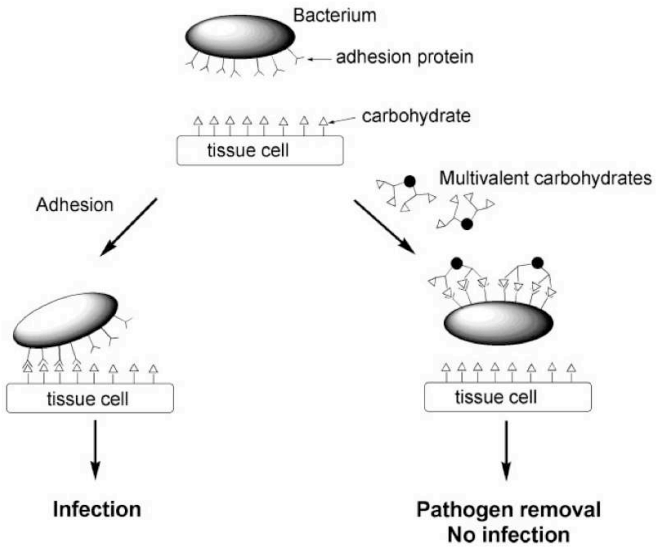

Figure 1-12. Scheme of bacterial adhesion followed by infection (left) and inhibition by multivalent carbohydrates to prevent infection (right), taken from Ref.[76]

However, many bacterial species employ additional strategies for environmental adaptation and host invasion, thus confounding therapies that depend on prevention of bacterial cell surface attachment or cell sequestration. Amongst these mechanisms are communication-systems such as quorum sensing (QS) described earlier.[1b, 1c, 77] Inhibition of QS is itself a potential

further method of controlling bacterial infection,[78] but targeting QS signals in isolation can still allow bacterial infection by alternative pathways. For instance, loss of QS can induce bacteria to switch on 'swarming'/aggregation responses to compensate, inducing in turn further infection mechanisms that can 'outmanoeuvre' conventional anti-adhesion therapeutics. Materials that could interfere with both communication mechanisms and cell adhesion/aggregation at the same time would allow greater flexibility in anti-infective strategies. The first phase of the project therefore involved the design and synthesis of polymers aimed to combine potent activity in binding QS autoinducers with effective adhesion at bacterial surfaces (*Figure 1-13*).

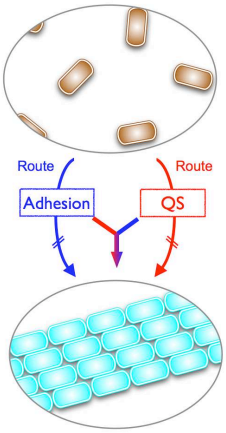

Figure 1-13. Scheme of investigated polymers interfering with both communication mechanism (QS Route, red) and cell adhesion/aggregation (Adhesion Route, blue) at the same time in anti-infective strategies

1.3.2 Polymersomes as artificial cells to cross talk with bacterial cells (2nd Phase)

Irrespective of organism complexity, the cell is the basic unit for all forms of life so far. The idea of establishing synthetic (and artificial) biology with polymers that might give structures and functions complementary to those in

nature, is of interest for both practical reasons (e.g. intelligent antibacterial agents), and for addressing more fundamental and philosophical questions (e.g. 'what is life?'). While the concept of a 'smart' polymersome for controlled release of antibacterials is a simple extension of current ideas, albeit difficult to realize in practice, the consideration of a polymersome as a proto-cell is more challenging. To describe of the concept of 'artificial cellularity', a discussion paper extending the famous 'Turing Test'[79] of intelligent machines towards biomimetic applications was suggested in 2006.[80] In the original Turing test, an 'imitation game' was introduced to identify if a machine can think or not (*Figure 1-14*, a). This test was performed between an intelligent interrogator (a human being) and two isolated subjects (a computer and another person). The interrogator was also separated from the intelligent subject (another human) and the computer/machine was allowed to ask questions in order to distinguish the two subjects between whether they were human or machine. If the computer gave an answer that was indistinguishable to the interrogator from an answer given by a human, Turing postulated that the machine could be considered as 'intelligent' - at least from a practical viewpoint. This system subtly avoids the problems suffered when researchers were trying to define the principles for an intelligent machine, but simplifies all the rules in terms of comparing a computer with a standard model that is a real intelligent subject – i.e. a human being. The UK 'Chell' consortium (Cronin *et al.*[80]) considered the same fundamental problems in the area of artificial cell definition, and suggested a strategy related to the original Turing test to determine if a synthetic/chemical cell could be considered 'intelligent' or not. (*Figure 1-14*, b)

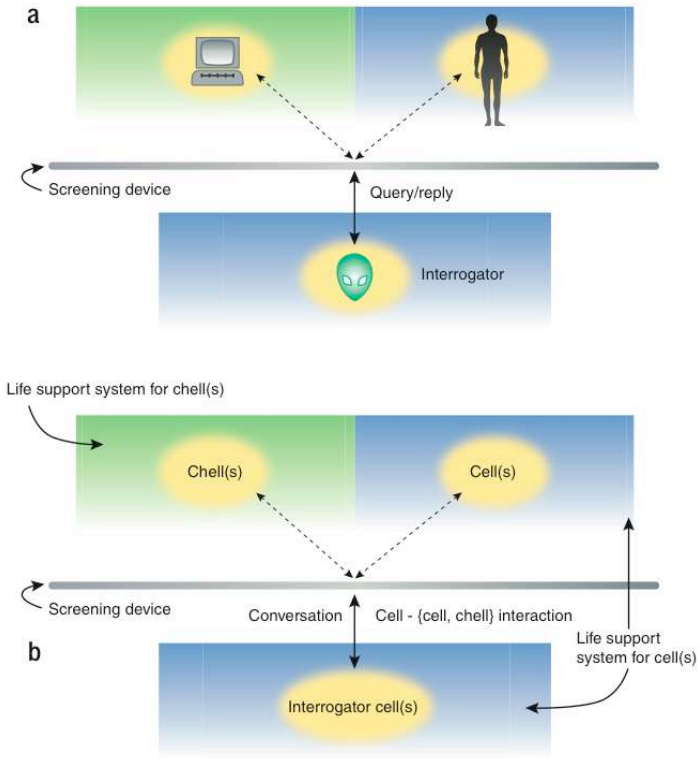

Figure 1-14. Scheme of the original Turing test for artificial intelligence (AI) (a); and the developed biological version of Turing test for artificial cellularity (chemical cell – chell) (b), taken from Ref.[80]

In this case, the roles of interrogator and intelligent human subject are replaced with two individual living cells, while artificial cells are tested instead of the computer machine to see if they could be judged as real alive cells so as to 'fool' the interrogator. Specifically, the language suggested to be the tool of communication between the two participants is designed around cell signal molecules, in this case the autoinducers already mentioned above relating to bacterial chemical communication – i.e. the QS network. One could envisage that if the synthetic objects are able to detect and sense the signal molecules produced by the real cells and also 'reply', for example by releasing certain mediators to regulate the behaviors of the living quorum, the communication

cycles between the real cell and the synthetic biomimicry might therefore be established. In such a way, the artificial cells so produced could probe the biological version of the Turing test, and thus circumvents the current lack of practical definitions in the area of artificial cellularity.

Although such a biological version of the Turing test leads to a practical definition of artificial cellularity, there is still a need to consider the properties of natural cells that confer 'life' to a living system. In this context, some of the key characteristics of alive cells have been considered in detail recently.[81] As a general rule, all living systems have 1) cells which possess a membrane, which separates the interior of the cell from the environment, and which controls the passage of nutrient molecules into the cell and the passage of waste out of the cells; 2) all cells store their heredity information in the form of double-stranded DNA; 3) all cells use similar molecular mechanisms for transcribing and translating the genetic information encoded in the DNA; 4) all cells use catalytically active proteins (enzymes) to catalyze chemical reactions inside the cell, the sum total of these reactions being the cell's metabolism; 5) all cells are 'biochemical factories' that transform nutrient molecules via metabolic pathways into components of the cell leading to cell growth, to a copying of the heredity information and finally to cell division; 6) all cells are self-regulating systems that are able to respond to certain stimuli; 7) the shape of cells depends on their function and can vary considerably, as does the size of cells, which is often 1-5 μm in the case of bacteria, and 10-30 μm (and more) in the case of eukaryotic cells; and 8) all known cells use the 'same type of chemistry' and many processes inside the cell use the same type of molecules (e.g. water, ATP, citric acid, DNA, proteins etc.), among which the

macromolecules are composed of the same set of building blocks.' It is not surprising therefore that it is still a challenge to build any type of artificial cell that can possess analogies of all the above features found in real cells.

In this case, the concepts of minimal cells and protocells have to be mentioned. A minimal cell is commonly recognized as a cell with very small genome sizes, which internalizes nutrients from other (host) cells, i.e. minimal cells do not produce its own nutrients. Thus, to establish a minimal cell system, researchers often adapt the 'top-down strategy' by removing most of the genes from an existing organism but retaining those which maintains some key properties such as self-maintenance, self-reproduction and possibility to evolve.[81] By contrast, a protocell is a simplified model only possessing some of the properties of a living cell but not necessarily all of them. Protocells may be more accessible for researchers as the first step towards synthetic artificial cells, adopting what is commonly defined as the 'bottom-up synthesis strategy'.[82] Polymersomes that can self-assemble from amphiphilic block copolymers are especially useful in the formation of protocells. Furthermore, as discussed above, polymersomes can be encoded with stimuli-responsive properties such as alterable permeability, enabling them to act potentially as cell-like containers for constructing artificial cells.[83] Examples of simple protocells have already been reported, including an intriguing multivesicular structure,[84] designed and synthesized by a double emulsion dispersion method. Such polymeric bilayer structures enable transfer of molecular 'information' from the exterior to interior in a pH-controllable manner (*Figure 1-15*).

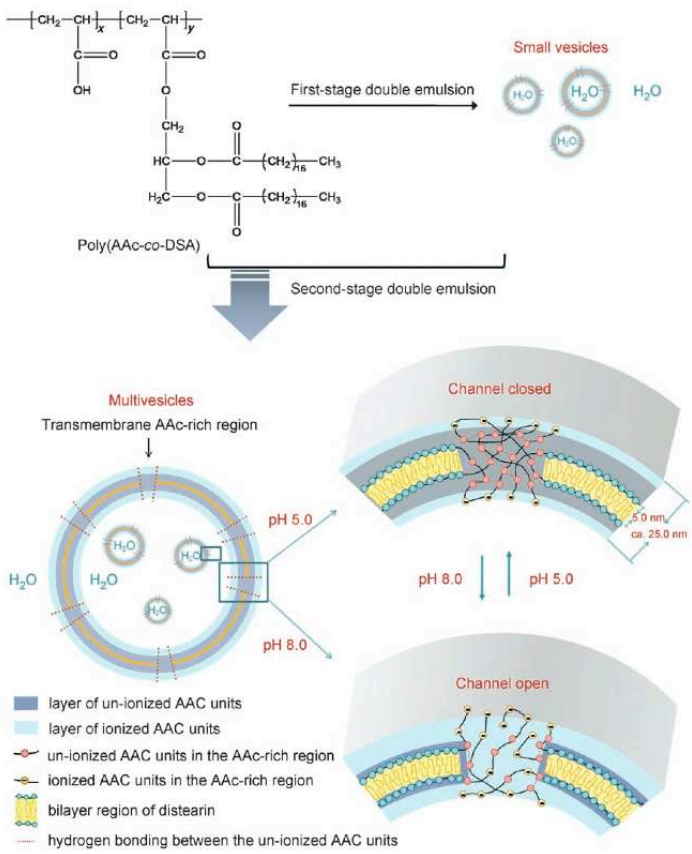

Figure 1-15. Structure of multivesicles composed of poly (acrylic acid-co-distearin acrylate) [p(AAc-co-DSA)], top; and schemes of on and off -gate controlled by tuning pH, bottom. Taken from Ref.[84]

Specifically, the channels linking the inter space and the outer environment switched off below pH 5.0 while opened above pH 8.0 via reversible transesterification of poly (acrylic acid-co-distearin acrylate) [p(AAc-co-DSA)]. Actually, such pH-dependent transmembrane channels formation mainly occurred in the AAc-rich region because the ionization of AAc in this region is easier to deprotonate than those copolymerized with DSA (*Figure 1-13*). This paper gives a good example of progress in synthetic biology applications particularly as an initial step towards the construction of artificial cell models.

For this thesis, it is the aim to establish a basic platform for understanding the principles of polymer-cell and polymer-signal molecule/boron interactions (1st stage, **Chapter 2** and **3**) in cell-cell communication processes, and then to develop a more meaningful test between real cells and artificial protocells. As reviewed above, polymersomes possessing continuous bilayer structures were able to be modified via tuning their hydrophobic and hydrophilic block compositions. They can also be decorated with functional groups to respond to cell signals, giving them potential to be exploited as the container components of artificial cells. In this case, polymersomes can be designed from hydrophilic blocks based on linear polymers investigated in Phase 1 of the PhD study combined with selected hydrophobic blocks, such that cell-like structures could form, which could also act as containers for QS interfering signals. In principle, the interaction of the polymersomes with real bacterial cells could form part of the QS network - detecting and responding/binding to bacterial signal molecules. However, considering the overall complexity of this study, to simplify the experiments it was first necessary to encapsulate only selected QS mediators, instead of reaction cascades that produce QS signals, and then to tune the cargo release rate via different kinds of hydrophobic monomers. However, if the full sets of chemistries in the PhD are achieved, and if the polymersomes can 'cross-talk' with real cells, the construction of artificial protocells and the implementation of the biological Turing test principle (*Figure 1-16*) will be achieved.

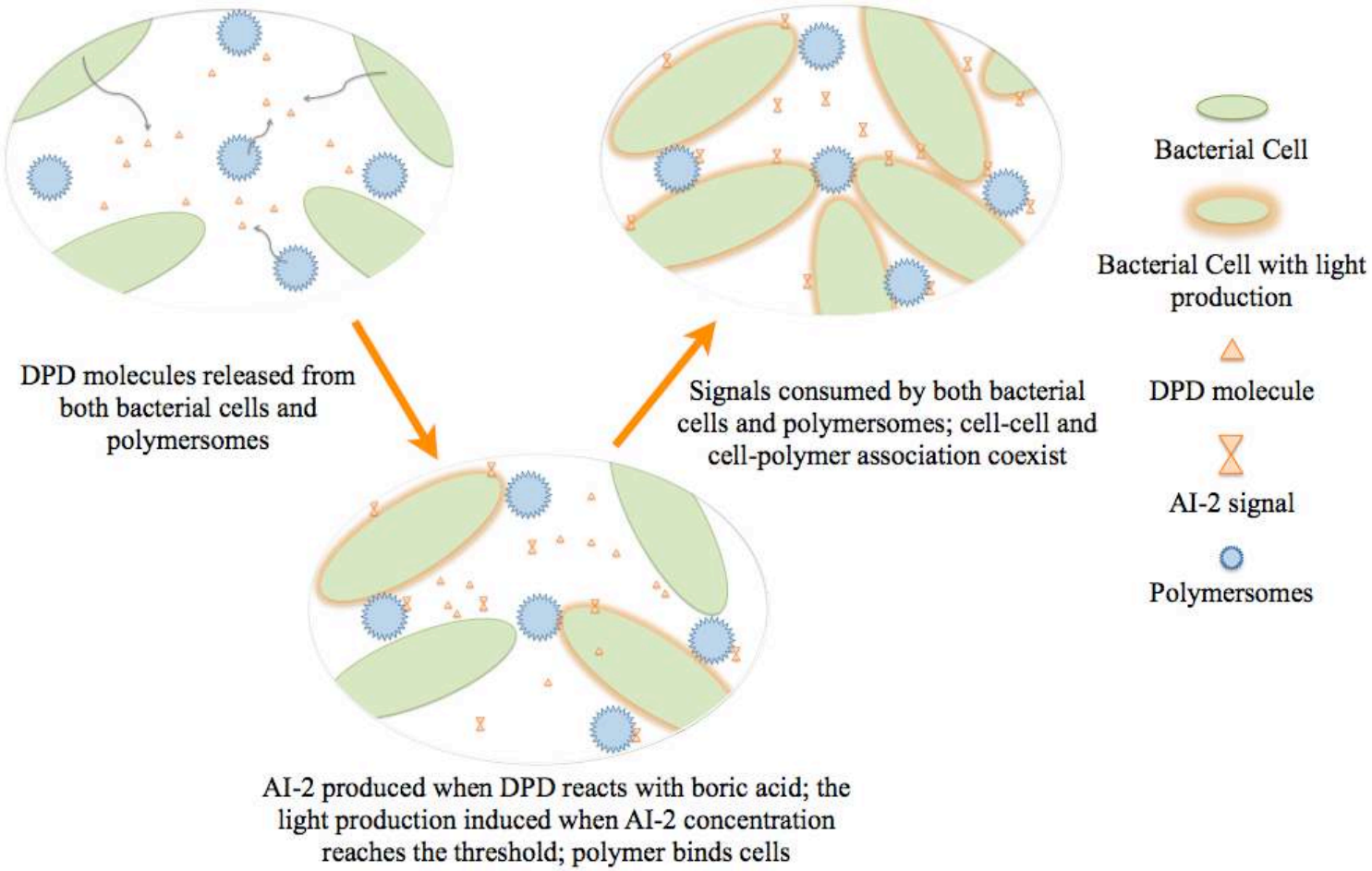

Figure 1-16. Scheme of cell-polymersome interactions for implementation of the cell-Chell Turing test

References

[1] aB. L. Bassler, *Cell* **2002**, *109*, 421-424; bC. M. Waters, B. L. Bassler, *Annu Rev Cell Dev Biol* **2005**, *21*, 319-346; cP. Williams, K. Winzer, W. C. Chan, M. Camara, *Philos Trans R Soc Lond B Biol Sci* **2007**, *362*, 1119-1134.

[2] aK. R. Hardie, K. Heurlier, *Nat Rev Microbiol* **2008**, *6*, 635-643; bN. N. Rao, M. R. Gomez-Garcia, A. Kornberg, *Annu Rev Biochem* **2009**, *78*, 605-647; cY. Irie, M. R. Parsek, *Curr Top Microbiol Immunol* **2008**, *322*, 67-84; dJ. S. Dickschat, *Nat Prod Rep* **2010**, *27*, 343-369.

[3] S. Derzelle, E. Duchaud, F. Kunst, A. Danchin, P. Bertin, *Appl Environ Microbiol* **2002**, *68*, 3780-3789.

[4] aM. B. Miller, K. Skorupski, D. H. Lenz, R. K. Taylor, B. L. Bassler, *Cell* **2002**, *110*, 303-314; bY. W. He, L. H. Zhang, *FEMS Microbiol Rev* **2008**, *32*, 842-857.

[5] aM. B. Miller, B. L. Bassler, *Annu Rev Microbiol* **2001**, *55*, 165-199; bB. L. Bassler, M. Wright, R. E. Showalter, M. R. Silverman, *Mol Microbiol* **1993**, *9*, 773-786; cB. L. Bassler, M. Wright, M. R. Silverman, *Mol Microbiol* **1994**, *13*, 273-286; dR. Czajkowski, S. Jafra, *Acta Biochim Pol* **2009**, *56*, 1-16; eP. K. Kambam, D. J. Sayut, Y. Niu, D. T. Eriksen, L. Sun, *Biotechnol Bioeng* **2008**, *101*, 263-272.

[6] I. B. Bischofs, J. A. Hug, A. W. Liu, D. M. Wolf, A. P. Arkin, *Proc Natl Acad Sci U S A* **2009**, *106*, 6459-6464.

[7] V. A. Lipasova, E. E. Atamova, I. A. Khmel, *Mol Gen Mikrobiol Virusol* **2009**, 8-11.

[8] A. L. Spoering, M. S. Gilmore, *Curr Opin Microbiol* **2006**, *9*, 133-137.

[9] X. Chen, S. Schauder, N. Potier, A. Van Dorsselaer, I. Pelczer, B. L. Bassler, F. M. Hughson, *Nature* **2002**, *415*, 545-549.

[10] J. M. Henke, B. L. Bassler, *J Bacteriol* **2004**, *186*, 6902-6914.

[11] K. B. Xavier, B. L. Bassler, *Current Opinion in Microbiology* **2003**, *6*, 191-197.

[12] S. Schauder, K. Shokat, M. G. Surette, B. L. Bassler, *Mol Microbiol* **2001**, *41*, 463-476.

[13] M. M. Meijler, L. G. Hom, G. F. Kaufmann, K. M. McKenzie, C. Sun, J. A. Moss, M. Matsushita, K. D. Janda, *Angew Chem Int Ed Engl* **2004**, *43*, 2106-2108.

[14] S. T. Miller, K. B. Xavier, S. R. Campagna, M. E. Taga, M. F. Semmelhack, B. L. Bassler, F. M. Hughson, *Mol Cell* **2004**, *15*, 677-687.

[15] B. M. Ahmer, *Mol Microbiol* **2004**, *52*, 933-945.

[16] M. P. DeLisa, C. F. Wu, L. Wang, J. J. Valdes, W. E. Bentley, *J Bacteriol* **2001**, *183*, 5239-5247.

[17] K. B. Xavier, B. L. Bassler, *J Bacteriol* **2005**, *187*, 238-248.

[18] A. F. Gonzalez Barrios, R. Zuo, Y. Hashimoto, L. Yang, W. E. Bentley, T. K. Wood, *J Bacteriol* **2006**, *188*, 305-316.

[19] L. Li, Z. Xu, Y. Zhou, T. Li, L. Sun, H. Chen, R. Zhou, *Microb Pathog* **2011**, *50*, 293-302.

[20] aS. P. Diggle, A. Gardner, S. A. West, A. S. Griffin, *Philosophical Transactions of the Royal Society B-Biological Sciences* **2007**, *362*,

1241-1249; bL. Keller, M. G. Surette, *Nature Reviews Microbiology* **2006**, *4*, 249-258.
[21] M. Manefield, S. L. Turner, *Microbiology* **2002**, *148*, 3762-3764.
[22] aM. I. More, L. D. Finger, J. L. Stryker, C. Fuqua, A. Eberhard, S. C. Winans, *Science* **1996**, *272*, 1655-1658; bM. R. Parsek, D. L. Val, B. L. Hanzelka, J. E. Cronan, Jr., E. P. Greenberg, *Proc Natl Acad Sci U S A* **1999**, *96*, 4360-4365.
[23] aT. A. Gould, H. P. Schweizer, M. E. Churchill, *Mol Microbiol* **2004**, *53*, 1135-1146; bA. Vannini, C. Volpari, C. Gargioli, E. Muraglia, R. Cortese, R. De Francesco, P. Neddermann, S. D. Marco, *EMBO J* **2002**, *21*, 4393-4401.
[24] A. W. Decho, R. L. Frey, J. L. Ferry, *Chem Rev* **2011**, *111*, 86-99.
[25] aV. Singh, G. B. Evans, D. H. Lenz, J. M. Mason, K. Clinch, S. Mee, G. F. Painter, P. C. Tyler, R. H. Furneaux, J. E. Lee, P. L. Howell, V. L. Schramm, *J Biol Chem* **2005**, *280*, 18265-18273; bM. B. Clarke, D. T. Hughes, C. Zhu, E. C. Boedeker, V. Sperandio, *Proc Natl Acad Sci U S A* **2006**, *103*, 10420-10425; cV. Singh, W. Shi, S. C. Almo, G. B. Evans, R. H. Furneaux, P. C. Tyler, G. F. Painter, D. H. Lenz, S. Mee, R. Zheng, V. L. Schramm, *Biochemistry* **2006**, *45*, 12929-12941.
[26] aR. Aharoni, M. Bronstheyn, A. Jabbour, B. Zaks, M. Srebnik, D. Steinberg, *Bioorg Med Chem* **2008**, *16*, 1596-1604; bM. Frezza, L. Soulere, D. Balestrino, M. Gohar, C. Deshayes, Y. Queneau, C. Forestier, A. Doutheau, *Bioorg Med Chem Lett* **2007**, *17*, 1428-1431; cD. Ren, J. J. Sims, T. K. Wood, *Environ Microbiol* **2001**, *3*, 731-736; dK. W. Widmer, K. A. Soni, M. E. Hume, R. C. Beier, P. Jesudhasan, S. D. Pillai, *J Food Sci* **2007**, *72*, M363-368; eJ. Lee, T. Bansal, A. Jayaraman, W. E. Bentley, T. K. Wood, *Appl Environ Microbiol* **2007**, *73*, 4100-4109; fD. Ren, R. Zuo, A. F. Gonzalez Barrios, L. A. Bedzyk, G. R. Eldridge, M. E. Pasmore, T. K. Wood, *Appl Environ Microbiol* **2005**, *71*, 4022-4034; gC. Niu, S. Afre, E. S. Gilbert, *Lett Appl Microbiol* **2006**, *43*, 489-494; hD. Ren, L. A. Bedzyk, R. W. Ye, S. M. Thomas, T. K. Wood, *Biotechnol Bioeng* **2004**, *88*, 630-642.
[27] N. Amara, B. P. Krom, G. F. Kaufmann, M. M. Meijler, *Chem Rev* **2011**, *111*, 195-208.
[28] E. V. Piletska, G. Stavroulakis, K. Karim, M. J. Whitcombe, I. Chianella, A. Sharma, K. E. Eboigbodin, G. K. Robinson, S. A. Piletsky, *Biomacromolecules* **2010**, *11*, 975-980.
[29] E. V. Piletska, G. Stavroulakis, L. D. Larcombe, M. J. Whitcombe, A. Sharma, S. Primrose, G. K. Robinson, S. A. Piletsky, *Biomacromolecules* **2011**, *12*, 1067-1071.
[30] A. L. Garner, J. Park, J. S. Zakhari, C. A. Lowery, A. K. Struss, D. Sawada, G. F. Kaufmann, K. D. Janda, *Journal of the American Chemical Society* **2011**, *133*, 15934-15937.
[31] D. E. Discher, A. Eisenberg, *Science* **2002**, *297*, 967-973.
[32] **H. L. Hsieh**, **R. P. Quirk**, *Marcel Dekker, New York* **1996**.
[33] aH. Bermudez, A. K. Brannan, D. A. Hammer, F. S. Bates, D. E. Discher, *Macromolecules* **2002**, *35*, 8203-8208; bG. Battaglia, A. J. Ryan, S. Tomas, *Langmuir* **2006**, *22*, 4910-4913.
[34] aH. Lomas, I. Canton, S. MacNeil, J. Du, S. P. Armes, A. J. Ryan, A. L. Lewis, G. Battaglia, *Advanced Materials* **2007**, *19*, 4238-4243; bT. O.

Pangburn, M. A. Petersen, B. Waybrant, M. M. Adil, E. Kokkoli, *Journal of biomechanical engineering* **2009**, *131*, 074005; cD. A. Christian, S. Cai, D. M. Bowen, Y. Kim, J. D. Pajerowski, D. E. Discher, *European Journal of Pharmaceutics and Biopharmaceutics* **2009**, *71*, 463-474; dG. Liu, S. Ma, S. Li, R. Cheng, F. Meng, H. Liu, Z. Zhong, *Biomaterials* **2010**, *31*, 7575-7585; eW. Chen, F. Meng, R. Cheng, Z. Zhong, *Journal of Controlled Release* **2010**, *142*, 40-46.

[35] M. C. Jones, J. C. Leroux, *European Journal of Pharmaceutics and Biopharmaceutics* **1999**, *48*, 101-111.

[36] K. S. Soppimath, T. M. Aminabhavi, A. R. Kulkarni, W. E. Rudzinski, *Journal of Controlled Release* **2001**, *70*, 1-20.

[37] A. Blanazs, S. P. Armes, A. J. Ryan, *Macromolecular Rapid Communications* **2009**, *30*, 267-277.

[38] J. S. Lee, J. Feijen, *Journal of Controlled Release* **2012**, *161*, 473-483.

[39] C. LoPresti, H. Lomas, M. Massignani, T. Smart, G. Battaglia, *Journal of Materials Chemistry* **2009**, *19*, 3576-3590.

[40] L. B. Luo, A. Eisenberg, *Journal of the American Chemical Society* **2001**, *123*, 1012-1013.

[41] aH. W. Shen, A. Eisenberg, *Macromolecules* **2000**, *33*, 2561-2572; bG. E. Yu, A. Eisenberg, *Macromolecules* **1998**, *31*, 5546-5549.

[42] D. Schmaljohann, *Advanced Drug Delivery Reviews* **2006**, *58*, 1655-1670.

[43] M. Grabe, G. Oster, *Journal of General Physiology* **2001**, *117*, 329-343.

[44] J. Z. Du, S. P. Armes, *Journal of the American Chemical Society* **2005**, *127*, 12800-12801.

[45] C. Giacomelli, V. Schmidt, R. Borsali, *Macromolecules* **2007**, *40*, 2148-2157.

[46] R. Jain, S. M. Standley, J. M. J. Frechet, *Macromolecules* **2007**, *40*, 452-457.

[47] S. Lin, F. Du, Y. Wang, S. Ji, D. Liang, L. Yu, Z. Li, *Biomacromolecules* **2008**, *9*, 109-115.

[48] W. Agut, A. Brulet, C. Schatz, D. Taton, S. Lecommandoux, *Langmuir* **2010**, *26*, 10546-10554.

[49] Y. Morishima, *Angewandte Chemie-International Edition* **2007**, *46*, 1370-1372.

[50] S. Qin, Y. Geng, D. E. Discher, S. Yang, *Advanced Materials* **2006**, *18*, 2905-2909.

[51] A. C. Couffin-Hoarau, J. C. Leroux, *Biomacromolecules* **2004**, *5*, 2082-2087.

[52] Y. Kim, M. Tewari, D. J. Pajeroski, S. Sen, W. Jason, S. Sirsi, G. Lutz, D. E. Discher, *Conference proceedings : ... Annual International Conference of the IEEE Engineering in Medicine and Biology Society. IEEE Engineering in Medicine and Biology Society. Conference* **2006**, *1*, 4350-4353.

[53] aA. S. Mathews, C. S. Ha, W. J. Cho, I. Kim, *Drug Delivery* **2006**, *13*, 245-251; bR. J. Mart, K. P. Liem, S. J. Webb, *Pharmaceutical Research* **2009**, *26*, 1701-1710; cA. E. Smith, X. Xu, D. A. Savin, C. L. McCormick, *Polymer Chemistry* **2010**, *1*, 628-630; dY. Cai, K. B. Aubrecht, R. B. Grubbs, *Journal of the American Chemical*

*Society***2011**, *133*, 1058-1065; eH. Xu, F. Meng, Z. Zhong, *Journal of Materials Chemistry* **2009**, *19*, 4183-4190.

[54] aA. Klaikherd, S. Ghosh, S. Thayumanavan, *Macromolecules* **2007**, *40*, 8518-8520; bS. Cerritelli, D. Velluto, J. A. Hubbell, *Biomacromolecules* **2007**, *8*, 1966-1972; cC. Lin, Z. Zhong, M. C. Lok, X. Jiang, W. E. Hennink, J. Feijen, J. F. J. Engbersen, *Bioconjugate Chemistry* **2007**, *18*, 138-145.

[55] aG. Wang, X. Tong, Y. Zhao, *Macromolecules* **2004**, *37*, 8911-8917; bX. K. Liu, M. Jiang, *Angewandte Chemie-International Edition* **2006**, *45*, 3846-3850; cE. Cabane, V. Malinova, W. Meier, *Macromolecular Chemistry and Physics* **2010**, *211*, 1847-1856; dE. Cabane, V. Malinova, S. Menon, C. G. Palivan, W. Meier, *Soft Matter* **2011**, *7*, 9167-9176.

[56] aP. J. Photos, L. Bacakova, B. Discher, F. S. Bates, D. E. Discher, *Journal of Controlled Release* **2003**, *90*, 323-334; bB. M. Discher, Y. Y. Won, D. S. Ege, J. C. M. Lee, F. S. Bates, D. E. Discher, D. A. Hammer, *Science* **1999**, *284*, 1143-1146; cJ. S. Lee, M. Ankone, E. Pieters, R. M. Schiffelers, W. E. Hennink, J. Feijen, *Journal of controlled release : official journal of the Controlled Release Society* **2011**, *155*, 282-288.

[57] M. Massignani, H. Lomas, G. Battaglia, in *Modern Techniques for Nano- and Microreactors/-Reactions* (Ed.: F. Caruso), **2010**, *229*, 115-154.

[58] aY. Lee, J.-B. Chang, H. K. Kim, T. G. Park, *Macromolecular Research* **2006**, *14*, 359-364; bS. Rameez, H. Alosta, A. F. Palmer, *Bioconjugate Chemistry* **2008**, *19*, 1025-1032; cH. C. Shum, J.-W. Kim, D. A. Weitz, *Journal of the American Chemical Society* **2008**, *130*, 9543-9549; dJ. S. Katz, D. H. Levine, K. P. Davis, F. S. Bates, D. A. Hammer, J. A. Burdick, *Langmuir* **2009**, *25*, 4429-4434; eG.-Y. Liu, L.-P. Lv, C.-J. Chen, X.-S. Liu, X.-F. Hu, J. Ji, *Soft Matter* **2011**, *7*, 6629-6636; fS. Li, B. Byrne, J. Welsh, A. F. Palmer, *Biotechnology Progress* **2007**, *23*, 278-285; gY. Kim, M. Tewari, J. D. Pajerowski, S. Cai, S. Sen, J. Williams, S. Sirsi, G. Lutz, D. E. Discher, *Journal of Controlled Release* **2009**, *134*, 132-140.

[59] aF. Axthelm, O. Casse, W. H. Koppenol, T. Nauser, W. Meier, C. G. Palivan, *Journal of Physical Chemistry B* **2008**, *112*, 8211-8217; bO. Onaca, D. W. Hughes, V. Balasubramanian, M. Grzelakowski, W. Meier, C. G. Palivan, *Macromolecular Bioscience* **2010**, *10*, 531-538; cV. Balasubramanian, O. Onaca, M. Ezhevskaya, S. Van Doorslaer, B. Sivasankaran, C. G. Palivan, *Soft Matter* **2011**, *7*, 5595-5603.

[60] aS. A. Joshi, S. S. Chavhan, K. K. Sawant, *European Journal of Pharmaceutics and Biopharmaceutics* **2010**, *76*, 189-199; bK. Ozturk, S. Caban, S. Kozlu, E. Kadayifci, F. Yerlikaya, Y. Capan, *Pharmazie* **2010**, *65*, 665-669; cZ. Yuan, D. Chen, S. Zhang, Z. Zheng, *Yakugaku Zasshi-Journal of the Pharmaceutical Society of Japan* **2010**, *130*, 1353-1359; dK. Hu, Y. Shi, W. Jiang, J. Han, S. Huang, X. Jiang, *International Journal of Pharmaceutics* **2011**, *415*, 273-283.

[61] F. H. Meng, G. H. M. Engbers, J. Feijen, *Journal of Controlled Release* **2005**, *101*, 187-198.

[62] G. Pasparakis, C. Alexander, *Angewandte Chemie-International Edition* **2008**, *47*, 4847-4850.
[63] C. C. Scott, R. J. Botelho, S. Grinstein, *Journal of Membrane Biology* **2003**, *193*, 137-152.
[64] aA. Descoteaux, *Memorias do Instituto Oswaldo Cruz* **1999**, *94*, 20-21; bP. Y. Zheng, N. L. Jones, *Gastroenterology* **2002**, *122*, A10-A10; cA. Amer, L. Franchi, T.-D. Kanneganti, M. Body-Malapel, N. Ozoren, G. Brady, S. Meshinchi, R. Jagirdar, A. Gewirtz, S. Akira, G. Nunez, *Journal of Biological Chemistry* **2006**, *281*, 35217-35223; dG. D. Fairn, E. Gershenzon, S. Grinstein, *Membrane Trafficking during Phagosome Formation and Maturation*, **2009**.
[65] P. Cossart, P. J. Sansonetti, *Science* **2004**, *304*, 242-248.
[66] M. Heinzelmann, M. Scott, T. Lam, *American Journal of Surgery* **2002**, *183*, 179-190.
[67] K. Hori, S. Matsumoto, *Biochem Eng J* **2010**, *48*, 424-434.
[68] K. C. Marshall, *Cc/Agr Biol Environ* **1992**, 8-8.
[69] aM. C. M. Vanloosdrecht, J. Lyklema, W. Norde, A. J. B. Zehnder, *Microbial Ecol* **1989**, *17*, 1-15; bM. C. M. Vanloosdrecht, A. J. B. Zehnder, *Experientia* **1990**, *46*, 817-822; cT. A. Camesano, N. I. Abu-Lail, *Biomacromolecules* **2003**, *4*, 1000-1012; dM. Hermansson, K. Otto, H. Elwing, *J Bacteriol* **1999**, *181*, 5210-5218; eB. E. Logan, Q. Li, *Water Res* **1999**, *33*, 1090-1100.
[70] aY. H. An, R. J. Friedman, *J Biomed Mater Res* **1998**, *43*, 338-348; bC. J. van Oss, *Cell Biophys* **1989**, *14*, 1-16; cC. J. Vanoss, *Colloid Surface A* **1993**, *78*, 1-49.
[71] C. J. van Oss, *J Mol Recognit* **2003**, *16*, 177-190.
[72] aD. W. Heinz, H. H. Niemann, W. D. Schubert, *Microbes Infect* **2004**, *6*, 101-112; bK. A. Barth, G. Coullerez, L. M. Nilsson, R. Castelli, P. H. Seeberger, V. Vogel, M. Textor, *Adv Funct Mater* **2008**, *18*, 1459-1469.
[73] M. Rohde, R. M. Graham, K. Branitzki-Heinemann, P. Borchers, C. Preuss, I. Schleicher, D. Zaehner, S. R. Talay, M. Fulde, K. Dinkla, G. S. Chhatwal, *Cellular Microbiology* **2011**, *13*, 450-468.
[74] aN. Jayaraman, *Chem Soc Rev* **2009**, *38*, 3463-3483; bR. T. Lee, Y. C. Lee, *Glycoconj J* **2000**, *17*, 543-551.
[75] aG. M. Whitesides, M. Mammen, S. K. Choi, *Angewandte Chemie-International Edition* **1998**, *37*, 2755-2794; bE. J. Toone, J. J. Lundquist, *Chemical Reviews* **2002**, *102*, 555-578; cT. K. Lindhorst, *Top Curr Chem* **2002**, *218*, 201-235; dC. F. Brewer, J. C. Sacchettini, L. G. Baum, *Biochemistry* **2001**, *40*, 3009-3015; eR. J. Pieters, *Trends Glycosci Glyc* **2004**, *16*, 243-254.
[76] R. J. Pieters, *Med Res Rev* **2007**, *27*, 796-816.
[77] aB. L. Bassler, A. Camilli, *Science* **2006**, *311*, 1113-1116; bJ. E. Gonzalez, N. D. Keshavan, *Microbiol Mol Biol R* **2006**, *70*, 859-875.
[78] T. Keshavarz, S. Raina, D. De Vizio, M. Odell, M. Clements, S. Vanhulle, *Biotechnol Appl Bioc* **2009**, *54*, 65-84.
[79] A. M. Turing, *Mind* **1950**, *59*, 433-460.
[80] L. Cronin, N. Krasnogor, B. G. Davis, C. Alexander, N. Robertson, J. H. G. Steinke, S. L. M. Schroeder, A. N. Khlobystov, G. Cooper, P. M. Gardner, P. Siepmann, B. J. Whitaker, D. Marsh, *Nature Biotechnology* **2006**, *24*, 1203-1206.

[81] P. Walde, *Bioessays* **2010**, *32*, 296-303.
[82] A. Moya, R. Gil, A. Latorre, J. Pereto, M. Pilar Garcillan-Barcia, F. de la Cruz, *Fems Microbiology Reviews* **2009**, *33*, 225-235.
[83] aA. Kishimura, S. Liamsuwan, H. Matsuda, W.-F. Dong, K. Osada, Y. Yamasaki, K. Kataoka, *Soft Matter* **2009**, *5*, 529-532; bC. Sanson, C. Schatz, J.-F. Le Meins, A. Soum, S. Lecommandoux, *Abstracts of Papers of the American Chemical Society* **2009**, *238*; cY. Fang, Z.-Y. Lai, P.-P. Pang, M. Jiang, *Acta Physico-Chimica Sinica* **2011**, *27*, 1712-1718; dS. S. Naik, J. G. Ray, D. A. Savin, *Langmuir* **2011**, *27*, 7231-7240; eY.-L. Tu, C.-C. Wang, C.-Y. Chen, *Journal of Polymer Science Part a-Polymer Chemistry* **2011**, *49*, 2866-2877; fQ. Cui, F. Wu, E. Wang, *Polymer* **2011**, *52*, 1755-1765; gC. Zheng, X. Yao, L. Qiu, *Macromolecular Bioscience* **2011**, *11*, 338-343; hJ.-C. Eloi, D. A. Rider, G. Cambridge, G. R. Whittell, M. A. Winnik, I. Manners, *Journal of the American Chemical Society* **2011**, *133*, 8903-8913; iH. Kim, S.-M. Jeong, J.-W. Park, *Journal of the American Chemical Society* **2011**, *133*, 5206-5209; jK. Wang, D.-S. Guo, X. Wang, Y. Liu, *Acs Nano* **2011**, *5*, 2880-2894.
[84] H.-C. Chiu, Y.-W. Lin, Y.-F. Huang, C.-K. Chuang, C.-S. Chern, *Angewandte Chemie-International Edition* **2008**, *47*, 1875-1878.

Chapter 2. Preparation and Characterization of Monomers: Binding Affinities for Boron

2. Introduction

As outlined in the 'Introduction Chapter', bacterial communication systems, prevalently termed quorum sensing (QS), regulate their community-scale behaviour to aid survival and develop their populations. Intervention in such systems has therefore been an attractive approach to treat bacterial infection.[1] In reality, the chemical 'language' autoinducer (AI) signal molecules for bacterial cell-to-cell 'talk' are generally species specific, and only autoinducer-2 (AI-2) can be considered to be a global signal for interspecies communication in both Gram-negative and Gram-positive bacteria.[2] Although bacteria coordinate their population-scale behaviours with multiple signals rather than a single type of AIs,[3] targeting AI-2 signal molecules can still be a 'universal' potential approach towards QS inhibition and also bacterial infection therapeutics. However, different bacteria generate distinct DPD derivatives that are generically termed as AI-2.[2d, 4] The active form of AI-2 (**1**) in *V. harveyi* species is a furanosyl borate formed as the product of reaction between DPD and borate in marine environment (*Figure 2-1*). In order to target AI-2 (**1**), the screening of small monomer candidates capable of binding boron and reducing AI-2 (**1**) concentration in solution was considered as the preliminary objective of the PhD.

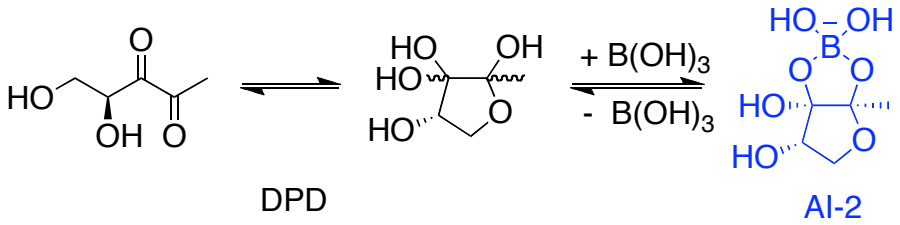

(**1**)

Figure 2-1. Structures of DPD derivatives and QS signal molecule AI-2 (**1**) in *V. harveyi*

Boric/boronic acids bind strongly with diol-containing compounds via reversible boronate ester formation (*Figure 2-2*).[5] Phenylboronic acid (PBA) converts from a trigonal boronic acid form to the tetrahedral boronate ion as the pH increases from below to above neutral pH (*Figure 2-2*). Although it was initially believed that a tetrahedral borate/boronate ion was the key reactant in alkaline solution of boric/boronic acid owing to its greater concentration compared to the trigonal state,[6] trigonal boric[7]/boronic[8] acid was eventually demonstrated to be the reactive form towards a diol-functional group even in alkaline solution. These results agreed with previous studies showing that the optimal pH value for diol-boron binding was not always above the pKa of the boric/boronic acid but around neutral value.[9] Numerous efforts have been made on synthesis of boric/boronic acid receptors for sensing diol-containing targets (e.g. saccharides).[9-10] Similarly, carbohydrate-binding agents, such as phenylboronic acids,[11] have been identified as potential lead structures for antiviral therapeutics targeting highly glycosylated enveloped viruses such as HIV type-1.[12] Interestingly, 3-aminophenylboronic acid was recently demonstrated as an rapid affinity sensor to detect total bacteria due to binding bacterial common cell wall component polysaccharide.[13] Boronic acid as tools

for sensing and separation have been reviewed this year by Nishiyabu R. *et al.*[14]

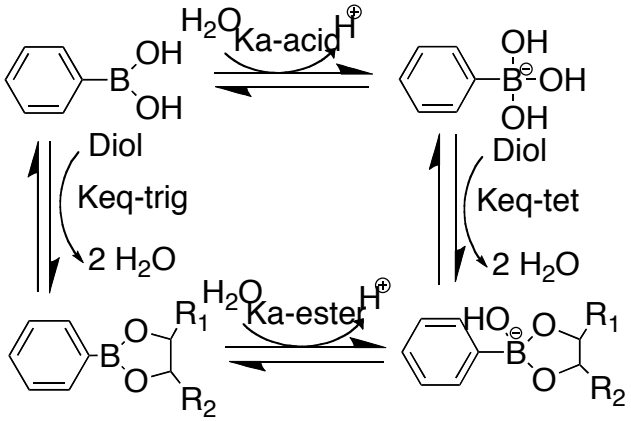

Figure 2-2. Scheme of mechanism of binding between phenylboronic acid and diols, taken from Ref.[9]

Understanding the factors that affect the stability of borate/boronate ester is essential for optimizing conditions that foster tight binding of boron-diol complexes. The Alizarin Red S (AR-S) assay can be used as a tool for measuring association constants of boron-diol complexes.[15] The AR-S system is a three-component assay allowing determination of the binding affinities of boric/boronic acid even without intrinsically fluorescent structures.[9] This assay is based on the affinity of two competing guests to one host.[16] The analyte competitively binds the host or receptor from the indicator, causing change in readout of its spectroscopic properties. Specifically, no fluorescence can be observed when AR-S exist in a free-state, due to the transfer of the excited state proton from the phenol hydroxyl group of AR-S to the ketone oxygen.[17] However, when AR-S forms complex with boron such fluorescence quenching was avoided. To briefly explain this assay, AR-S is used as the indicator that becomes fluorescent upon binding to boric/boronic acid

(host/receptor). However, diol-containing compounds (analyte) are also able to reversibly binding boron via boronate ester formation. In the presence of diol-containing compounds, two competing binding equilibria are established in the media between receptor (boric/boronic acid) and indicator (AR-S), as well as receptor and analyte (diol) (*Figure 2-3*). The fluorescent intensity of boric/boronic acid-AR-S complex will be decreased due to the transfer of AR-S complex to AR-S free molecule when the concentration of diol increases in the solution. By keeping the concentration of AR-S, boric/boronic acid and all the other contents the same but with different concentrations of diols, the relation between the diol concentration and fluorescent intensity can be established. Thus, the formation of a boronate ester between boric/boronic acid and diols controls the fluorescence of the whole system, which enables the determination of binding constants.[9, 18] Recent work has described a new class of water-soluble fluorescent boronic acids that change their fluorescence properties significantly upon binding of diol-containing compounds at physiological pH. This has simplified the fluorescence reporting system and can be an alternative for the conventional AR-S assay.[19]

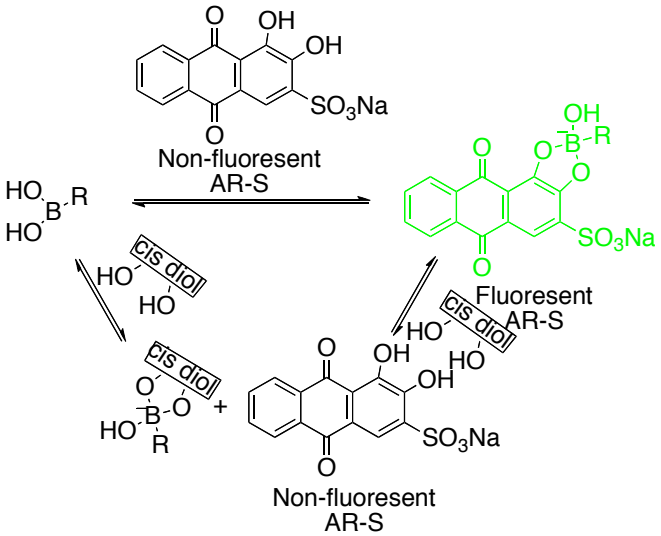

Figure 2-3. Scheme of mechanism of AR-S assay

In this chapter, representative diols will be investigated as potential AI-2 scavengers via reversible boronate ester formation, with special attention to carbohydrate derivatives. The binding constants of boron (sodium borate and PBA) with a series of diols will be established via AR-S assay. Esterification of boron with catechols will be confirmed by both mass spectrometry and ^{11}B-NMR techniques, both of which are commonly used to identify boron-diol bindings for decades.[20] Monomer candidates capable of QS quenching will be synthesized and characterized prior to subsequent polymer studies (**Chapter 3**).

2.1 Experiments

2.1.1 Binding affinities for boron using Alizarin Red S (AR-S) assay

Binding affinities were calculated at pH 7.4 and 37 ºC following the protocol described by Wang *et al*.[9, 21] In brief, Solution A, containing AR-S in phosphate buffer, Solution B, containing both AR-S (same concentration as solution A) and boronic acid in phosphate buffer, were mixed in different ratios in order to make solutions with a constant concentration of AR-S and a range of concentrations of the boronic acid. At least 8 different solutions were made in order to cover as much of the binding curve as possible. The experiments were carried out in triplicate and the plotted curves are derived from the mean value. The fluorescence intensities were measured with an excitation wavelength of 468 nm. The relationship between fluorescence intensity changes and the equilibrium constant can be expressed using the Benesi-Hildebrand equation (**Eq. 1**) so that the association constant for the AR-S-boronic acid complex (K_{a1}) can be obtained from the equation of the intercept

and the slope in a plot of 1/[B] vs $1/\Delta I_f$.[9] Where I_f means the fluorescent intensity, Δkp_0 is a constant derived from the intrinsic fluorescence and the laser power, $[AR\text{-}S]_0$ represents the original concentration of AR-S and [B] is the concentration of boric/boronic acid at each measurement. (See **Appendix** for more information)

Equation 1

$$\frac{1}{\Delta I_f} = \frac{1}{\Delta k \cdot p_0 \cdot [AR^{-}S]_0 \cdot K_{a1}} \cdot \frac{1}{[B]} + \frac{1}{\Delta k \cdot p_0 \cdot [AR^{-}S]_0}$$

In order to calculate the binding affinities between the boronic acids and the different diols employed in this work, Solution B and Solution C (containing the same concentration of AR-S and boronic acid as Solution B and at least 20 eq of the diol) were mixed in different ratios in order to make different solutions with a constant concentration of both AR-S and boric/boronic acid and a range of concentrations of the diols. At least 6 different solutions were made in order to cover as much of the binding curve as possible. Once again, the experiments were carried out in triplicate and the fluorescence intensities were measured with an excitation wavelength of 468 nm. The binding affinity (K_a) was determined by plotting *1/P* vs *Q* (**Eq. 2**), where *P* according to **Eq. 3** and **Eq. 4**, $[B]_0$ represents the original concentration of boric/boronic acid, $[Diol]_0$ is the highest concentration of diols applied through the testing time, [AR-S-B] means the concentration of AR-S-boron binding complex at each measurement, and [AR-S] is the concentration of free AR-S at each measurement. For a more detailed description see Ref.[9]

Equation 2 **Equation 3** **Equation 4**

$$\frac{[Diol]_0}{P} = \frac{K_{a1}}{K_a}Q + 1 \qquad P = [B]_0 - \frac{1}{Q \cdot K_{a1}} - \frac{[AR^-S]_0}{Q+1} \qquad Q = \frac{[AR^-S]}{[AR^-S^-B]}$$

2.1.2 Binding confirmation by mass spectrometry

Samples of diols were initially dissolved in $Na_2B_4O_7$ buffer (50 mM, pH 7.4). Aliquots (200 µL) of this solution were further diluted with a 1:1 mixture of H_2O : Acetonitrile (200 µL).

2.1.3 Binding confirmation by ^{11}B-NMR

A 25 mM solution of $Na_2B_4O_7$ was prepared in phosphate buffer (250 mM, pH 7.4) and 10% in volume of D_2O was added. This borate/phosphate buffer was used to prepare samples with different amounts of the diols of interest and NMR spectra were acquired for each of them. A collection of 128 scans was averaged for each spectrum with a 0.20 s recycle time.

For the competitive binding experiments, a 20 mM solution of DPD was prepared in borate/phosphate buffer (25 mM, 100 mM, pH 7.4, 10% in D_2O) and an NMR spectrum was recorded. 2 eq of the diol were then dissolved in this DPD solution and a new NMR spectrum was recorded.

2.1.4 Synthesis of diol-monomers

2.1.4.1 Synthesis of N-(3,4-dihydroxyphenethyl) methacrylamide (DMAm)[22]

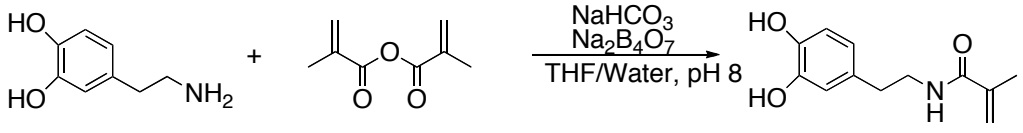

dopamine methacrylic anhydride DMAm

The reaction media were prepared by adding $Na_2B_4O_7$ (10 g, 26 mmol) and $NaHCO_3$ (4.0 g, 48 mmol) to distilled water (100 mL). Both $Na_2B_4O_7$ and $NaHCO_3$ were saturated in water in these amounts, and demonstrated some insolubility. Dopamine hydrochloride (5.0 g, 26 mmol) was added to this solution. Methacrylic anhydride solution (4.7 mL, 32 mmol) in tetrahydrofuran (THF, 25 mL) was prepared separately and added dropwise into the aqueous dopamine solution. In order to keep the reaction mixture moderately basic (pH 8 or above) sodium hydroxide (1.0 M) was added dropwise. The reaction mixture was stirred overnight at room temperature. At this time, a dark black slurry-like solution had formed; this was washed twice with ethyl acetate (50 mL). The resulting solid was vacuum filtered and the obtained aqueous solution was acidified to pH 2 with hydrochloric acid solution (6.0 M). The crude product was extracted with ethyl acetate (50 mL) three times from the acidified aqueous solution and then dried over magnesium sulfate. The solution volume was reduced to 25 mL with a rotary evaporator. The obtained solution was added to hexane (250 mL) with vigorous stirring to precipitate a brownish slurry-like solid. Then the formed suspension was dissolved with ethyl acetate (50 mL). The solvent was removed with a rotary evaporator. Precipitation was carried out another time and the final white solid (3.9 g, 66%) was dried under vacuum overnight. ^{1}H-NMR (DMSO-d_6, 400 MHz) δ (ppm) 8.70 (*br s*, 2H, OH), 7.93 (*s*, 1H, NH), 6.62 (*d*, J = 2.0 Hz, 1H, Ar-H), 6.57 (*d*, J = 8.0 Hz, 1H, Ar-H), 6.42 (*dd*, J = 8.0, 2.0 Hz, 1H, Ar-H), 5.61 (*s*, 1H, C=CH), 5.29 (*s*, 1H, C=CH), 3.49-3.18 (*m*, 2H, N-CH_2), 2.67-2.38 (*m*, 2H, Ar-CH_2), 2.08 (*s*, 3H, CH_3-MAm).

2.1.4.2 Synthesis of 3,4-dihydroxy-L-phenylamanine methacrylamide (L-DMAm)[22]

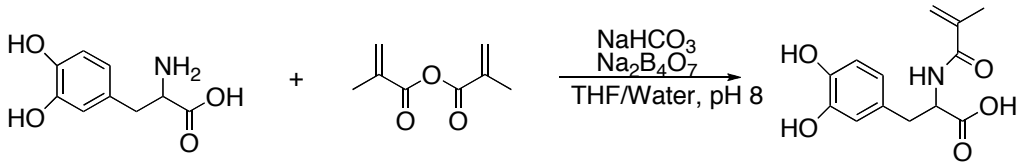

L-DOPA methacrylic anhydride L-DMAm

L-DMAm was prepared following the same procedure as described for synthesis of DMAm. In a typical experiment, 3,4-dihydroxy-L-phenylamanine (L-DOPA) (5.0 g, 25 mmol) in distilled water (100 mL) with $Na_2B_4O_7$ (10 g, 26 mmol) and $NaHCO_3$ (4.0 g, 48 mmol) solution was prepared. Methacrylic anhydride solution (4.7 mL, 32 mmol) in tetrahydrofuran (THF, 25 mL) was prepared separately. The methacrylic anhydride solution was added dropwise into the aqueous solution. The mixture was then adjusted to pH 8 or above with sodium hydroxide (1.0 M). The reaction was carried out overnight at room temperature. The title compound L-DMAm was purified by extraction and precipitation and recovered as brown powder (4.3 g, 64%) after dried under vacuum overnight. ^{1}H-NMR (DMSO-d_6, 400 MHz) δ (ppm) 12.62 (*s*, 1H, COOH), 8.72 (*br s*, 2H, OH), 7.96 (*d*, J = 8.1, 1H, NH), 6.62 (*d*, J = 2.0 Hz, 1H, Ar-H), 6.60 (*d*, J = 8.0 Hz, 1H, Ar-H), 6.48 (*dd*, J = 8.0, 2.0 Hz, 1H, Ar-H), 5.64 (*s*, 1H, C=CH), 5.34 (*s*, 1H, C=CH), 4.38-4.30 (*m*, 1H, N-CH), 2.96-2.75 (*m*, 2H, CH-C$\underline{H_2}$), 1.80 (*s*, 3H, CH_3-MAm). ^{13}C-NMR (DMSO-d_6, 100 MHz) δ (ppm) 173.7 (COOH), 167.9 (CONH), 145.3 (C-OH), 144.1 (C-OH), 139.9 (-C=), 129.2 (Ar C-), 120.2 (Ar CH), 120.0 (=CH_2), 116.8 (Ar CH), 115.7 (Ar CH), 54.5 (CH-NH), 36.1 (CH_2), 19.0 (CH_3). IR (KBr) ν (cm^{-1}) 3517 (N-H), 3382 (Carboxyl O-H), 3204 (Ar O-H), 1713 (Carboxyl C=O), 1654 (Amide C=O), 1537 and 1519 (N-H). ESI-MS: m/z 266.11 (MH^+, 100%), 220.11 (MH^+

- COOH, 38%). HR-MS Calcd for $C_{13}H_{16}N_1O_5$ (MH^+): 266.1028 found: 266.1122.

2.2 Results and discussions

2.2.1 Binding affinities for boron using Alizarin Red S (AR-S) assay

In the initial study, phenylboronic acid (PBA) and sodium borate were examined as boron models and their affinities with AR-S were calculated by fitting the AR-S assay data with Benesi-Hildebrand equation (**Eq. 1**) (*Figure 2-4 to 2-7*). As expected, the formation of a borate/boronate ester complex between boric/boronic acid and AR-S enabled AR-S to be fluorescent by removing the quenching structure in AR-S.[17] The fluorescent intensity was getting strong with the increase of boron concentrations (AR-S concentration and all other conditions were constant all through the experiment), owing to the increased formation of AR-S-boron complex in the system (*Figure 2-4 to 2-7*, upper). Also, the color change of solution was observed varying from dark pink (no fluorescent free AR-S structure) to orange (fluorescent AR-S-boron complex form) upon addition of boric/boronic acid into AR-S/PBS buffer. The initial buffer composition and pH conditions followed previous reports by Wang and coworkers[9] ([**AR-S**] = 0.009 mM, [**PBA**] = 2 mM, [$\mathbf{Na_2B_4O_7}$] = 2 mM. [$\mathbf{PO_4^-}$] = 100 mM) (*Figure 3-4 and 3-5*). Buffer composition and concentration were retained throughout each experiment, for the constant between AR-S and boric/boronic acid varies significantly when buffer conditions are changing.[9] The same experiments were repeated with a modified buffer conditions in due course, which verified the prior conclusion that different associate constants were achieved under different testing

conditions ([**AR-S**] = 0.12 mM, [**PBA**] = 1 mM, [$\mathbf{Na_2B_4O_7}$] = 1 mM. [$\mathbf{PO_4^-}$] = 200 mM) (*Figure 2-6 and 2-7*). When AR-S concentration was fixed to 0.009 mM, and PBS was 100 mM, the associate constant of PBA-AR-S binding was 477.8 ± 10.3 M^{-1} and $Na_2B_4O_7$-AR-S was 317.8 ± 35.8 M^{-1} (*Figure 2-4 and 2-5*). However, if the buffer condition was changed (e.g. [AR-S] = 0.012mM, [PBS] = 200 mM], the binding affinity also altered (Ka_1 (PBA) = 432.2 ± 15.7 M^{-1}; Ka_1 ($Na_2B_4O_7$) = 368.4 ± 48.4M^{-1}) (*Figure 2-6 and 2-7*). Therefore, the binding constant is only applicable in its applied assay conditions.

Specifically, by using the AR-S assay, the binding constants (K_{a1}) of AR-S with phenyboronic acid (PBA) and $Na_2B_4O_7$ were determined, respectively. The titration of PBA/$Na_2B_4O_7$ from 86.3 to 222.7 equivalents (*Figure 2-4 and 2-5*) or 1.1 to 8.3 equivalents (*Figure 2-6 and 2-7*) of AR-S was employed under constant conditions (AR-S, PBS, pH and temperature) (Here the 'equivalent' was defined as the value of PBA/$Na_2B_4O_7$ concentration divided by AR-S concentration). The concentration range of boron applied in solution was slightly different under the two different buffer conditions, which would not impact the calculated value of the constants as long as different boron concentrations were employed and induced big enough fluorescent change. Analyzing fluorescence data at different wavelengths made it possible to cover as wide range of fluorescence as possible and minimize intrinsic instrument errors. Therefore, three sets of data have been selected for inclusion in **Eq. 1** (*Figure 2-4* to *2-7*, bottom). These three are: the fluorescence intensity at 592 nm wavelength (emission wavelength for AR-S), intensities at 572 nm wavelength and average intensities in the range of 573-614 nm. All the three sets were analyzed independently. The constants shown here are the average

values of the three. In addition, this assay was carried out twice independently under the two different solution conditions.

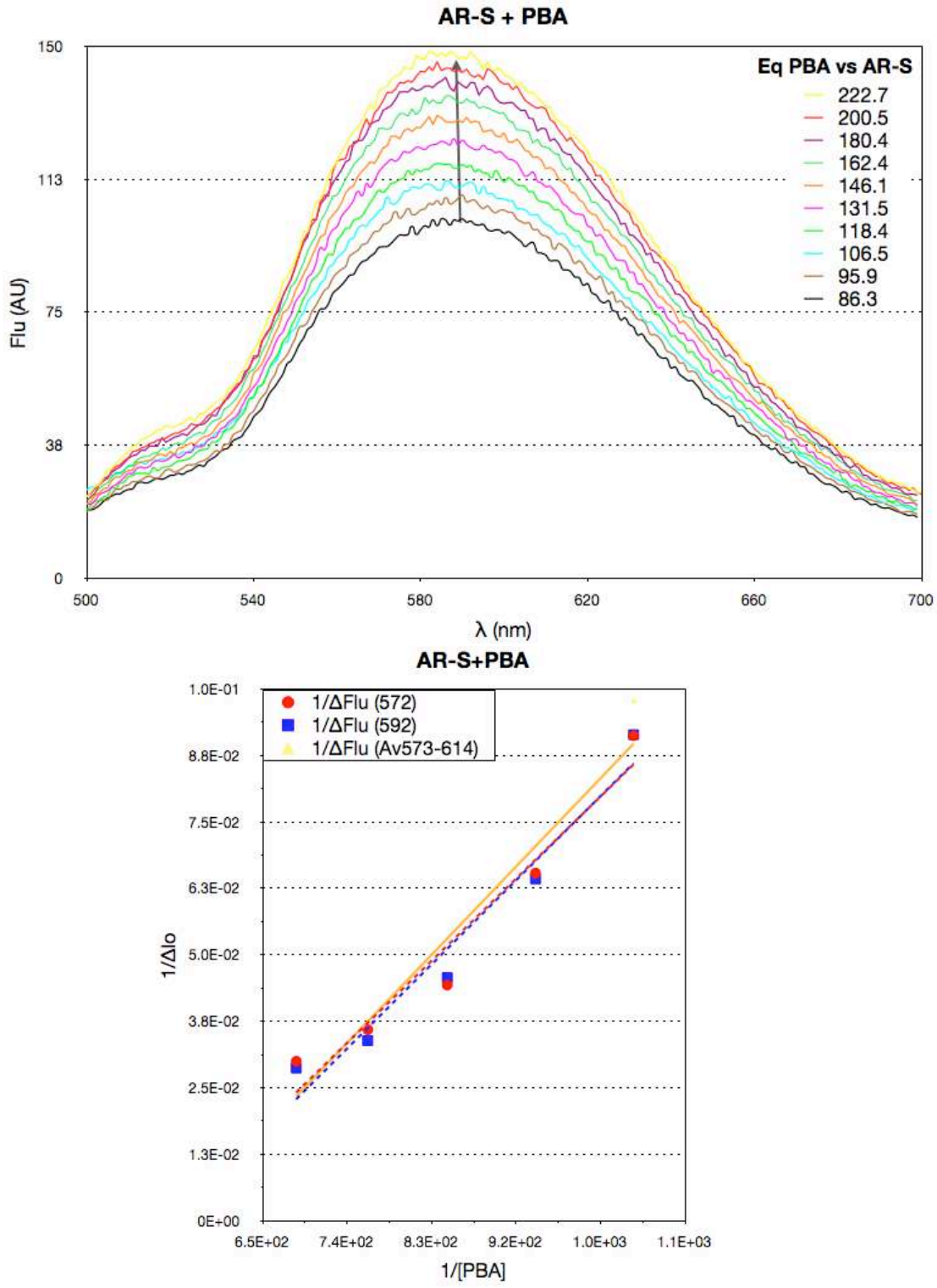

Figure 2-4. Fluorescence profile of **AR-S** and phenylboronic acid (**PBA**) and the corresponding fitting plots. [**AR-S**] = 0.009 mM, [**PBA**] = 2 mM, [$\mathbf{PO_4^-}$] = 100 mM; $\mathbf{K_{a1}}$ **(PBA)** = 477.8 ± 10.3 M^{-1}

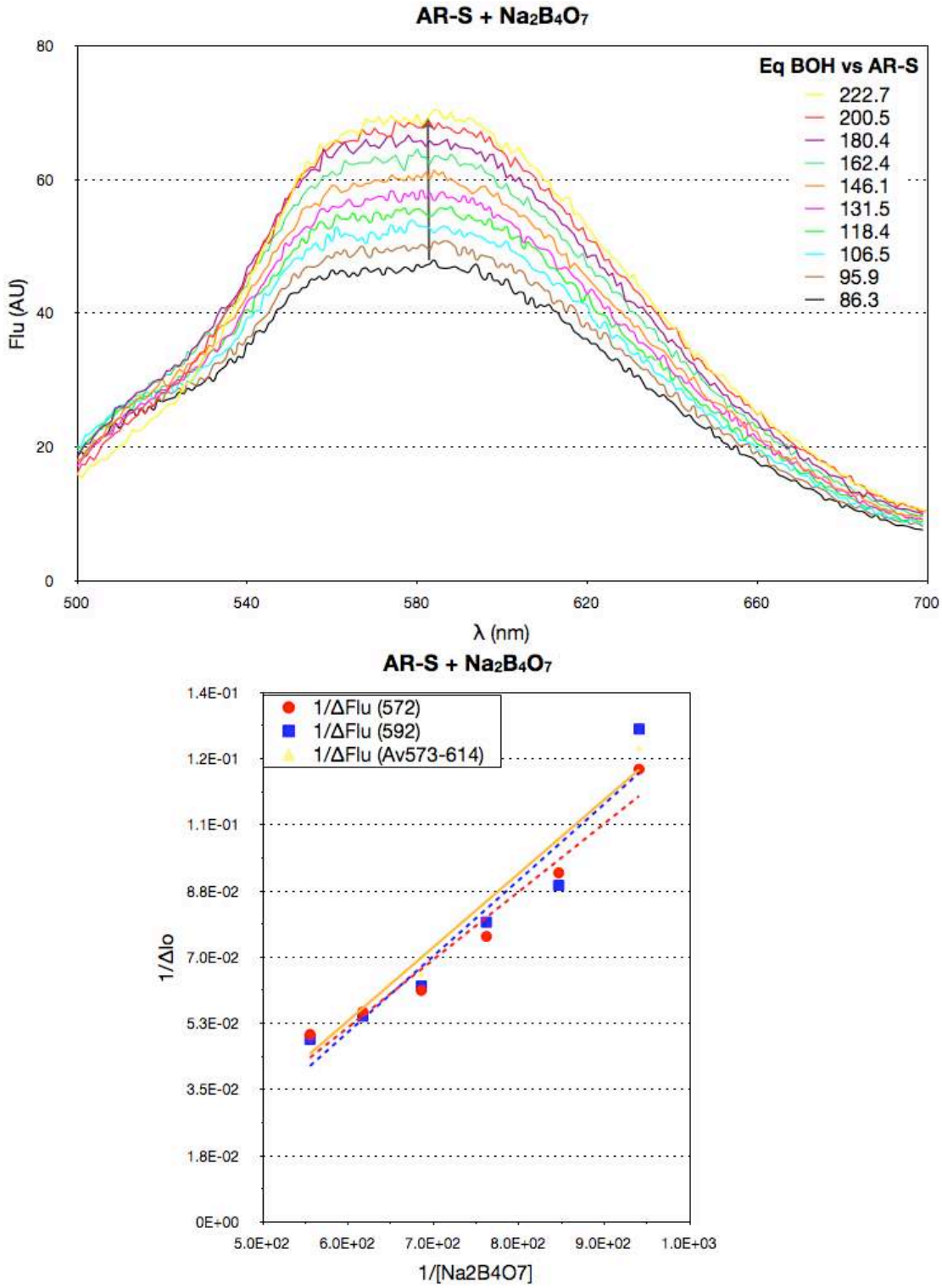

Figure 2-5. Fluorescence profile of **AR-S** and sodium borate and the corresponding fitting plots. [**AR-S**] = 0.009 mM, [$\mathbf{Na_2B_4O_7}$] = 2 mM, [$\mathbf{PO_4^-}$] = 100 mM; $\mathbf{K_{a1}\ (Na_2B_4O_7)}$ = 317.8 ± 35.8 M^{-1}

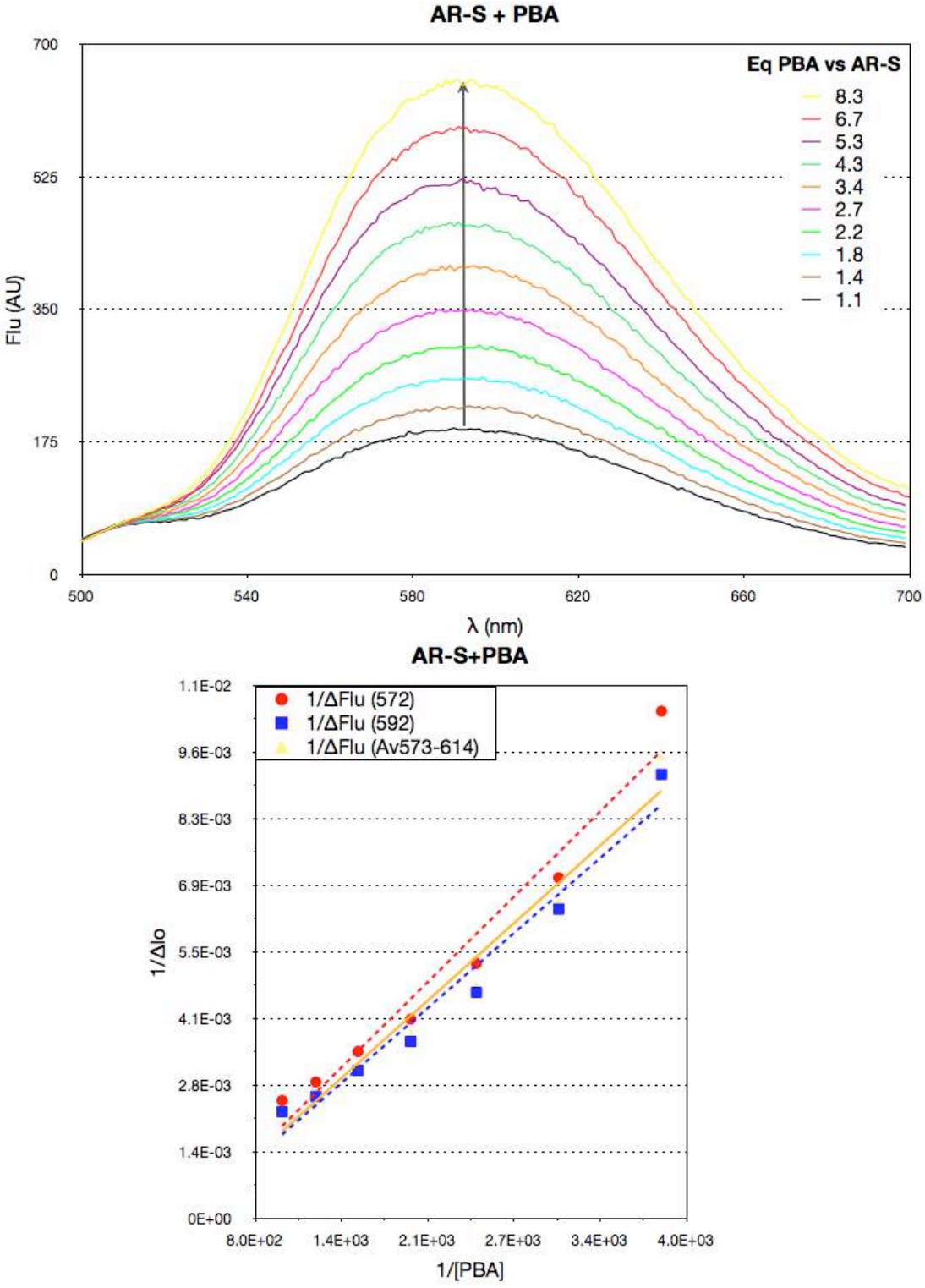

Figure 2-6. Fluorescence profile of **AR-S** and phenylboronic acid (**PBA**) and the corresponding fitting plots. [**AR-S**] = 0.12 mM, [**PBA**] = 1 mM, [$\mathbf{PO_4^-}$] = 200 mM; $\mathbf{Ka_1}$ **(PBA)** = 432.2 ± 15.7 M^{-1}

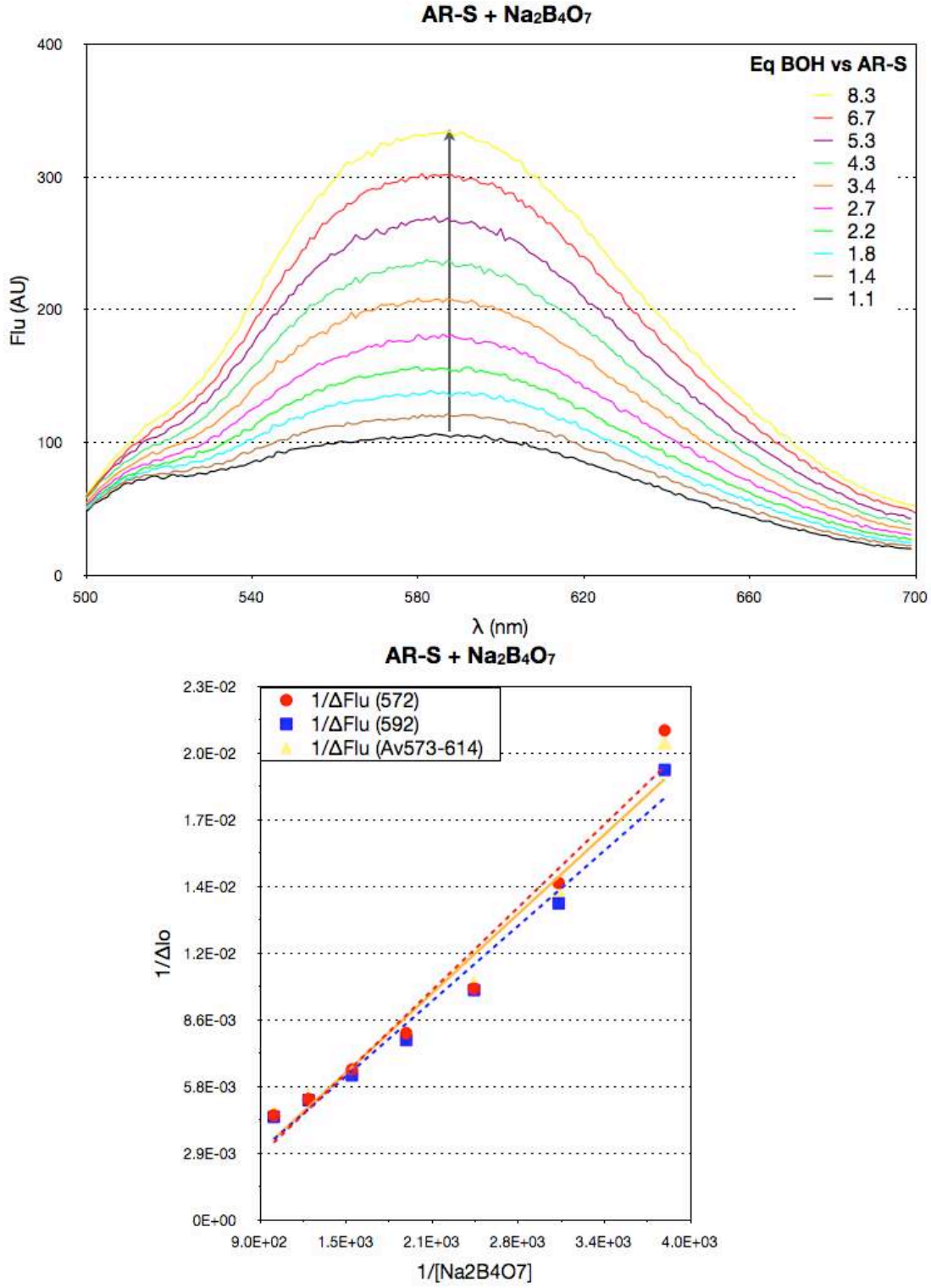

Figure 2-7. Fluorescence profile of **AR-S** and sodium borate and the corresponding fitting plots. [**AR-S**] = 0.12 mM, [$\mathbf{Na_2B_4O_7}$] = 1 mM, [$\mathbf{PO_4^-}$] = 200 mM; $\mathbf{Ka_1\ (Na_2B_4O_7)}$ = 368.4 ± 48.4M^{-1}

Based on the AR-S three-composition system, the binding affinity constants (K_a) of a series of diol-containing compounds including DPD molecules to boron were established at pH 7.4 in PBS buffer fitting with **Eq. 2, 3 & 4** (see **Appendix** for more details). Linear diols such as 3-methoxy-1,2-propanediol, 2-methyl-1,3-propanediol and 2-amino-1,3-propanediol (*Figure 3-8*) have very low affinities ranging from 0.212 M^{-1} to 12.7 M^{-1} for PBA and from 0.169 M^{-1} to 9.86 M^{-1} for sodium borate. Methoxy-β-D-glucopyranoside and methoxy-β-D-galactopyranoside (*Figure 3-8*) have moderate K_a values: 0.765 M^{-1} and 0.882 M^{-1} for PBA and 0.444 M^{-1} and 1.07 M^{-1} for sodium borate, respectively. Catechols such as dopamine and L-DOPA (*Figure 3-8*) have high affinities for both PBA and sodium borate with K_a values in the range of 32.5 M^{-1}-108 M^{-1}. These results were in accord with prior reports i.e.: linear diols < cyclic diols (sugars) < aromatic diols or catechols.[9, 23] Even though DPD (*Figure 3-8*) (K_a: 81 for PBA and 84.5 for sodium borate) has a similar structure to carbohydrates, its affinity was much higher than that obtained for the other saccharides analyzed, and only the catechols (Dopamine and L-DOPA) gave comparable affinities. On the other hand, the binding affinity of dopamine with boric acid was much higher than its derivative structure L-DOPA and also higher than its own affinity but with the other boron model PBA. This value was demonstrated to be more or less the same for the different repeats. The reason for this unexpected high value was not very clear. However, through this AR-S experiments, dopamine and its derivative molecule L-DOPA were believed to be selectively important, for they gave higher ability to competitively bind boron from DPD than the other analyzed diols. And thus,

dopamine and L-DOPA were considered as the potential candidates involved in 'QS quenching' system.

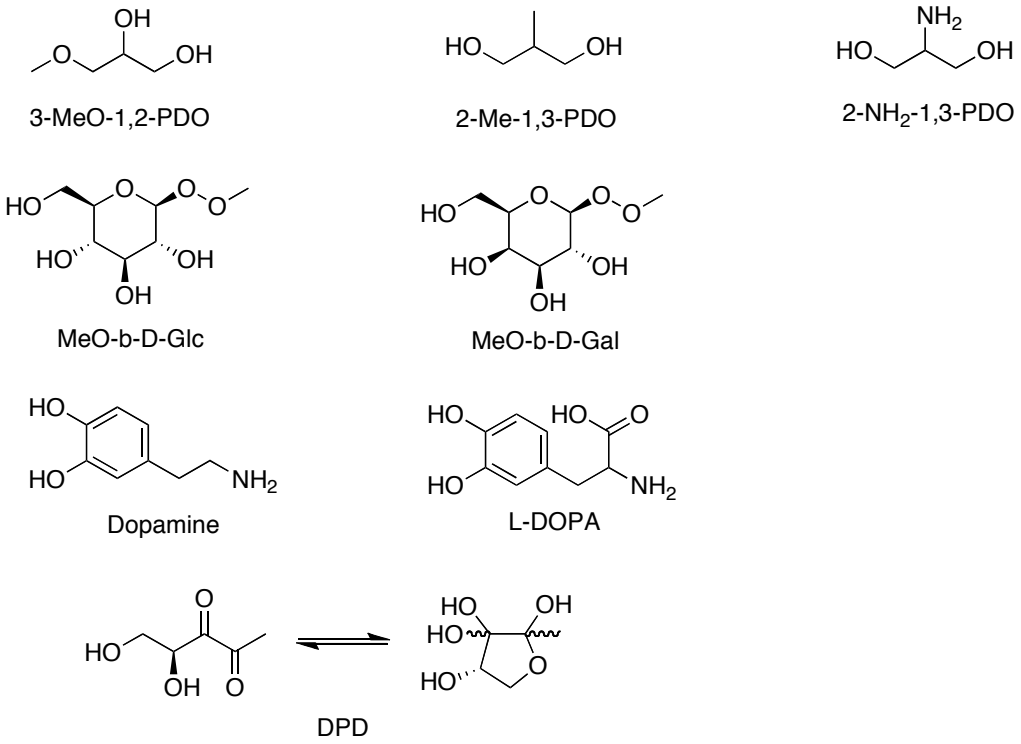

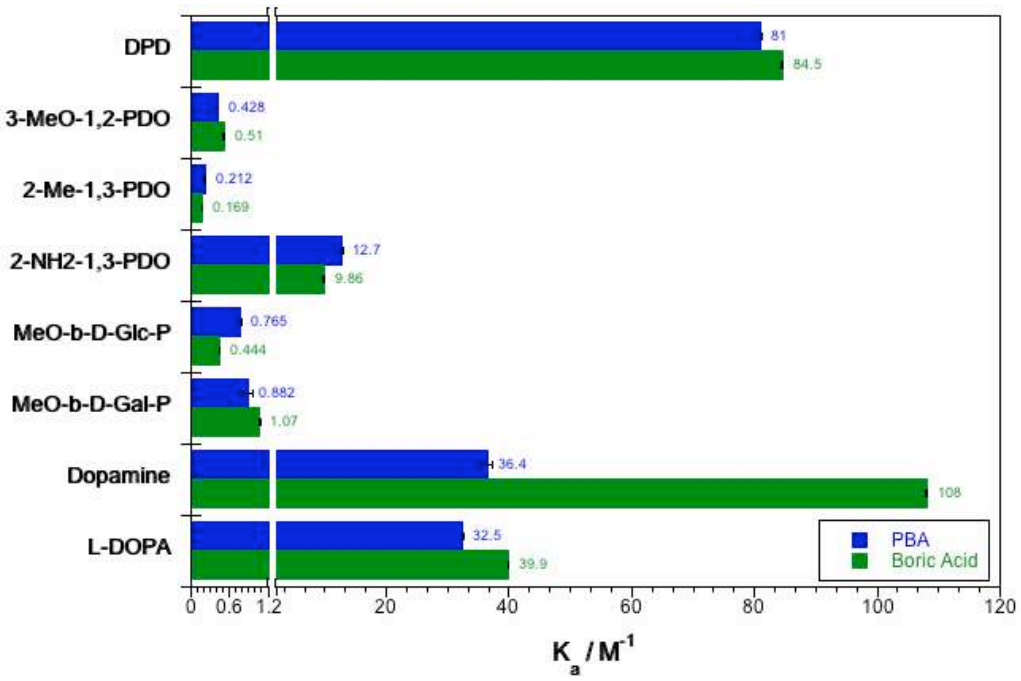

Figure 2-8. Binding affinities of DPD, model diols and polymers for phenylboronic acid (PBA - Blue bars) and boric acid (Green Bars). (PDO = Propanediol, Glc = Glucopyranoside, Gal = Galactopyranoside)

Specifically, the graphs below (*Figure 2-9 to 2-24*) gave the detailed information to explain how the above binding affinity values (*Figure 2-8*) came. The full scan profiles (500 nm to 750 nm wavelength) of fluorescence were recorded with fluorimeter under the condition of constant concentration of PBS, AR-S and PBA/$Na_2B_4O_7$, but a series concentration of diols (*Figure 2-9 to 2-24*, upper). Such graphs gave a direct view that fluorescent intensity decreased with the increase of diol concentration due to the competitive binding of boron from AR-S induced quenching of AR-S-boron fluorescence. Again, the concentrations of diols employed were not the same, as displayed on the legend, for each type of diols (e.g. *Figure 2-9 and Figure 2-11*). However, this has nothing to do with their binding affinity values, as long as significant fluorescent change was obtained with a series concentration of diols. This is obviously because that binding affinity represents the intrinsic binding ability of one type of molecule to another, which should be constant through out the same testing conditions. And also, even with the same type of diol molecule and similar diol concentrations, the fluorescence could be different (e.g. *Figure 2-11* and Figure *2-12*). This is expected that phenylboronic acid (PBA) has only one binding site for one boron-containing molecule, but sodium borate has two. And thus, their affinities for one specific type of diol molecule can be different. In addition, these fluorescence data at three different wavelengths (572 nm, 592 nm and 573 to 614 nm) were then fitting with Benesi-Hildebrand equation (**Eq. 2, 3 &4**) to form the equation profiles (*Figure 2-9 to 2-24*, bottom). The binding affinities (Ka) of each type of diol with each type of boron model at each wavelength were calculated

individually (*Figure 2-9 to 2-24*) (see more details in **Appendix**). The values of binding affinity were the average of the three and concluded in *Figure 2-8*.

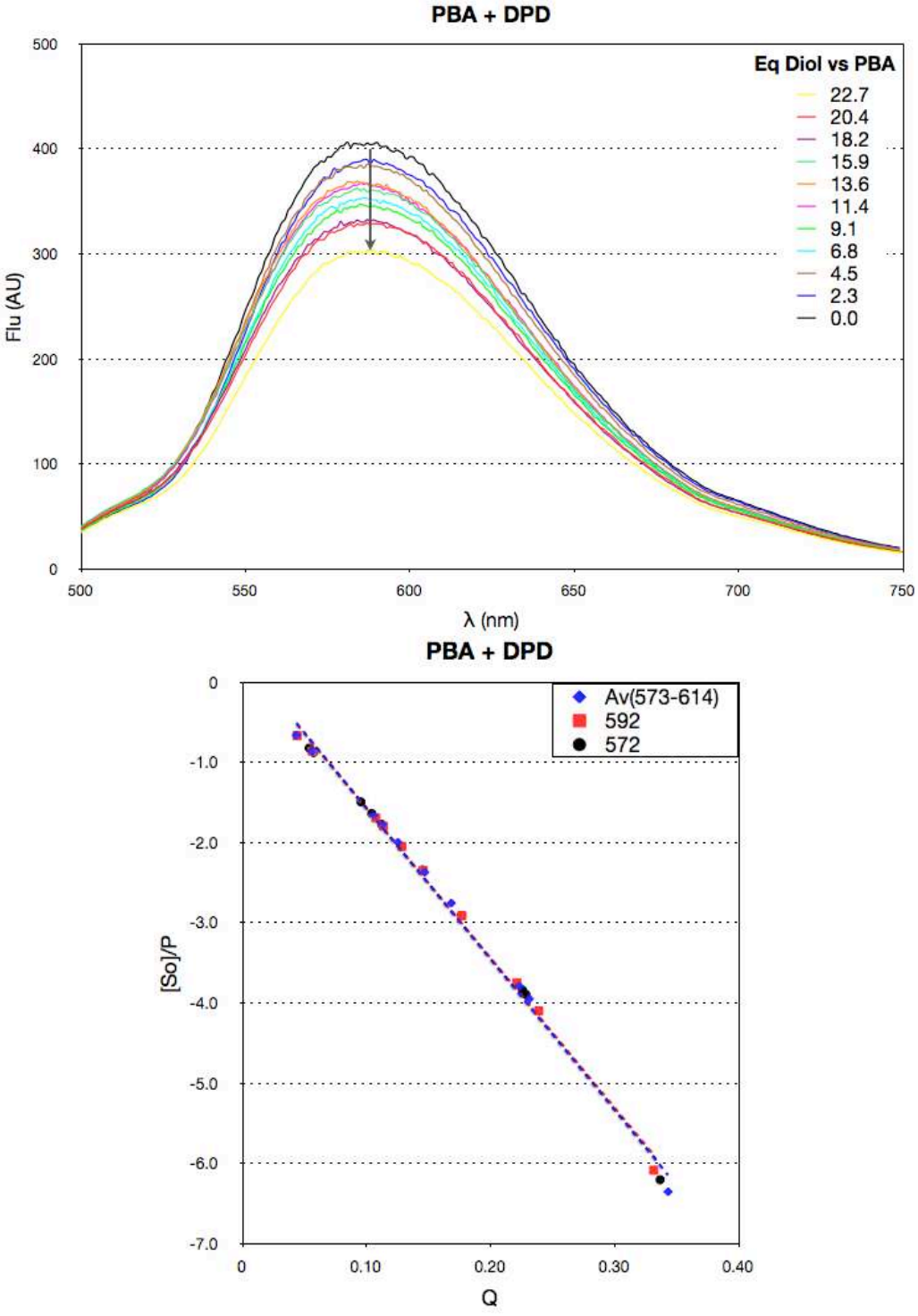

Figure 2-9. Fluorescence profile of **PBA** and **DPD** titration and the corresponding fitting plot. [**AR-S**] = 0.06 mM, [**PBA**] = 0.5 mM, [**DPD**] = 11.4 mM, [$\mathbf{PO_4^-}$] = 100 mM. $\mathbf{K_a}$ = 81.0 ± 0.1 M^{-1}

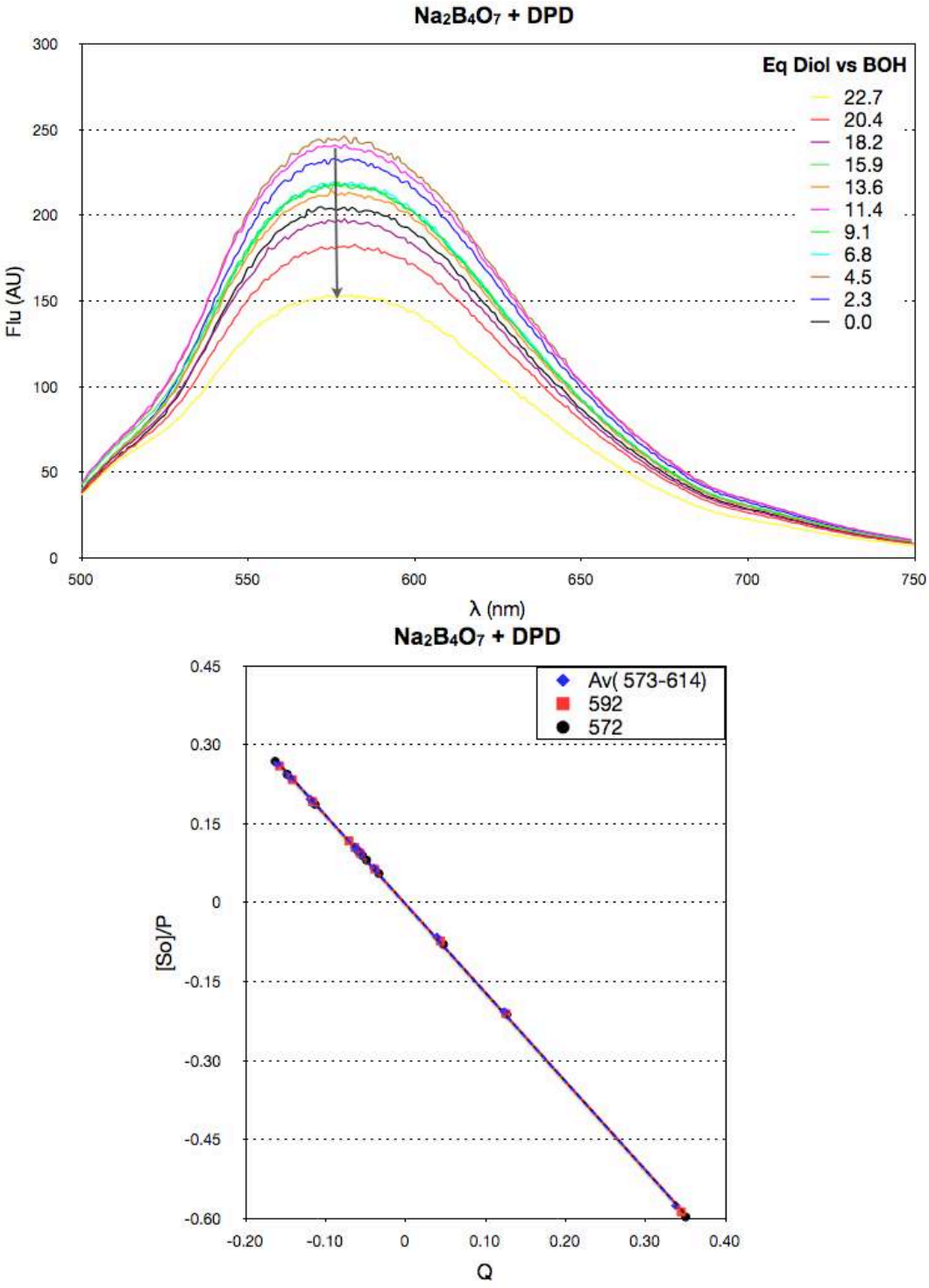

Figure 2-10. Fluorescence profile of Sodium Borate and **DPD** titration and the corresponding fitting plot. [**AR-S**] = 0.06 mM, [$\mathbf{Na_2B_4O_7}$]=0.5 mM, [**DPD**] = 11.4 mM, [$\mathbf{PO_4^-}$] = 100 mM. $\mathbf{K_a}$ = 84.5 ± 0.1 M^{-1}.

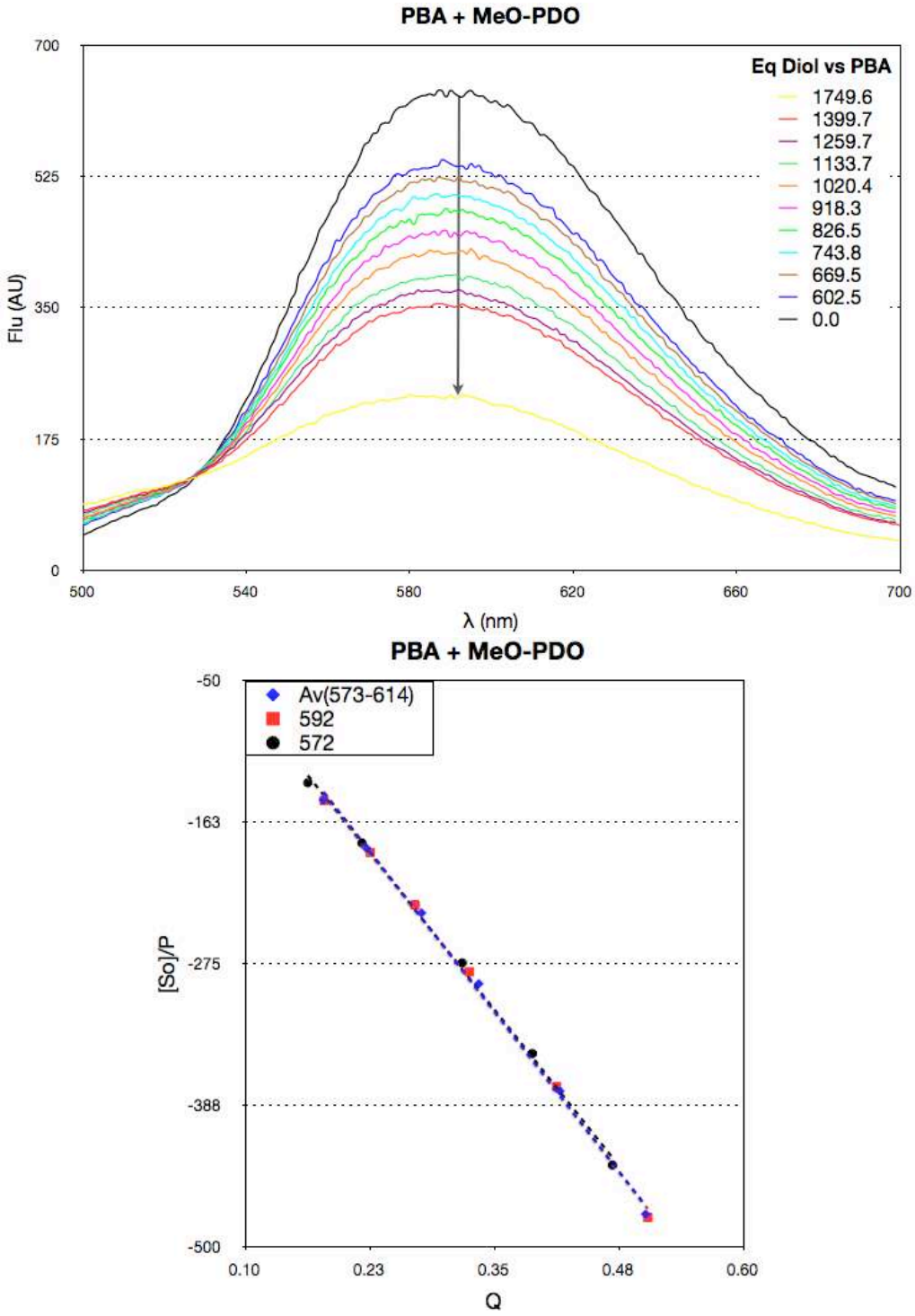

Figure 2-11. Fluorescence profile of **PBA** and 3-Methoxy-1,2-propanediol (**MeO-PDO**) titration and the corresponding fitting plot. [**AR-S**] = 0.12 mM, [**PBA**] = 1 mM, [**MeO-PDO**] = 1749.6 mM, [$\mathbf{PO_4^-}$] = 200 mM. $\mathbf{K_a}$ = 0.4 ± 0.006 M^{-1}.

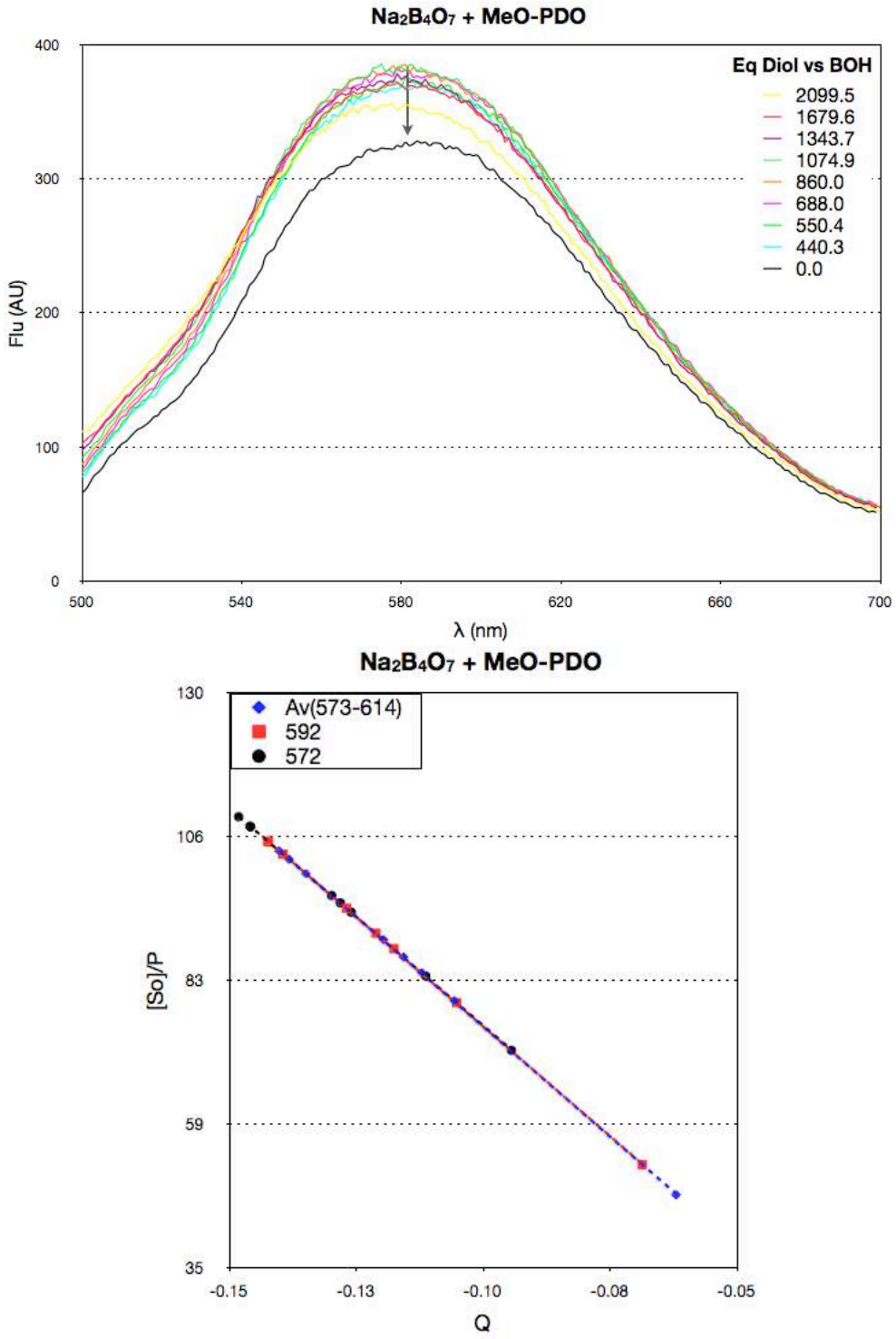

Figure 2-12. Fluorescence profile of Sodium Borate and 3-Methoxy-1,2-propanediol (**MeO-PDO**) titration and the corresponding fitting plot. [**AR-S**] = 0.12 mM, [$\mathbf{Na_2B_4O_7}$] = 1 mM, [**MeO-PDO**] = 2099.5 mM, [$\mathbf{PO_4^-}$] = 200 mM. $\mathbf{K_a}$ = 0.5 ± 0.003 M^{-1}.

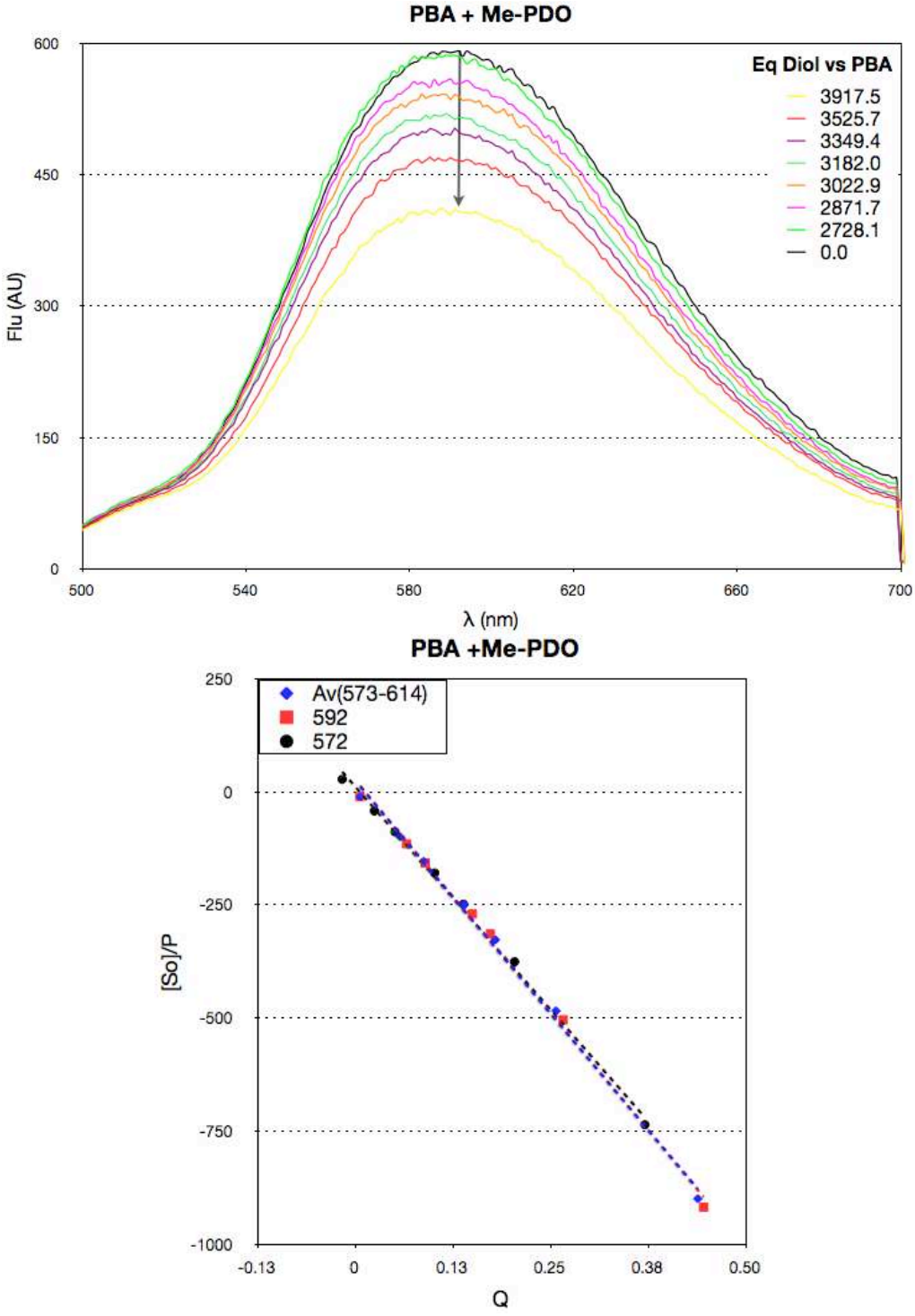

Figure 2-13. Fluorescence profile of **PBA** and 2-Methyl-1,3-propanediol (**Me-PDO**) titration and the corresponding fitting plot. [**AR-S**] = 0.12 mM, [**PBA**] = 1 mM, [**Me-PDO**] = 3917.5 mM, [$\mathbf{PO_4}$] = 200 mM. $\mathbf{K_a}$ = 0.2 ± 0.006 M^{-1}.

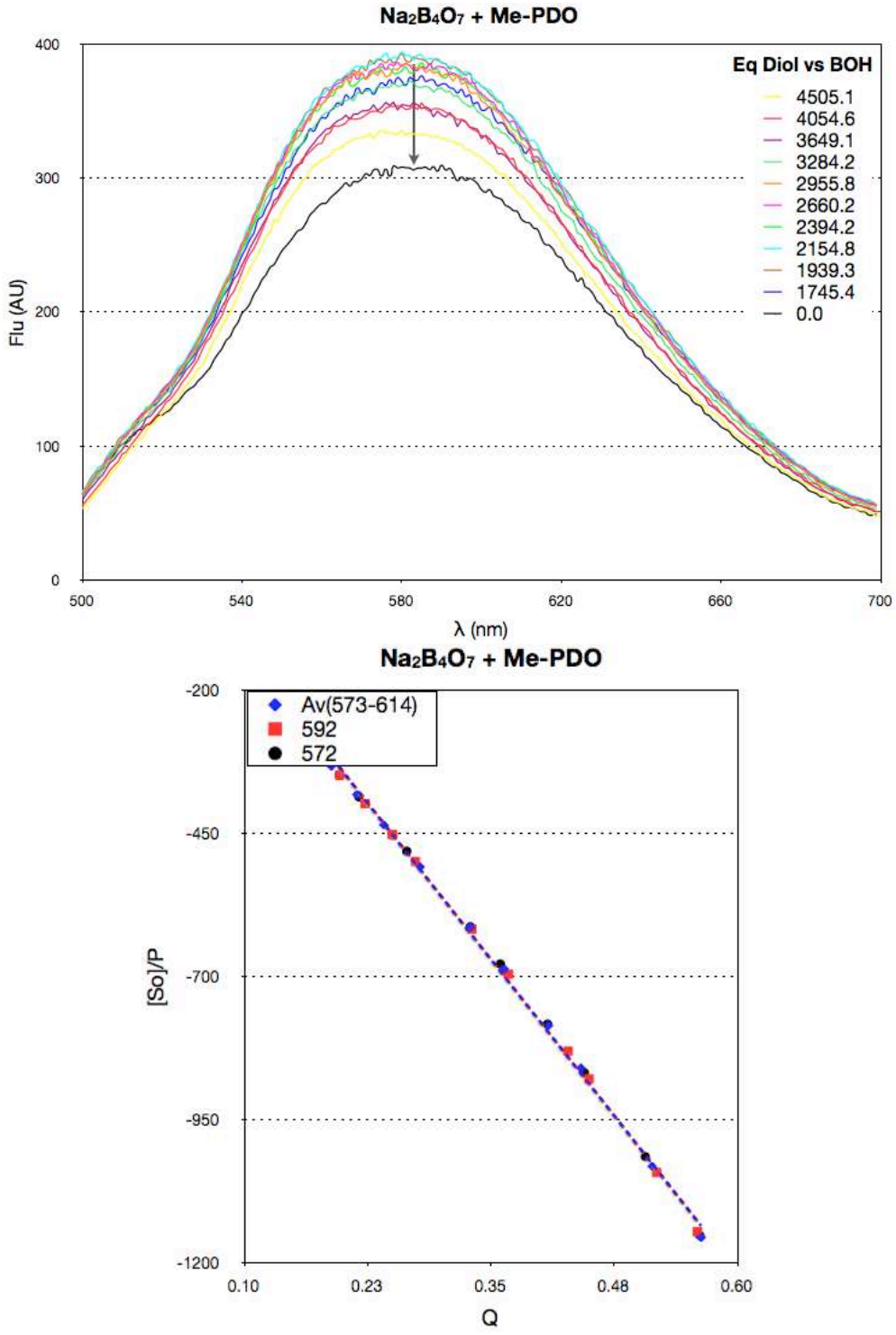

Figure 2-14. Fluorescence profile of Sodium Borate and 2-Methyl-1,3-propanediol (**Me-PDO**) titration and the corresponding fitting plot. [**AR-S**] = 0.12 mM, [$\mathbf{Na_2B_4O_7}$] = 1 mM, [**Me-PDO**] = 4505.1 mM, [$\mathbf{PO_4^-}$] = 200 mM. $\mathbf{K_a} = 0.2 \pm 0.001\ M^{-1}$.

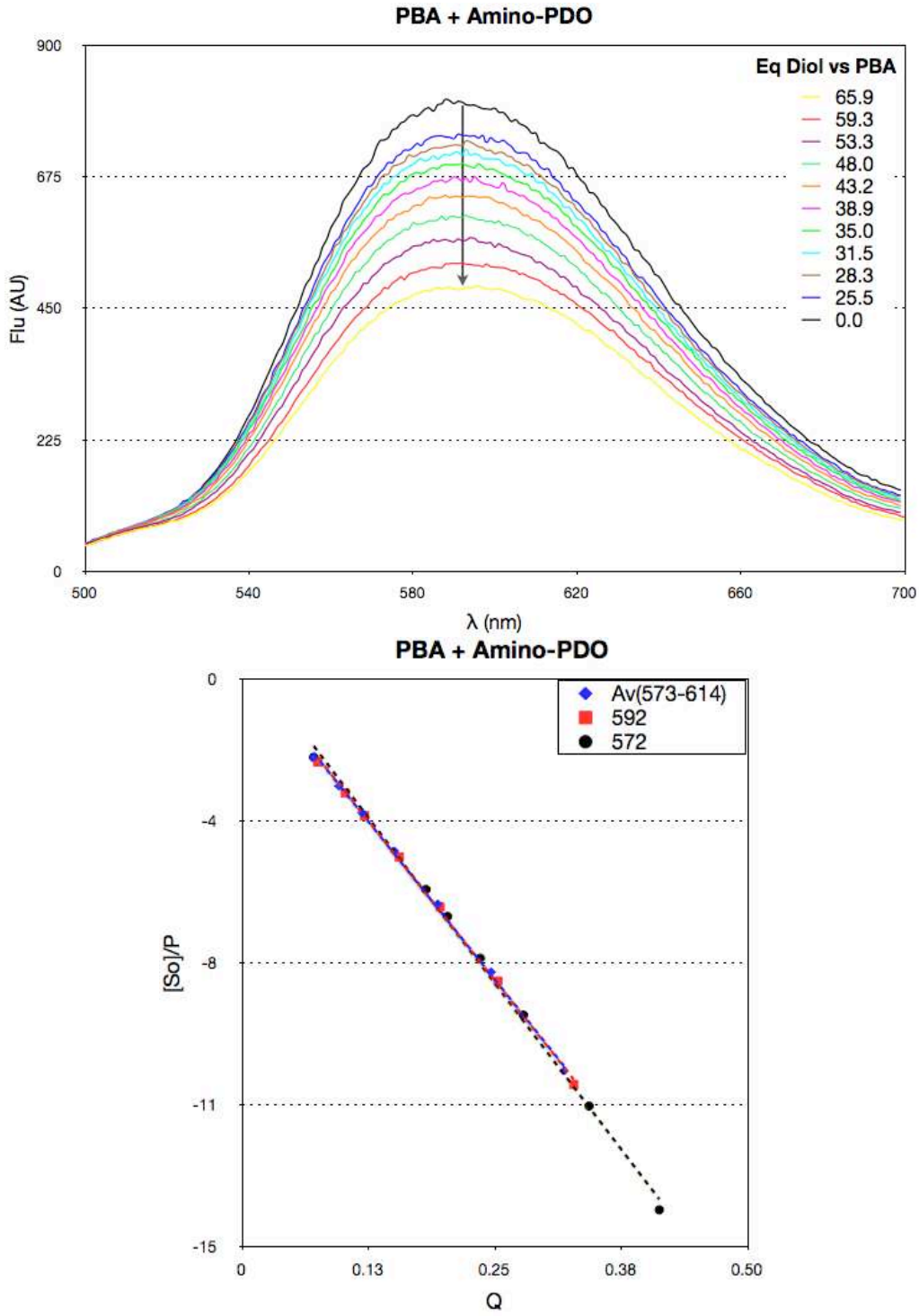

Figure 2-15. Fluorescence profile of **PBA** and 2-Amino-1,3-propanediol (**Amino-PDO**) titration and the corresponding fitting plot. [**AR-S**] = 0.12 mM, [**PBA**] = 1 mM, [**Amino-PDO**] = 65.9 mM, [$\mathbf{PO_4^-}$] = 200 mM. $\mathbf{K_a}$ = 12.7 ± 0.3 M^{-1}.

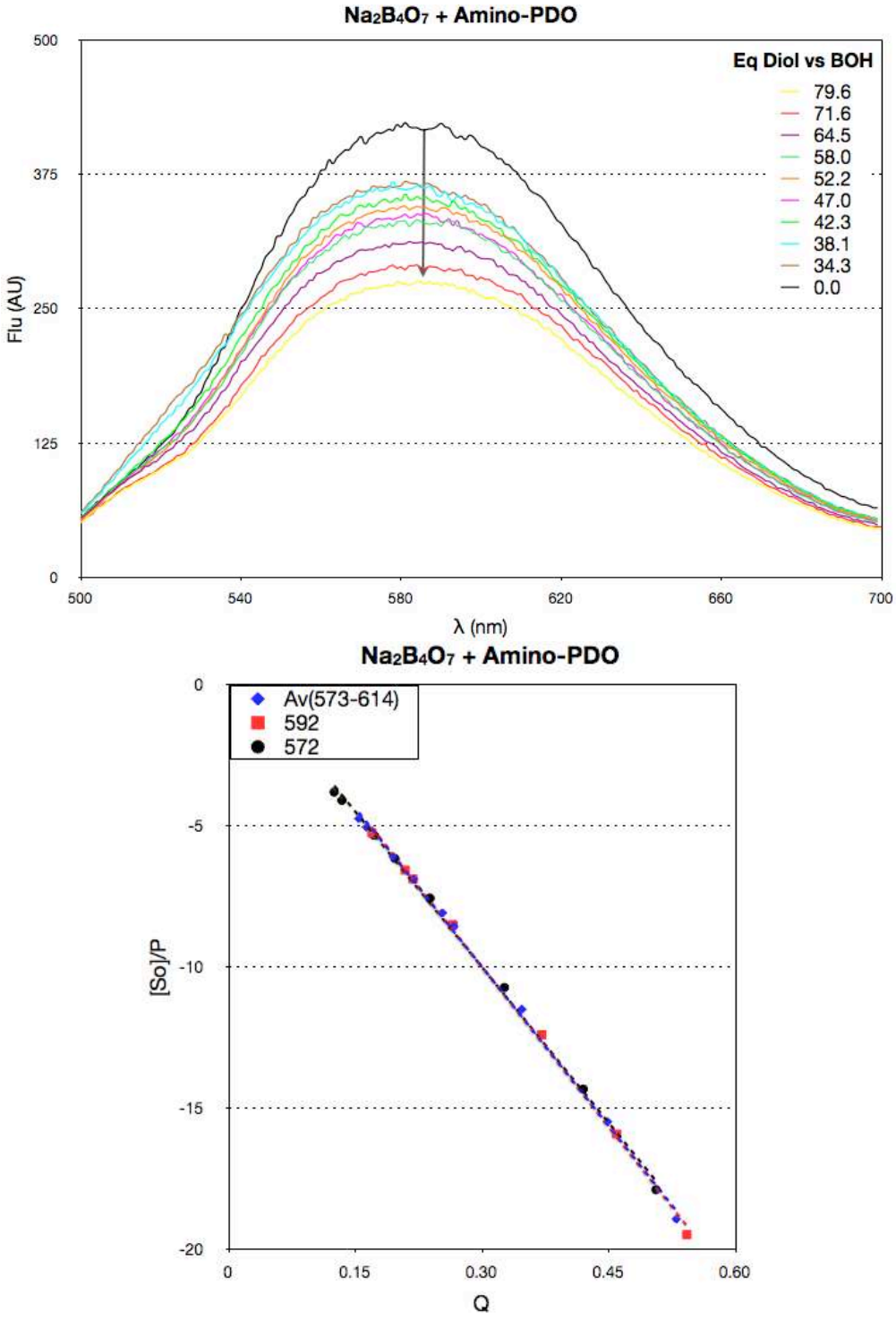

Figure 2-16. Fluorescence profile of Sodium Borate and 2-Amino-1,3-propanediol (**Amino-PDO**) titration and the corresponding fitting plot. [**AR-S**] = 0.12 mM, [$\mathbf{Na_2B_4O_7}$] = 1 mM, [**Amino-PDO**] = 79.6 mM, [$\mathbf{PO_4^-}$] = 200 mM. $\mathbf{K_a}$ = 9.9 ± 0.2 M^{-1}.

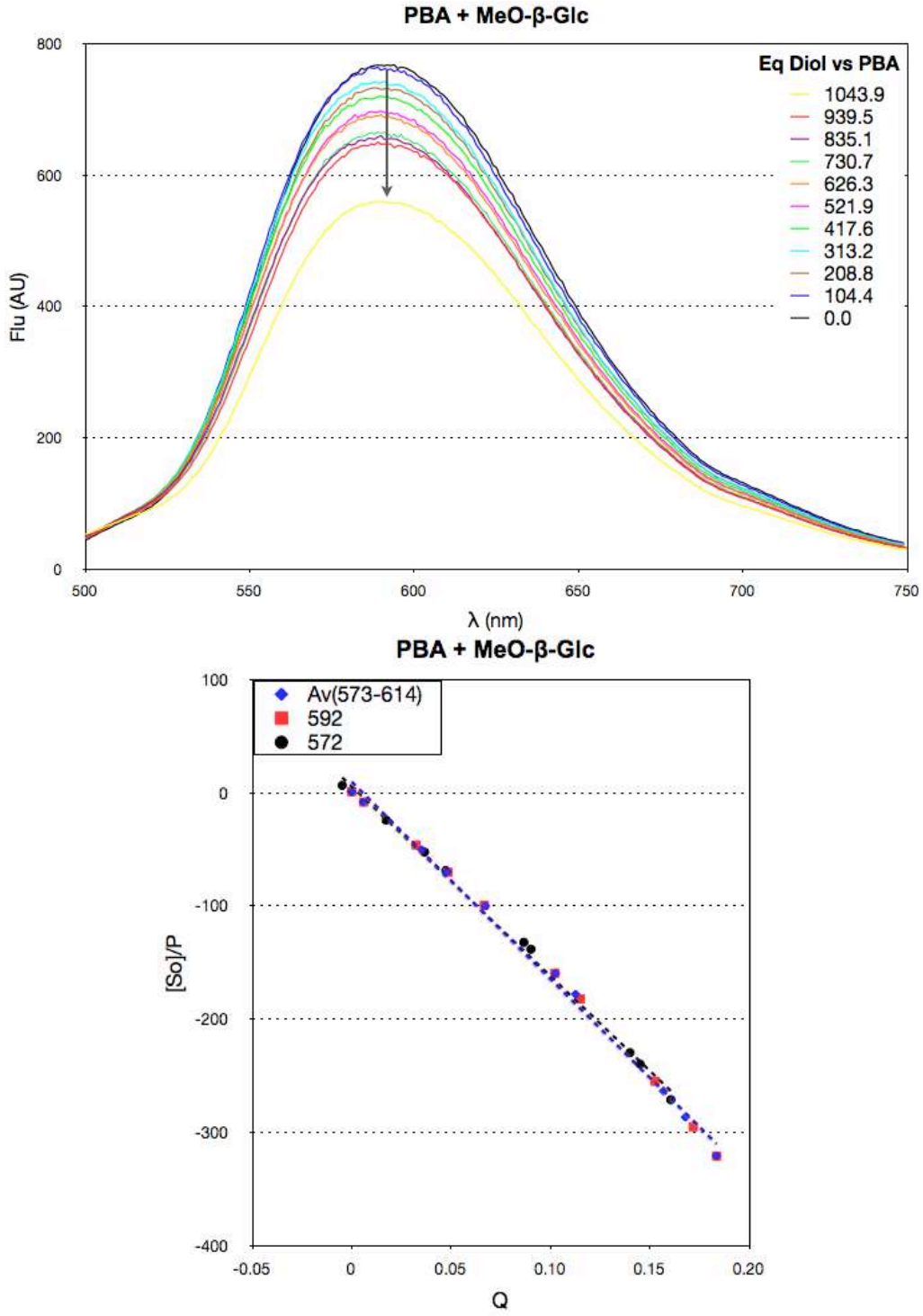

Figure 2-17. Fluorescence profile of **PBA** and MeO-β-glucopyranoside (**MeO-β-Glc**) titration and the corresponding fitting plot. [**AR-S**] = 0.12 mM, [**PBA**] = 1 mM, [**MeO-β-Glc**] = 1043.9 mM, [$\mathbf{PO_4^-}$] = 200 mM. $\mathbf{K_a}$ = 0.8 ± 0.017 M^{-1}.

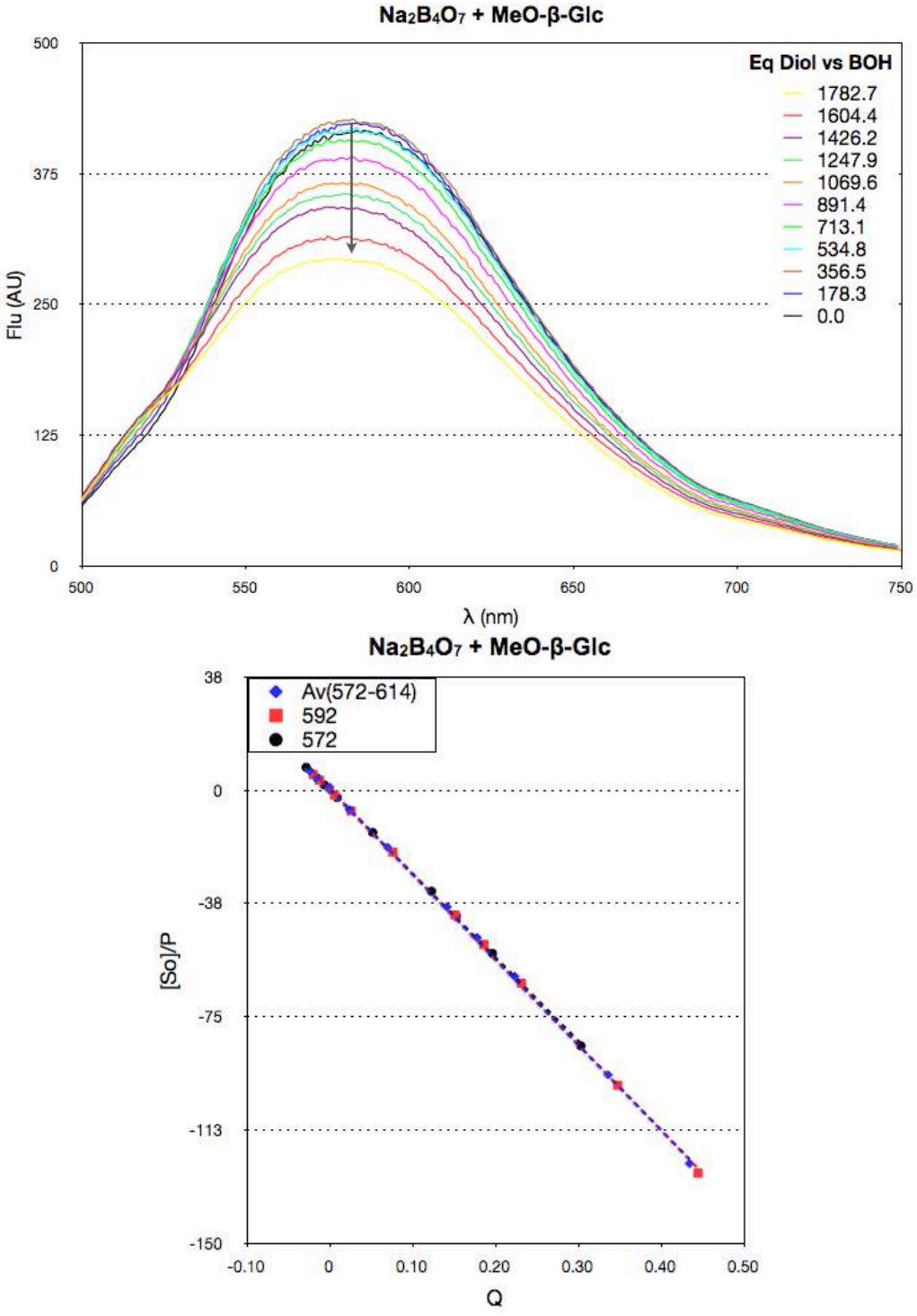

Figure 2-18. Fluorescence profile of Sodium Borate and MeO-β-glucopyranoside (**MeO-β-Glc**) titration and the corresponding fitting plot. [**AR-S**] = 0.12 mM, [$\mathbf{Na_2B_4O_7}$] = 1 mM, [**MeO-β-Glc**] = 1782.7 mM, [$\mathbf{PO_4^-}$] = 200 mM. $\mathbf{K_a}$ = 0.4 ± 0.006 M^{-1}.

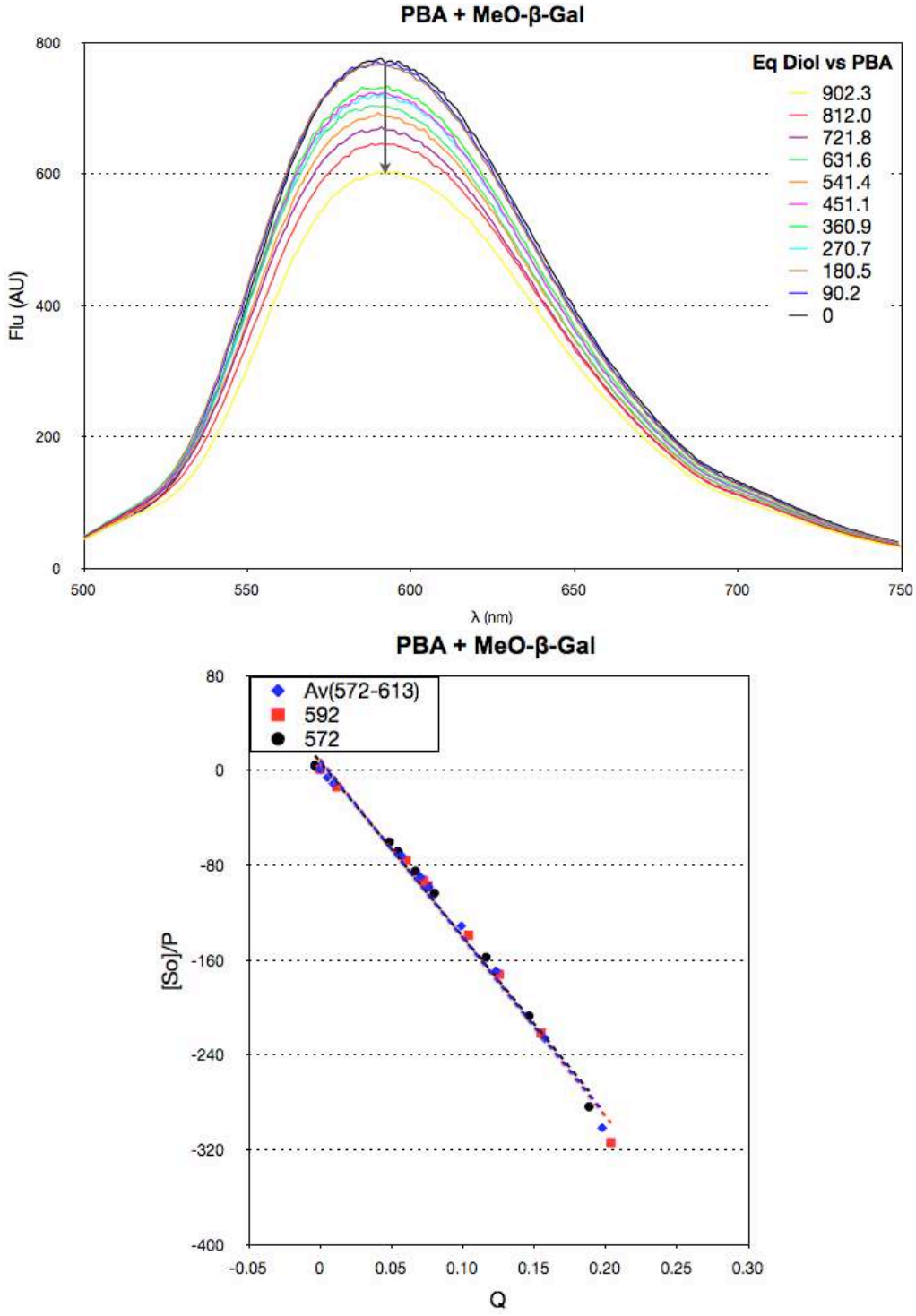

Figure 2-19. Fluorescence profile of **PBA** and MeO-β-galactopyranoside (**MeO-β-Gal**) titration and the corresponding fitting plot. [**AR-S**] = 0.12 mM, [**PBA**] = 1 mM, [**MeO-β-Gal**] = 902.3 mM, [$\mathbf{PO_4^-}$] = 200 mM. $\mathbf{K_a}$ = 0.9 ± 0.1 M^{-1}.

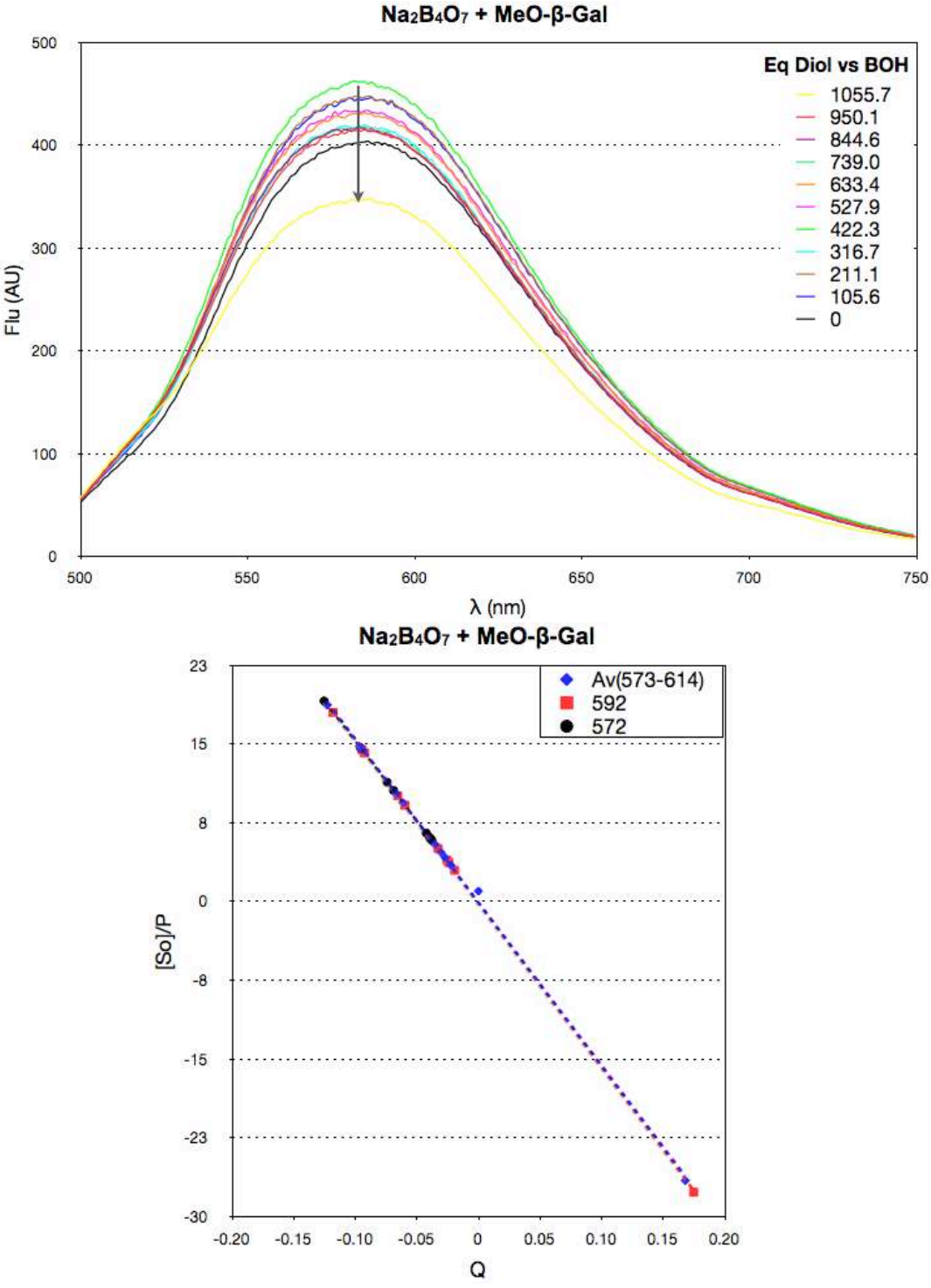

Figure 2-20. Fluorescence profile of Sodium Borate and MeO-β-galactopyranoside (**MeO-β-Gal**) titration and the corresponding fitting plot. [**AR-S**] = 0.12 mM, [$\mathbf{Na_2B_4O_7}$] = 1 mM, [**MeO-β-Gal**] = 1055.7 mM, [$\mathbf{PO_4^-}$] = 200 mM. $\mathbf{K_a}$ = 1.1 ± 0.014 M^{-1}.

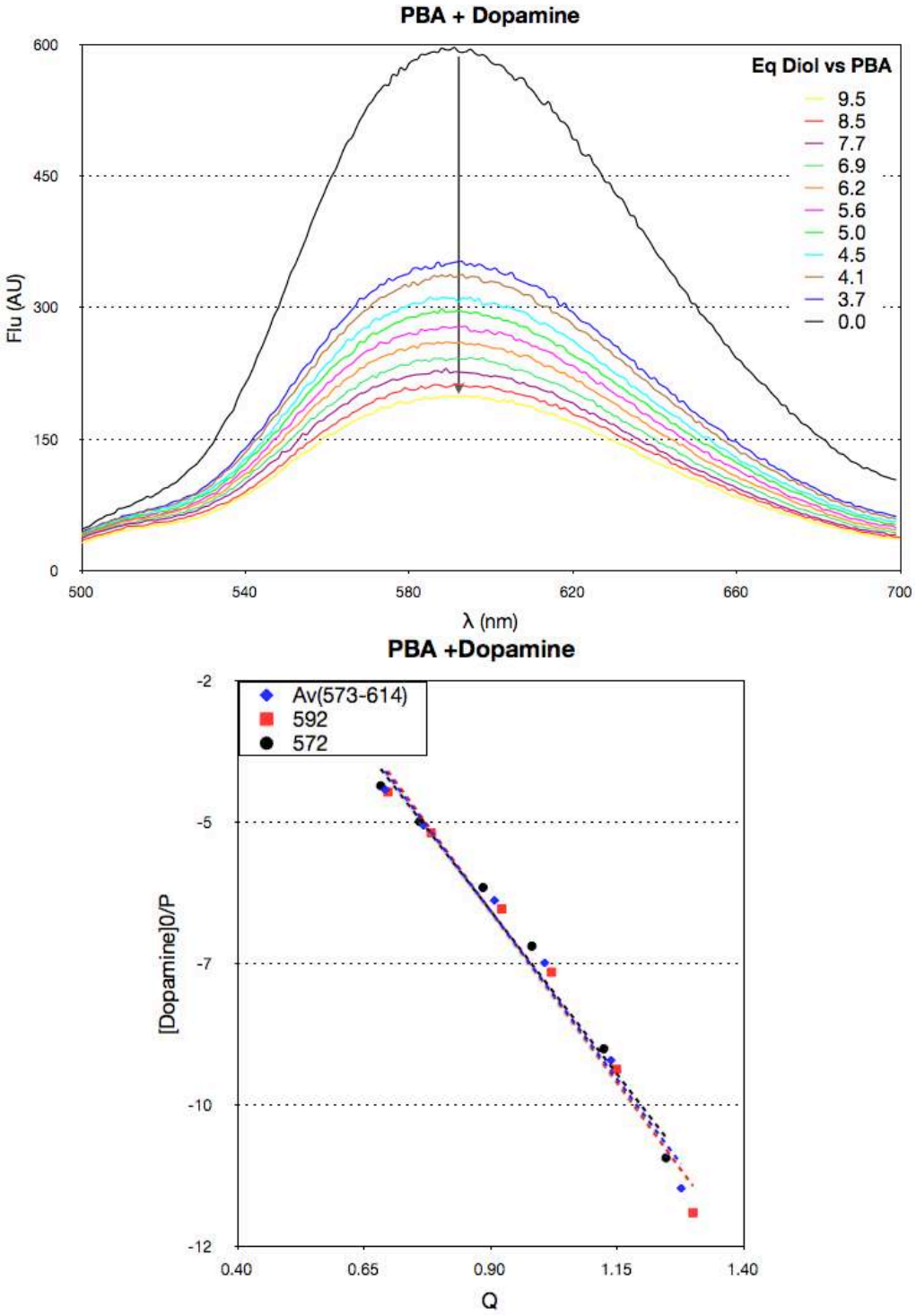

Figure 2-21. Fluorescence profile of **PBA** and Dopamine Hydrochloride (**Dopamine**) titration and the corresponding fitting plot. [**AR-S**] = 0.12 mM, [**PBA**] = 1 mM, [**Dopamine**] = 9.5 mM, [$\mathbf{PO_4^-}$] = 200 mM. $\mathbf{K_a}$ = 36.4 ± 0.9 M^{-1}.

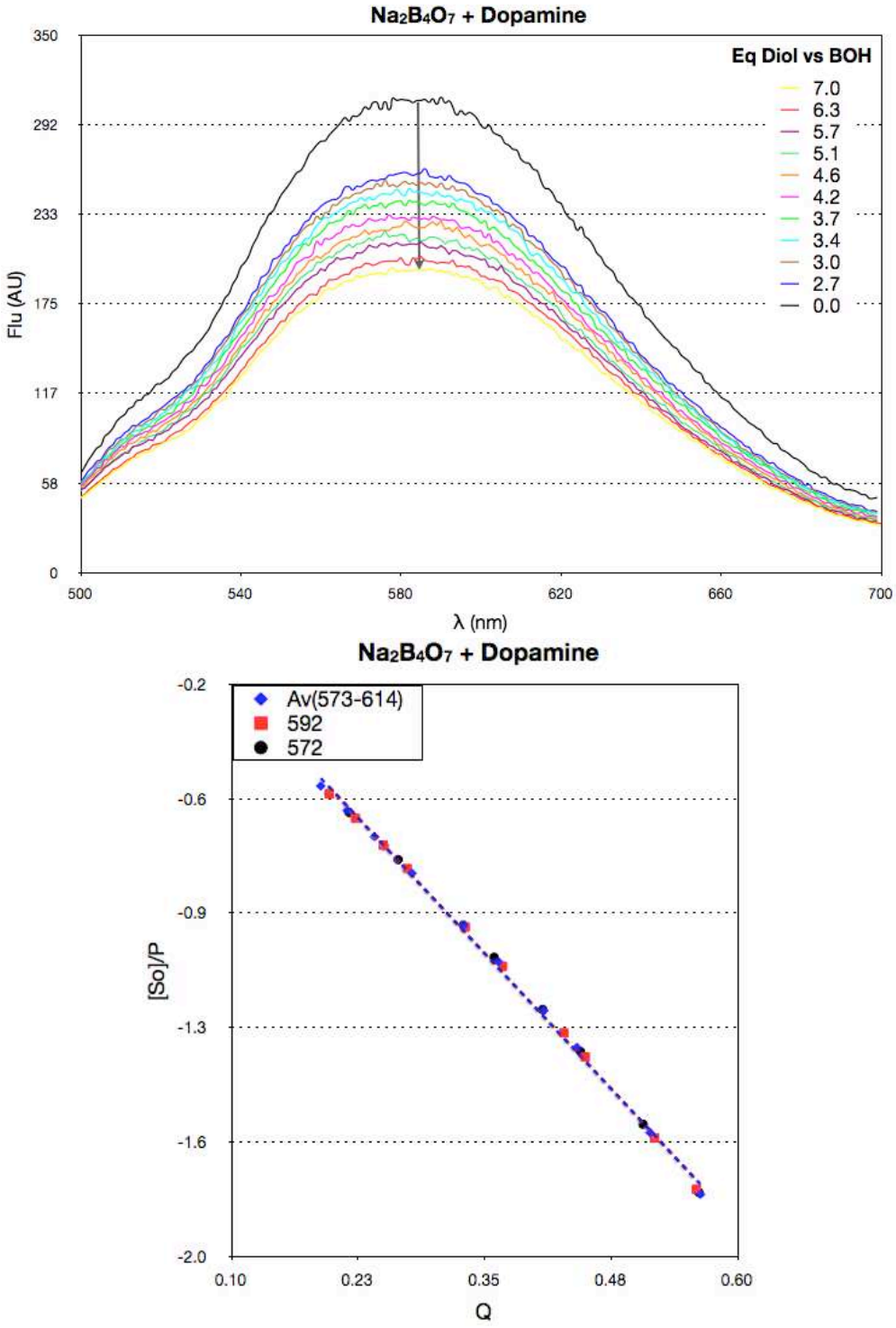

Figure 2-22. Fluorescence profile of Sodium Borate and Dopamine Hydrochloride (**Dopamine**) titration and the corresponding fitting plot. [**AR-S**] = 0.12 mM, [$\mathbf{Na_2B_4O_7}$] = 1 mM, [**Dopamine**] = 7.0 mM, [$\mathbf{PO_4^-}$] = 200 mM. $\mathbf{K_a}$ = 108.0 ± 0.1 M^{-1}.

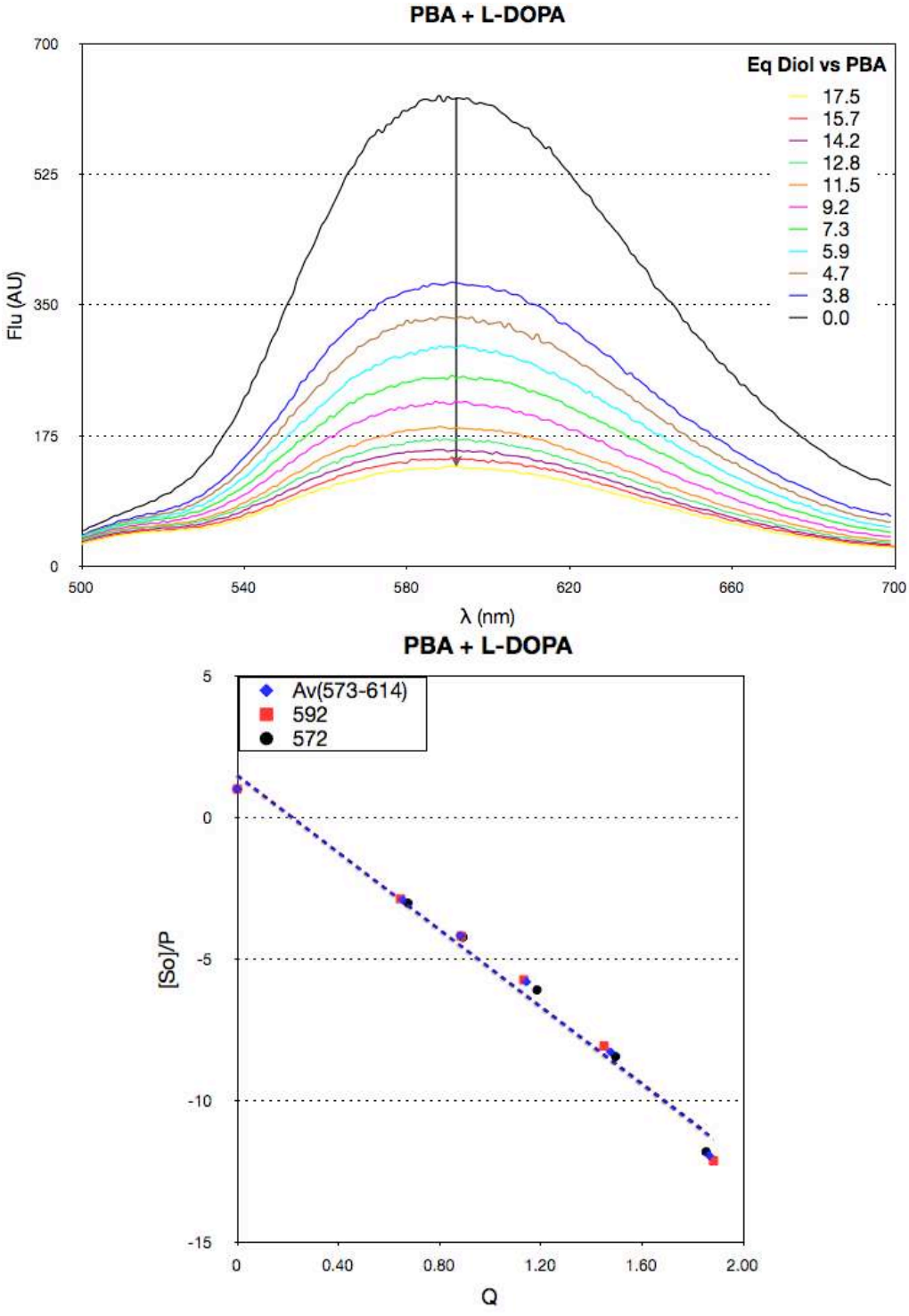

Figure 2-23. Fluorescence profile of **PBA** and 3,4-Dihydroxy-L-phenylalanine (**L-DOPA**) titration and the corresponding fitting plot. [**AR-S**] = 0.12 mM, [**PBA**] = 1 mM, [**L-DOPA**] = 17.5 mM, [$\mathbf{PO_4^-}$] = 200 mM, $\mathbf{K_a}$ = 32.5 ± 0.1 M^{-1}.

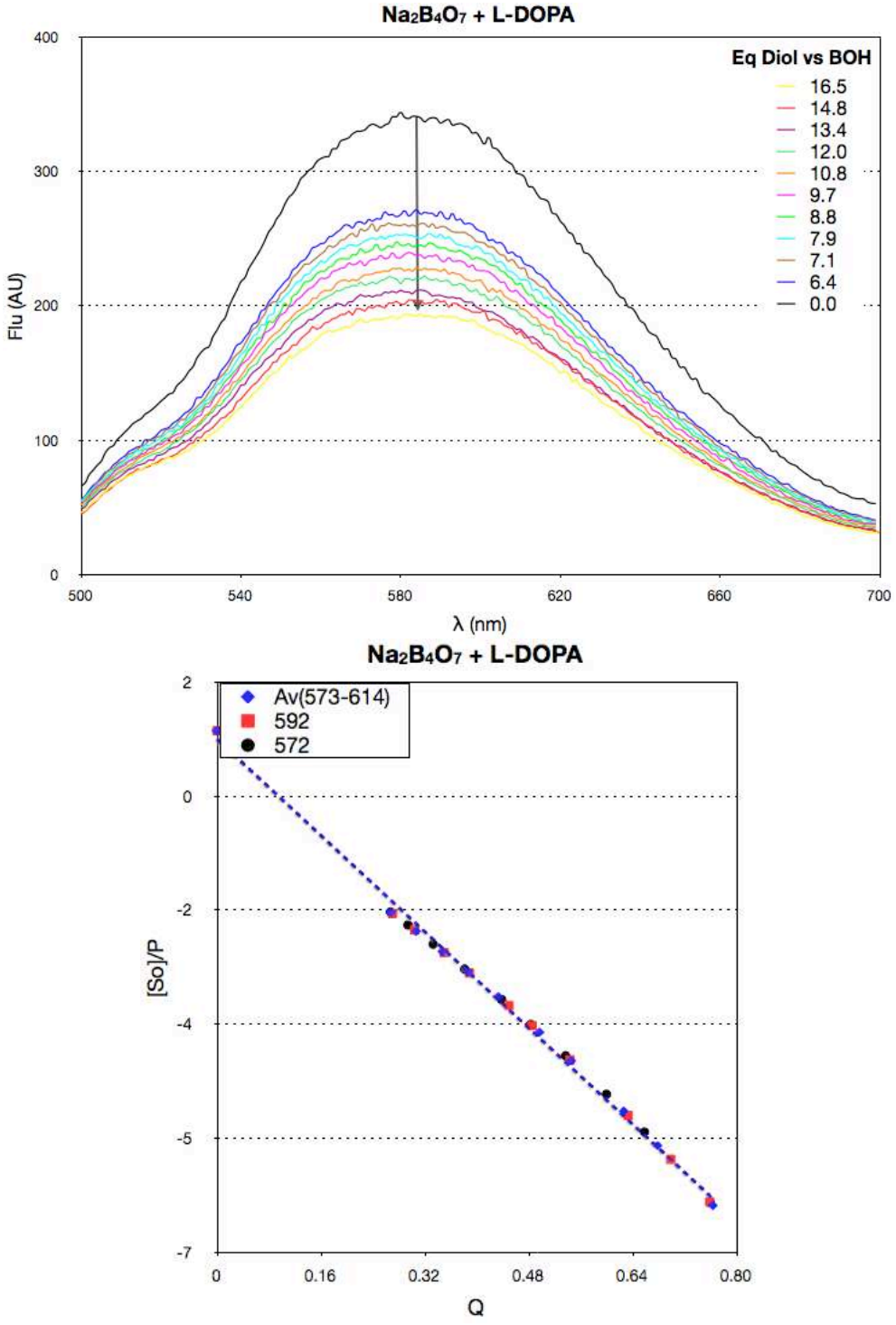

Figure 2-24. Fluorescence profile of Sodium Borate and 3,4-Dihydroxy-L-phenylalanine (**L-DOPA**) titration and the corresponding fitting plot. [**AR-S**] = 0.12 mM, [$\mathbf{Na_2B_4O_7}$] = 1 mM, [**L-DOPA**] = 16.5 mM, [$\mathbf{PO_4^-}$] = 200 mM. $\mathbf{K_a}$ = 39.9 ± 0.1 M^{-1}.

2.2.2 Binding confirmation by mass spectrometry

The complexes formed between catechol and sodium borate in neutral buffer were also confirmed by MS spectrometry. As shown, the complexes existed in two forms: 196.07886 m/z corresponded to 1 to 1 binding between dopamine and sodium borate and 178.06810 m/z was also the 1 to 1 binding complex but the amine group was involved to form a eight-member cyclic structure which was of interest and not anticipated. The free ionized dopamine was observed at 152.07170 m/z. Also, L-DOPA and sodium borate binding complexes showed two forms of existence (m/z: 240.06849 and 220.05793) and its free ionized molecule appeared at m/z 196.0794. (*Figure 2-25*)

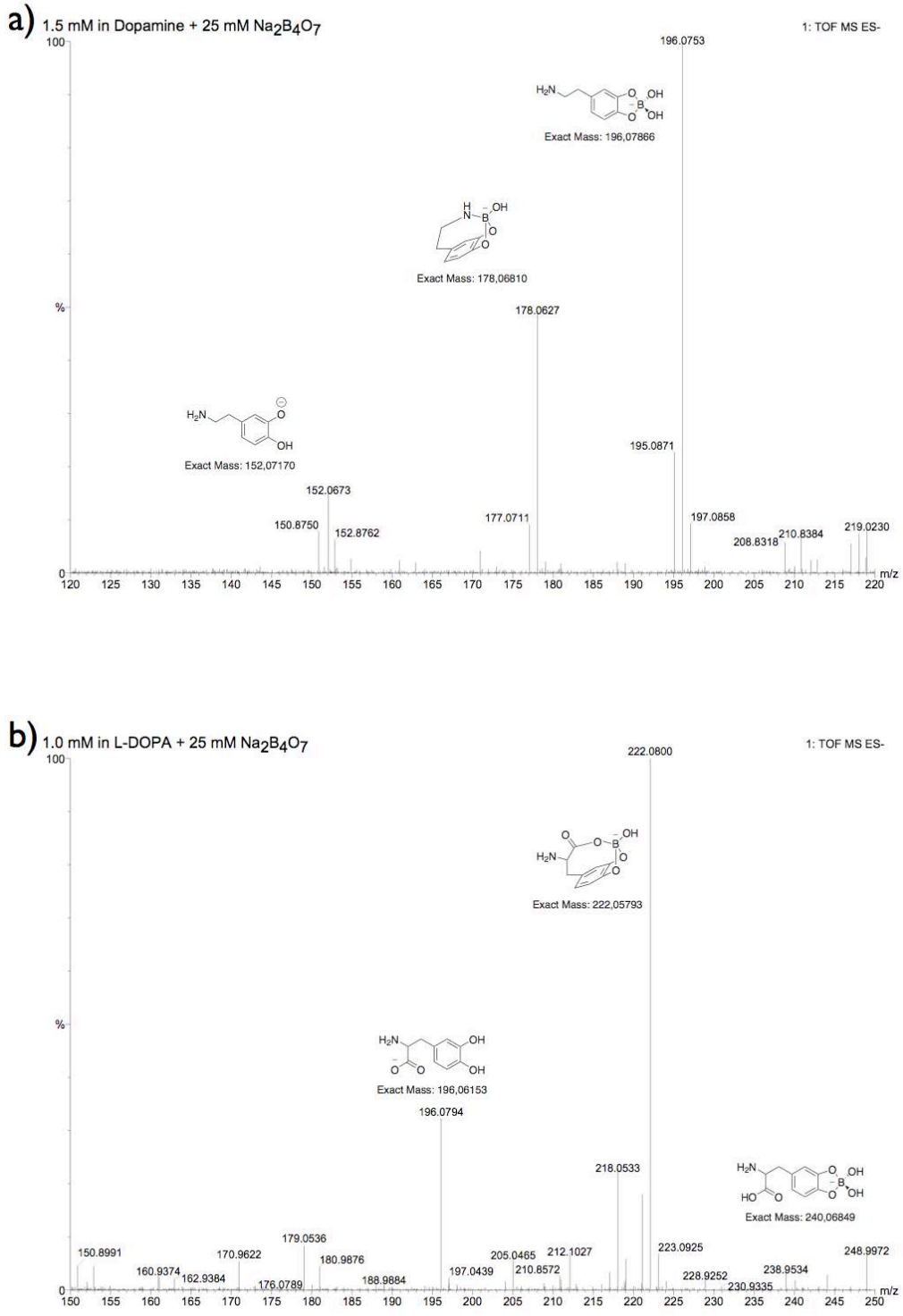

Figure 2-25. MS spectra showing the presence of 1:1 complexes formed between a) dopamine and b) L-DOPA and $Na_2B_4O_7$. Complexes for MeO-β-glucopyranoside could not be detected under the same conditions.

2.2.3 Binding confirmation by ^{11}B-NMR

The observation of complex formation was also confirmed by ^{11}B-NMR. B-diol complexes could not be detected in the case of any of the monosaccharides analyzed. For instance, complexes for MeO-β-glucopyranoside could not be detected even in the presence of 30 eq of the saccharide. ^{11}B-NMR technique confirmed the presence of 1:1 and 1:2 complexes between boric acid and dopamine or L-DOPA. As shown, the peak at 18.3 ppm corresponded to the excess of $Na_2B_4O_7$. With increasing addition of catechols, a signal appeared at 6.9 ppm (dopamine) and 7.9 ppm (L-DOPA) for formation of 1:1 complex. As more catechol was added, a second peak at 12.4 ppm (dopamine) or 13.5 ppm (L-DOPA) became predominant and represented 1:2 complexes. With the molar ratio of catechol : borate of approximately 2:1, the sodium borate peak (18.3 ppm) disappeared. Theoretically, only the peak assigned to the 2:1 complex should remain. The limitation of aqueous solubility of the catechols did not allow confirmation of 2:1 complex formation in all cases.

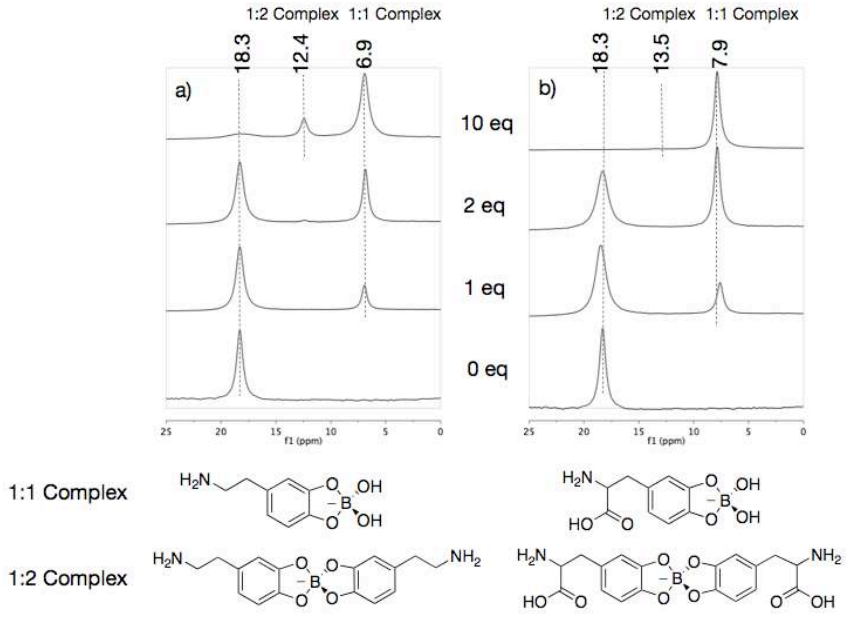

Figure 2-26. ^{11}B-NMR of $N_2B_4O_7$ titration with different amounts of a) dopamine and b) L-DOPA

The ability of the catechol molecules to quench the 'active' AI-2 (**1**) (*Figure 2-1*) was also verified using ^{11}B-NMR. When a solution of DPD in a borate/phosphate buffer at pH 7.4 was treated with 2 eq of the catechols, complete suppression of the signals at 4.8 and 6.2 ppm, corresponding to the AI-2 (**1**) (*Figure 2-1*),[24] occurred, while new signals at 6.9 and 7.9 ppm, assigned to the dopamine and L-DOPA 1:1 to sodium borate complexes respectively, could be observed. The peak at 18.3 ppm, corresponding to the excess of $Na_2B_4O_7$ has been left out for a better comparison.

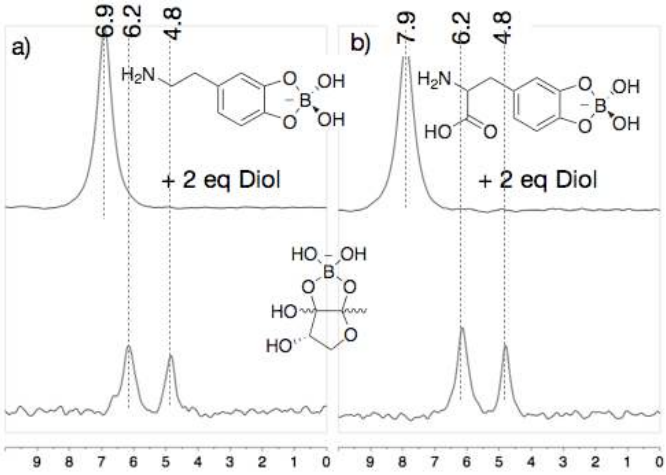

Figure 2-27. Quenching of AI-2 boronated form by a) dopamine and b) L-DOPA as shown by ^{11}B-NMR

2.2.4 Synthesis of diol-monomers

According to the above assay results, catechols were demonstrated to give highest affinities to boric and boronic acid among all the small molecules analyzed, DMAm[22] and L-DMAm[22] were therefore synthesized as the monomer candidates. Specifically, L-DMAm was designed to confer better water-solubility in neutral aqueous solutions, as DMAm was reported to be insoluble in such conditions.[22b] L-DMAm is a monomer product whose synthesis has not been published before and was prepared based on the previous report for synthesis of DMAm.[22b] The reaction was performed under moderately basic conditions between 3,4-dihydroxy-L-phenylamanine (L-DOPA) and methacrylic anhydride in an aqueous solution of saturated sodium borate and sodium bicarbonate. The presence of sodium borate was aimed to protect the catechol moiety by forming a transient borate ester. The synthesized L-DMAm monomer was a water-soluble solid white powder. The final product was fully characterized by ^{1}H-NMR, ^{13}C-NMR (*Figure 2-28*), MS spectrum and FT-IR (see **Appendix**).

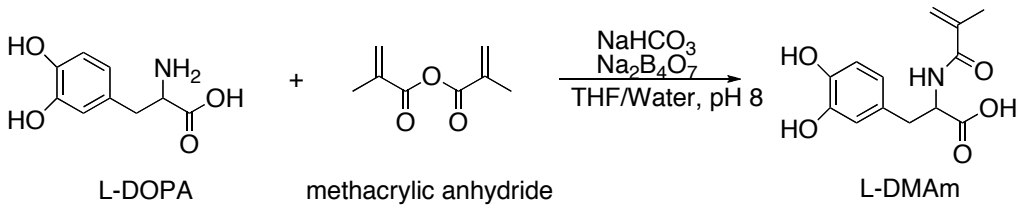

L-DOPA methacrylic anhydride L-DMAm

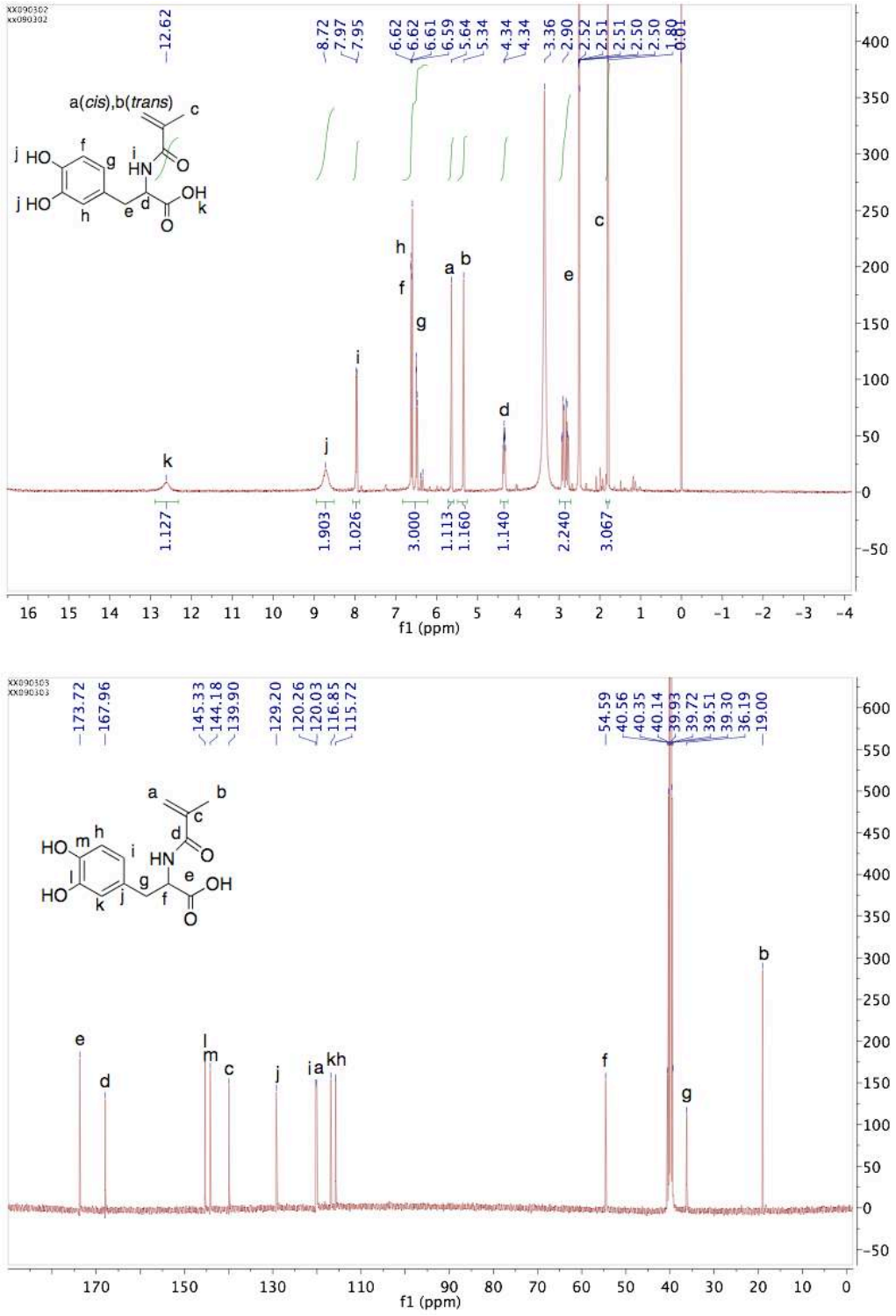

Figure 2-28. ^{1}H NMR (upper) and ^{13}C NMR (bottom) spectrum of L-DMAm in DMSO-d_6

2.3 Conclusions

In this chapter, representative diols were investigated as potential AI-2 scavengers via reversible ester formation with boric and boronic acids, with special attention to carbohydrate derivatives. Titration studies at pH 7.4 using the AR-S assay established binding affinities for boron-diol species, which were in accord with prior reports i.e.: linear diols < cyclic diols (sugars) < aromatic diols or catechols.[9, 23] Even though DPD has a similar structure to carbohydrates, its affinity was much higher than that obtained for the other saccharides analyzed, and only the catechols gave comparable affinities. These observations were confirmed by using mass spectrometry and ^{11}B-NMR spectroscopy.

These experiments suggested that dopamine was the best candidate for polymeric QS control, showing a similar affinity for boron compared to DPD and the potential ability to decrease the concentration of AI-2 (**1**) (*Figure 2-1*) in solution. Two catechol monomers with different water-solubility were therefore synthesized and characterized in order to be ready for the polymer synthesis.

References

[1] S. Raina, D. De Vizio, M. Odell, M. Clements, S. Vanhulle, T. Keshavarz, *Biotechnol Appl Biochem* **2009**, *54*, 65-84.

[2] aB. L. Bassler, *Cell* **2002**, *109*, 421-424; bC. M. Waters, B. L. Bassler, *Annu Rev Cell Dev Biol* **2005**, *21*, 319-346; cP. Williams, K. Winzer, W. C. Chan, M. Camara, *Philos Trans R Soc Lond B Biol Sci* **2007**, *362*, 1119-1134; dX. Chen, S. Schauder, N. Potier, A. Van Dorsselaer, I. Pelczer, B. L. Bassler, F. M. Hughson, *Nature* **2002**, *415*, 545-549.

[3] B. L. Bassler, M. Wright, M. R. Silverman, *Mol Microbiol* **1994**, *13*, 273-286.

[4] S. T. Miller, K. B. Xavier, S. R. Campagna, M. E. Taga, M. F. Semmelhack, B. L. Bassler, F. M. Hughson, *Mol Cell* **2004**, *15*, 677-687.

[5] aJ. Yoon, A. W. Czarnik, *J Am Chem Soc* **1992**, *114*, 5874-5875; bK. Kondo, Y. Shiomi, M. Saisho, T. Harada, S. Shinkai, *Tetrahedron* **1992**, *48*, 8239-8252; cS. Liu, U. Wollenberger, J. Halamek, E. Leupold, W. Stocklein, A. Warsinke, F. W. Scheller, *Chemistry* **2005**, *11*, 4239-4246.

[6] aR. Pizer, L. Babcock, *Inorganic Chemistry* **1977**, *16*, 1677-1681; bL. Babcock, R. Pizer, *Inorganic Chemistry* **1980**, *19*, 56-61; cE. Pezron, A. Ricard, F. Lafuma, R. Audebert, *Macromolecules* **1988**, *21*, 1121-1125; dE. Pezron, L. Leibler, F. Lafuma, *Macromolecules* **1989**, *22*, 2656-2662; eP. C. Harris, *Journal of Petroleum Technology* **1993**, *45*, 264-269.

[7] M. Rietjens, P. A. Steenbergen, *European Journal of Inorganic Chemistry* **2005**, 1162-1174.

[8] S. Iwatsuki, S. Nakajima, M. Inamo, H. D. Takagi, K. Ishihara, *Inorganic Chemistry* **2007**, *46*, 354-356.

[9] G. Springsteen, B. H. Wang, *Tetrahedron* **2002**, *58*, 5291-5300.

[10] aY. Qin, B. Peng, *Anal Chem* **2008**, *80*, 6137-6141; bJ. Tan, H. F. Wang, X. P. Yan, *Anal Chem* **2009**, *81*, 5273-5280.

[11] aP. C. Trippier, C. McGuigan, J. Balzarini, *Antivir Chem Chemother* **2010**, *20*, 249-257; bP. C. Trippier, J. Balzarini, C. McGuigan, *Antivir Chem Chemother* **2011**, *21*, 129-142.

[12] J. Balzarini, *Antivir Chem Chemother* **2007**, *18*, 1-11.

[13] R. Wannapob, P. Kanatharana, W. Limbut, A. Numnuam, P. Asawatreratanakul, C. Thammakhet, P. Thavarungkul, *Biosens Bioelectron* **2010**, *26*, 357-364.

[14] R. Nishiyabu, Y. Kubo, T. D. James, J. S. Fossey, *Chem Commun (Camb)* **2011**, *47*, 1106-1123.

[15] aA. J. Tong, A. Yamauchi, T. Hayashita, Z. Y. Zhang, B. D. Smith, N. Teramae, *Anal Chem* **2001**, *73*, 1530-1536; bT. D. James, P. Linnane, S. Shinkai, *Chemical Communications* **1996**, 281-288; cM. Yamamoto, M. Takeuchi, S. Shinkai, *Tetrahedron* **1998**, *54*, 3125-3140.

[16] K. S. Suslick, C. J. Musto, *Curr Opin Chem Biol* **2010**, *14*, 758-766.

[17] D. Palit, H. Pal, T. Mukherjee, J. Mittal, *J Chem Soc, Faraday Trans* **1990**, *86*, 3861-3869.

[18] aJ. N. Weiss, *FASEB J* **1997**, *11*, 835-841; bN. Sakai, S. Matile, *J Am Chem Soc* **2003**, *125*, 14348-14356.

[19] B. H. Wang, Y. F. Cheng, N. T. Ni, W. Q. Yang, *Chem-Eur J* **2010**, *16*, 13528-13538.
[20] aD. H. Kim, B. N. Marbois, K. F. Faull, C. D. Eckhert, *J Mass Spectrom* **2003**, *38*, 632-640; bS. Z. Ackloo, P. C. Burgers, B. E. McCarry, J. K. Terlouw, *Rapid Commun Mass Spectrom* **1999**, *13*, 2406-2415.
[21] G. Springsteen, B. Wang, *Chem Commun (Camb)* **2001**, 1608-1609.
[22] aH. Lee, B. P. Lee, P. B. Messersmith, *Nature* **2007**, *448*, 338-341; bP. Glass, H. Chung, N. R. Washburn, M. Sitti, *Langmuir* **2009**, *25*, 6607-6612.
[23] J. P. Lorand, J. O. Edwards, *J Org Chem* **1959**, *24*, 769-774.
[24] aM. F. Semmelhack, S. R. Campagna, C. Hwa, M. J. Federle, B. L. Bassler, *Org Lett* **2004**, *6*, 2635-2637; bM. F. Semmelhack, S. R. Campagna, M. J. Federle, B. L. Bassler, *Org Lett* **2005**, *7*, 569-572.

Chapter 3. Preparation and Characterization of Linear Polymers: Dual-action Polymers for Simultaneous Bacterial Sequestration and Quorum Sense (QS) Interference

3. Introduction

Invasive bacteria gain their access to the intracellular milieu through actively inducing their own uptake, and subsequently exploit the host's immune system, replicate and also disseminate in an actin-based motility process between host cells.[1] Although the entry mechanisms and their intracellular life cycle may vary from different bacterial species,[1] bacterial adhesion is the initial step in colonization and the formation of biofilm.[2] Therefore, anti-adhesion strategies have been developed to reduce contact between host and pathogens, by the means of preventing adhesion of the potential intruders.[3] Hori and Matsumoto[2] suggested that antimicrobial agents (antibiotics, oxidants and biocides) could be employed in advance of biofilm formation in order to control bacterial adhesion effectively, but the limitations of their utilization in anti-infection, such as the need for high concentrations to achieve an effective therapy as well as harmful by-products, and also the occurrence of bacterial resistance invoked from their continuous administration, were also described.

Significantly, the disconcerting fact on therapeutics of infectious pathogens is the appearance of resistance in response to selection pressure by drugs and the possible discontinuation of current drug regimens.[4] The general mechanisms of resistance are mutation, recombination, or horizontal gene transfer.[5] Compared to the other two strategies, mutation is an approach to give rise to resistance in almost every disease, while the use of antimicrobials is a powerful selective force for promoting the emergence of resistant mutants in

epidemiological history.[6] Additionally, the prolonged use of antibiotics clearly causes the cumulative effect of resistance to the whole organisms, and thus asymptomatic colonization typically happens even before infection.[7] On the other hand, some researchers noticed that the resistance in bacteria invoked by antibiotics has become a global issue.[8] Evolution of multidrug resistance (MDR) has increased as a result of excessive antibiotic use and environmental factors (greater movement of people and increased industrialization).[8]

As noted earlier, synthetic polymers that interfere with bacteria-host interactions are an attractive approach for controlling infectious diseases without selection pressure and resistance invoked in bacteria by antibiotics, since adhesion of bacteria to tissues of host is one of the initial stages of the infectious process and resistance are seldom arisen by non-bactericidal materials.[3] In this study, the 'smart' polymer materials combined dual-actions of bacterial sequestration and at the same time interfering with bacterial QS signalling, will be developed (*Figure 3-1*).

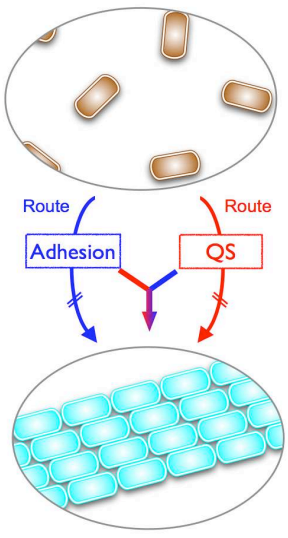

Figure 3-1. The scheme of investigated polymers interfering with both communication mechanism (QS Route, red) and cell adhesion/aggregation (Adhesion Route, blue) at the same time in anti-infective strategies

In this chapter, polymers are designed to attach to *Vibrio* species (such as the human pathogen *V. cholera*), while at the same time binding specific autoinducers for QS. For this, marine bacterium *V. harveyi* is selected as the bacterial model, because QS in this species not only controls virulence but also bioluminescence, thereby facilitating readout of the effects of polymers on the QS network. It is considered that if polymers are able to bind bacteria while at the same time sequester borate, the levels of 'active' AI-2 should be reduced and QS, as reported by bioluminescence, should be suppressed.

Bacteria strongly bind cationic surfaces[9] and glycopolymers[10], but less is known about the ability of polymers to quench AI-2 in *Vibrio* species.[11] As discussed in **Chapter 2**, dopamine was found to be the best candidate for polymeric QS control, showing a similar affinity for boron compared to DPD and the ability to decrease the concentration of AI-2 in solution. To test for effects on both bacterial adhesion and QS interference, DMAm[12] will be copolymerized with N-[3-(dimethylamino)propyl]methacrylamide (DMAPMAm) to form a cationic polymer. The amine functionality is designed to confer water solubility at neutral pH and bacterial adhesion, as well as coordinate boronic acids.[13] Since dopamine and L-DOPA showed similar affinities for borate, L-DMAm will be polymerized, thereby generating novel anionic water-soluble homopolymers, which should bind AI-2 strongly but attach less readily to bacterial surfaces because of charge-charge repulsion. Also, carbohydrate-based poly(β-D-glucosyloxyethyl methacrylate) (p(GlcEMA)) will be used in bacterial assays, for it showed a highly active bacterial sequestration ability in prior assays.[14]

Structures of Dual-action Linear Polymers Investigated in this Chapter:

Polymer **1**

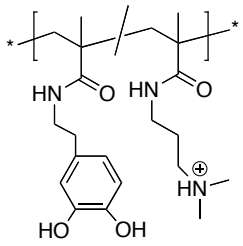

DMAm : DMAPMAm
a: 14 : 86; **b**: 29 : 71

Polymer **2**

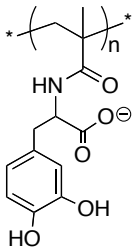

a: n = 15; **b**: n = 26

Polymer **3**

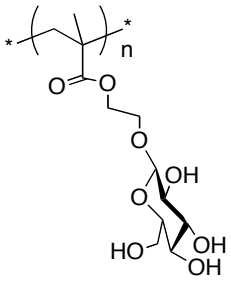

n = 16

3.1 Experiments

3.1.1 Synthesis of polymers

General protocol for RAFT polymerization:[15]

Polymerizations were conducted in round bottom flasks sealed with a rubber septum and parafilm. An NMR spectrum was recorded at the beginning of the experiment. The polymerization solutions were degassed using argon for at least 10 min and transferred to an oil bath preheated to 70 °C. After reaction, the solution was quenched by cooling in ice-water and opening to air. Another NMR spectrum was recorded to enable calculation of degree of conversion. For the removal of CTA, the reaction was carried out at 70 ºC, and the absence of CTA was confirmed by UV spectroscopy.

3.1.1.1 p(DMAm): poly(N-dopamine methacrylamide)

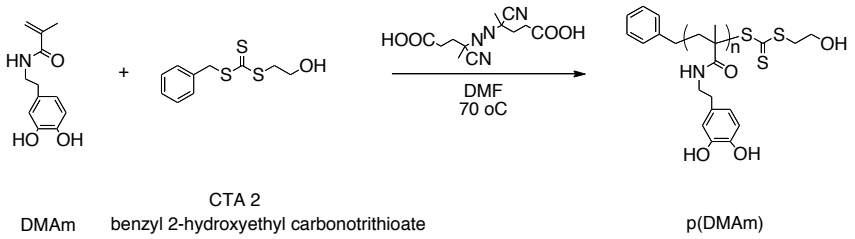

DMAm — CTA 2 benzyl 2-hydroxyethyl carbonotrithioate

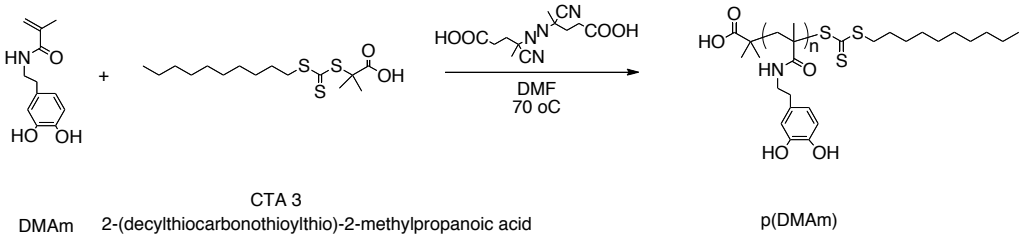

DMAm — CTA 3 2-(decylthiocarbonothioylthio)-2-methylpropanoic acid

In a typical experiment, DMAm (500 mg, 2.3 mmol, 2.7 M) in DMF (0.84 mL), CTA (0.023 mmol, 0.12 M) in DMF (0.19 mL) and V-501 (3.2 mg, 0.011 mmol, 0.060 M) in DMF (0.19 mL) were prepared separately and then mixed together (to make a final 0.27 M concentration of DMAm). The polymerization was carried out overnight.

3.1.1.2 p(DMAm-*c*-DMAPMAm): poly{N-(3,4-dihydroxyphenethyl) methacrylamide-co-N-[3-(dimethylamino)propyl] methacrylamide}

- Polymer 1

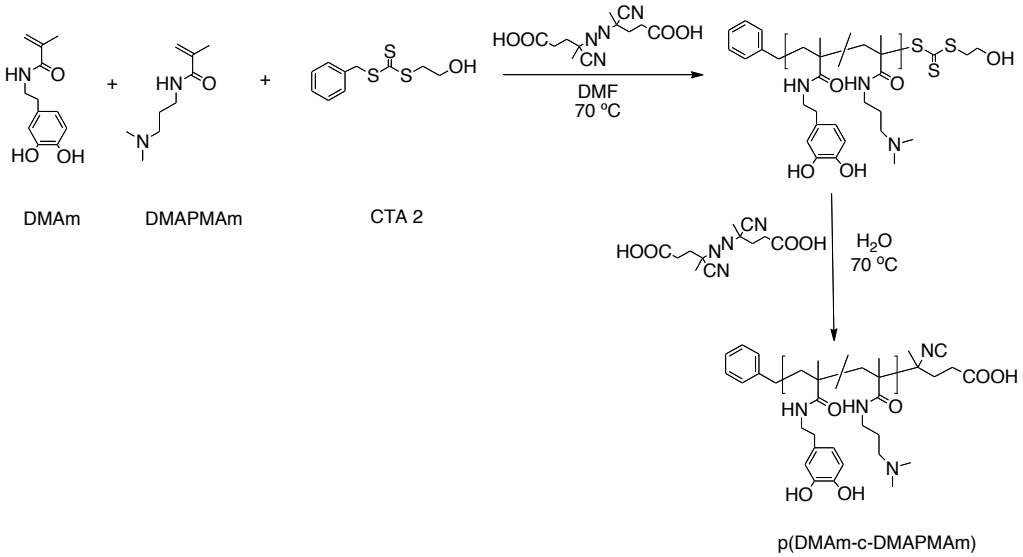

DMAm — DMAPMAm — CTA 2

p(DMAm-c-DMAPMAm)

In a typical experiment, DMAm (50 mg, 0.23 mmol, 2.5 M) in DMF (0.091 mL), N-[3-(dimethylamino)propyl] methacrylamide (DMAPMAm) (0.37 mL, 2.0 mmol), CTA (5.5 mg, 0.023 mmol, 0.12 M) in DMF (0.19 mL) and V-501 (3.2 mg, 0.011 mmol, 0.060 M) in DMF (0.19 mL) were prepared separately and then mixed together (to make a final 0.27 M concentration of DMAm). The polymerization was carried out overnight. The polymer products were purified by dialysis against water and recovered as a light brown powder (0.18 g, 45 %) after freeze-drying from water (dark, 2 days). Solutions of the polymer (148 mg, 0.019 mmol, 0.010 M) in H_2O (1.8 mL) and V-501 (151 mg, 0.54 mmol, 1.4 M) in ethanol (0.40 mL) were prepared separately and then mixed together (to make a final ratio 1 : 30 of polymer to initiator). In order to remove CTA, this mixture was degassed and allowed to react at 80 ºC overnight. The title compound p(DMAm-co-DMAPMAm) was purified by dialysis against water and recovered as a light brown powder (0.12 g, 81 %) after freeze-drying from water (dark, 2 days) ^{1}H-NMR (D_2O/TFA 5 : 1, 400 MHz) δ (ppm) 7.55-6.36 (*m*, 3H, Ar-H), 3.52-3.34 (*m*, 2H, CH_2-N DMAm), 3.33-2.95 (*m*, 4H, CH_2-N DMAPMAm), 2.93-2.66 (*m*, > 8H, N-CH_2-$C\underline{H_2}$ DMAm + CH_3 DMAP), 2.15-1.53 (*m*, > 5H, CH_3-MAm + HN-CH_2-$C\underline{H_2}$-DMAPMAm), 1.24-0.63 (*m*, 2H, CH_2-MAm backbone) Mw (GPC) 6.6 KDa, PDI (GPC) 1.05.

- Macro-CTA-1 (polymer 1 with active trithiocarbonate end group)

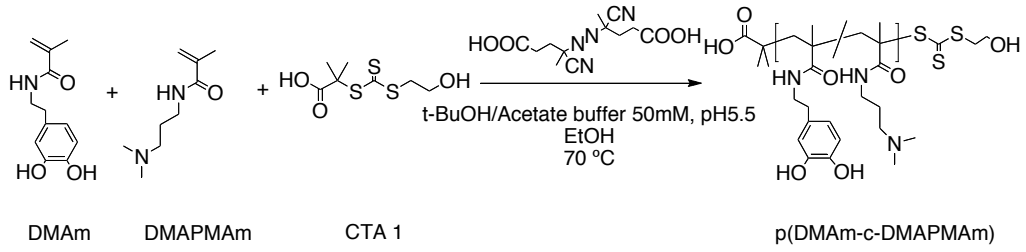

In a typical experiment, DMAm (150 mg, 0.68 mmol, 0.21 M) in t-BuOH/acetate buffer (50 mM, pH 5.5, 0.62 mL), N-[3-(dimethylamino) propyl] methacrylamide (DMAPMAm) (1.1 mL, 6.1 mmol), RAFT agent (17 mg, 0.068 mmol, 0.12 M) in EtOH (0.57 mL) and V-501 (3.8 mg, 0.014 mmol, 0.060 M) in EtOH (0.23 mL) were prepared separately and then mixed together. The pH of mixture was ajusted with HCl (10 M, 0.50 mL; 5.0 M, 0.070 mL) and NaOH (4.0 M, 0.15 mL) to 5.5 and to make a final 0.21 M concentration of DMAm. The polymerization was carried out overnight. The macro-RAFT agent compound p(DMAm-*c*-DMAPMAm) was purified by dialysis against water and recovered as a light brown powder (0.40 g, 33%) after freeze-drying from water (dark, 2 days). ^{1}H-NMR (D_2O, 400 MHz) δ (ppm) 6.83-6.40 (*m*, 3H, Ar-H), 3.18-2.89 (*m*, 2H, CH_2-N-DMAm), 2.79-2.56 (*m*, 4H, CH_2-N-DMAPMAm), 2.56-2.22 (*m*, >8H, N-CH_2-$\underline{CH_2}$-DMAm + CH_3-DMAP), 1.94-1.43 (*m*, >5H, CH_3-MAm + HN-CH_2-$\underline{CH_2}$-DMAPMAm), 1.11-0.53 (*m*, 2H, CH_2-MAm backbone) Mw (GPC) 12.9 KDa, PDI (GPC) 1.36

3.1.1.3 p(L-DMAm): poly(3,4-dihydroxy-L-phenylalanine methacrylamide)

- Polymer 2

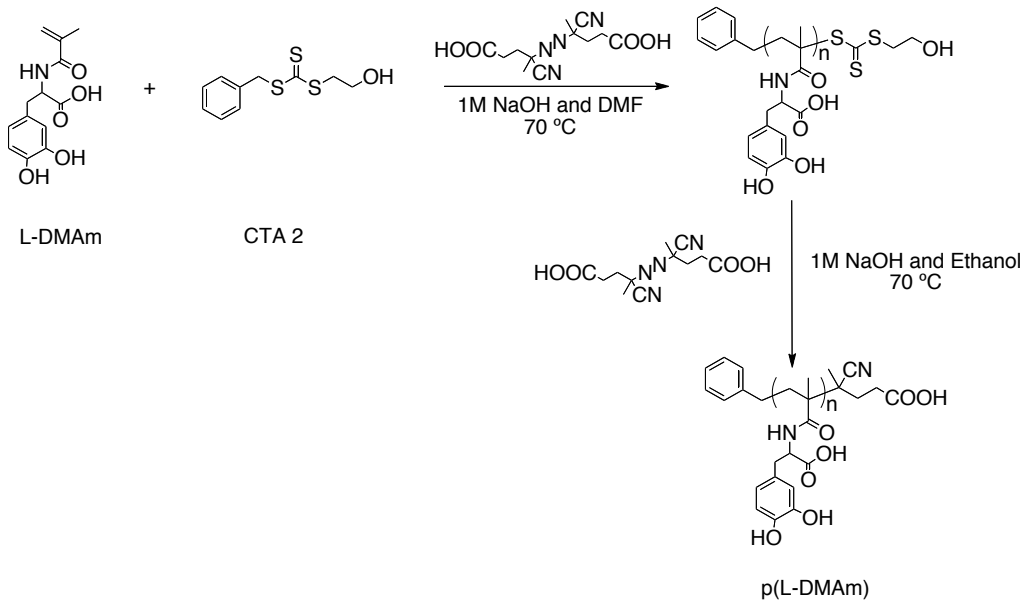

In a typical experiment, L-DMAm (500 mg, 1.9 mmol, 3.1 M) in sodium hydroxide (1.0 M, 0.62 mL), CTA (23 mg, 0.094 mmol, 0.12 M) in DMF (0.79 mL) and V-501 (13 mg, 0.047 mmol, 0.060 M) in DMF (0.79 mL) were prepared separately and then mixed together (to make a final 0.86 M concentration of L-DMAm). The polymerization was carried out overnight. The polymer products were purified by dialysis against water and recovered as a white powder (0.31 g, 62 %) after freeze-drying from water (dark, 2 days). Solutions of the polymer (310 mg, 0.079 mmol, 0.020 M) in NaOH solution (0.12 M, 3.4 mL) and V-501 (663 mg, 2.4 mmol, 1.7 M) in ethanol (1.4 mL) were prepared separately and then mixed together (to make a final ratio 1:30 of polymer to initiator). In order to remove CTA, this mixture was degassed and allowed to react at 80 ºC overnight. The title compound p(L-DMAm) was purified by dialysis against water and recovered as a white powder (0.23 g,

74 %) after freeze-drying from water (dark, 2 days) ^{1}H-NMR (D_2O/NaOH (1.0 M) 5 : 1, 400 MHz) δ (ppm) 7.44-5.80 (*m*, 3H, Ar-H), 4.38-3.76 (*m*, 1H, N-CH), 3.23-1.90 (*m*, > 5H, CH-C<u>H</u>$_2$ + CH_3-MAm), 1.83-0.00 (*m*, 2H, CH_2-MAm backbone).

3.1.2 Synthesis of Reversible Addition-Fragmentation Chain Transfer (RAFT) Agent / (CTA)

3.1.2.1 2-((2-hydroxyethylthio)carbonothioylthio)-2-methylpropanoic acid[16]

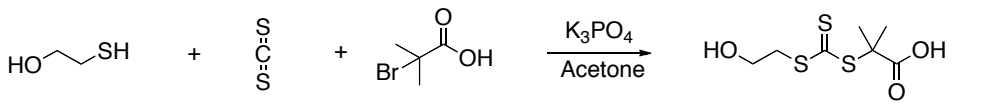

2-mercaptoethanol carbon disulfide 2-bromoisobutyric acid 2-((2-hydroxyethylthio)carbonothioylthio)-2-methylpropanoic acid

2-mercaptoethanol (2.0 g, 25 mmol) and a suspension of K_3PO_4 (6.0 g, 28 mmol) were mixed in acetone (60 mL) and stirred for 10 min. CS_2 (5.2 g, 68 mmol) was added to the above mixture. After 10 min stirring, 2-bromoisobutyric acid (4.2g, 25 mmol) was added. The mixture was stirred for 13 hour (overnight). The solution was bubbled under N_2 for 30 min to remove CS_2. Solvent was removed under reduced pressure. The residue was extracted into CH_2Cl_2 from 1.0 M HCl and washed with H_2O and NaCl (Sat). Again, the solvent was removed under reduced pressure. The crude product was purified by column chromatography on silica using ethyl acetate/hexane gradient ratio from 2 : 1 to 3 : 2 to yield a bright yellow solid (17 %) that crystallized upon cooling. ^{1}H-NMR ($CDCl_3$, 400 MHz) δ (ppm) 4.96 (*br*, 1H, <u>H</u>O-CH_2-CH_2), 3.89 (*t*, *J* = 6.4 Hz, 2H, HO-C<u>H$_2$</u>-CH_2), 3.55 (*t*, *J* = 6.4, 2H, HO-CH_2-C<u>H$_2$</u>), 1.75 (*s*, 6H, CH_3).

3.1.3 Binding affinities for boron using Alizarin Red S (AR-S) assay

Similarly to small molecule analysis, in order to calculate the binding affinities between the boronic acids and polymers investigated in this work, Solution B and Solution C (containing the same concentration of AR-S and boronic acid as Solution B and at least 20 eq of the diol) were mixed in different ratios in order to make varying solutions with a constant concentration of both AR-S and boric/boronic acid, and a range of concentrations of the diols. At least 6 different solutions were made in order to cover as much of the binding curve as possible. The experiments were carried out in triplicate and the fluorescence intensities were measured with an excitation wavelength of 468 nm. For the polymers, due to their multivalent nature, binding affinities (K_a) were determined using the Hill Equation (**Eq. 1**), where ΔI_f is again the change in fluorescence intensity, ΔI_∞ the change in fluorescence upon saturation, and n is the Hill coefficient.[17]

Equation 1

$$\Delta I_f = \frac{\Delta I_\infty}{1 + [\frac{1}{[Diol] \cdot K_a}]^n}$$

3.1.4 Binding confirmation by ^{11}B-NMR

A 25 mM solution of $Na_2B_4O_7$ was prepared in phosphate buffer (250 mM, pH 7.4) and 10% in volume of D_2O was added. This borate/phosphate buffer was used to prepare samples with different amounts of the diols of interest and NMR spectra were acquired for each of them. A collection of 128 scans was averaged for each spectrum with a 0.20 s recycle time.

For the competitive binding experiments, a 20 mM solution of DPD was prepared in borate/phosphate buffer (25 mM, 100 mM, pH 7.4, 10% in D_2O) and an NMR spectrum was recorded. Polymers were then dissolved in this DPD solution and a new NMR spectrum was recorded.

3.1.5 Bacterial aggregation assay

3.1.5.1 UV spectrum

V. harveyi MM32 grown on Luria Bertani (LB) agar plate containing kanamycin (50 μg/ml) and chloramphenicol (10 μg/ml), were used to inoculate 2 mL Assay Broth (AB) from a fresh plate. The bacteria were then grown with aeration at 30ºC overnight. 285 μL of the medium were placed in a UV cuvette and combined with 15 μL of the samples to be analyzed. Optical density (OD, 600 nm) was recorded at 30 ºC every 30 seconds for at least 40 min. Because of the difficulties found in reproducing exactly the same initial bacteria conditions, experiments were carried out in duplicate. Aggregation Index ($\boldsymbol{X_{Ag}}$) was determined using **Eq. 2**, where *[P]* was the concentration of polymer expressed in weight percentage and *%Ag*, the percentage of aggregation of each sample calculated according to **Eq. 3**. Because of *V. Harveyi's* fast sedimentation, its aggregation was subtracted from that observed in the presence of polymers. For a better comparison $\boldsymbol{X_{Ag}}$ has been normalized to the lowest value.

LB Medium: 10 g/L of tryptone, 5 g/L of yeast extract and 10 g/L of NaCl. AB Medium: 0.3 M NaCl, 0.05 M $MgSO_4 \cdot 7H_2O$, 0.2% vitamin-free casamino acids, 1 mM L-arginine, 1% glycerol, 0.01 M K_2HPO_4, pH 7.0. Both Solutions are autoclaved at 120 ºC for 20 min.

Equation 2

$$X_{Ag} = \frac{\%Ag}{[P]}$$

Equation 3

$$\%Ag = \frac{OD_0 - OD}{OD_0}$$

Aggregation was also investigated in PBS (10 mM, pH 7.4). This way, *V. Harveyi* were sampled in the midexponential phase, washed twice, and resuspended in sterile PBS to a final OD (600 nm) of ~1.9. This medium were placed in UV cuvettes and combined with the polymer water solution to be analyzed. The final concentration of polymers were 0.25 mg/mL in all cases, except poly (β-D-glucosyloxyethyl methacrylate) (p(GlcEMA) (Polymer **3**) which was set to 0.05 mg/mL due to the limited amount of material.

In order to investigate the effect of polymer concentration, the same experimental procedure was undertaken, but the cell suspension in PBS and a p($DMAm_{14}$-co-$DMAPMAm_{86}$) (Polymer **1a**) solution were mixed in different ratios in order to make different solutions with a range of concentrations of the polymer. In addition, aggregation in the presence of different concentrations of PVA was also investigated.

3.1.5.2 Microscopy

For optical microscopy, Aliquots (10 μL) of the previous samples in AB medium were collected with a micropipette, mounted on a glass slide with a cover slip on top and examined with an optical microscope.

3.1.6 Bioluminescence assay with *V. harveyi* species

3.1.6.1 MM32 assay

Protocol 1:

1. Vibrio harveyi MM32 was grown from frozen stock in LB medium (2 mL) with kanamycin (antibiotic, 30 μg/mL) at 30 °C, shaking in an incubator overnight.

2. 50% glycerol (400 μL), K_2HPO_4 (200 μL of 1 M) and arginine (200 μL of 0.1 M) were added to 19.0 mL of autoinducer bioassay media (AB medium, see below), and inoculated with 4 μL of the overnight culture of MM32. DPD (195 μL of 2.27 mM commercial available) filtered through sterile membrane (0.2 μM) was added into the above media to have a concentration of 22 μM.

3. 180 μL aliquots were placed in a 96 well plate.

4. 20 μL of supernatants were added to the aliquots of inoculated AB media, separately (triplicate for each supernatant sample), such that DPD reached a final concentration of 19.9 μM.

5. A 96-well plate was then put in a combined luminometer/spectrometer, recording OD (600 nm) and light output every 30 minutes for 22 h.

(AB medium: sodium chloride (17.52 g/L), $MgSO_4$ (12.33 g/L) and casamino acids (2.0 g/L), pH adjusted to 7.5 with KOH.)

Protocol 2: - Boron concentration controlled

1. Vibrio harveyi MM32 was grown from frozen stock in LB medium (2mL) with kanamycin (antibiotic, 30μg/mL) at 30 °C, shaking in an incubator overnight.

2. 50% glycerol (400 μL), $B(OH)_3$ (300 μL of 29.6 mM, 11.3 mg/mL), K_2HPO_4 (200 μL of 1M) and arginine (200 μL of 0.1M) were added to 18.7 mL of autoinducer bioassay media (AB medium, see below), and inoculated with 4 μL of the overnight culture of MM32. DPD (195 μL of 2.27 mM commercial available) filtered through sterile membrane (0.2 μM) was added into the above media to have a concentration of 22 μM.

3. 180 μL aliquots were placed in a 96-well plate.

4. 20 μL of supernatants were added to the aliquots of inoculated AB media, separately (triplicate for each supernatant sample) 4 h after keeping 96-well plate in 30 °C incubator, so that DPD reached a final concentration of 19.9 μM and $B(OH)_3$ reached a final concentration of 400 μM.

5. A 96-well plate was then put in a combined luminometer/spectrometer, recording OD (600 nm) and light output every 30 minutes for 22 h.

(AB medium: sodium chloride (17.52 g/L), $MgSO_4$ (12.33 g/L) and casamino acids (2.0 g/L), pH adjusted to 7.5 with KOH.)

Protocol 3:[18] -Boron concentration and media evaperation controlled

1. Vibrio harveyi MM32 (2.5 μL) was grown from frozen stock in LB medium (5mL) with kanamycin (antibiotic, 50 mg/mL, 5 μL) at 30 °C, shaking in an incubator 12 h. Finally OD was controlled to be 0.9~1.0 (600 nm).

2. 50% glycerol (400 μL), $B(OH)_3$ (300 μL of 29.6 mM, 11.3 mg/mL), K_2HPO_4 (200 μL of 1M) and arginine (200 μL of 0.1 M) were added to 18.7 mL of autoinducer bioassay media (AB medium, see below), and inoculated with 4 μL of the overnight culture of MM32. DPD (195 μL of 2.27 mM

synthesized) filtered through sterile membrane (0.2 μM) was added into the above media to have a concentration of 22 μM.

3. 180 μL aliquots were placed in a 96 well plate.

4. 20 μL of supernatants were added to the aliquots of inoculated AB media, separately (triplicate for each supernatant sample), so that DPD reached a final concentration of 19.9 μM and $B(OH)_3$ reached a final concentration of 400 μM.

5. A 96-well plate was sealed with aluminum cover then put in a combined luminometer/spectrometer, recording OD (490 nm) and light output every 2 h manually for 16 h.

(AB medium: sodium chloride (10.52 g/L), $MgSO_4$ (0.36 g/L) and casamino acids (1.2 g/L), pH adjusted to 7.5 with NaOH.)

Protocol 4: -Boron concentration and media evaperation controlled with modification

a. Borate-depleted procedure:[19]

V. harveyi was grown in borate-depleted autoinducer bioassay (AB) medium. To remove borate, the media were filtered through a borate anion-specific resin, Amberlite IRA743 (Sigma-Aldrich). Specifically, 100 mL of medium was passed three times through 6 mL of resin (suspended in distilled water) and the column was regenerated between each passage according to the method described as follows.[20]

In a plastic separation column, 6 mL of Amberlite resin (suspended in distilled water) was treated, in sequence, with the following: 30 mL 3 mol/L ammonia hydroxide, 120 mL distilled water, 60 mL of 1 mol/L hydrochloric acid, 30 mL distilled water, 60 mL of 0.16 mol/L nitric acid, 120 mL distilled water

followed by 100 mL of media. All liquid was allowed to filter through the resin at an effluent rate of ~2 drops/s. Media were collected in a plastic bottle, filter-sterilized and stored at 4 °C until used.

Following filtration, the pH of the medium was adjusted to 7.5 using KOH made with borate-depleted water.

b. DPD concentration optimization assay

1. *V. harveyi* MM32 was grown from frozen stock in LB medium (2 mL) with kanamycin (antibiotic, 30 μg/mL) at 30 °C, shaking in an incubator overnight.

2. Boron-depleted glycerol (400 μL of 50%, v/v), boron-depleted K_2HPO_4 (200 μL of 1 M) and boron-depleted arginine (200 μL of 0.1 M) were added to 18.9 mL of boron-depleted AB medium.

3. $B(OH)_4$ (300 μL of 29.6 mM, 11.3 mg/mL) made with borate-depleted water and 4 μL of the overnight culture of MM32 were added to above media.

4. 180 μL aliquots were placed in a 96 well plate

5. 20 μL of DPD solution were added to the aliquots of inoculated AB media, separately (triplicate for each DPD concentration), so that $B(OH)_4$ reached a final concentration of 400 μM.

6. A 96-well plate sealed with aluminum tape was incubated for 4 h.

7. A 96-well plate was then put in a combined luminometer/spectrometer, recording OD and light output every 30 minutes for 22 hours.

(AB medium: sodium chloride (17.52 g/L), $MgSO_4$ (12.33 g/L) and casamino acids (2.0 g/L), pH adjusted to 7.5 with KOH.)

c. Polymer assay

1. *V. harveyi* MM32 was grown from frozen stock in LB medium (2 mL) with kanamycin (antibiotic, 30 μg/mL) at 30 °C, shaking in an incubator overnight.

2. Boron-depleted glycerol (400 μL of 50%, v/v), boron-depleted K_2HPO_4 (200 μL of 1 M) boron-depleted arginine (200 μL of 0.1 M), $B(OH)_3$ (prepared from boron-depleted H_2O, 300 μL of 29.6 mM, 11.3 mg/mL) were added to 18.6 mL of boron-depleted AB medium. The overnight culture of MM32 (4 μL, OD adjusted to 1.0) and DPD (119 μL of 3.7 mM) were added to above media. (All of the above solution/media were filtered through sterile membrane (0.2 μM) before mixing.)

3. 180 μL aliquots were placed in a 96 well plate.

5. 20 μL of polymer supernatants were added to the aliquots of inoculated AB media, separately (triplicate for each sample), so that DPD reached a final concentration of 19.9 μM and $B(OH)_3$ reached the final concentration of 400 μM.

6. A 96-well plate sealed with aluminum tape was incubated for 4 h at 30 °C.

7. A 96-well plate was then put in a combined luminometer/spectrometer, recording OD and light output every 30 minutes for 22 hours.

(AB medium: sodium chloride (17.52 g/L), $MgSO_4$. $7H_2O$ (25.18 g/L) and casamino acids (2.0 g/L), pH adjusted to 7.5 with KOH.)

3.1.6.2 BB170 assay

1. BB170 was grown from frozen stock on LB plate with kanamycin (30 μg/mL) at 30 °C.

2. 2 mL overnight culture was set up (LB with Km at 30 μg/mL) inoculating from fresh plate, shaking in an incubator at 30 °C.

3. 50% glycerol (400 μL), HEPES (500 μL of 1 M, pH 7.8), K_2PO_4 (200 μL of 1 M) and arginine (200 μL of 0.1 M) were added to 18.7 mL of autoinducer bioassay media (AB media - sodium chloride 17.52 g/L, $MgSO_4$ 12.33 g/L, casamino acids 2.0 g/L, pH adjusted to 7.5 with KOH, autoclaved), and inoculated with 4 μL of the overnight culture of BB170.

4. 180 μL aliquots were placed in a 96-well plate.

5. 20 μL of supernatants were added to the aliquots of inoculated AB media (triplicate for each supernatant sample and also blank sample)

6. A 96-well plate was then put in a combined luminometer / spectrometer, recording OD and light output every 30 min for 12 h.

3.2 Results and discussions

3.2.1 Polymer synthesis

3.2.1.1 Synthesis of p(DMAm)

P(DMAm) homopolymers was synthesized by using the general polymerization procedure at the very beginning of the project. In the initial reaction conditions, CTP (*Figure 3-5*, **4**) was used as CTA and V-501 was used as a water-soluble initiator. DMAm monomer was initially dissolved in H_2O. CTP and V-501 were dissolved in ethanol to reach the concentration of 0.12 M and 0.06 M respectively as stock solutions. The above three portions were mixed to get a final molar ratio: 100 : 1 : 0.5 (monomer : CTP : V-501) and monomer concentration 0.86 M. After overnight reaction, the mixture was cloudy and hard to dissolve in any solvent. This phenomenon suggested that

polymerization was occurred. However, the polymer produced under these conditions exhibited poor solubility in most of the organic solvents and aqueous solutions. In order to improve polymer solubility, different solvents (e.g. DMF, DMSO, H_2O with $Na_2B_4O_7/Na_2OH$ to adjust pH > 6) were employed to adjust polymerization conditions. The stock solutions of CTA and initiator were fresh made for each polymerization. Also, the oxygen-excluding process was checked and carried out very carefully. Temperature was controlled to be 70 °C all through the reaction. However, the solubility of RAFT-prepared p(DMAm) did not improve in all the tested solutions. On the other hand, p(DMAm) with improved solubility in DMF was made successfully via repeating the standard free radical polymerization conditions reported in the literature.[21]

It was well known that the key to a successful RAFT polymerization was the proper choice of CTA. In this case, the last attempt to improve polymer properties was to use different CTAs. The monomer conversion (calculated by comparing the integration of vinyl proton signals from the monomers to the aromatic groups in ^{1}H-NMR, see **Appendix** for details) was increased to 59.9% and 79.9% by using benzyl 2-hydroxyethyl carbonotrithioate (*Figure 3-5*, **2**) and 2-(dodecylthiocarbonothioylthio)-2-methylpropanoic acid (*Figure 3-5*, **3**) as CTAs, respectively, in DMF solvent. However, the poor solubility of the resultant polymer product in most of the organic solvent (methanol, THF, methylene chloride and dichloromethane) as well as aqueous media at neutral pH was still limited. Therefore, no further work was carried out with this polymer.

3.2.1.2 Synthesis of p(DMAm-*c*-DMAPMAm) hydrophilic statistic copolymers and p(L-DMAm) homopolymers

As discussed above, in order to improve the water-solubility of homo-p(DMAm) polymer in neutral pH as well as testing for effects on both bacterial adhesion and QS interference, two strategies have been explored here: 1) DMAm[12] was copolymerized with DMAPMAm to form a cationic polymer. The amine functionality is designed to confer water solubility at neutral pH and bacterial adhesion, as well as coordinate to boronic acids.[13] 2) Since dopamine and L-DOPA showed similar affinities for borate, L-DMAm was also synthesized and polymerized to homopolymer, thereby generating novel anionic water-soluble homopolymers, which should still bind AI-2 strongly but attach less readily to bacterial surfaces because of charge-charge repulsion.

In order to have different binding affinities to either bacteria surfaces or QS signals, a series of hydrophilic polymers with various monomer composition and/or degree of polymerization were prepared. All the prepared polymers were screened based on their solubility in neutral aqueous media. A series of synthetic polymers with distinct water-solubility was presented in Table **3-1** and **3-2**. However, only polymer **1a**, **1b** (statistic copolymer with randomly polymerized DMAm and DMAPMAm constructions) and polymer **2a**, **2b** (homopolymer) gave promising solubility in water at neutral pH, and therefore remained as potential candidates for dual-intervention of both bacteria to host invasion and QS network. Also, it was notable that the final composition percentage calculated from ^{1}H-NMR (Table **3-1**, values in brackets) of DMAm was bigger than the target value (Table **3-1**, values outside the brackets), while such final composition percentage of DMAPMAm was smaller than its target

one. This gave an insight into kinetics of the polymerization progress that DMAm was polymerized faster than DMAPMAm monomer in the applied conditions. In addition, to optimize polymerization conditions, different CTAs (*Figure 3-5*, **1** and **2**) and solvents (DMF, DMSO, aqueous acetic acid pH 2 with t-butanol) were employed. Finally, the polymerization conditions to prepare p(DMAm-*c*-DMAPMAm)-CTA were modified (t-BuOH and acetate buffer (50 mM) at pH 5.5, with CTA **1** stock solution in EtOH) in order to keep the macro-CTA active to grow the second block of copolymer, because the alkaline conditions are known to quench CTA easily.

Table 3-1

No.	DMAm	DMAPMAm	Conversion (^{1}H-NMR)	Mn (GPC)	PDI
1a [a]	10 % (14 %)	90 % (86 %)	45 %	6633	1.05
1b [a]	20 % (29 %)	80 % (71 %)	35 %	9911	1.05
1c[b]	40 %	60 %	-	-	-
1d[b]	50 %	50 %	-	-	-

[a] The composition percentage in brackets is the final value calculated from ^{1}H-NMR; [b] Polymer products were not dissolved in any solvent available in our lab.

Aqueous GPC was used to characterize polymer **2**. However, it gave poor solubility at pH 7.4 buffer solution and very low concentration remained after being filtered through 0.2 μm membrane. The low solubility of polymers **2** at concentrations needed for GPC prevented them from being characterized by means of aqueous GPC, and therefore the PDI of the polymers could not be calculated. The polymers were also insoluble in other common solvents employed for GPC, such as DMF (0.1% LiBr), $CHCl_3$ or THF. Although the poor solubility of polymer **2** in neutral aqueous media was not expected, the low concentration in solution was assumed to be high enough to interfere with QS and cell activities (see 'aggregation assay' and 'bioluminescence assay').

Table 3-2

No.	Monomer	DP [a]	Conversion (^{1}H-NMR)	Mn [b] (^{1}H-NMR)
2a	L-DMAm	20 (15)	74 %	3934
2b	L-DMAm	40 (26)	66 %	6989
2c	L-DMAm	100 (89)	89 %	23510

[a] The degree of polymerization (DP) in the brackets is the final value calculated from ^{1}H-NMR,
[b] A proper solvent for GPC analysis was not found.

The overall monomer conversion was calculated from ^{1}H-NMR by comparing the vinyl proton signals from the monomers (5.6 and 6.1 ppm) to the overall integration from the aromatic groups (6.5-6.8 ppm). For the copolymers the composition of DMAm in the polymer was calculated from the ^{1}H-NMR spectra of the purified polymer in D_2O, by comparing the integral of the two protons **a**, α to the amido group in DMAm (3.6 ppm) to the protons **c** and **d** in DMAPMAm (3.2 ppm) (*Figure 4-2*).

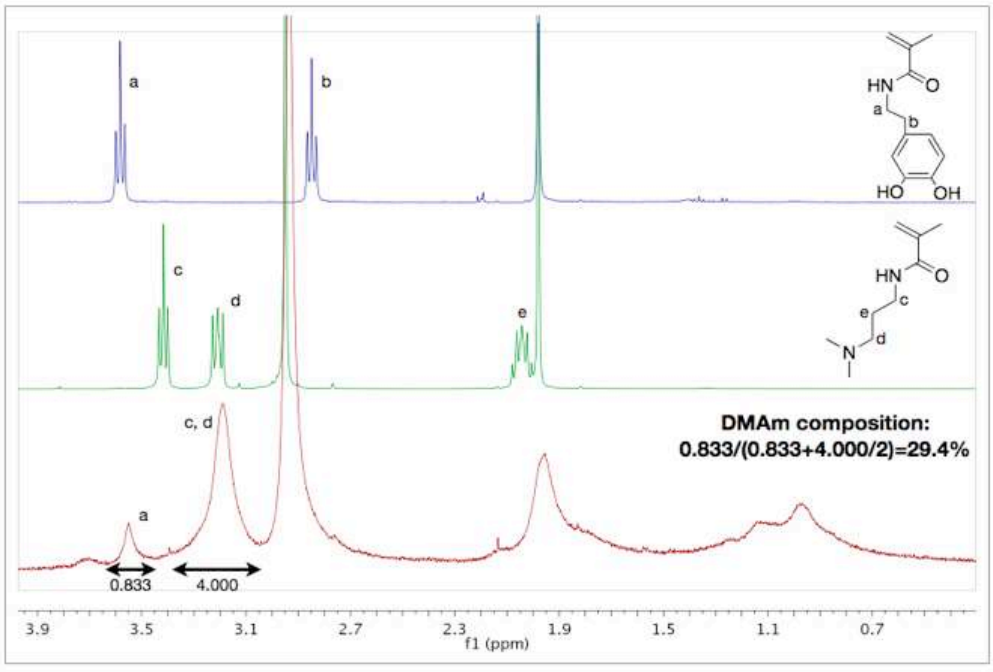

Figure 3-2. Representative example of copolymer composition calculation: ^{1}H-NMR spectra of monomer DMAm (blue) and DMAPMAm (green), and copolymer p(DMAm-*c*-DMAPMAm) - Polymer **1b** (red, bottom) in D_2O.

3.2.2 DLS analysis

Polymers **1** and **2** were also characterized by dynamic light scattering (DLS) in H_2O (*Figure 3-3 and Figure 3-4*). The results indicated that at high concentrations (0.5 mg/ml polymer **1** and 0.2 mg/mL polymer **2**) polymer **1** and **2** led to self-assembled aggregates that resulted in lower diffusion rates. Polymer **1** induced self-aggregation as expected, for DMAm and DMAPMAm shows distinct hydrophilic properties in H_2O. The particles formed from polymer **2** - p(L-DMAm) homopolymers may be attributed to their intrinsic low solubility in neutral aqueous solutions.

Polymer **1**

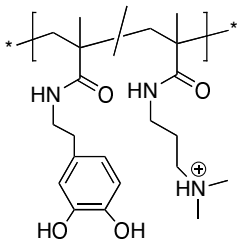

DMAm : DMAPMAm
a: 14 : 86; **b**: 29 : 71

Polymer **2**

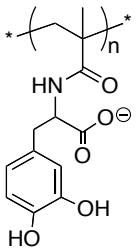

a: n = 15; **b**: n = 26

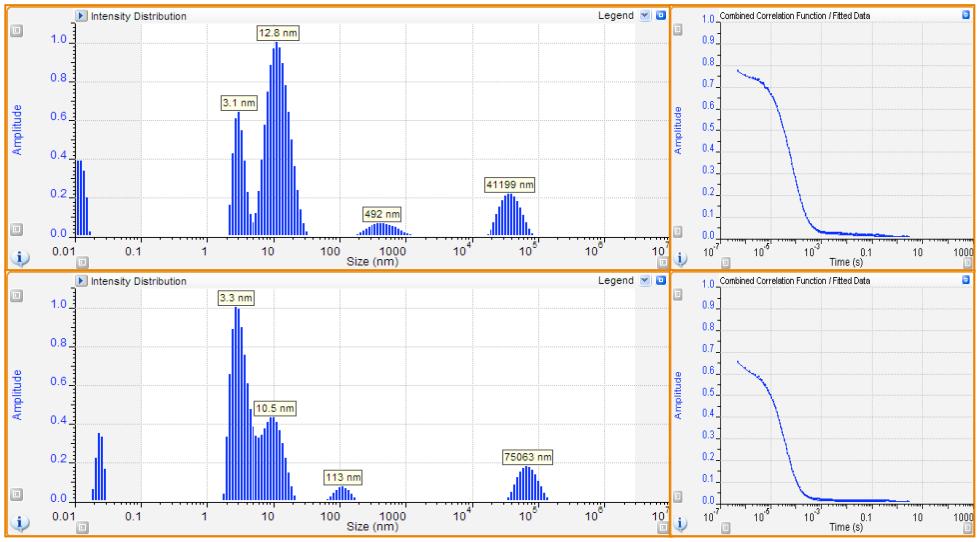

Figure 3-3. DLS data for polymer **1a** (top) and **1b** (bottom) (0.5 mg/mL H_2O)

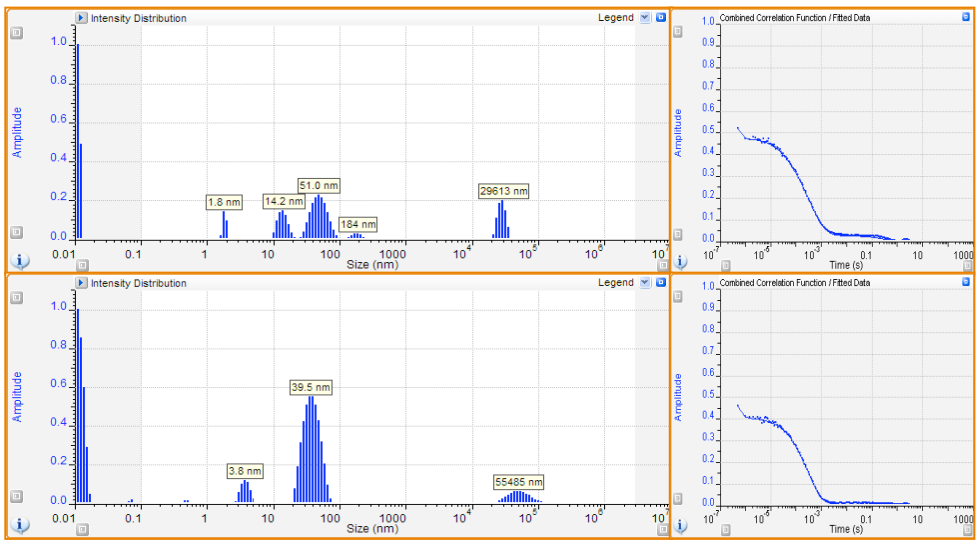

Figure 3-4. DLS data for polymer **2a** (top) and **2b** (bottom) (0.2 mg/mL H_2O)

3.2.3 Chain transfer agent (CTA)

As discussed in the Introduction Chapter, RAFT operates on a conventional free radical polymerization process with degenerative chain transfer. The key to a successful RAFT process is to choose an appropriate CTA or so-called RAFT agent for selected monomers. Hence, appropriate choice of CTA for a given monomer/monomer family is important and has been well-reviewed recently.[22] Among the major employed thiocarbonylthio families, 4-cyanopentanoic acid dithiobenzoate (CTP) (*Figure 3-5*, **4**) has been proved to be extremely useful for diverse monomers and has been employed for the synthesis of water-soluble polymers directly in both aqueous solution and organic solvents. Specifically, some CTAs are more effective under certain polymerization conditions and/or for certain types of monomers.[23] In this case, a series of CTAs (*Figure 3-5*, **1**-**5**) was ready for polymer preparation, for the purpose of establishing proper polymerization conditions and thus achieving well-defined water-soluble polymers.[23]

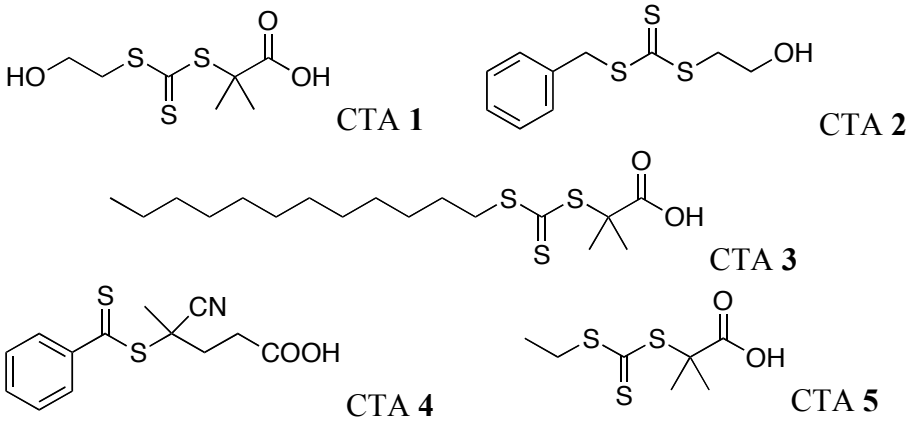

Figure 3-5. Structures of CTA being considered and/or used in RAFT polymerization in this Chapter

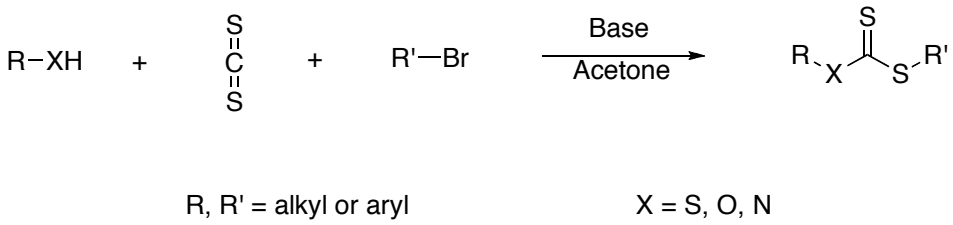

Figure 3-6. General approach of CTA synthesis[16]

Since to appropriately choose CTAs is key to a successful RAFT polymerization process, synthesis of CTAs with distinct functional groups was required.[22a, 22c, 22d, 24] The CTAs presented here were synthesized via the method developed by O'Reilly (*Figure 3-6*).[16] There apparently exist advantages of this strategy: 1) no need to exclude oxygen from the reactions, 2) comparable high product yields, 3) applicable to prepare various types of CTAs, 4) one step one pot reaction, facile. CTA **1** (*Figure 3-5*) was therefore synthesized and characterized by ^{1}H-NMR. However, the yield was not as high as reported (approximately 83%). Some of the crude product was remained in the aqueous phase while extracted by CH_2Cl_2 and washed with H_2O. This was

anticipated that the polarity of the product was in between of the employed organic and aqueous phase. And thus, the product could not be extracted thoroughly. No further exploration was made to optimize purification conditions and skills, for our interest only focused on its application in the following polymerization process.

The reasons for design and synthesis of CTA **1** are as follows: CTAs with alcohol, amine or carboxylic acid functionality are able to facilitate post-polymerization coupling or further functionalization of polymers;[16] S-dodecyl-S-(α,α-dimethyl-α-acetic acid) trithiocarbonate (DDMAT) has been demonstrated as CTA for acrylamides polymerization;[16] for the synthesis of hydrophilic polymers, alcohol end group that is also hydrophilic will facilitate polymer morphology in aqueous media rather than hydrophobic alkyl or phenyl groups.

3.2.4 Binding affinities for Boron

As described in **Chapter 2**, binding affinities of investigated polymer **1** and polymer **2** were calculated via fitting the AR-S assay data with equations. Briefly, a series concentration of each polymer was applied in constant concentration of AR-S, boric/boronic acid and PBS solution at pH 7.4. The fluorescence data at each selected wavelength (572 nm, 592 nm and 573 to 615 nm) were recorded under fluorimeter and fitted with equations to achieve the binding affinity (K_a) for boron. The final K_a value reported (*Figure 3-7*) was the average of the three calculated from different wavelength data and the standard deviation was also for the three K_a at different wavelength. As shown in *Figure 3-8 and 3-9*, the fluorescence was not significantly decreased with

the concentration of polymer **1** employed in this assay. Unlike its small molecule analogues, polymer analysis was limited by the lack of saturation in some of the cases. This has been mainly attributed to the low amount of material and/or low affinity. For polymer **2**, higher concentration was applied and therefore more significant decrease of fluorescence can be obtained (*Figure 3-10 to 3-13*). However, a new band at 545 nm from the catechol structures in polymer can be observed with the increase of polymer concentrations that could overlap with that of AR-S (592 nm) preventing its further analysis (*Figure 3-10 to 3-13*). For the same reason, the standard deviations of K_a for polymer **2** were much bigger than those of its small molecule analogues (*Figure 3-7*). Also, the binding affinities of polymer **1** and sodium borate were not accessible under our assay conditions. This may be because one sodium borate provides two binding positions for diols. Thus the formation of 1:1 or 1:2 complexes in the solution were exchanging depending on the ratio of diol to sodium borate. In another word, there is a chance that fluorescence would not decrease with the increase of diol concentration, which made the analysis of experimental data more complicated. To simplify, for those polymers where binding saturation could be achieved, due to their multivalent nature, binding affinities (K_a) were determined using the Hill Equation (**Eq. 1**) (*Figure 3-10* to *3-13*).

However, according to the data all polymers quenched significantly the fluorescence signal corresponding to the AR-S : B complex, and in most cases affinities were higher than those calculated for the small molecule analogues (*Figure 3-7*). Due to the low amount of polymer **3** available, saturation of binding could not be achieved during the titration of the AR-S : B complex.

Nevertheless, the enhancement of affinity is clearly apparent, as similar changes in fluorescence could be obtained with 20 eq of diol in polymer **3** and 100 eq of methyl-β-D-glucopyranoside. Thus, a 5-fold increase in affinity was observed when comparing polymer **3** to methyl-β-D-glucopyranoside, suggesting that, at least in the case of the carbohydrates, multivalency could play a significant role in the binding with boronic acids, and therefore in QS-control.

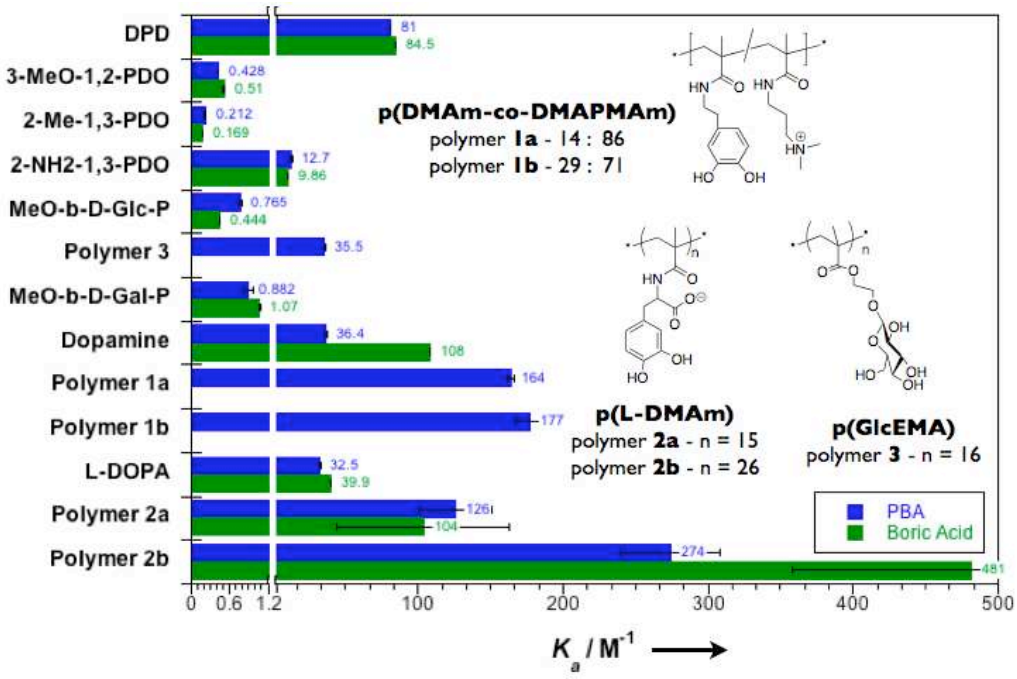

Figure 3-7. Binding affinities of DPD, model diols and polymers for phenylboronic acid (PBA, blue bars) and boric acid (green bars).

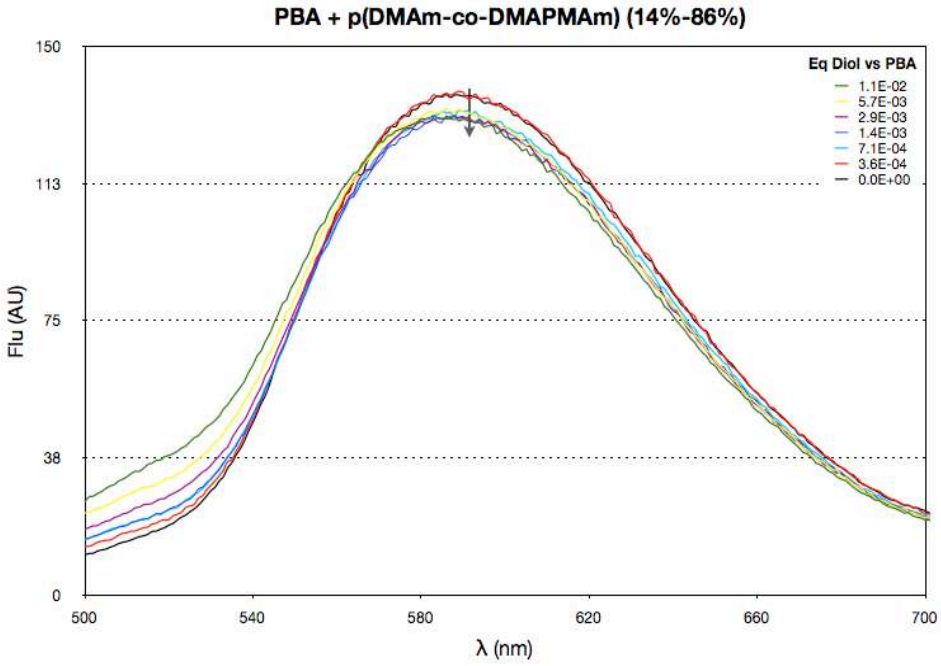

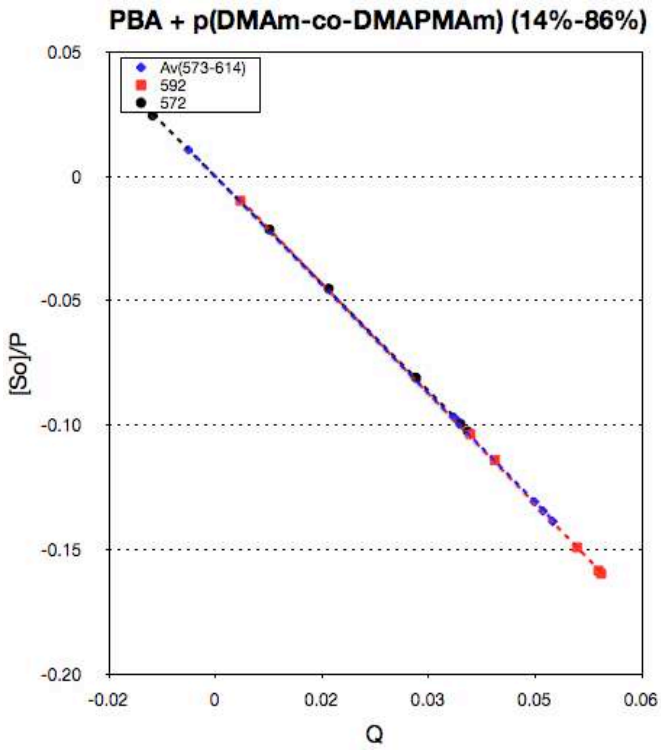

Figure 3-8. Fluorescence profile of **PBA** and polymer **1a** (**p(DMAm-co-DMAPMAm) 14%-86%**) titration and the corresponding fitting plot. [**AR-S**] = 0.009 mM, [**PBA**] = 2 mM, [**DMAm**] = 0.02 mM, [$\mathbf{PO_4^-}$] = 100 mM. $\mathbf{K_a}$ = 164.3 ± 2.3 M^{-1}

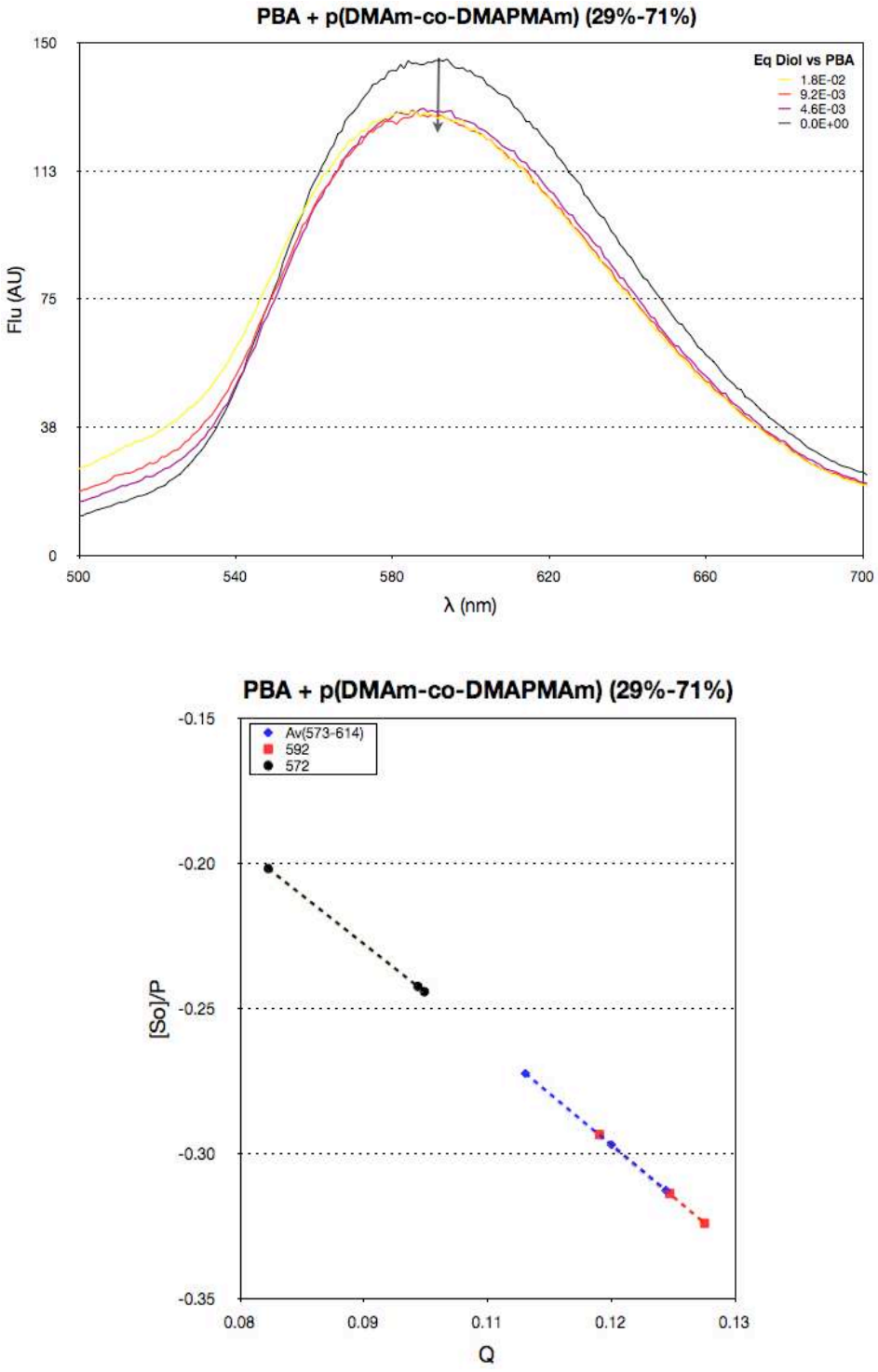

Figure 3-9. Fluorescence profile of **PBA** and polymer **1b** (**p(DMAm-co-DMAPMAm) 29%-71%**) titration and the corresponding fitting plot. [**AR-S**] = 0.009 mM, [**PBA**] = 2 mM, [**DMAm**] = 0.04 mM, [$\mathbf{PO_4^-}$] = 100 mM. $\mathbf{K_a}$ = 177.1 ± 9.9 M^{-1}.

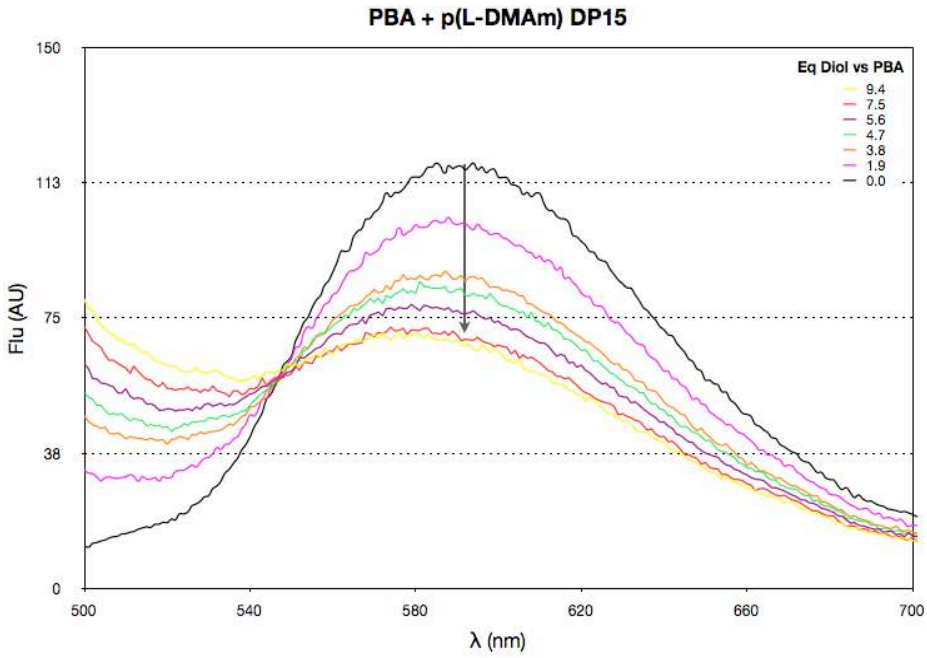

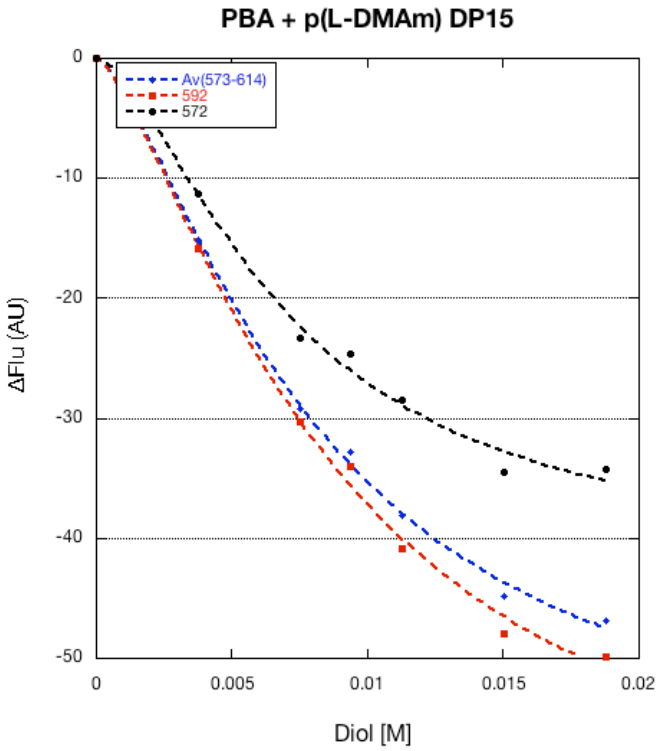

Figure 3-10. Fluorescence profile of **PBA** and polymer **2a** (**p(L-DMAm) DP15**) titration and the corresponding fitting plot. [**AR-S**] = 0.009 mM, [**PBA**] = 2 mM, [**L-DMAm**] = 18.8 mM, [$\mathbf{PO_4^-}$] = 100 mM. $\mathbf{K_a}$ = 126.0 ± 25.3 M^{-1}, n = 1.50 ± 0.31.

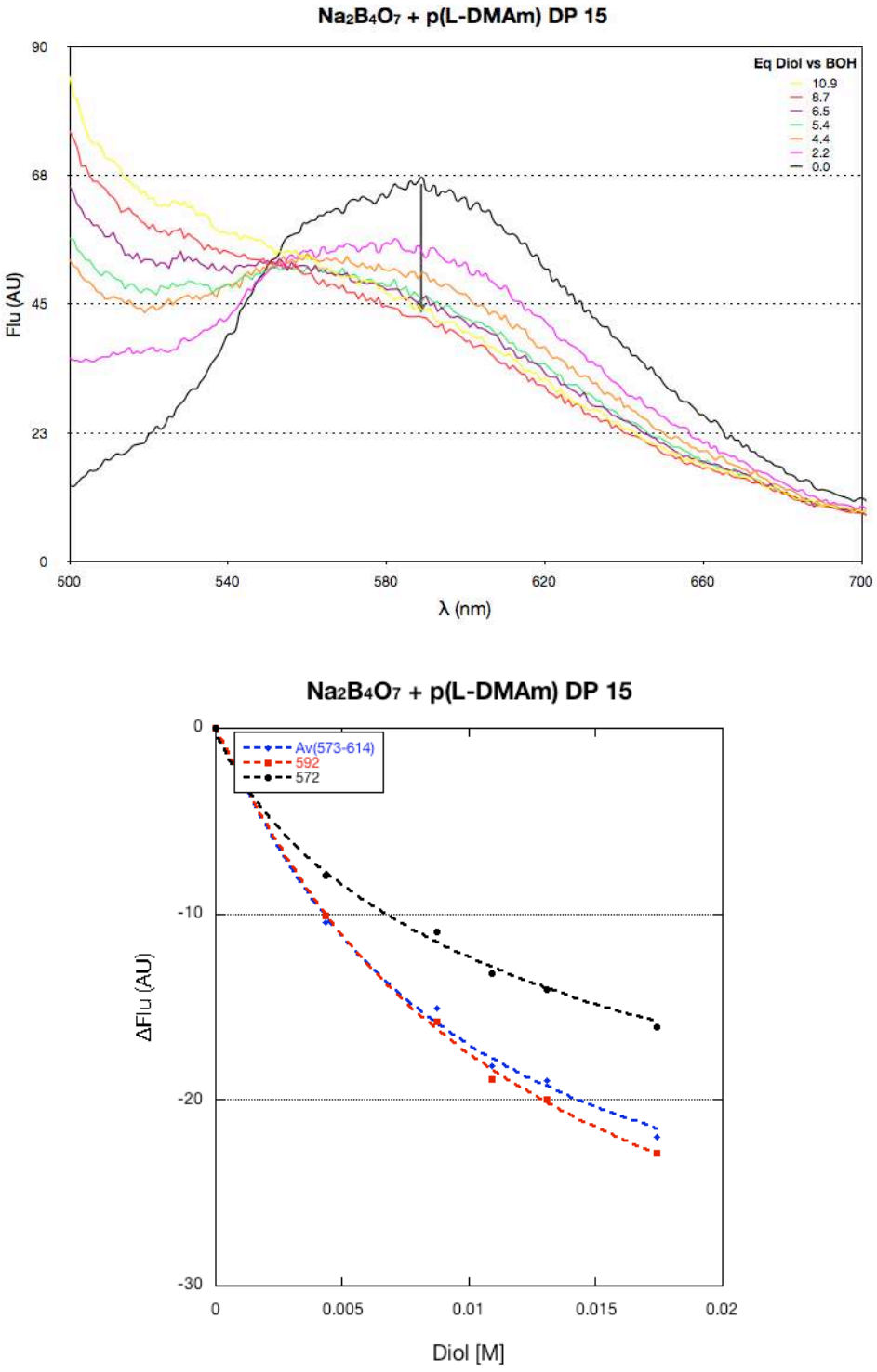

Figure 3-11. Fluorescence profile of Sodium Borate and polymer **2a** (**p(L-DMAm) DP15**) titration and the corresponding fitting plot. [**AR-S**] = 0.009 mM, [$\mathbf{Na_2B_4O_7}$] = 2 mM, [**L-DMAm**] = 21.8 mM, [$\mathbf{PO_4^-}$] = 100 mM. $\mathbf{K_a}$ = 103.7 ± 59.7 M^{-1}, n = 1.00 ± 0.32.

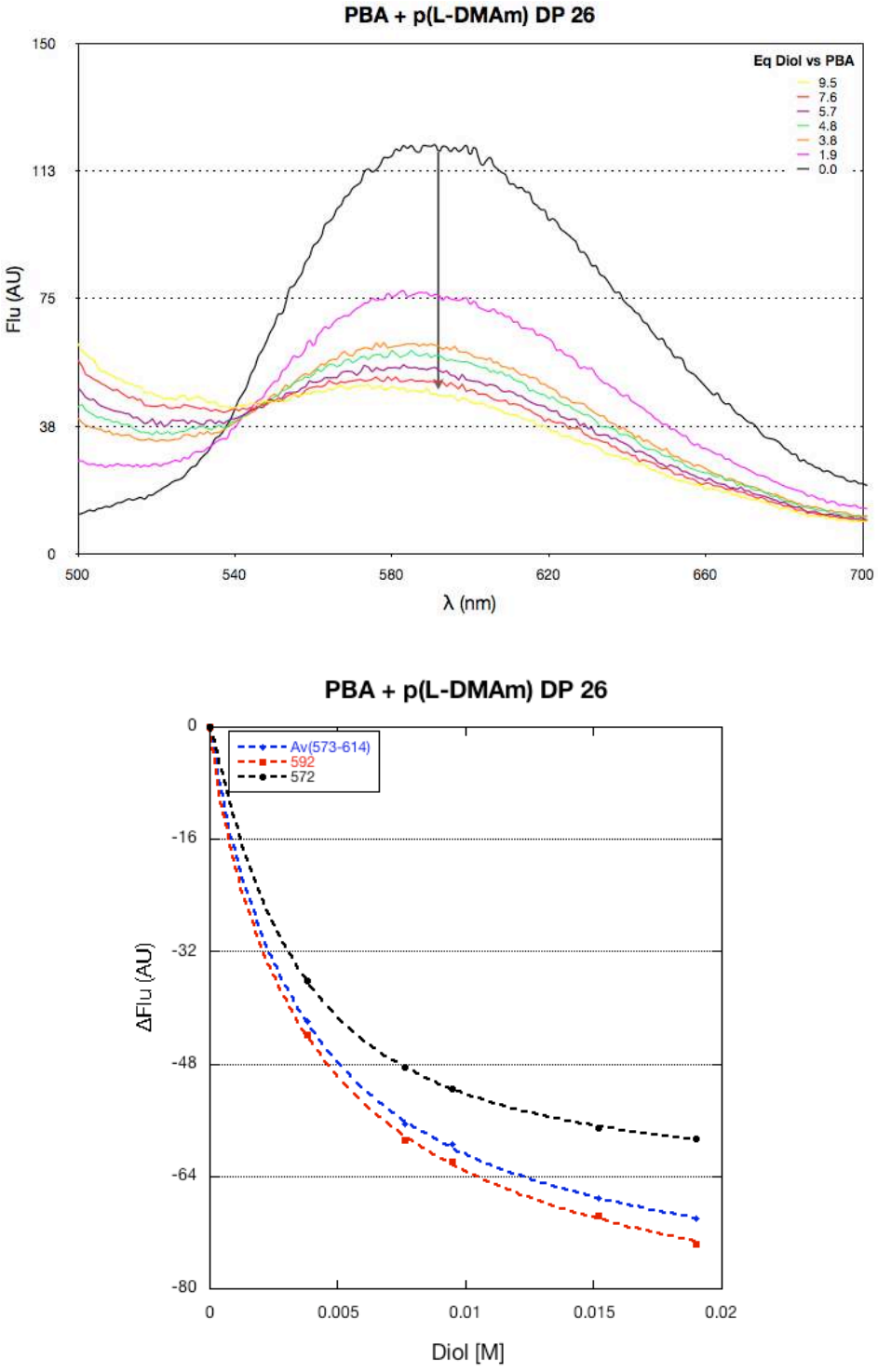

Figure 3-12. Fluorescence profile of **PBA** and polymer **2b** (**p(L-DMAm) DP26**) titration and the corresponding fitting plot. [**AR-S**] = 0.009 mM, [**PBA**] = 2 mM, [**L-DMAm**] = 19.0 mM, [$\mathbf{PO_4^-}$] = 100 mM. $\mathbf{K_a}$ = 274.0 ± 34.4 M^{-1}, n = 1.03 ± 0.13.

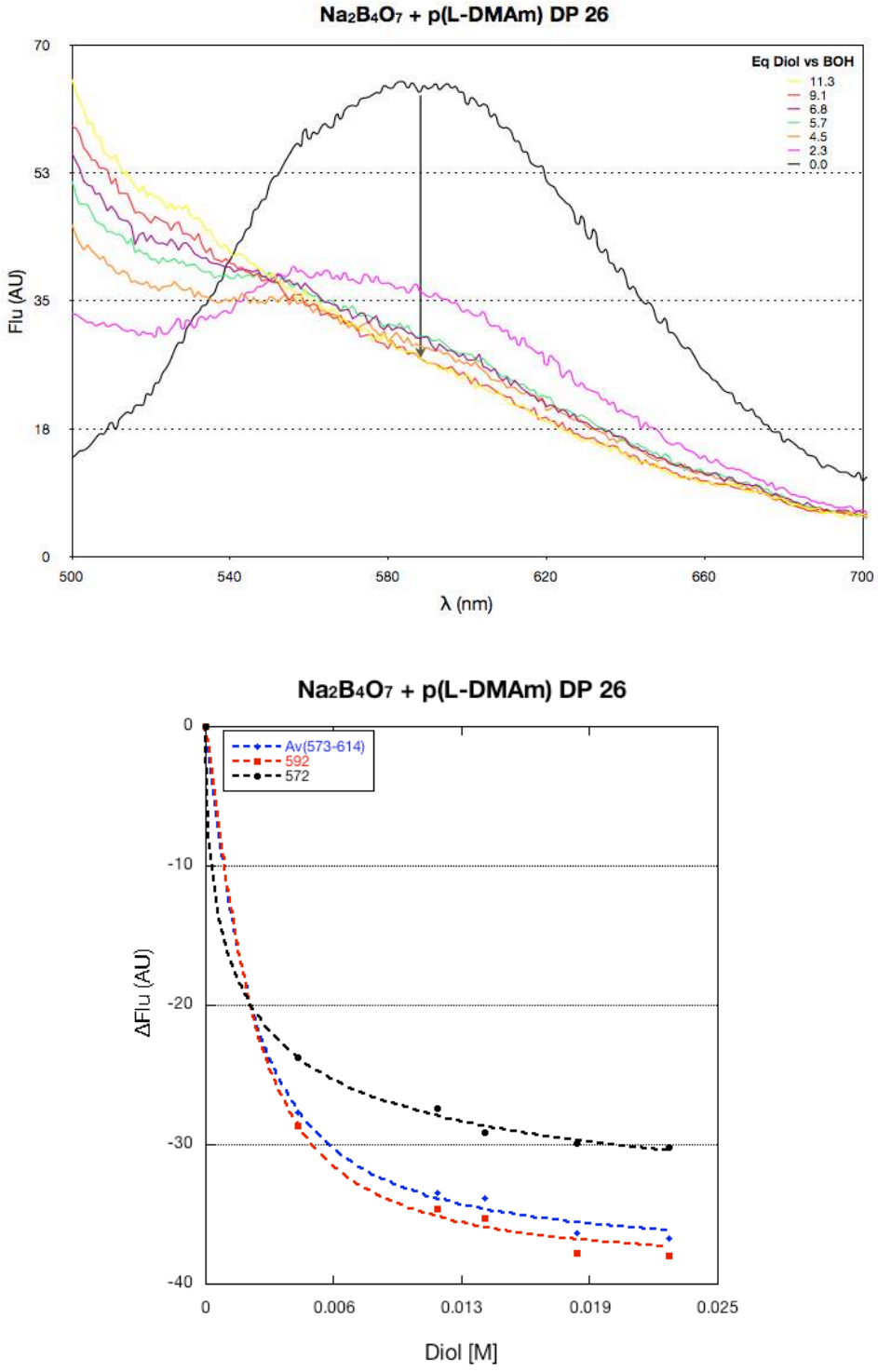

Figure 3-13. Fluorescence profile of Sodium Borate and polymer **2b** (**p(L-DMAm) DP26**) titration and the corresponding fitting plot. [**AR-S**] = 0.009 mM, [$\mathbf{Na_2B_4O_7}$] = 2 mM, [**L-DMAm**] = 22.6 mM, [$\mathbf{PO_4^-}$] = 100 mM. $\mathbf{K_a}$ = 481.1 ± 122.9 M^{-1}, n = 1.28 ± 0.66.

3.2.5 Binding confirmation by ^{11}B-NMR

Experiments by ^{11}B-NMR were carried out with polymers **1a** and **2a** in order to confirm binding between AI-2 molecule and designed polymers. Unfortunately, polymer solubility at the concentrations employed for the NMR analysis (up to 25 mg/mL), limited the amount of diol that could be added, especially in the case of polymer **1a**. Also, the baseline of ^{11}B-NMR spectra became noisy while increasing the polymer concentrations, which caused difficulty to compare the signal intensities. In addition, polymers **1** and **2** led to self-assembled aggregates (*Figures 3-3 and 3-4*, DLS data) at high concentrations, resulting in lower diffusion rates and decreased signals in the NMR, limiting the significance of the assay.

However, polymer **2a** was able to reduce the concentration of AI-2 in solution. As shown in *Figure 3-14*, when a solution of DPD in a borate/phosphate buffer at pH 7.4 was treated with 1 eq of diols in polymer **2a**, a decrease of the signals at 4.8 and 6.2 ppm, corresponding to the AI-2 (**1**)[25] occurred, while such an observation was more significant when diol to sodium boronate ratio was increased to 2.5 eq in the media (*Figure 3-14*). These data indicated that ^{11}B-NMR could be an alternative technique to characterize such competitive binding, but only for cases where aqueous solubility of the polymers was sufficient.

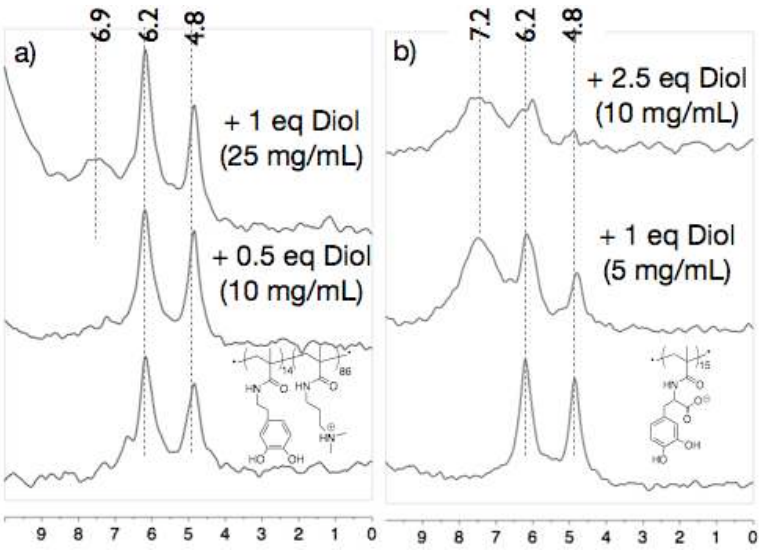

Figure 3-14. Quenching of AI-2 boronated form by a) Polymer **1a** and b) Polymer **2a** acid as shown by ^{11}B-NMR (The peak corresponding to the excess of $Na_2B_4O_7$ has been left out for a better comparison. Number in parenthesis corresponds to the concentration of polymer)

3.2.6 Bacterial aggregation assay

3.2.6.1 UV spectrum

The bacterial aggregation rate was quantified by measuring the bacterial optical density (OD) at a wavelength of 600 nm. It was assumed that all the aggregates should be precipitated to the bottom of the UV cuvets and thus the suspended cells and the OD would decrease. This is because in UV/Vis spectrometer light goes through the cuvet from front to back window and OD referring to the amount of light transmitted or reflected from an object (here were cells) would therefore become small when cells were precipitated from suspension. Therefore, by measuring the decrease of OD (at 600 nm) in the absence and presence of polymers, the function that polymers give to sequester cells could be quantified. In order to compare the binding affinities of polymer

to bacterial MM32 cells, the same set of data was presented in three different ways: OD at 600 nm as a function of time (*Figure 3-15* and *3-16*, a), which showed an overall view of the whole process; aggregation percentage, which showed the aggregation rate compared to blank (i.e. a measure of polymer sequestration affinity) (*Figure 3-15* and *3-16*, b); the value of aggregation percentage divided by polymer concentration, as an alternative way to show the binding rate for unit polymer concentration (*Figure 3-15* and *3-16*, c). All the polymers tested here (Polymer **1a**, **1b**, **2a**, **2b** and **3**) induced bacterial aggregation compared to the 'blank' (no addition of polymers) in both AB (*Figure 3-15*) and PBS (*Figure 3-16*) medium via giving decreases of OD (600 nm) with time in graph a) and high aggregation percentage value in graph b) (*Figure 3-15* and *3-16*). Importantly, these results also showed that the strength of the binding affinity of polymer to bacteria surfaces could be tuned with different monomer compositions. On the other hand, these behaviors were confirmed again with dose-dependent cell sequestration action in the presence of different concentrations of polymer **1a** (*Figure 3-17*). Interestingly, X_{Ag} of homopolymer p(L-DMAm) (Polymer **2a** and Polymer **2b**) was always smaller than those of Polymer **1** and Polymer **3** in either solution, maybe indicating that Polymer **2** attached bacteria more rapidly, but with a relatively low affinity compared to the other two polymer types (*Figure 3-15* and *3-16*, c).

In order to understand the mechanism of polymer to bacteria binding, one more experiment with a series of **PVA** solutions as the control polymer was performed under the same conditions. These demonstrated that the abilities of Polymer **2a** and Polymer **2b** to sequester bacteria adhesion were not due to non-specific association of polymeric alcohols with *V. harveyi*, as no

significant bacterial aggregation was observed in the presence of different concentrations of **PVA** solutions (*Figure 3-18*).

Polymer **1**	Polymer **2**	Polymer **3**	**PVA**
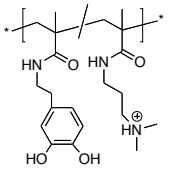	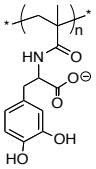	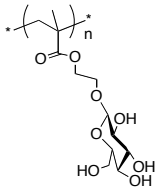	
DMAm : DMAPMAm **a**: 14 : 86; **b**: 29 : 71	**a**: n = 15 **b**: n = 26	n = 16	n = 13000~23000

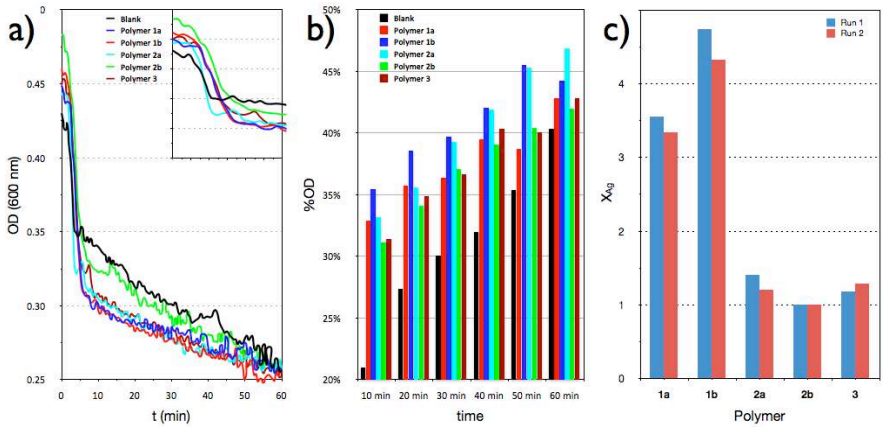

Figure 3-15. a) OD (600nm) as a function of time in the absence and presence of polymers, and amplification of the first 10 min, b) %Ag as a function of time and c) X_{Ag} for the 2 duplicates in AB media

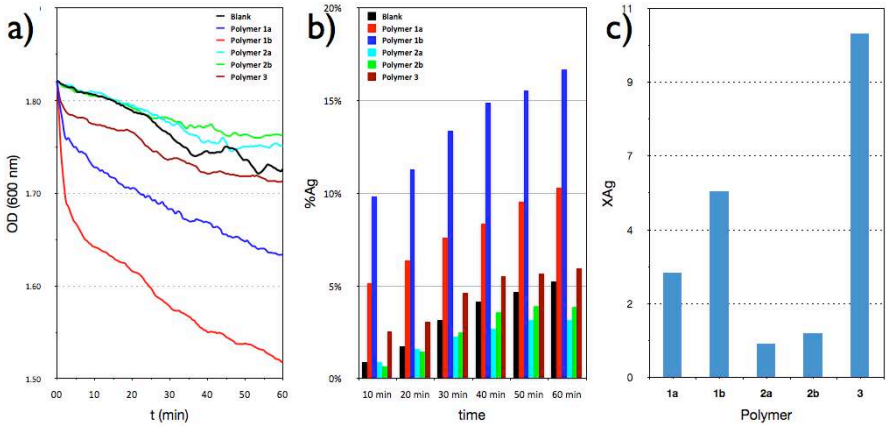

Figure 3-16. a) OD (600 nm) as a function of time in the absence and presence of polymers, b) %Ag as a function of time and c) X_{Ag} in PBS.

Polymer **01**	Polymer **02**	Polymer **03**
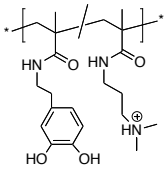	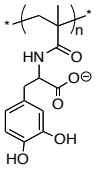	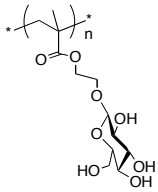
DMAm : DMAPMAm **a**: 14 : 86; **b**: 29 : 71	**a**: n = 15 **b**: n = 26	n = 16

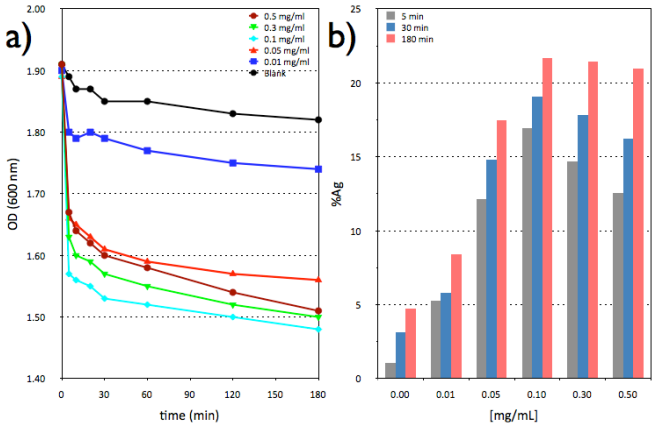

Figure 3-17. a) OD (600 nm) as a function of time in the absence and presence of different amounts of Polymer **1a**, b) %Ag as a function of Polymer **1a** concentration and time.

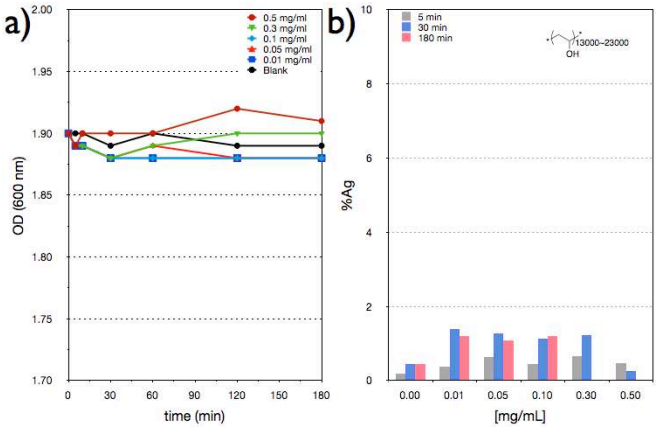

Figure 3-18 a) OD (600 nm) as a function of time in the absence and presence of different amounts of **PVA**, b) %Ag as a function of **PVA** concentration and time

3.2.6.2 Microscopy

Dense ‘mats’ of polymer-cell aggregates were apparent in the presence of all the tested polymers. Polymers clustered of bacterial cells more significantly than the blank controls, as shown in images (*Figure 3-19*).

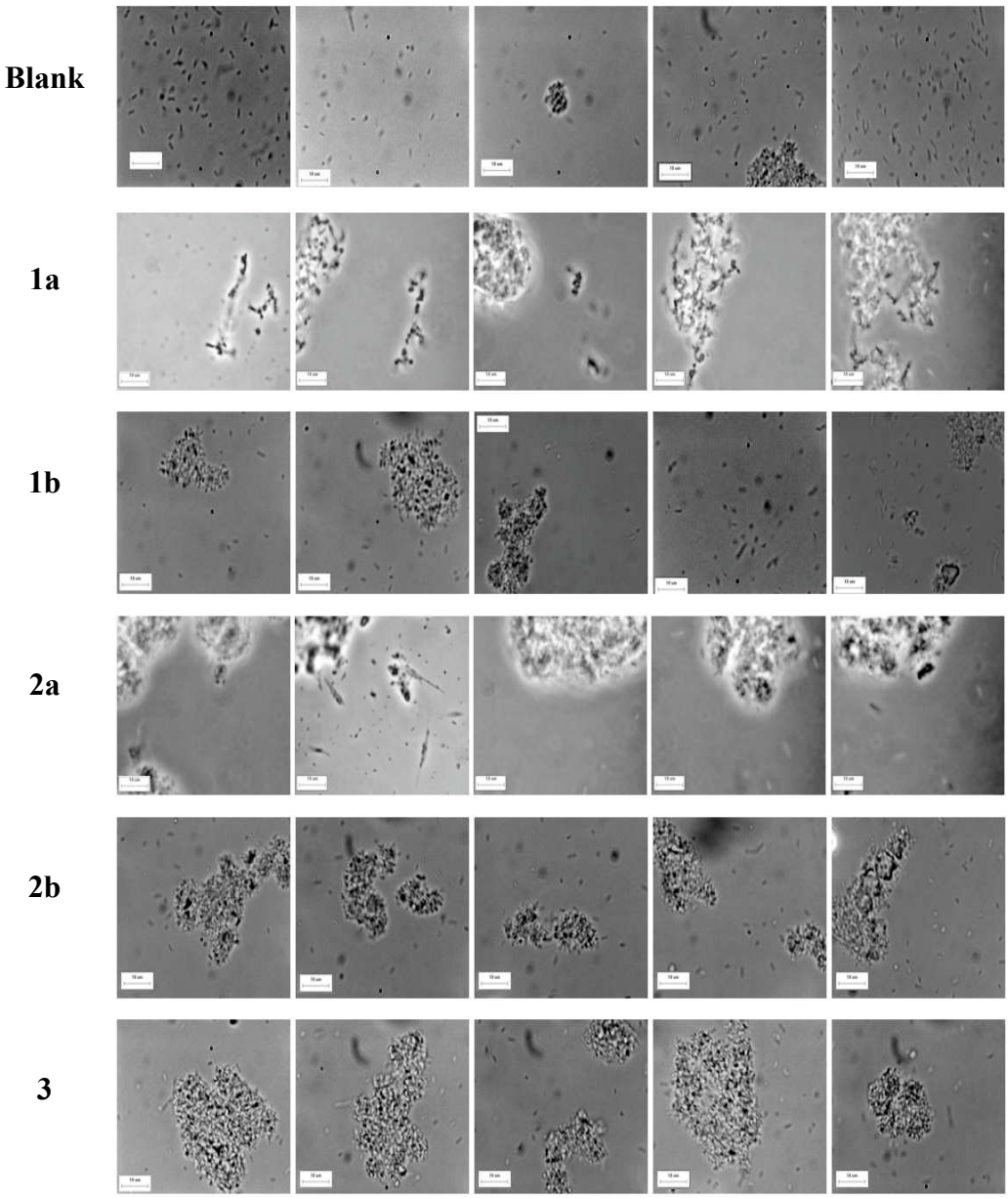

Figure 3-19. Representative examples of the *V. harveyi*-polymer aggregates in AB media, as seen by Optical Microscopy, scale bars = 10 μm

All the above experimental results indicated that, as expected, the cationic polymers (polymer **1a** and **1b**) sequestered the negatively charged *V. harveyi*, with the formation of dense 'mats' of polymer-cell aggregates (*Figure 3-19*). In addition, since *V. harveyi* has been shown to bind to glucose,[26] the fact that polymer **3** induced bacterial aggregation was also anticipated (*Figure 3-15*, *3-16* and *3-19*). The negatively-charged polymers (polymer **2a** and **2b**) also formed dense polymer-cell aggregates (*Figure 3-19*), a less predictable outcome, attributed to the inherent adhesive properties of L-DOPA-derived catechols.[27]

3.2.7 Bioluminescence assays

3.2.7.1 MM32 assay

Bioluminescence assays were carried out with *V. harveyi* bacteria - MM32 mutant ($LuxN^-$ and $LuxS^-$), in which no DPD molecule is produced by the bacterial cells themselves due to the lack of DPD biosynthesis protein LuxS. In this case, the concentration of DPD in solution would be constant all through the experiment, by externally adding DPD into the assay media, which simplified cells' feedback loop with polymer materials. On the other hand, as described in the first chapter, the QS controlled behaviors, for example bioluminescence, are coordinated with different types of AI systems (i.e. AI-1 and AI-2). MM32 mutant without LuxN protein (responsible for AI-1 production) would only response to AI-2 signals (the product of reaction between exogenous added DPD and boric acid in assay media) in the solution to produce light. In another word, in this assay condition light production was only under control of AI-2 QS system. *V. harveyi* MM32 assays were

performed under a range of conditions (***protocol 1-4***) adapted from prior publications.[18-19] Actually, there were several factors that might be significantly related to the intensity of light output with time. For example, boron concentration was one of the most essential issues that directly affect the AI-2 concentration available for bacterial QS. In addition, as described, in each individual experimental unit (well) only 200 μL mixture solution was loaded, so that evaporation at the 30 °C incubation temperature would significantly change its in-total volume, and therefore the concentration of each component, and even the growth of bacteria. Moreover, the growing state of the bacteria in different overnight cultures was not possible to be controlled.

V. harveyi MM32 was grown on LB agar plate containing kanamycin (50 μg/ml) and chloramphenicol (10 μg/ml), which were antibiotics for most of the other bacteria except of the *Vibrio* species, thus excluded any impact from other bacterial species. Bacteria were then precultured in 2 mL LB media with aeration at 30 ºC overnight to reach a high OD in nutrient-rich media. AB medium, in which *V. harveyi* can produce light, was inoculated with this preculture (5000:1) and DPD was added externally to a final concentration of 22 μM. 180 μL of the inoculated medium were placed in each of the wells of a 96 well plate and combined with 20 μL of the samples to be analyzed (triplicate for each polymer). This way, the concentration of DPD in each of the wells was 20 μM. This optimal DPD concentration was determined by measuring the effect of DPD concentration in light production in the absence of polymer samples. As shown in *Figure 4-20*, the maximum bioluminescence changed significantly as a function of DPD concentrations when it was around 20 μM following ***protocol 1***. Thus, the bioluminescence was believed to be

highly sensitive to the change of DPD concentration around this concentration range (20 μM), which gave the possibility to understand better the effect of polymer on bacterial QS network with more reliable readout data (bioluminescence).

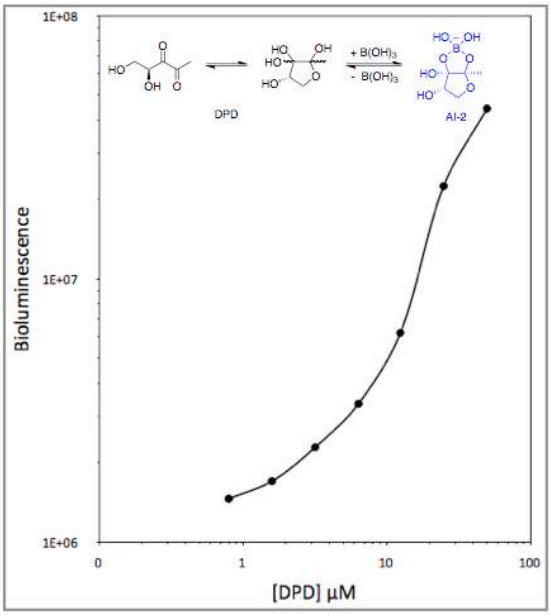

Figure 3-20. Effect of **DPD** concentration in light production under the condition of ***protocol 1***

The same experiments were performed again for each new batch of commercial DPD and/or if a different protocol was followed, e.g. ***protocol 4***. This time, the effect of different concentrations of boron was also taken into account. Although the maximum bioluminescence varied (*Figure 3-21*) which might be attributed to the independent overnight cultures (at different growing state, hard to know), the intrinsic variations in response of instrumentation, the difference of the protocol, DPD batch and/or the boron concentrations, the optimal final concentration of DPD in assay media was fixed to 20 μM. For the same reason as described above, the readout (bioluminescence) data were changed significantly on changing DPD concentration at around 20 μM. And

also, to keep DPD exogenous concentration the same allowed comparability as much as possible. s

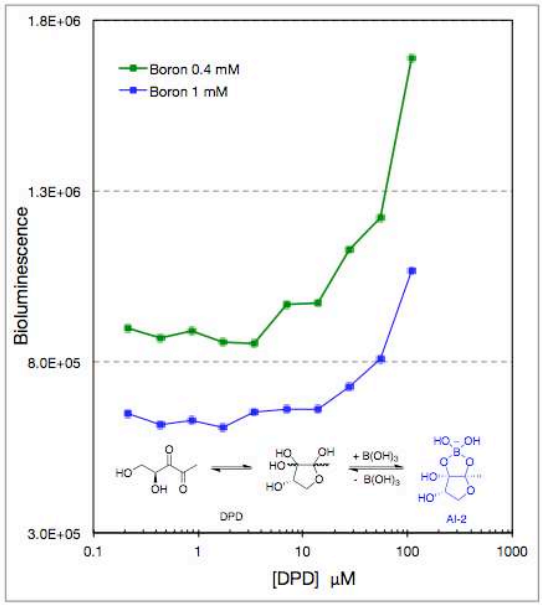

Figure 3-21. Effect of **DPD** concentration in light production under the condition of ***protocol 4***, but in the presence of 0.4 mM (green) and 1 mM (blue) of boron prepared in boron-depleted media (no extra boron in the solution)

For MM32 assay following ***protocol 1***, in order to get dose response profiles for the different analytes, each compound was tested at least for 5 different concentrations. Light production and optical density (600 nm) were recorded at 30 ºC every 30 minutes for at least 6 hours in a 96-well plate. The experiments were carried out in triplicate and the plotted curves are derived from the mean value. The normalized bioluminescence was calculated by dividing the mean light output by the mean optical density at each time point. Significant differences in optical density (OD) between those cultures in the presence and absence of polymers were observed with increasing time (after about 8 h), for the impact from solution evaporation cannot be ignored at this stage, so that

every component in the solution was concentrated, which interfered with cell growth reflected by the dramatically increase of OD (more light transmission/reflection from cells was recorded). In this experiment, bioluminescence and OD were taken in the mean time by using Tecan instrument. Different from the aggregation assay carried out with the UV spectrometer, 96-well plate was used to locate samples instead of cuvet, and thus the light provided by Tecan went from the bottom of the wells to the top (not from the front to the back window of cuvets which only tested the particle in suspension) to record the OD of particles/cells in both suspension and precipitation, giving information of the cell growth but not its sequestration rate. The analysis of bioluminescence vs diol concentration was restricted to the 4-10 h timeframe, where almost no differences in OD were observed for most of the polymers and conditions analyzed.

Having established binding of bacteria and boric acids by polymers **1-3**, and their potential to reduce the concentration of AI-2 in solution, their effect on bacterial QS was investigated by means of bioluminescence. Unlike the expected dose-dependent suppression observed for conventional small molecule AI-2 quenchers,[28] or polymers without the ability to bind bacteria,[11b] such as PVA (*Figure 3-18*) the bioluminescence profiles reflected a more complex behaviour of *V. harveyi* in the presence of the dual-action polymers. Intriguingly, variations in time of onset, as well as magnitude, of light production were observed as the concentrations of different polymers in suspensions of bacteria varied (*Figure 3-22 to 3-26*).

At the earlier time points (5h, *Figure 3-22 to 3-26*) all the polymers exhibited dose-dependent suppression of light production except the lower molar mass

anionic polymer **2a** (for which the effects were small). However, at intermediate time periods (7h, *Figure 3-22* to *3-26*) increases in light production were observed in the presence of polymers **1a**, **2a** (and to a lesser extent **3**) with bioluminescence only suppressed at higher polymer concentrations. Over more extended times (*Figure 3-22 to 3-26*) light production again was increased for low polymer concentrations and decreased at higher doses for all the polymers investigated here. These data suggest that the onset and duration of any quenching effects were strongly dependent on the cell density (cell growth cycle/time) as well as the affinity of the polymers towards the boron moiety and their ability to bind bacteria. Importantly, since QS itself partially depends on cell density[29] and clustering[30] it is likely that those polymers able to aggregate bacteria as well as remove DPD were interfering in the cell signalling pathways by both a 'cell-binding' and a 'QS-quenching' mechanism. Since each of these processes could be in feedback, an apparent 'oscillation' in light production could be inferred. In another word, the increase of polymer concentration would not always decrease the light output (sometimes enhance it), which resulted from both cell growth cycle and polymer affinity for both cells and QS signals. However, for the 'control' polymer PVA (*Figure 3-27*) with no cell sequestration function, there was no 'oscillation' in bioluminescence correlated to the different polymer concentrations. Instead, the light production was suppressed in proportion to the polymer concentrations. These data of experiments were in accord with the 'single function' (QS quenching, but no cell sequestration) assumption. PVA incorporates 1,3-propanediol units in its polymer backbone. The affinity for 2-methyl-1,3-propanediol for PBA and boric acid was assessed using the AR-S

assay (*Figure 2-8*) and it was shown to be smaller than the catechol derivatives. Therefore, PVA was expected to bind boric acid with a decreased affinity when compared with the polymers investigated during this research. On the other hand, PVA did not induce extra cell aggregation (*Figure 3-18*), which means no dual function (no light oscillation) but only 'QS signal quenching' (more polymer more quenching) should be observed in MM32 assay (*Figure 3-27*).

Two experimental repeats were performed independently for each of the polymers analysed (*Figure 3-28*). Despite the difference between the two batches of cells causing slight differences of the bioluminescence reading and OD, the overall trends at each testing time point were quite similar. This gave the strong evidence that polymers interfering with the bacterial coordination network based on the assumption of 'dual function' theory were true and the experimental results were reproducible.

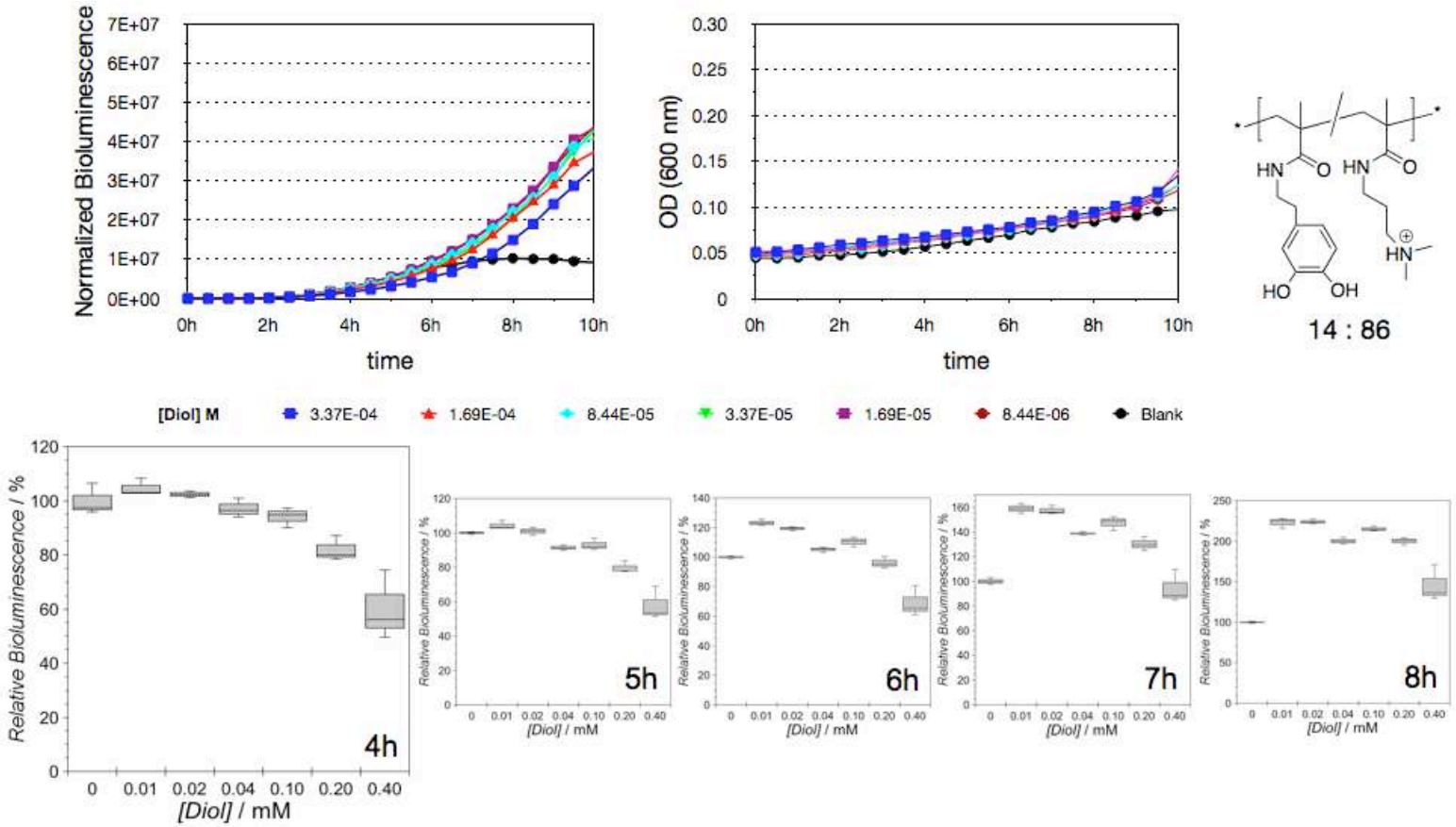

Figure 3-22. Light production curves and OD (600 nm), as a function of time for *V. harveyi* MM32 in the absence and presence of Polymer **1a**.

Bottom: Effect of diol concentration in light production. (***protocol 1***)

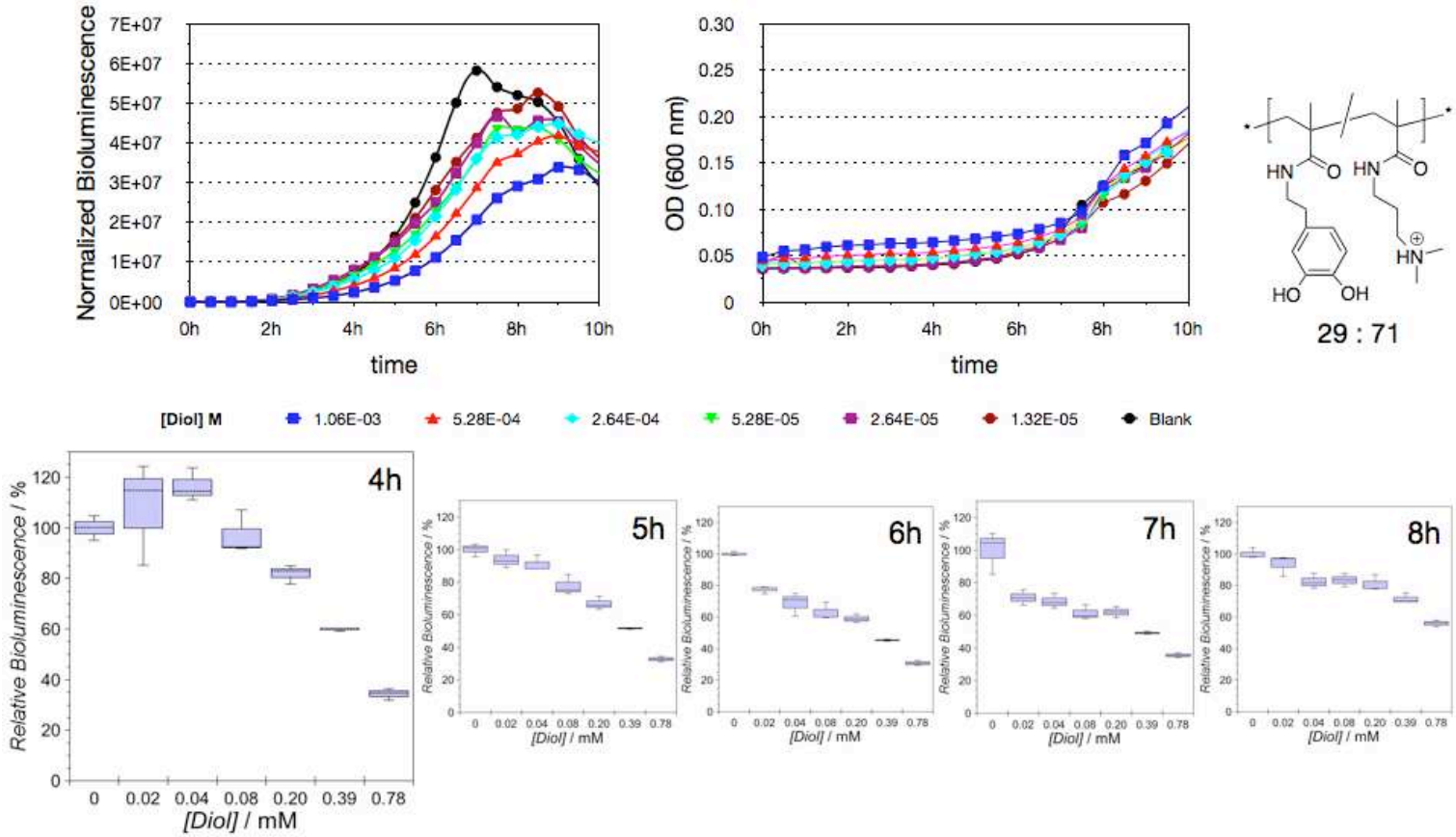

Figure 3-23. Light production curves and OD (600 nm), as a function of time for *V. harveyi* MM32 in the absence and presence of Polymer **1b**.

Right: Effect of diol concentration in light production. (***protocol 1***)

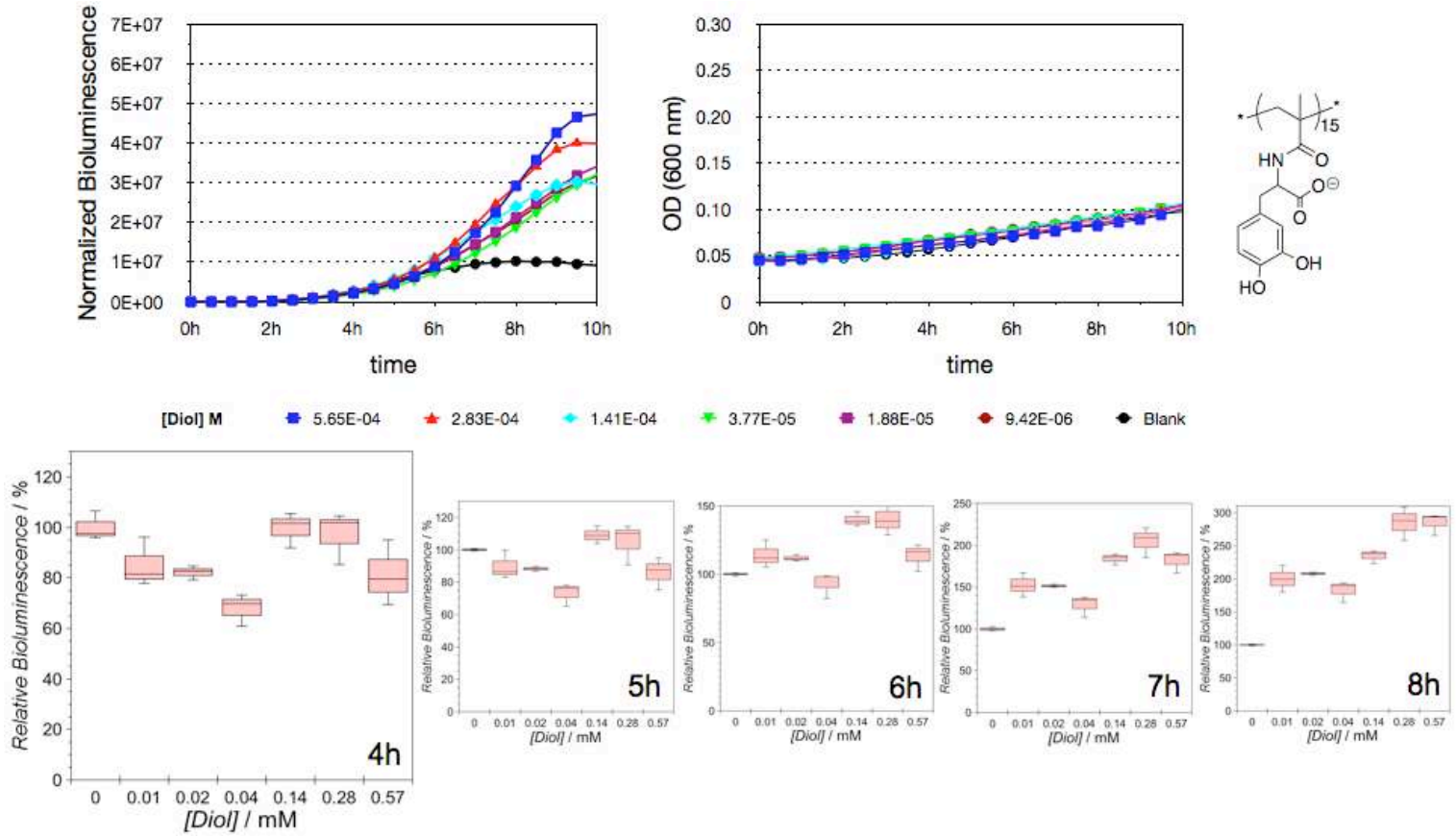

Figure 3-24. Light production curves and OD (600 nm), as a function of time for *V. harveyi* MM32 in the absence and presence of Polymer **2a**.

Bottom: Effect of diol concentration in light production. (***protocol 1***)

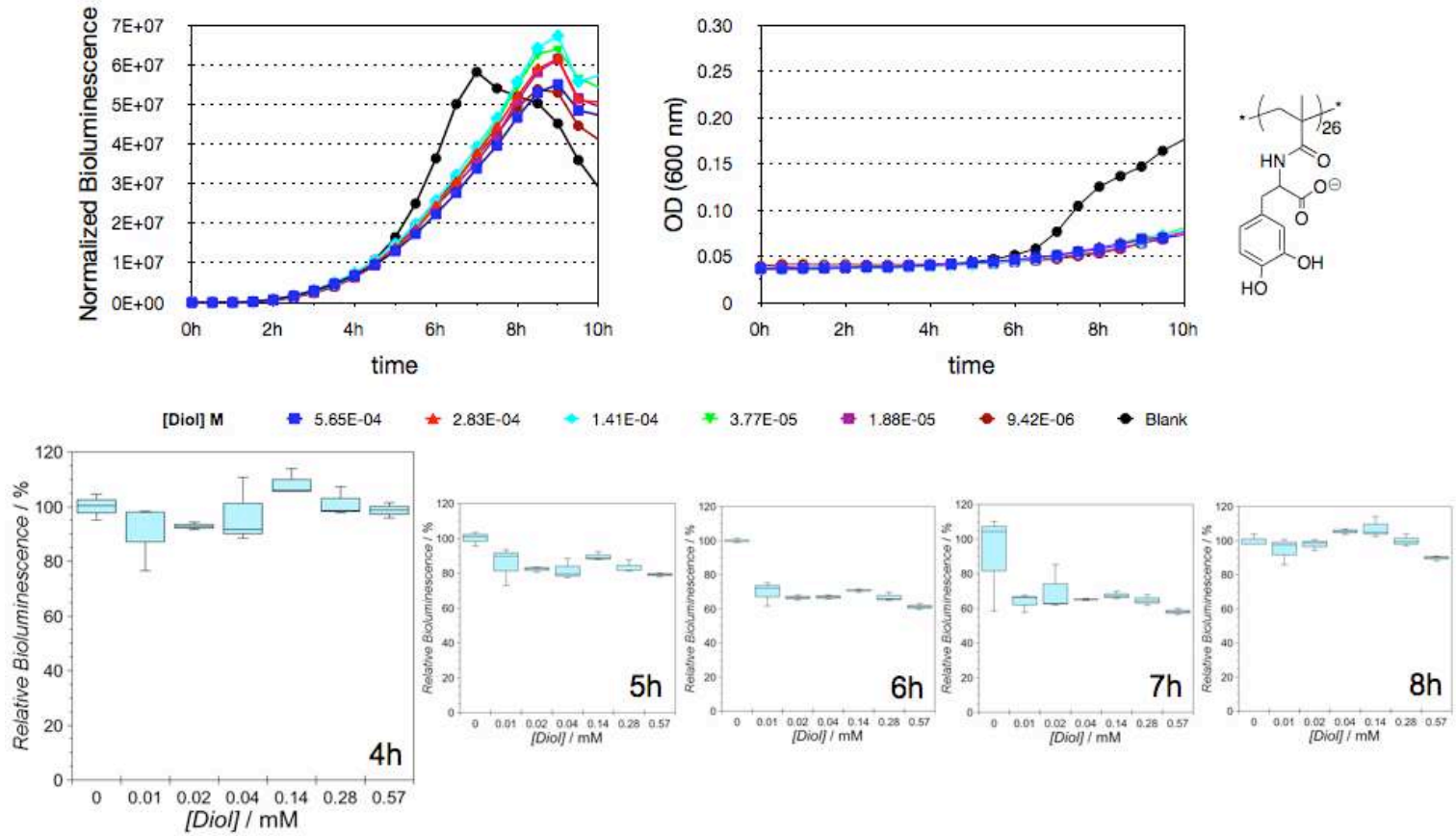

Figure 3-25. Light production curves and OD (600 nm), as a function of time for *V. harveyi* MM32 in the absence and presence of Polymer **2b**.

Bottom: Effect of diol concentration in light production. (***protocol 1***)

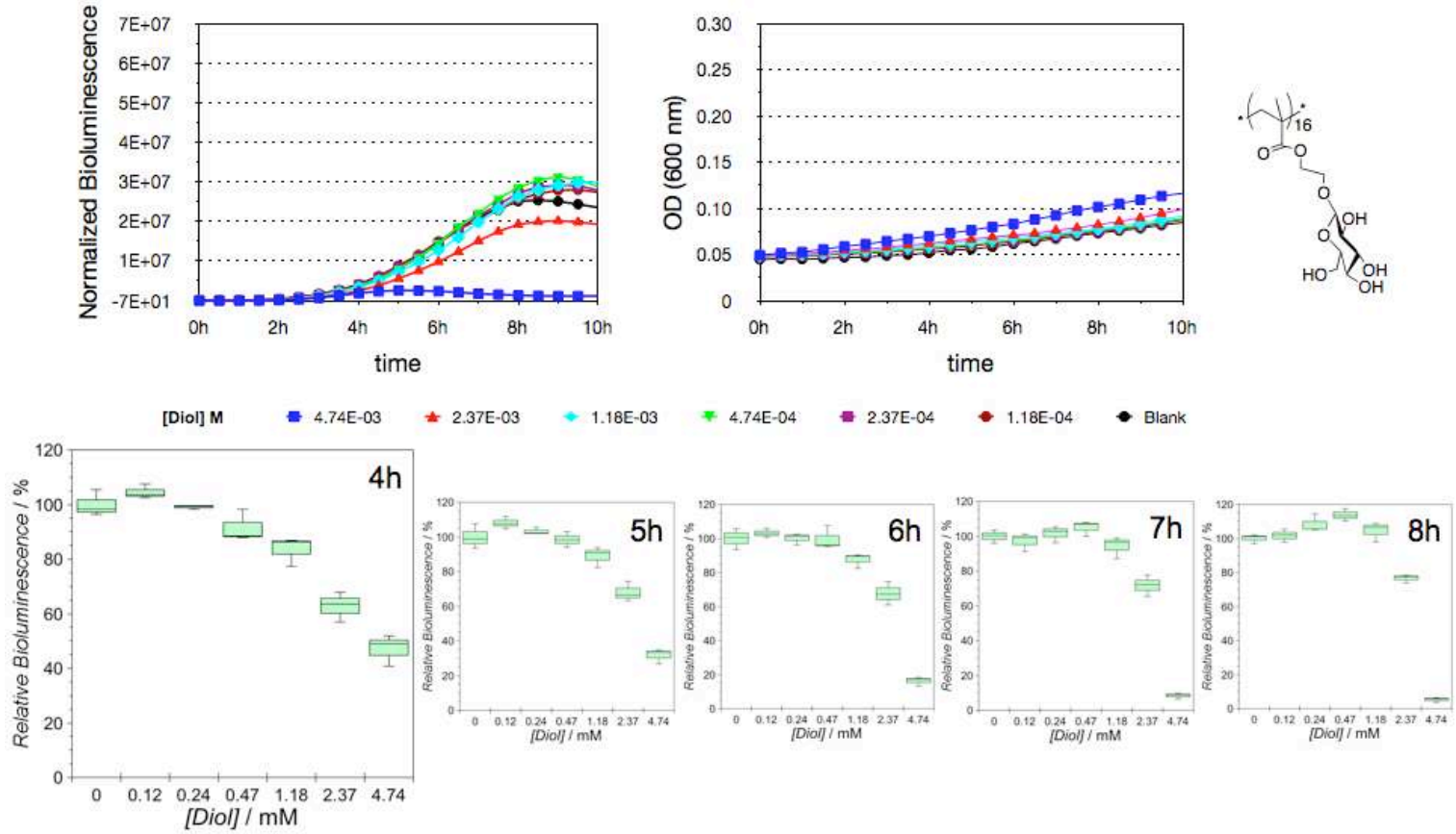

Figure 3-26. Light production curves and OD (600 nm), as a function of time for *V. harveyi* MM32 in the absence and presence of Polymer **3**.

Bottom: Effect of diol concentration in light production. (***protocol 1***)

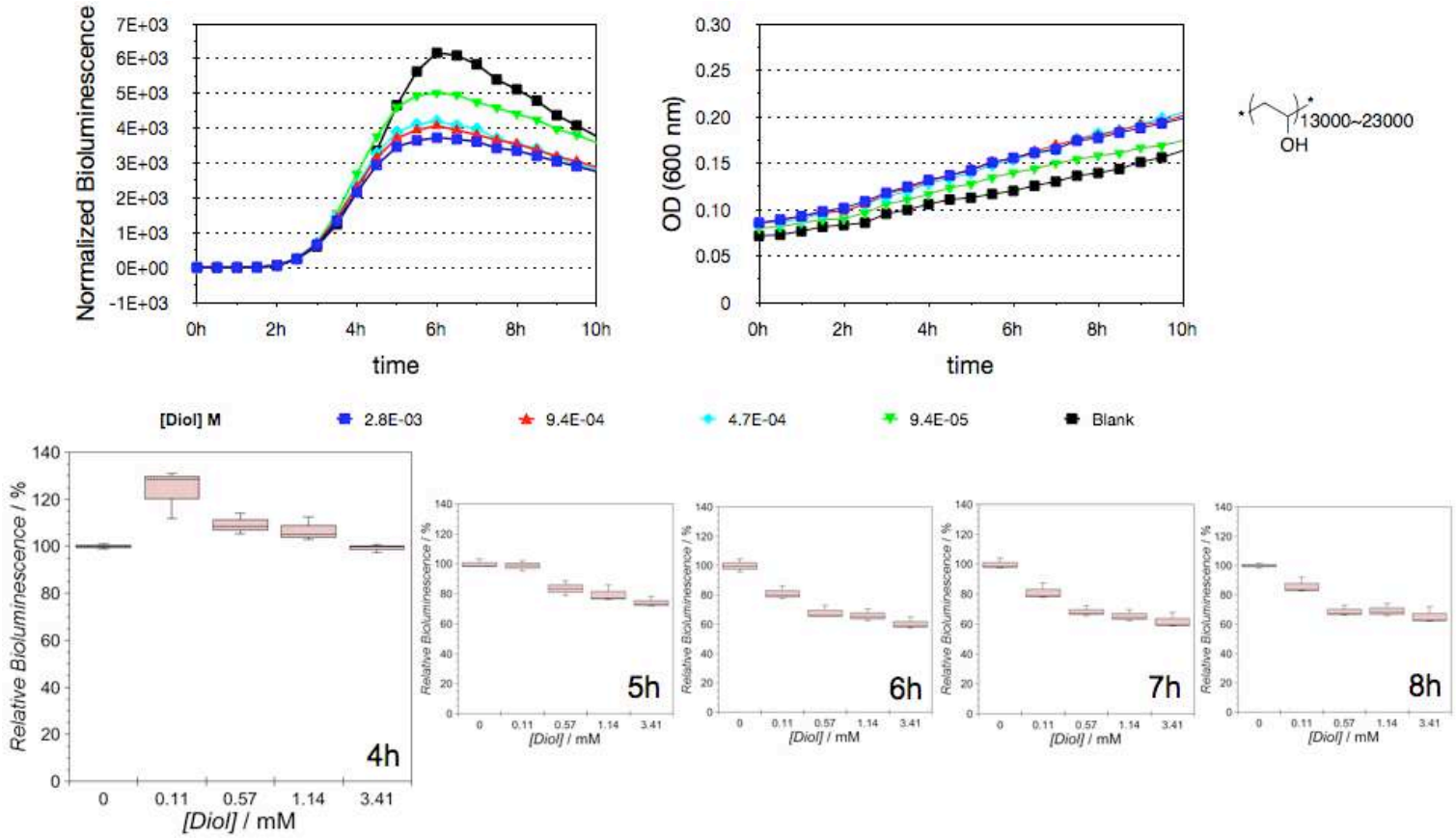

Figure 3-27. Light production curves and OD (600 nm), as a function of time for *V. harveyi* MM32 in the absence and presence of Polymer **PVA**.

Bottom: Effect of diol concentration in light production. (***protocol 1***)

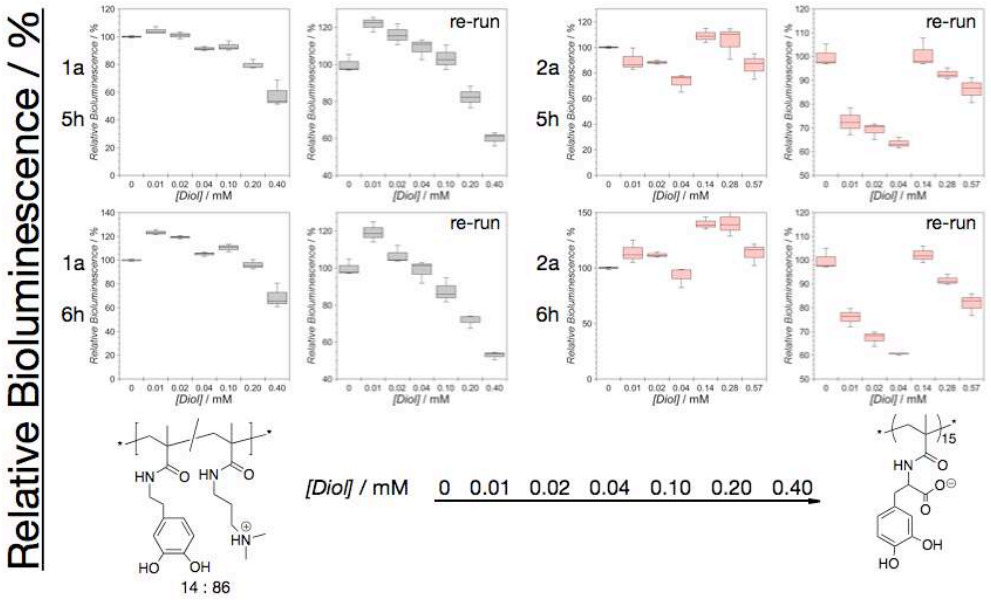

Figure 3-28. Similar results of bioluminescence MM32 assay in the presence of polymer **1a** and **2a** from two independent repeats. (***protocol 1***)

In addition, experiments were carried out with the same overnight culture of *V. Harvey* MM32 and Polymer **1a,b** and Polymer **2a,b**, which show similar water solubility and boron affinity, but whose main difference was their ability to cluster bacteria. In these experiments the concentration of boron was fixed (0.4 mM) in order to saturate AI-2 production and the addition of polymers was delayed 4 h, approximately the time of onset of light production for the previous experiments, in order to synchronize bacterial response prior to polymer addition. This way, not only the efficiency of the polymers could be properly compared but also different experimental conditions could be tested in order to see if they had an effect in the dual activity of the polymers (*Figures 3-29 to 3-33*). In these cases, the same dual behavior (bioluminescence inhibition vs enhancement) was observed in additional assays at applied polymer concentrations as those reported before, but responses in the presence of polymers were significantly enhanced. Such enhancement was attributed to

the 0.4 mM boron externally added to the media (compared to ***protocol 1*** in which the only boron source is the small amount that exists in water and media salts) that amplified the response of QS. This is because DPD molecules could react with boron to form active signal (AI-2) more effectively with higher boron concentration (fixed the concentration of DPD and other salts) and thus induced more lights (This has been proved by later work performed by Cheng Sui in my PhD group, data not shown). On the other hand, polymer **1a** and **1b** were tested together by using the same overnight culture, while polymer **2a** and **2b** were examined together with another batch of overnight culture. Thus, the much bigger enhancement of light in the presence of polymer **1a** and **1b** after 7 h (*Figure 3-29 and 3-30*) than that with addition of polymer **2a** and **2b** (*Figure 3-31 and 3-32*) were resulted from the difference between the two cultures. Here, the relative bioluminescence as a function of polymer-diol concentration at 3.5 h, 5 h and 7 h time points were presented together (*Figure 3-33*) to give a better comparation. Similar to the results of ***protocol 1***, 'oscillation' of light output with varied polymer-diol concentration could be observed due to the 'dual' function competitively existence in the system, expect of polymer **2a**, in the presence of which such phenomenon was not that significant. This is anticipated that polymer **2a** gave comparable binding affinity for boron/QS signal to the other three polymers but lowest affinity to binding cells and thus the effect of QS quenching was much higher than cell sequestration (no enhancement for the first 7 h). However, the enhancement of bioluminescence was observed at later time point even for polymer **2a** (*Figure 3-31*, left, at 9-10 h), which reconfirmed its dual functionality. It was notable that the reduction and enhancement of light production appeared at different time point and also

gave varied value when different protocols and/or overnight cultures were used, but the overall trends were always the same.

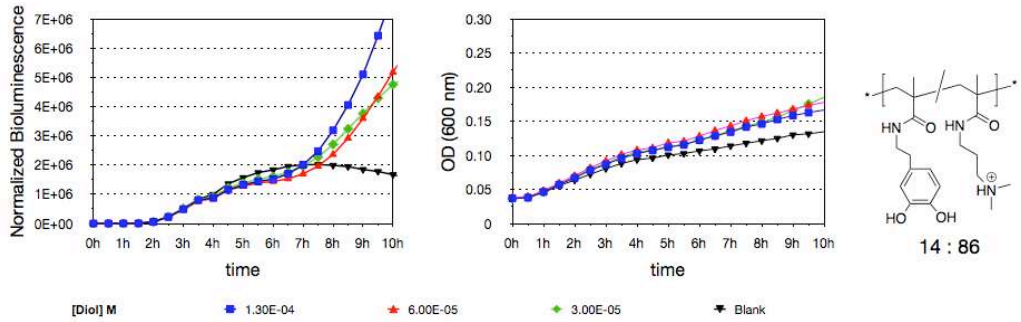

Figure 3-29. Light production curves and OD (600 nm), as a function of time for *V. harveyi* MM32 in the absence and presence of Polymer **1a** (***protocol 2***)

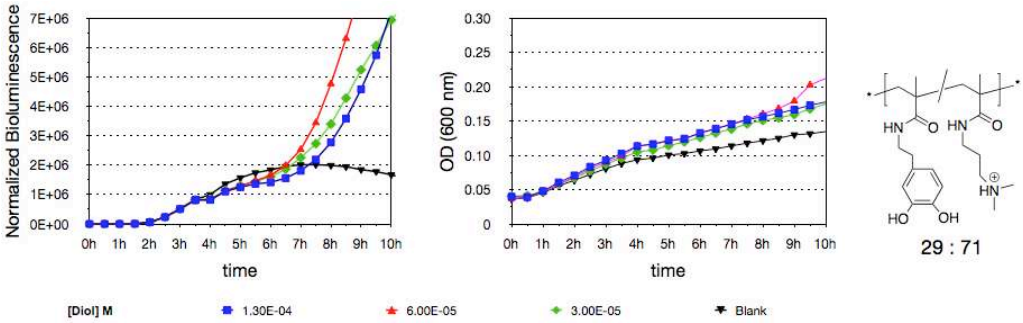

Figure 3-30. Light production curves and OD (600 nm), as a function of time for *V. harveyi* MM32 in the absence and presence of Polymer **1b** (***protocol 2***)

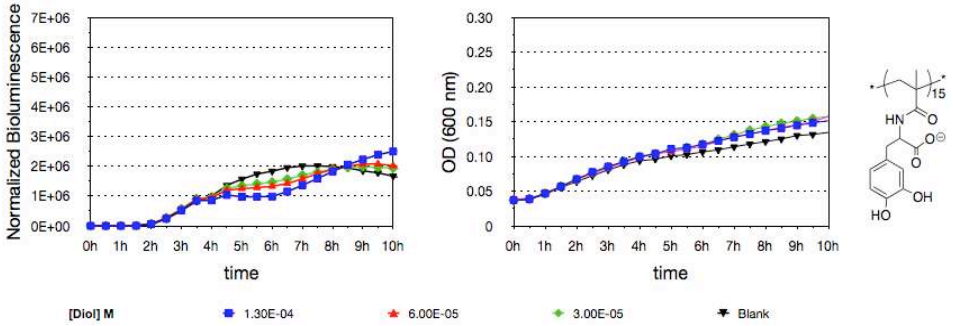

Figure 3-31. Light production curves and OD (600 nm), as a function of time for *V. harveyi* MM32 in the absence and presence of Polymer **2a** (***protocol 2***)

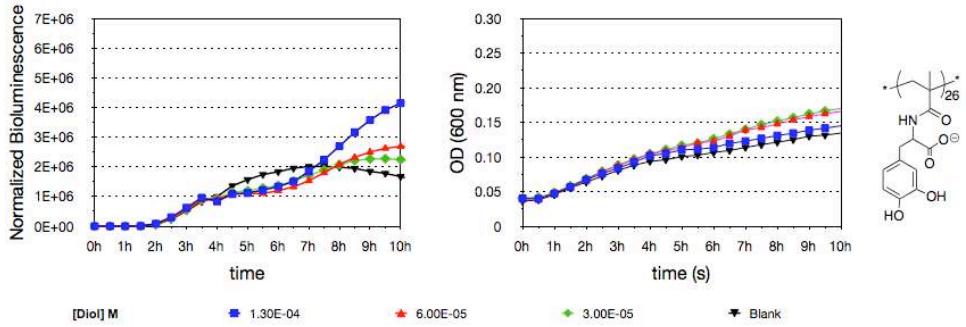

Figure 3-32. Light production curves and OD (600 nm), as a function of time for *V. harveyi* MM32 in the absence and presence of Polymer **2b** (***protocol 2***)

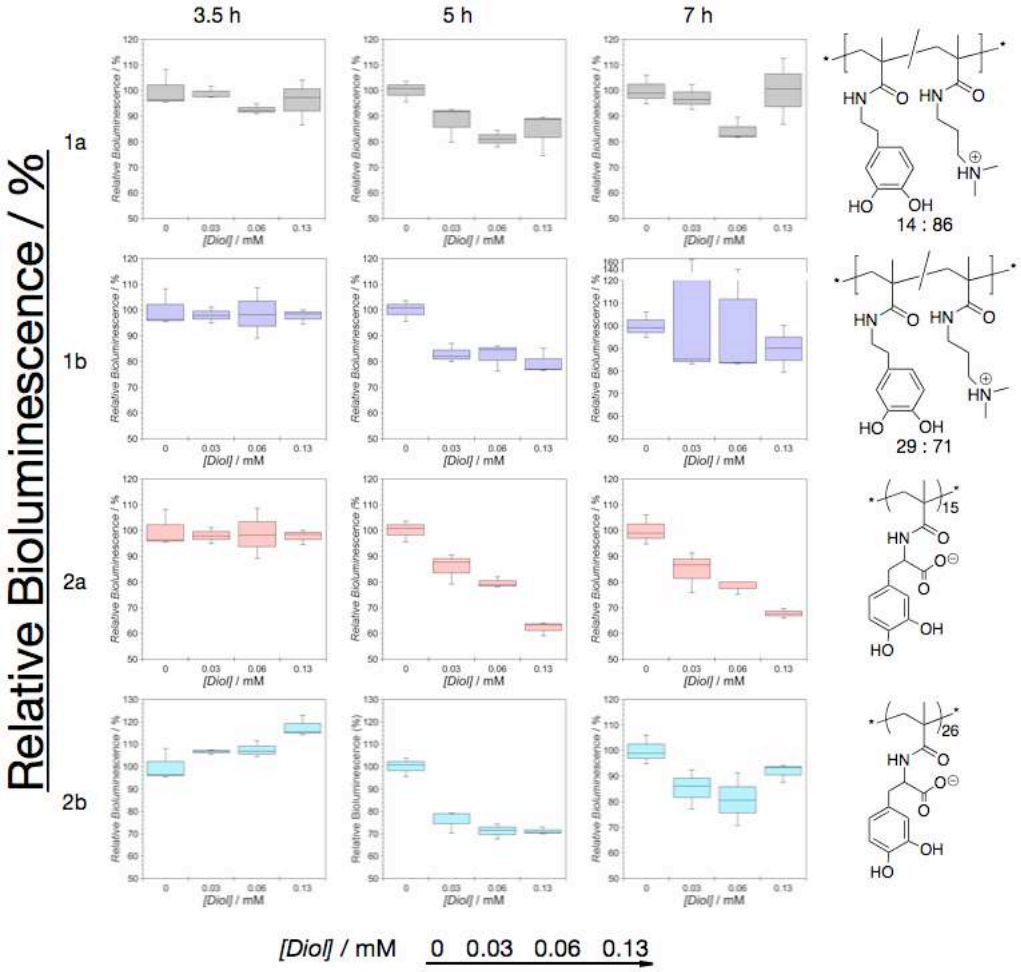

Figure 3-33. Effect of diol concentration in light production, in the absence and presence of Polymers **1** and **2** (***protocol 2***)

These results suggested that in these systems reversible borate-diol binding reactions compete with irreversible bacteria-polymer clustering as well as bacteria-QS binding interactions. While the detailed mechanisms by which these interactions were occurring are still not fully clear, support for a feedback-competition model was obtained from experiments with PVA, which did not bind to bacteria, but was able to sequester borate with low affinity, giving rise to simpler dose-dependent QS quenching (*Figure 3-27*) but with no cell sequestration or cell-growth dependent binding. By contrast, the dual-action polymers **1-3**, having three different functional group types (cationic, saccharide and catechol), each of which varied in total aggregation efficacy, were able to sequester *V. harveyi* through adhesion and interference with their QS network. Of crucial importance was that this range of polymers was able to maintain bacterial capture and suppression of QS signalling, but without damaging cell viability[31] (as judged by continuing growth in optical density measurements) (*Figure 3-22 to 3-27*, *3-29* to *3-32*).

In order to minimize any error coming from the protocol, another approach aimed to achieve constant volumes of bacterial media of each well in the 96-microplate was applied. To explain the difference, in ***protocol 3*** samples composed of polymers, bacteria and media placed in each wells and sealed with aluminum plate cover were incubated in a 30 °C incubator all through the assay, (except 10 min/2 h testing time in room temperature) while in the ***protocol 1*** and ***2***, a 30 °C Tecan plate reader automatically reads light production and optical density every 30 min without cover to prevent sample media evaporation.

According to the data presented (*Figure 3-34* to *3-37*), the linear polymers decreased the light production in a dose-dependent way in all cases at earlier time points. However, compared to the results from the previous protocol, the maximum output of light production moved from 9 h to 11 h, and even after 12 h there was no sign to show a reduction of light production. These results were anticipated. The new method to some extent decreased the media evaporation rate. In this case, the change of OD and concentration of the contents (e.g. AI-2 molecules, DPD and free boron) correlated to media volume, but was slower. However, the overall trend of each polymer addition assay was in accord with what was obtained before. The 'oscillation' of light output with different polymer-diol concentrations, which was believed to be the feature in the presence of dual function polymers, could be observed (*Figure 3-38*). The results suggested two basic mechanisms operate in tandem in terms of polymers inhibiting light production based initially on boron-diol binding, but also enhancing light production as the polymer induced bacteria aggregation occurs. This conclusion was verified again when the assay data of control polymer PVA was compared to those of the other proposed diol-functional polymers. PVA lacks the ability to induce bacterial aggregation and thus could change the bacterial communication via only one mechanism (QS quenching).

It should be noted that an issue for the bioassays is the variation of factors arising from the cell environment that are difficult to be fixed exactly the same for each assay. For example, the end-point assay and time-course assay were performed with the same bacterial overnight culture, 96-well plate, incubator and plate-reader, but results were on occasions different. Therefore, it is worth

focusing on the overall trend of each assay result rather than specific individual values.

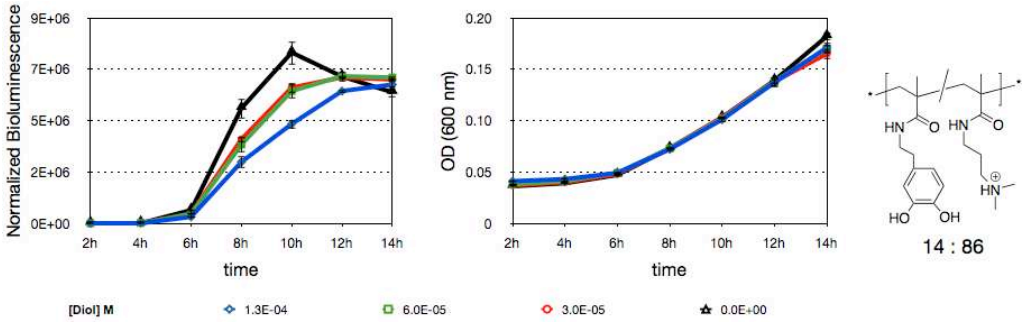

Figure 3-34. Light production curves and OD (600 nm), as a function of time for *V. harveyi* MM32 in the absence and presence of Polymer **1a** (***protocol 3***)

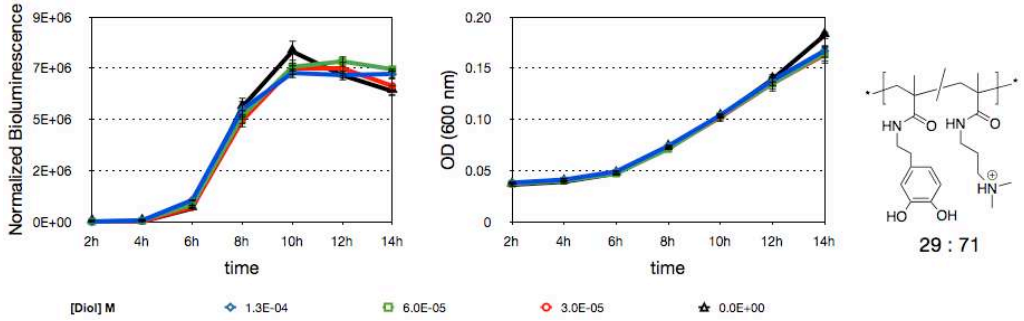

Figure 3-35. Light production curves and OD (600 nm), as a function of time for *V. harveyi* MM32 in the absence and presence of Polymer **1b** (***protocol 3***)

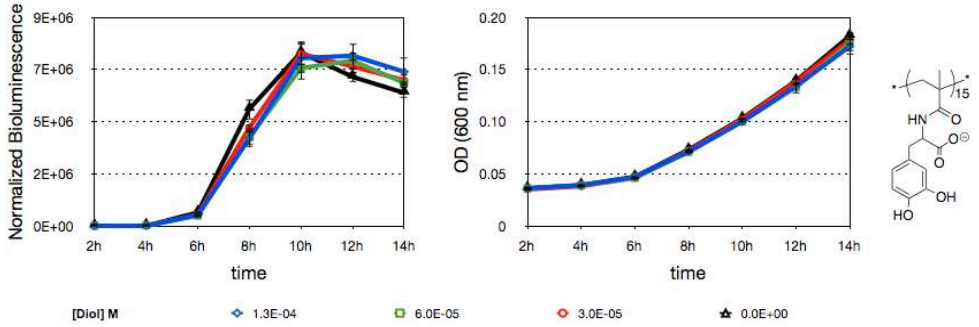

Figure 3-36. Light production curves and OD (600 nm), as a function of time for *V. harveyi* MM32 in the absence and presence of Polymer **2a** (***protocol 3***)

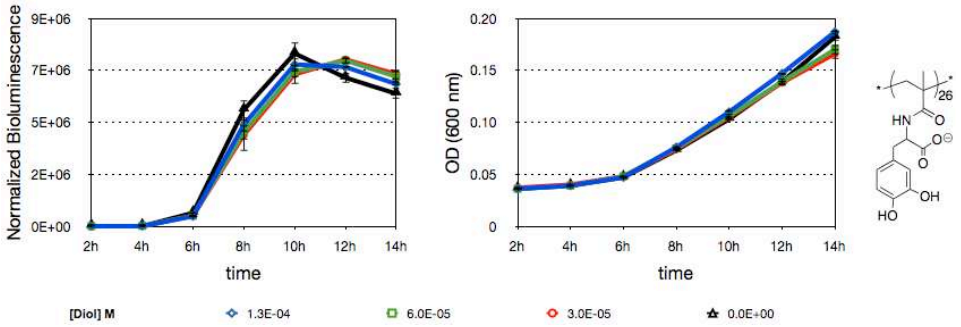

Figure 3-37. Light production curves and OD (600 nm), as a function of time for *V. harveyi* MM32 in the absence and presence of Polymer **2b** (***protocol 3***)

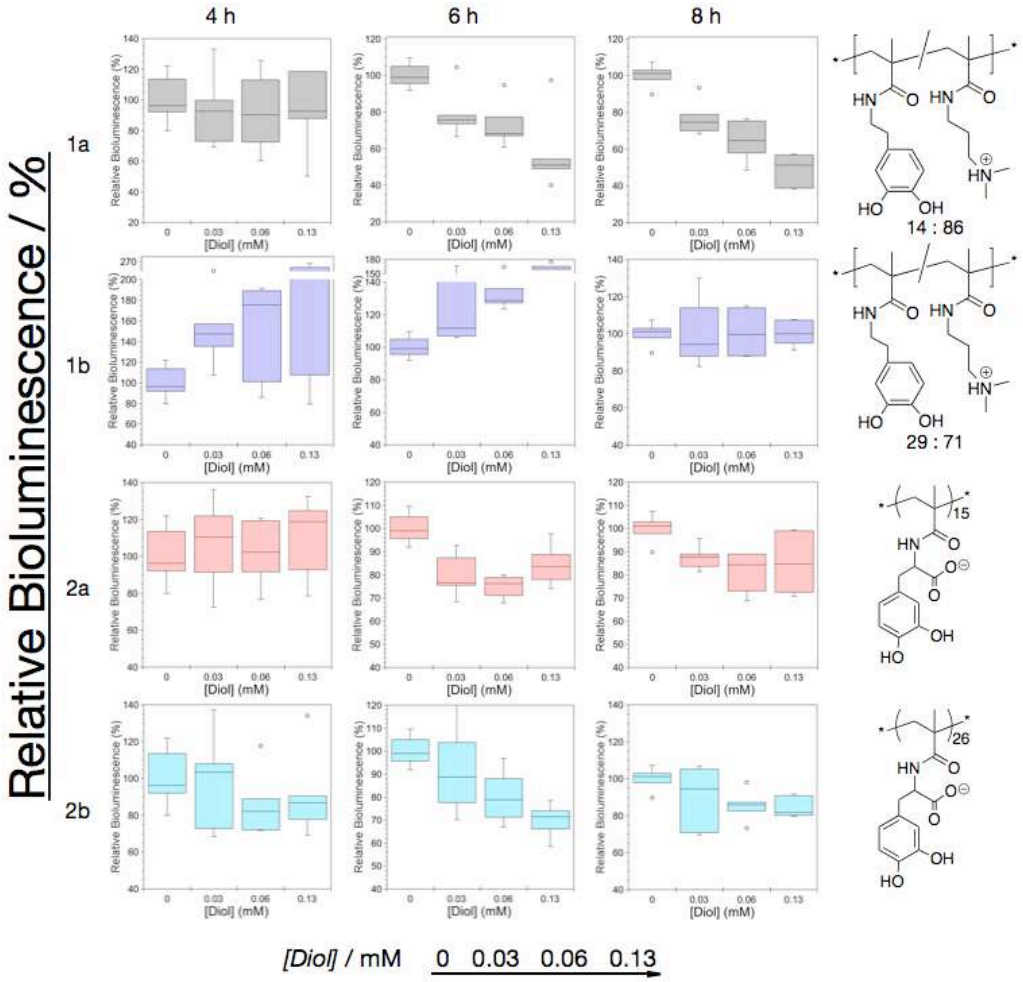

Figure 3-38. Effect of diol concentration in light production, in the absence and presence of Polymers **1** and **2** (***protocol 3***)

To address some of the issues above, future bioluminescence assays were considered to compromise with ***protocols 1, 2 and 3*** (*Figure 3-39* to *3-41*). In this case, sample loaded well-plates are incubated in the 30 °C incubator for the first 4 h (the light onset time point) and then kept in the plate reader to automatically record the intensity of bioluminescence and cell optical density every 30 min (***protocol 4***). The resutls showed the same 'oscillation' of bioluminescence in the presence of different concentrations of polymer **1a**, **1b**, **2a** and **2b**, which demonstrated again the dual function as described above (*Figure 3-42*).

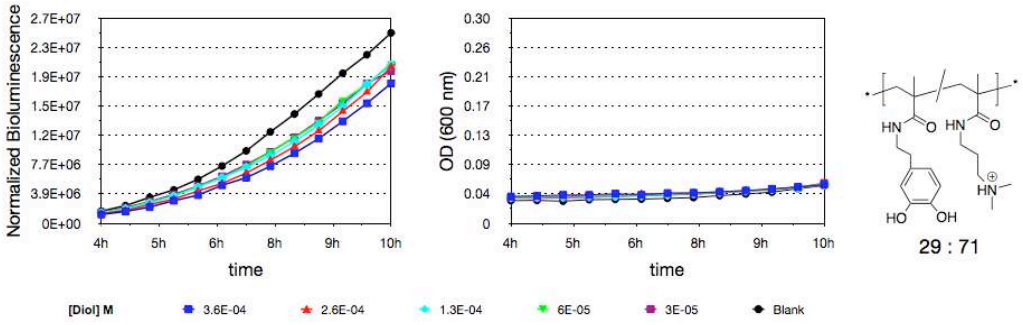

Figure 3-39. Light production curves and OD (600 nm), as a function of time for V. harveyi MM32 in the absence and presence of Polymer **1b**. (***protocol 4***)

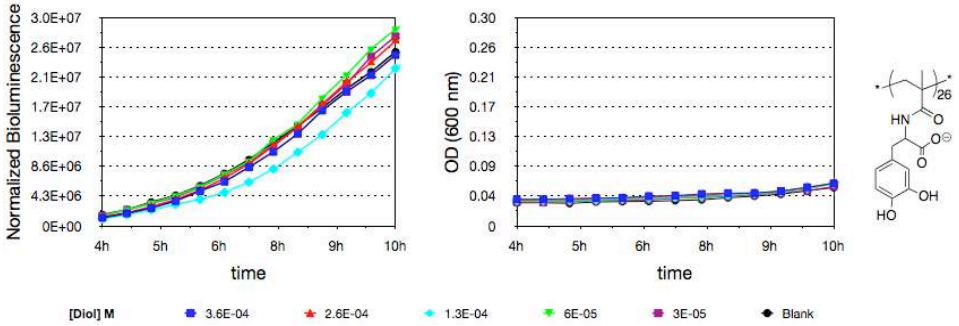

Figure 3-40 Light production curves and OD (600 nm), as a function of time for V. harveyi MM32 in the absence and presence of Polymer **2b**. (***protocol 4***)

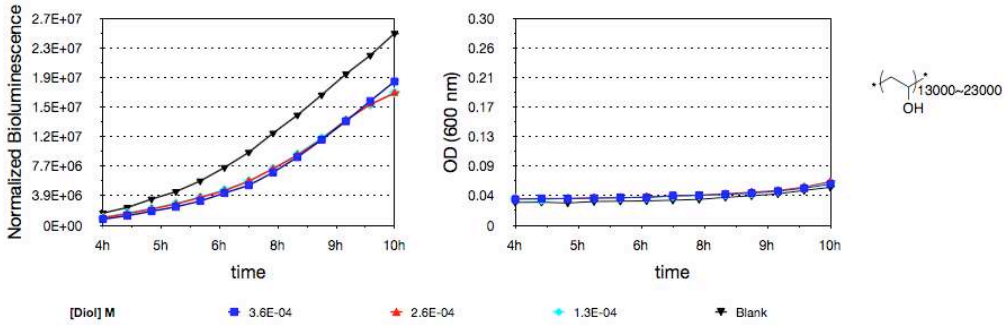

Figure 3-41 Light production curves and OD (600 nm), as a function of time for *V. harveyi* MM32 in the absence and presence of Polymer **PVA**. (***protocol 4***)

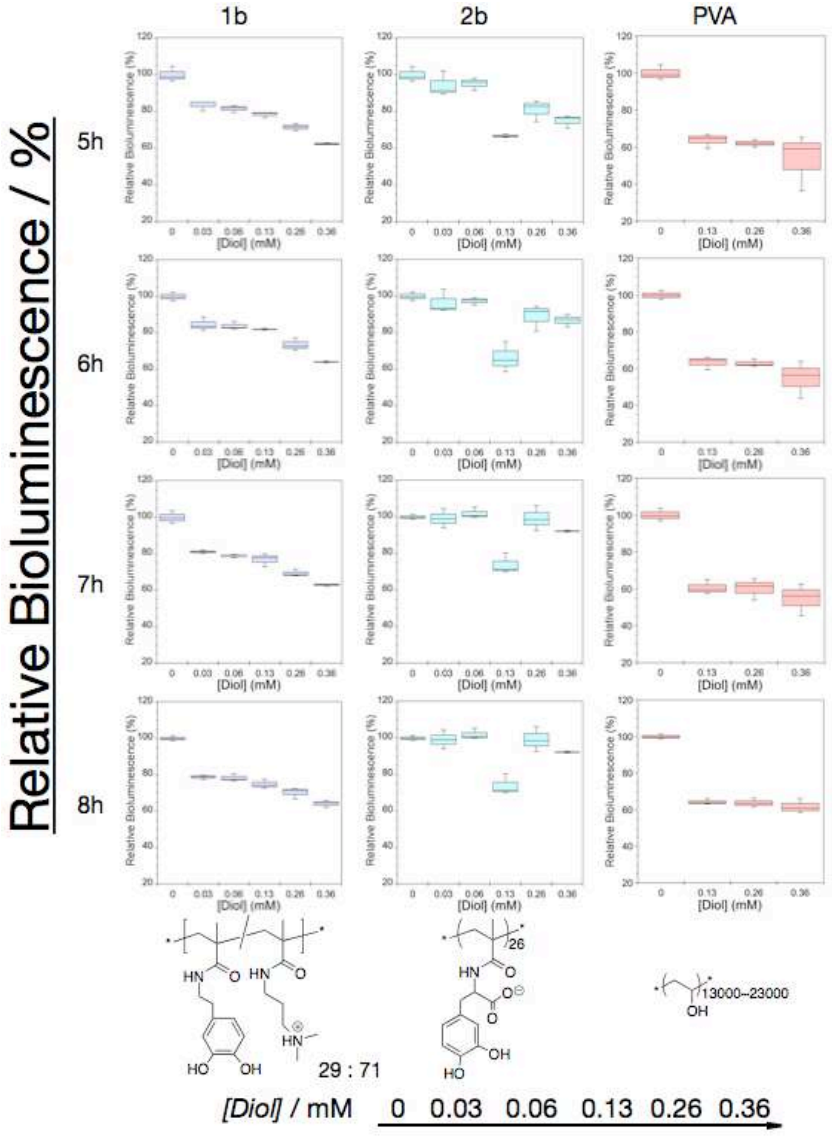

Figure 3-42. Effect of diol concentration in light production, in the absence and presence of Polymers **1b**, **2b** and **PVA** (***protocol 4***)

3.2.7.2 BB170 assay

Bioluminescence assay were also performed with *V. harveyi* bacteria - BB170 mutant ($LuxN^-$), in the presence and absence of linear polymers. Unlike *V. harveyi* MM32 mutant ($LuxN^-$ and $LuxS^-$), the BB170 strain is able to produce its own AI-2 precursor - DPD molecules, as it possesses LuxS protein responsible for DPD biosynthesis, while similar to MM32 that no other signal molecule (AI-1) generated by BB170 due to the lack of protein LuxN responsible for AI-1 signal molecule biosynthesis. In this case, the light production was only under control of AI-2 QS system. The whole assay procedure was the same as described in ***protocol 1*** for MM32 assay and no modification to prevent evaporation for this initial stage, but without external addition of DPD. As mentioned, MM32 strain was selected as the main bacterial model was because it is a *V. harveyi* mutant which lacks LuxS protein and therefore cannot produce DPD by its own. By externally adding DPD molecule into the assay media, its overall concentration should be constant all through the experiment, which simplifies the bacteria QS feedback system. On the other hand, for BB170 the concentration of QS signals increase as the number of bacteria in a local population increase. When reaching a threshold concentration, the signaling molecules (AI-2) activate specific receptors to regulate QS-dependent gene expression.[29, 32] Herein, the bioluminescence outputs for BB170 strain in the presence of investigated polymers are anticipated to be more complicated than those for MM32 mutant.

Similarly, variations in time of onset, as well as magnitude of light production were observed as the concentrations of different polymers in suspensions of bacteria varied (*Figure 3-43 to 3-46*). Intriguingly however, unlike MM32

assay for which all the polymers exhibited dose-dependent suppression of light production (except polymer **2a**, see 'MM32 data') at earlier time points (5h, *Figure 3-22* to *3-27*), the assay performed with BB170 mutant showed dose-dependent enhancement of light output all through the assay (*Figure 3-43* to *3-46*). Apparently, the light onset of BB170 was earlier (around 2h) than that of MM32 strain (around 4h), so more attention was paid on earlier time points (2h, 4h, 6h) for the effect of diol concentration on light output (*Figure 3-43 to 3-46*, bottom). At early time periods (2h, *Figure 3-43 to 3-46*, bottom) increases in light production were observed in the presence of polymers **1a**, **1b**, **2c** and **3** without bioluminescence suppression at any time points, while over time (4h and 6h, *Figure 3-43 to 3-46*, bottom) the same dose-dependent trends but varied rates of light enhancement were observed. Interestingly, the 'oscillation' of the light with different polymer concentrations could be observed again.

These initial results of BB170 assay suggested that the onset and duration of polymer effects were dependent on the bacterial mutant as well as their cell growth stage. Since binding of bacteria (MM32) and boronic acids by polymers **1-3**, and their potential to reduce the concentration of AI-2 in solution have already been demonstrated (AR-S assay and bacterial attachment assay), it was assumed that polymers retained their dual-action on QS and bacterial sequestration for BB170 strain (light 'oscillation' responsed to different polymer concentration). However, to identify its feedback mechanism, more experiments are needed such as polymer sequestration assay with BB170 cells, repeated bioluminescence assays with modified protocols and investigation of new in-vitro assays.

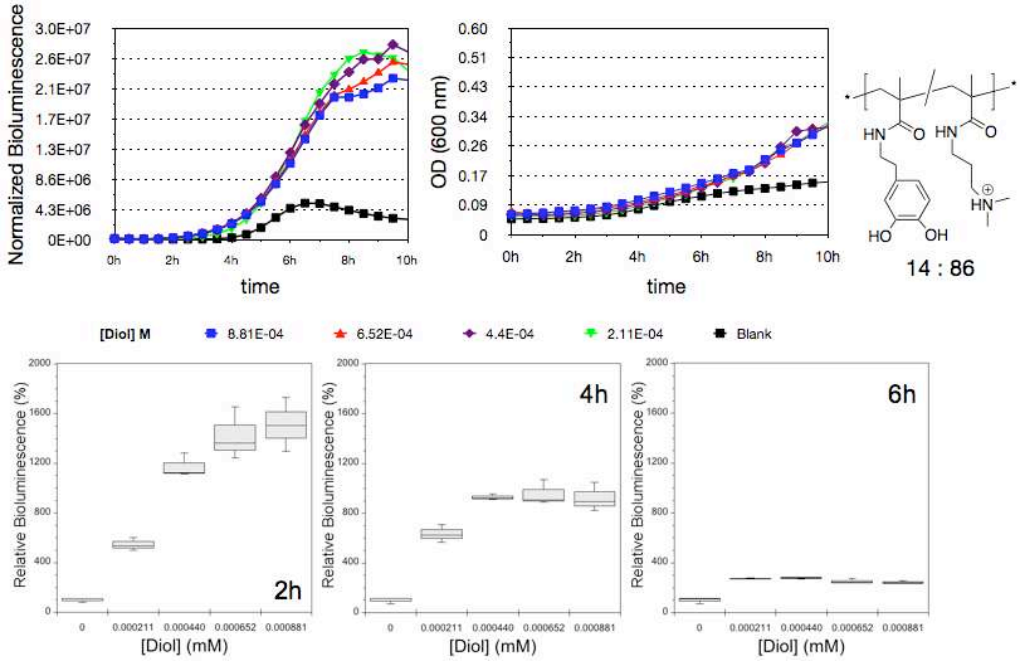

Figure 3-43. Top: Light production curves and OD (600 nm), as a function of time for V. harveyi MM32 in the absence and presence of Polymer **1a**. Bottom: Effect of diol concentration in light production.

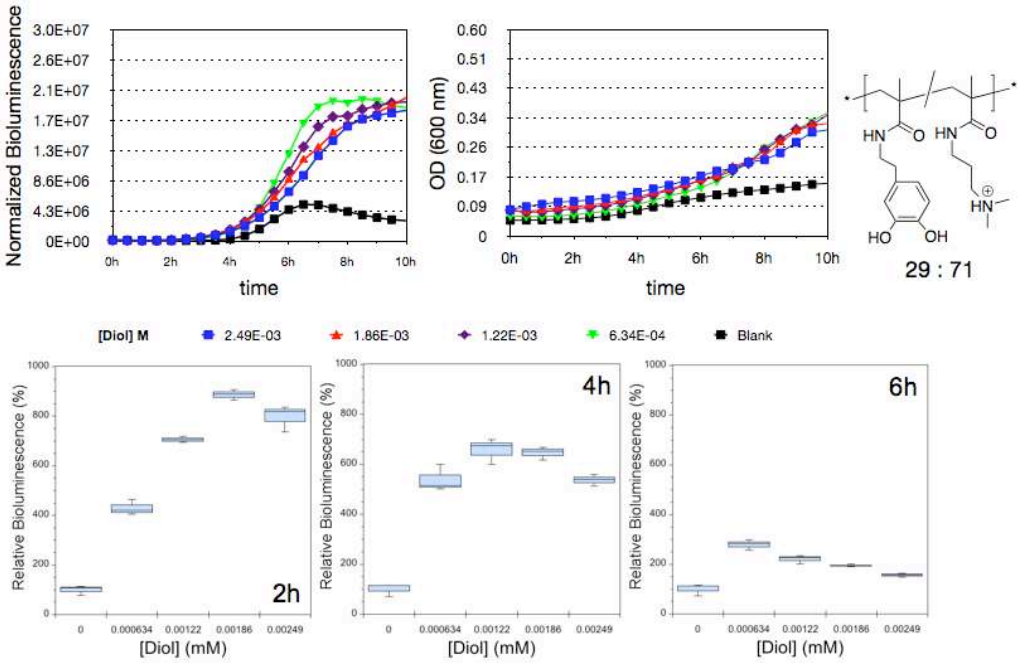

Figure 3-44. Top: Light production curves and OD (600 nm), as a function of time for V. harveyi MM32 in the absence and presence of Polymer **1b**. Bottom: Effect of diol concentration in light production.

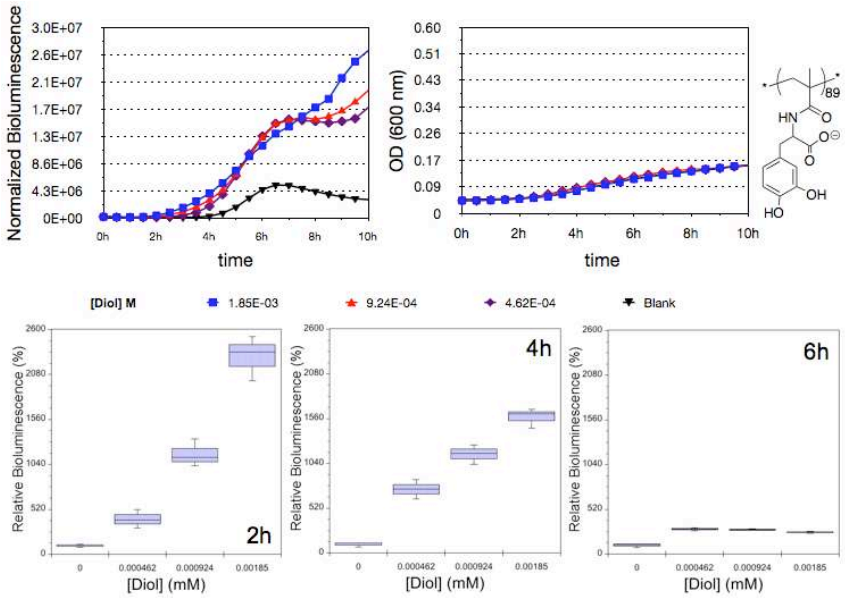

Figure 3-45. Top: Light production curves and OD (600 nm), as a function of time for V. harveyi MM32 in the absence and presence of Polymer **2c** (DP 89). Bottom: Effect of diol concentration in light production. (Polymer **2c** was used instead of polymer **2a** and **2b** (limited amount).)

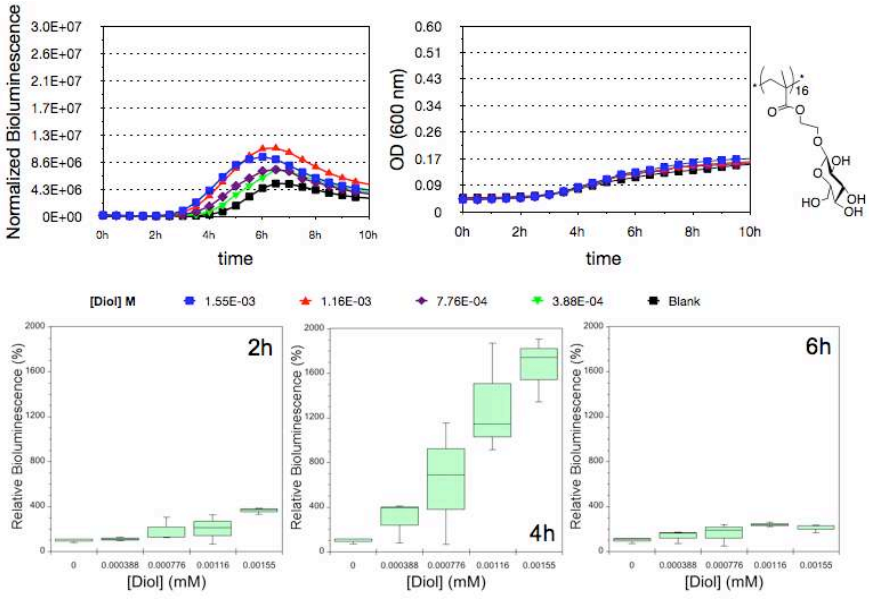

Figure 3-46. Top: Light production curves and OD (600 nm), as a function of time for V. harveyi MM32 in the absence and presence of Polymer **3**. Bottom: Effect of diol concentration in light production.

3.3 Conclusions

In this chapter, a series of polymers were successfully synthesized via RAFT polymerization process and characterized by ^{1}H-NMR, GPC (see **Appendix**) and DLS analysis. The binding abilities of the reported polymers with boric/boronic acid were established by the AR-S assay and confirmed by ^{11}B-NMR spectra. In all cases, polymers with multivalent effects gave higher affinities to boric and boronic acids than their corresponding small molecule analogous. In order to test cell sequestration of the polymers, bacterial attachment assays were performed in both AB-media and PBS buffer at pH 7.4. In this case, all the three types of investigated polymers were demonstrated to induce bacterial aggregation. All the above in-vitro experimental results suggested that polymers made in this chapter had dual function to the AI-2 controlled bacterial communication network.

In this case, the three types of polymers and 'control' polymer PVA were employed in a complex biological environment. The data showed the polymers had dual-function in binding and deactivating population responses in *V. harveyi*. Although MM32 assays were performed in different conditions (batch of cells, protocols and batch of DPD), the trends of light output in the presence of each individual polymer were constant all the experiments. Significantly this range of polymers was able to maintain bacterial capture and suppression of QS signaling without damaging the cells as judged by continuing growth in optical density measurements.

References

[1] P. Cossart, P. J. Sansonetti, *Science* **2004**, *304*, 242-248.
[2] K. Hori, S. Matsumoto, *Biochem Eng J* **2010**, *48*, 424-434.
[3] I. Ofek, D. L. Hasy, N. Sharon, *Fems Immunol Med Mic* **2003**, *38*, 181-191.
[4] S. Bonhoeffer, M. Lipsitch, B. R. Levin, *Proc Natl Acad Sci U S A* **1997**, *94*, 12106-12111.
[5] P. A. zur Wiesch, R. Kouyos, J. Engelstadter, R. R. Regoes, S. Bonhoeffer, *Lancet Infect Dis* **2011**, *11*, 236-247.
[6] C. Wongsrichanalai, A. L. Pickard, W. H. Wernsdorfer, S. R. Meshnick, *Lancet Infect Dis* **2002**, *2*, 209-218.
[7] M. Lipsitch, M. H. Samore, *Emerg Infect Dis* **2002**, *8*, 540-540.
[8] P. M. Hawkey, A. M. Jones, *J Antimicrob Chemother* **2009**, *64 Suppl 1*, 3-10.
[9] G. P. Treweek, J. J. Morgan, *J Colloid Interf Sci* **1977**, *60*, 258-273.
[10] R. J. Pieters, *Med Res Rev* **2007**, *27*, 796-816.
[11] aD. M. Lynn, A. S. Breitbach, A. H. Broderick, C. M. Jewell, S. Gunasekaran, Q. Lin, H. E. Blackwell, *Chemical Communications* **2011**, *47*, 370-372; bE. V. Piletska, G. Stavroulakis, K. Karim, M. J. Whitcombe, I. Chianella, A. Sharma, K. E. Eboigbodin, G. K. Robinson, S. A. Piletsky, *Biomacromolecules* **2010**, *11*, 975-980.
[12] H. Lee, B. P. Lee, P. B. Messersmith, *Nature* **2007**, *448*, 338-341.
[13] G. Wulff, *Pure Appl Chem* **1982**, *54*, 2093-2102.
[14] aC. Alexander, G. Pasparakis, A. Cockayne, *Journal of the American Chemical Society* **2007**, *129*, 11014-11015; bC. Alexander, G. Pasparakis, *Angewandte Chemie-International Edition* **2008**, *47*, 4847-4850.
[15] L. Albertin, M. H. Stenzel, C. Barner-Kowollik, T. P. Davis, *Polymer* **2006**, *47*, 1011-1019.
[16] J. Skey, R. K. O'Reilly, *Chem Commun (Camb)* **2008**, 4183-4185.
[17] aN. Sakai, S. Matile, *Journal of the American Chemical Society* **2003**, *125*, 14348-14356; bJ. N. Weiss, *FASEB J* **1997**, *11*, 835-841.
[18] M. B. Neiditch, F. M. Hughson, *Methods Enzymol* **2007**, *423*, 250-263.
[19] S. T. Miller, K. B. Xavier, S. R. Campagna, M. E. Taga, M. F. Semmelhack, B. L. Bassler, F. M. Hughson, *Mol Cell* **2004**, *15*, 677-687.
[20] A. Bennett, R. I. Rowe, N. Soch, C. D. Eckhert, *J Nutr* **1999**, *129*, 2236-2238.
[21] P. Glass, H. Chung, N. R. Washburn, M. Sitti, *Langmuir* **2009**, *25*, 6607-6612.
[22] aG. Moad, E. Rizzardo, S. H. Thang, *Australian Journal of Chemistry* **2005**, *58*, 379-410; bA. Favier, M.-T. Charreyre, *Macromolecular Rapid Communications* **2006**, *27*, 653-692; cG. Moad, E. Rizzardo, S. H. Thang, *Australian Journal of Chemistry* **2006**, *59*, 669-692; dG. Moad, E. Rizzardo, S. H. Thang, *Australian Journal of Chemistry* **2009**, *62*, 1402-1472.
[23] A. B. Lowe, C. L. McCormick, *Progress in Polymer Science* **2007**, *32*, 283-351.

[24] aS. H. Thang, Y. K. Chong, R. T. A. Mayadunne, G. Moad, E. Rizzardo, *Tetrahedron Letters* **1999**, *40*, 2435-2438; bM. R. Wood, D. J. Duncalf, S. P. Rannard, S. Perrier, *Organic Letters* **2006**, *8*, 553-556.
[25] aM. F. Semmelhack, S. R. Campagna, C. Hwa, M. J. Federle, B. L. Bassler, *Organic Letters* **2004**, *6*, 2635-2637; bM. F. Semmelhack, S. R. Campagna, M. J. Federle, B. L. Bassler, *Organic Letters* **2005**, *7*, 569-572.
[26] G. A. Vydryakova, *Applied Biochemistry and Microbiology* **2006**, *42*, 364-368.
[27] aH. Lee, B. P. Lee, P. B. Messersmith, *Nature* **2007**, *448*, 338-342; bH. Lee, J. Rho, P. B. Messersmith, *Advanced Materials* **2009**, *21*, 431-434.
[28] aN. Ni, G. Choudhary, M. Li, B. Wang, *Bioorganic & Medicinal Chemistry Letters* **2008**, *18*, 1567-1572; bC. A. Lowery, N. T. Salzameda, D. Sawada, G. F. Kaufmann, K. D. Janda, *Journal of Medicinal Chemistry* **2010**, *53*, 7467-7489.
[29] C. M. Waters, B. L. Bassler, *Annu Rev Cell Dev Biol* **2005**, *21*, 319-346.
[30] aJ. Q. Boedicker, M. E. Vincent, R. F. Ismagilov, *Angewandte Chemie-International Edition* **2009**, *48*, 5908-5911; bE. C. Carnes, D. M. Lopez, N. P. Donegan, A. Cheung, H. Gresham, G. S. Timmins, C. J. Brinker, *Nature Chemical Biology* **2010**, *6*, 41-45.
[31] C.-W. Chang, E. Bays, L. Tao, S. N. S. Alconcel, H. D. Maynard, *Chemical Communications* **2009**, 3580-3582.
[32] aB. L. Bassler, A. Camilli, *Science* **2006**, *311*, 1113-1116; bP. Williams, K. Winzer, W. C. Chan, M. Camara, *Philos Trans R Soc Lond B Biol Sci* **2007**, *362*, 1119-1134.

Chapter 4. Preparation and Characterization of Polymeric Vesicles/Polymersomes: Biological Application Studies

4. Introduction

Having established a basic platform for understanding the principles of polymer-cell and polymer-signal molecule/boron interactions (**Chapter 2** and **3**) in cell-cell communication process as well as in the bacterial-colony invasion network, the research in this chapter extends towards a more meaningful test between real cells and artificial protocells.

As noted earlier, in this project the research was mainly focused on three key hypotheses underlying the concepts of protocells.

1. Synthesis of artificial materials that interact with natural networks;
2. Interference of Quorum Sense (QS) signaling and sequestration of cells;
3. Establishment and development of artificial-natural signal feedback loops.

The first two aspects have been addressed by developing diol-functional linear polymers capable of interfering bacterial chemical communication pathways as well as binding cells into clusters (**Chapter 3**). However, the linear polymers have a limited ability to establish communication cycles between real cells and artificial materials as they cannot encapsulate and release signals. Herein, polymersomes self-assembled from amphiphilic block copolymers with a liposome-like membrane and an aqueous compartment are investigated. The concept is to contain a series of small functional molecules, such as QS mediator - DPD into the aqueous compartment of the polymersomes and then to release the signals in a controlled manner by tuning the chemical composition and architecture of block copolymers. In this chapter, polymersomes will be designed to release, detect and respond to signal

molecules, as an interim step towards establishing communication loops with the real bacterial cells. These polymersomes might in future function as protocells if they could incorporate a simple metabolism.[1]

Polymersomes are usually self-assembled from three types of amphiphilic block copolymers: regular block copolymers - coil to coil, block copolymers with rigid blocks - rod to coil and rod to rod, and block copolymers with intermolecular interactions such as charge interactions, ligand binding, H-bonds, dipolar interactions, etc.[2] There are two commonly used approaches for preparing polymersomes: 1) film rehydration, and 2) solvent-exchange techniques. In both methods, a good solvent for both hydrophilic and hydrophobic components has to be properly selected, such as tetrahydrofuran (THF), ethanol, methanol or even mixture solvents, to completely dissolve the amphiphilic copolymers. Polymersomes are subsequently prepared through solvent evaporation to form a thin film, which is then rehydrated in the aqueous phase in the 'film rehydration' approach. Alternatively, the organic phase loaded with copolymer can be added to aqueous media or vice versa and then the organic solvent either evaporates or diffuses into the aqueous phase, leaving the polymersomes.

Typically, the size and shape of the aggregates are determined by chemical constitution, the length of each individual block, the properties of the solvent, the environmental conditions of the solution (e.g. pH, temperature, ions and concentration), the volume ratio of organic phase and aqueous phase, the solvent removing rate and also the preparation method.[3] For typical polymer materials the effects of solvents and process variables are key parameters in formulation development. A recent paper reported the preparation of

doxorubicin-loaded nanopolymersomes and investigation of various solvents and process variables as a function of size and drug loading during the whole preparation process.[4] The polymersome preparation method adopted in this study was based on nanoprecipitation and 'solvent-exchange' techniques and has been recognized as a valid and efficient approach toward preparing polymersomes.[5] After polymersome formation, the solvent residue or free drug if applicable was removed by dialysis against aqueous solution. A number of variables can be optimized in order to achieve targeted size and dispersity of nanopolymersomes in this process, which was demonstrated in this report that many experimental parameters including ratio and composition of organic and aqueous phase, order of addition of phases, copolymer concentration and external energy input can be important factors.

An important part of the design and preparation process is characterization of polymersomes using particle analysis techniques. The most commonly applied technique to determine particle size and distribution in suspension or solution is Dynamic Light Scattering (DLS) also known as Photon Correlation Spectroscopy.[6] Another important characteristic of polymersomes is the surface electrical charge in colloidal suspension or emulsion, which is usually measured by DLS and recorded as zeta potential.[7] Some polymersomes tend to ionize to form a charged-film on particle surfaces, while others may gain charges by adsorbing ions from their surroundings. In either case, the overall condition of the solution is always neutral since the numbers of counter ions are evenly balanced. Such property of polymersomes is important, as it reflects several properties of the media suspension or emulsion. Microscopy can also be used to characterize polymersomes in terms of size, size distribution,

morphology and homogeneity.[8] For example, optical microscopy is suitable to assess particles with diameter greater than 1 μm, while Transmission Electron Microscopy (TEM) and Scanning Electron Microscopy (SEM) are good alternatives to record the nano-sized particles (> 5 nm). Particularly, Confocal Laser Scanning Microscopy (CLSM), a fluorescence microscopy, allows to record images of large polymersomes (> 1 μm) with fluorescence either from its own chemical structure or from labeling fluorochromes.[9] For surface analysis, Atomic Force Microscopy (AFM) measures surface morphology by testing the change in surface height with a cantilever tip on an atomic scale.[10] Surface roughness values calculated from AFM data are an important parameter in several biological applications, for such property may be related to cell adhesion.[11]

This chapter will mainly describe the synthesis of amphiphilic block copolymers and the preparation of polymersomes, while the effect of functional polymersomes for QS network and bacterial invasion system in a specific strain compared to their corresponding linear polymers investigated early in this study will also be discussed. Also, the encapsulation of DPD molecules in the aqueous compartment of polymersomes and the release of these signal molecules will be demonstrated as the first step toward constructing synthetic-natural feedback loops.

4.1 Experiments

4.1.1 Synthesis of amphiphilic block copolymers

4.1.1.1 Synthesis of monomers

4.1.1.1.1 N-(2-ethylhexyl) methacrylamide (2-EHMAm)[12]

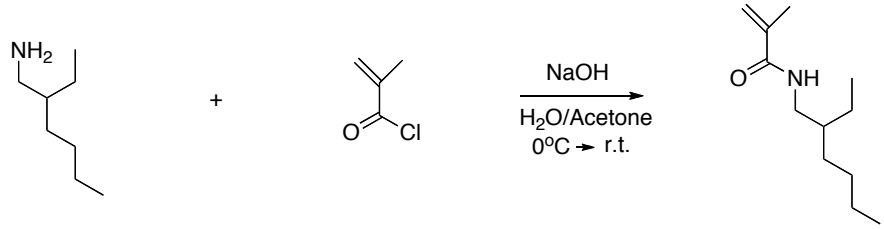

2-ethylhexan-1-amine methacryloyl chloride N-(2-ethylhexyl)methacrylamide

2-Ethylhexan-1-amine (5.0 g, 38 mmol) was dissolved in 57 mL acetone and 57 mL sodium hydroxide solution and cooled in an ice bath. Methylacryloyl chloride (7.4 mL, 76 mmol) was added dropwise over 30 mins, and the reaction mixture was stirred at 0 °C in the ice bath overnight. Then, sodium chloride solid was added to saturate the mixture. The product was extracted with ethyl acetate three times and then washed with sodium chloride solution once. The extract was concentrated on a rotary evaporator (~ 30 °C) and the residue was purified by flash chromatography using a mixed eluent of hexane and ethyl acetate (3:1 ~ 7:3 v/v). After the solvent was removed, the title compound was recovered (5.6 g, 76%) and stored in the refrigerator. ^{1}H-NMR ($CDCl_3$, 400 MHz) δ (ppm) 5.61 (*s*, 1H, C=CH, *trans*), 5.25 (*s*, 1H, C=CH, *cis*), 3.30-3.17 (*m*, 2H, N-CH_2), 1.99 (*m*, 1H, CH), 1.92 (*s*, 3H, CCH_3), 1.52-1.36 (*m*, 2H, $CHCH_2CH_3$), 1.37-1.15 (*m*, 6H, $CH_2CH_2CH_2$), 0.99-0.80 (*m*, 6H, CH_2CH_3). ^{13}C-DEPT (CD_3Cl, 400 MHz) δ (ppm) 118.84 ($=CH_2$), 42.54 ($NHCH_2$), 39.34 (CH), 31.04 ($CHCH_2CH_2$), 28.85 ($CHCH_2CH_2$), 24.30 ($CHCH_2CH_3$), 22.96 ($CH_2CH_2CH_3$), 18.71 (CCH_3), 14.00 ($CH_2CH_2CH_3$)), 10.84 ($CHCH_2CH_3$). IR (KBr) ν (cm^{-1}) 3318 (N-H), 3089 (=C-H), 2958, 2926,

2872 and 2859 (-C-H), 1655 (Amide C=O), 1618 and 1538 (N-H), ESI-MS: m/z 198.18 (MH^+, 100%), 197.28 (M, 1%).

4.1.1.1.2 N-(2-ethylhexyl) acrylamide (2-EHAm)[12]

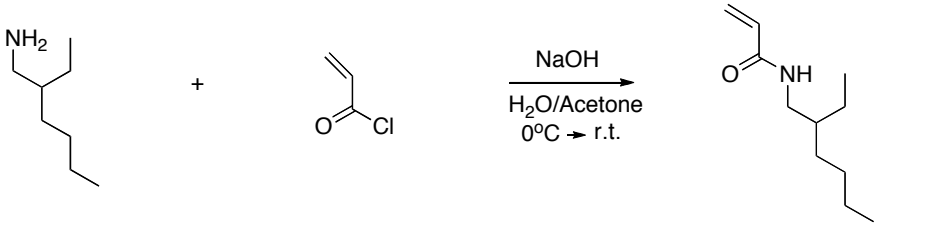

2-ethylhexan-1-amine acryloyl chloride N-(2-ethylhexyl)acrylamide

2-Ethylhexan-1-amine (5.0 g, 38 mmol) was dissolved in 57 mL acetone and 57 mL sodium hydroxide solution and cooled in an ice bath. Acryloyl chloride (7.4 mL, 76 mmol) was added dropwise over 30 min, and the reaction mixture was stirred at 0 °C in the ice bath overnight. Then, sodium chloride solid was added to saturate the mixture. The product was extracted with ethyl acetate three times and then washed with sodium chloride solution once. The extract was concentrated on a rotary evaporator (~ 30 °C) and the residue was purified by a flash chromatography using a mixed eluent of hexane and ethyl acetate (1:4 ~ 3:7 v/v). After the solvent was removed, the title compound was recovered (2.4 g, 34%) and stored in the refrigerator. ^{1}H-NMR ($CDCl_3$, 400 MHz): δ (ppm) 6.31-6.21 (*m*, 1H, CHC=O), 6.16-6.03 (*m*, 1H, C=CH, *trans*), 5.69-5.51 (*m*, 1H, C=CH, *cis*), 3.27 (*m*, 2H, N-CH_2), 2.62 (*m*, 1H, CH), 1.55-1.36 (*m*, 2H, CHC$\underline{H_2}$CH$_3$), 1.37-1.20 (*m*, 6H, C$\underline{H_2}$C$\underline{H_2}$C$\underline{H_2}$), 1.00-0.77 (*m*, 6H, CH_2C$\underline{H_3}$).

4.1.1.1.3 4-acrylamidobutanoic acid (4-AmBA)[12]

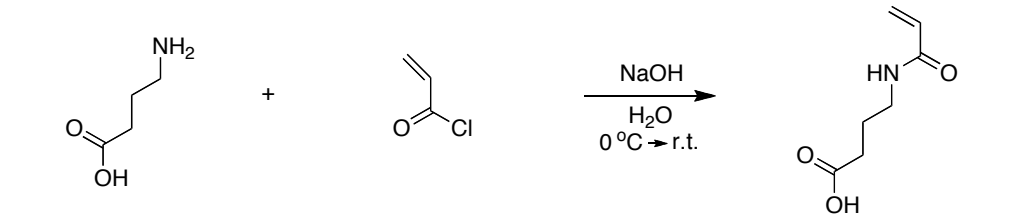

4-aminobutanoic acid acryloyl chloride 4-acrylamidobutanoic acid

4-Aminobutanoic acid (4-ABA) (10 g, 96 mmol) was dissolved in 191 mL sodium hydroxide solution (2M) and cooled in an ice bath. Acryloyl chloride (16 mL, 191 mmol) was added dropwise over 30 min, and the reaction mixture was stirred at 0 °C in the ice bath overnight. Then, chlorine hydride (2M) was added to adjust the pH to 1.0. The solution was saturated with sodium chloride solid. The product was extracted with ethyl acetate three times and then dried over magnesium sulfate. The filtrate was concentrated on a rotary evaporator (~ 30 °C) and the residue was diluted with ethyl acetate again and cooled in ice bath. The solid was collected through filtering and washed with cold diethyl ether three times. The resultant crystals (6.8 g, 45%) were kept in desiccator to remove the residue solvent. ^{1}H-NMR (D_2O, 400 MHz): δ (ppm) 6.28-5.96 (*m*, 2H, $C\underline{H}_2$=C$\underline{H}$, *trans*), 5.70-5.62 (*m*, 1H, $C\underline{H}_2$=CH, *cis*), 3.31-3.13 (*m*, 2H, N-CH_2), 2.42-2.24 (*m*, 2H, $C\underline{H}_2$COOH), 1.87-1.67 (*m*, 2H, $CH_2C\underline{H}_2CH_2$).

4.1.1.2 Synthesis of amphiphilic di-block copolymers

General protocol for RAFT polymerization:[13]

Polymerizations were conducted in round bottom flasks sealed with a rubber septum and parafilm. An NMR spectrum was recorded at the beginning of the experiment. The polymerization solutions were degassed using argon for at least 10 min and transferred to an oil bath preheated to 70 °C. After reaction, the solution was quenched by cooling in ice-water and another NMR spectrum was recorded to enable calculation of degree of conversion. For the removal of the CTA, the reaction was carried out at 70 ºC, and the absence of CTA was confirmed by UV spectroscopy.

4.1.1.2.1 p(L-DMAm)-*b*-p(2-EHAm): poly(3,4-dihydroxy-L-phenylalanine methacrylamide)-*block*-poly[N-(2-Ethylhexyl) acrylamide]

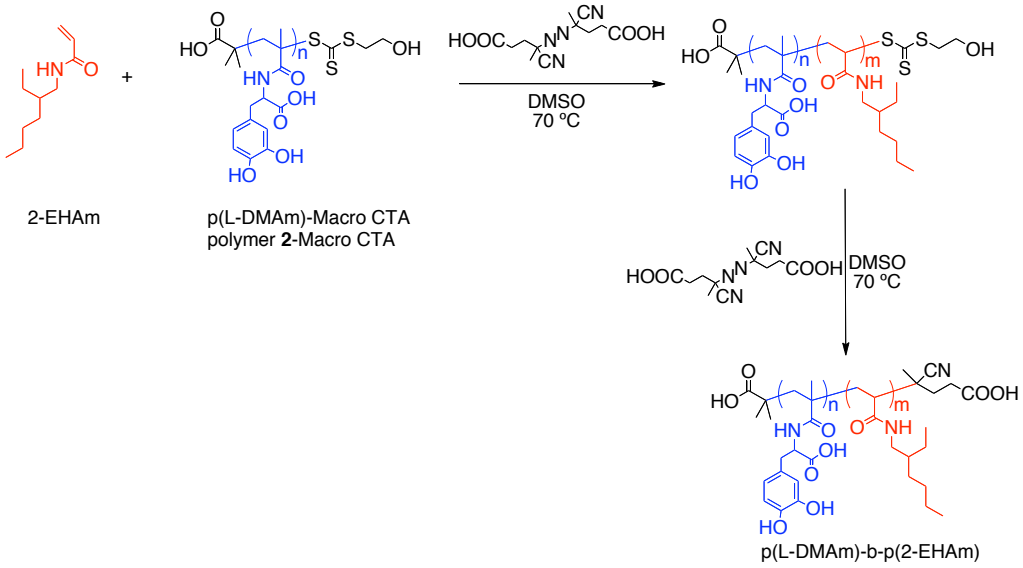

In a typical experiment, 2-EHAm (436 mg, 2.4 mmol, 1.0 M) in DMSO (2.4 mL), p(L-DMAm)-macro CTA (polymer **2**-macro CTA) (100 mg, 0.024 mmol, 0.12 M) in DMSO (0.20 mL) and V-501 (1.3 mg, 0.0050 mmol, 0.060 M) in DMSO (0.080 mL) were prepared separately and then mixed together (to make

a final 0.90 M concentration of 2-EHAm). The polymerization was carried out overnight. The polymer product was purified by dialysis against water and recovered as a white powder (0.36 g, 67%) after freeze-drying from water (dark, 2 days). In order to remove the CTA, the polymer (339 mg, 0.019 mmol, 0.0050 M) and V-501 (152 mg, 0.54 mmol, 0.15 M) were dissolved in DMSO (3.6 mL) (to make a final ratio 1:30 of polymer to initiator). This mixture was degassed for 15 min and allowed to react at 70 ºC overnight. The title compound p(L-DMAm)-*b*-p(2-EHAm) was purified by dialysis against water and recovered as a white powder (0.27 g, 80 %) after freeze-drying from water (dark, 2 days) ^{1}H-NMR (DMSO, 400 MHz) δ (ppm) 12.45 (*br*, 1H, COOH), 8.71 (*br*, >2H, NH), 7.22-6.04 (*m*, 3H, Ar-H), 4.54-3.88 (*m*, 1H, N-CH), 3.13-2.70 (*m*, >5H, CH-C$\underline{H_2}$-L-DMAm + N-C$\underline{H_2}$-C$\underline{H}$-EHAm), 2.33-1.87 (*m*, 3H, CH_3-MAm), 1.41-1.06 (*m*, >8H, C$\underline{H_2}$C$\underline{H_2}$C$\underline{H_2}$ + CHC$\underline{H_2}$$CH_3$), 1.04-0.57 (*m*, 6H, CH_2C$\underline{H_3}$), 1.84-0.00 (*br*, >2H, CH_2-MAm/Am backbone).

4.1.1.2.2 p(L-DMAm)-*b*-p(PAm): poly(3,4-dihydroxy-L-phenylalanine methacrylamide)-*block*-poly(N-phenylacrylamide)

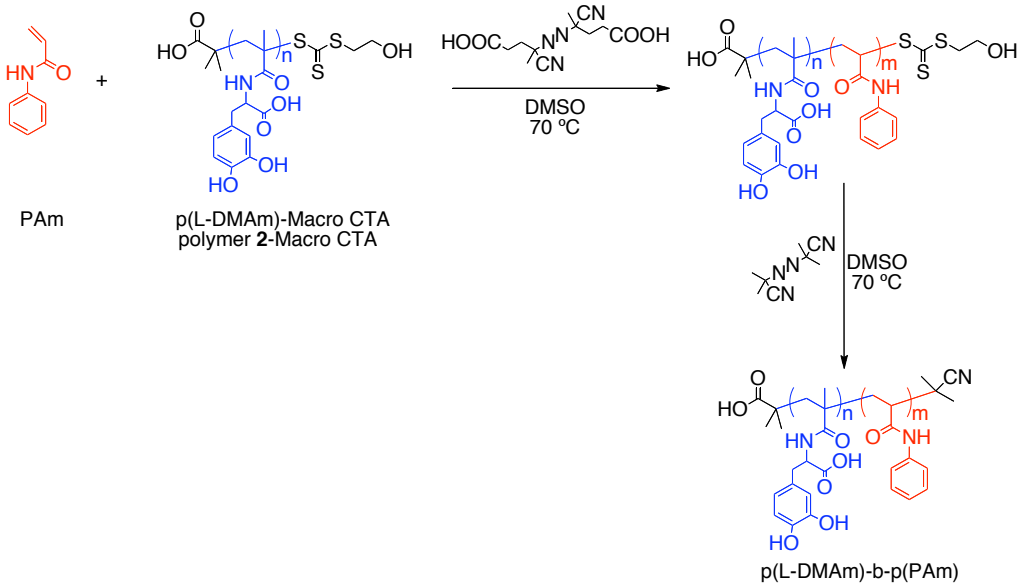

In a typical experiment, PAm (440 mg, 3.0 mmol, 1.0 M) in DMSO (3.0 mL), p(L-DMAm)-macro CTA (polymer **2**-macro CTA) (100 mg, 0.030 mmol, 0.12 M) in DMSO (0.25 mL) and V-501 (1.7 mg, 0.0060 mmol, 0.060 M) in DMSO (0.10 mL) were prepared separately and then mixed together (to make a final 0.90 M concentration of PAm). The polymerization was carried out for 90 min. The polymer product was purified by dialysis against water and recovered as a white powder (0.39 g, 72%) after freeze-drying from water (dark, 2 days). In order to remove the CTA, the polymer (390 mg, 0.023 mmol, 0.010 M) and AIBN (75 mg, 0.46 mmol, 0.15 M) were dissolved in DMSO (3.0 mL) (to make a final ratio 1:20 of polymer to initiator). This mixture was degassed for 15 min and allowed to react at 70 ºC for 3 h. The title compound p(L-DMAm)-*b*-p(PAm) was purified by dialysis against water and recovered as a white powder (0.30 g, 76%) after freeze-drying from water (dark, 2 days) ^{1}H-NMR (DMSO, 400 MHz) δ (ppm) 12.46 (*br*, 1H, COOH), 8.68 (*br*, >2H, NH), 7.87-6.37 (*m*, >8H, Ar-H), 4.56-3.88 (*m*, 1H, N-CH), 2.47-2.08 (*m*, >5H, CH-C$\underline{H_2}$ + CH_3-MAm), 2.08-0.00 (*br*, >4H, CH_2-MAm/Am backbone).

4.1.1.2.3 p(4-AmBA)-*b*-p(PAm): poly(4-acrylamidobutanoic acid)-*block*-poly(N-phenylacrylamide)

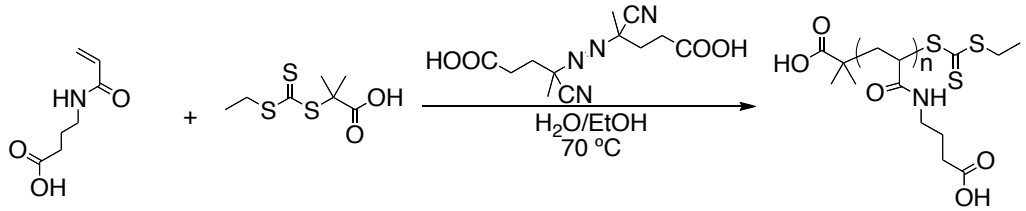

4-AmBA RAFT agent p(4-AmBA)

In a typical experiment, 4-AmBA (500 mg, 3.2 mmol, 0.88 M) in H_2O (3.6 mL), RAFT agent (20 mg, 0.091 mmol, 0.24 M) in ethanol (0.38 mL) and V-

501 (2.6 mg, 0.0090 mmol, 0.030 M) in ethanol (0.27 mL) were prepared separately and then mixed together (to make a final 0.75 M concentration of 4-AmBA). The polymerization was carried out for 60 min. The compound p(4-AmBA) was purified by dialysis against water and recovered as a white powder (464 g, 85%) after freeze-drying from water (dark, 2 days). ^{1}H-NMR (DMSO, 400 MHz) δ (ppm) 12.06 (*br*, 1H, COOH), 8.04 (*br*, 1H, NH), 3.82-2.73 (*m*, 2H, N-CH_2), 2.17 (*br*, 2H, $C\underline{H_2}COOH$), 1.92 (*br*, 2H, $CH_2C\underline{H_2}CH_2$), 1.69-0.85 (*br*, 2H, CH_2-Am backbone).

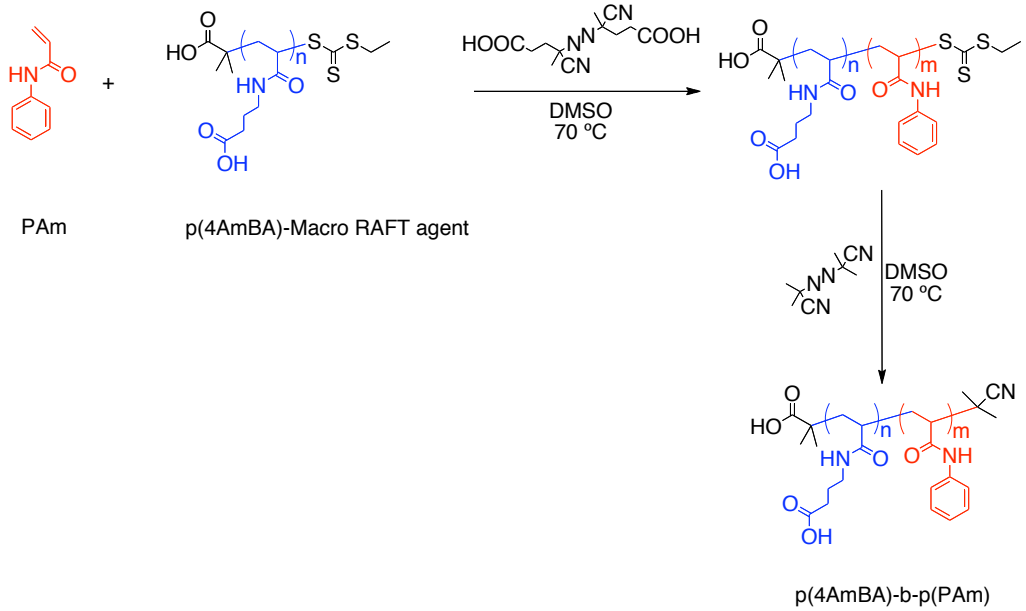

In a typical experiment, PAm (330 mg, 2.2 mmol, 0.50 M) and p(4-AmBA)-macro CTA (100 mg, 0.022 mmol, 0.0050 M) in DMSO (4.5 mL), and V-501 (1.6 mg, 0.0060 mmol, 0.060 M) in DMSO (0.094 mL) were prepared separately and then mixed together (to make a final 0.49 M concentration of PAm). The polymerization was carried out for 5 h. The polymer product was purified by diluted in THF and precipitated into hexane as a white powder (0.25 g, 90%) after desiccated (dark, 2 days). In order to remove the CTA, the polymer (251 mg, 0.014 mmol, 0.0050 M) and AIBN (47 mg, 0.28 mmol, 0.094 M) were dissolved in DMSO (3.0 mL) (to make a final ratio 1:20 of

polymer to initiator). This mixture was degassed for 15 min and allowed to react at 70 ºC for 5 h. The title compound p(4-AmBA)-*b*-p(PAm) was purified by purified by diluted in THF and precipitated into hexane as a white powder (0.20 g, 78%) after desiccated (dark, 2 days). ^{1}H-NMR (DMSO, 400 MHz) δ (ppm) 12.06 (*br*, 1H, COOH), 9.65 (*br*, >2H, NH), 7.70-6.68 (*m*, 5H, Ar-H), 3.73-2.88 (*m*, 2H, N-CH_2), 2.21 (*br*, 2H, $C\underline{H_2}COOH$), 1.76 (*br*, 2H, $CH_2C\underline{H_2}CH_2$), 2.03-0.73 (*br*, >4H, CH_2-Am backbone).

4.1.1.2.4 p(DMAm-*c*-DMAPMAm)-*b*-p(PAm): poly{N-(3,4-dihydroxy-phenethyl)methacrylamide-co-N-[3-(dimethylamino)propyl] methacrylamide}-*block*-poly(N-phenylacrylamide)

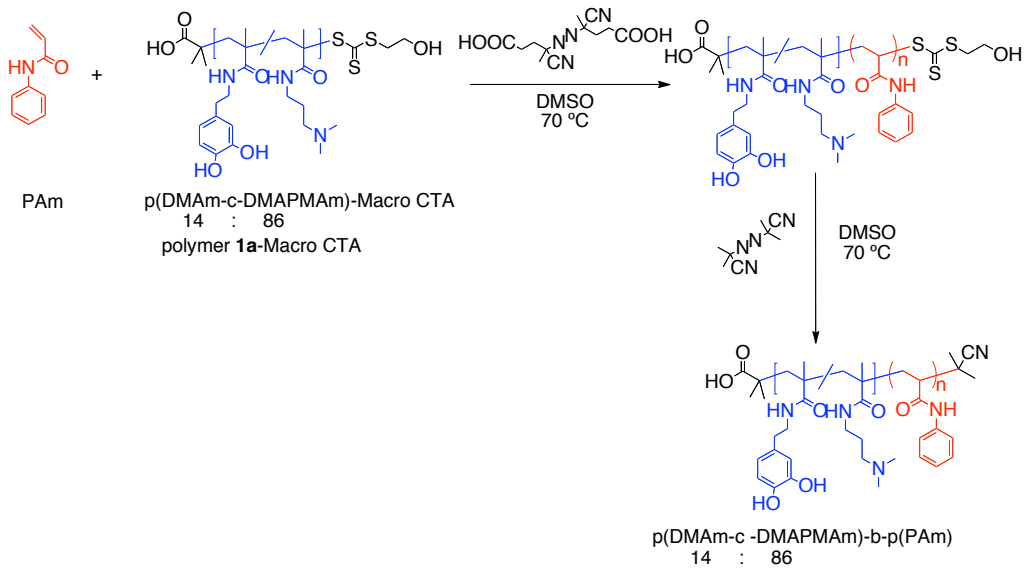

In a typical experiment, PAm (526 mg, 3.6 mmol, 0.93 M) in DMSO (3.8 mL), p(DMAm-*c*-DMAPMAm)-macro CTA (polymer **1a**-macro CTA) (150 mg, 0.011 mmol, 0.12 M) in DMSO (0.090 mL) and V-501 (0.61 mg, 0.0020 mmol, 0.060 M) in DMSO (0.036 mL) were prepared separately and then mixed together (to make a final 0.90 M concentration of PAm). The polymerization was carried out for 4 h. The polymer product was purified by dialysis against

water and recovered as a light brown powder (0.34 g, 50%) after freeze-drying from water (dark, 2 days). In order to remove the CTA, the polymer (341 mg, 0.0070 mmol, 0.0035 M) and AIBN (23 mg, 0.14 mmol, 0.070 M) were dissolved in DMSO (2.0 mL) (to make a final ratio 1:20 of polymer to initiator). This mixture was degassed for 15 min and allowed to react at 70 ºC for 3 h. The title compound p(DMAm-*c*-DMAPMAm)-*b*-p(PAm) was purified by dialysis against water and recovered as a light brown powder (0.28 g, 81%) after freeze-drying from water (dark, 2 days) ^{1}H-NMR (D_2O, 400 MHz) δ (ppm) 9.65 (*br*, >3H, NH), 7.84-6.59 (*m*, >8H, Ar-H), 3.13-2.82 (*m*, 2H, CH_2-N-DMAm), 2.72-2.48 (*m*, 4H, CH_2-N-DMAPMAm), 2.47-2.03 (*m*, >8H, N-CH_2-C$\underline{H_2}$-DMAm + CH_3-DMAP), 2.00-1.35 (*m*, >5H, CH_3-MAm + HN-CH_2-C$\underline{H_2}$-DMAPMAm), 1.10-0.59 (*m*, 2H, CH_2-MAm backbone).

4.1.2 Preparation of vesicles

General procedure to prepare vesicles:[14]

Amphiphilic diblock copolymer (5.0 mg) was completely dissolved in a volatile organic solvent (e.g. THF, Methanol or mixture, 1mL). The aqueous phase (1.0 mL, 10 mM HEPES, 10 mM NaCl and 50 mM dye, pH 7.4) was placed in a narrow neck flask (25 mL) with continuous stirring. Organic phase and polymer samples were added dropwise into the aqueous solution. The top of the flask was covered with clean tissues, and the mixture was stirred over night at room temperature to allow evaporation of all the organic solvent.

To remove the free dye and purify the vesicles, two approaches were applied. The simpler way was to dialyze the crude vesicle solution with 1000 MW dialysis membrane against osmotic buffer (5000 mL, 10 mM HEPES, 100 mM

NaCl) for 2 days with twice osmotic buffer change. For those polymers with improved permeability (see details in **4.2.3**), the crude sample was purified through a Sephadex G-50 (Dry bead diameter 20-80 μm, bed volume 9-11 mL/g) column. The pure vesicle solution was collected for the following tests.

4.1.3 Measurement of membrane permeability using 5(6)-carboxyfluorescein

5-Carboxyfluorescein loaded polymeric vesicles were prepared as described above. The fluorescence emission spectra from 500 to 600 nm, λ*ex* 470 nm, were recorded with slit widths 10 nm excitation 5 nm emission. The original vesicle solution (100 μL) was mixed with osmotic buffer (2.0 mL) pH 7.4 and pH 12 separately, and the fluorescence spectra recorded with the parameters as above. The above solution (1.0 mL) were then taken out and solubilized with 10% Triton-X-100 (20 μL) and after 30 min the fluorescence was recorded. If this initial assay worked, kinetics would be carried out as described below.

Kinetics of fresh diluted vesicle solutions were recorded with λ*ex* 470 nm, λ*em* 517 nm, slit widths 10 nm excitation 5 nm emission for 2 h at pH 7.4 and pH 12, separately. The diluted vesicle solutions (1.0 mL) were then solubilized with 10% Triton-X-100 (20 μL), and the fluorescence was recorded as above for another 2 h.

4.1.4 Measurement of membrane permeability to pH using pyranine

Pyranine loaded polymeric vesicles were prepared as described above. The fluorescence emission spectra from 480 to 600 nm, λ*ex* 460 nm, were recorded with slit widths 10 nm excitation 5 nm emission. The original vesicle solution

(100 μL) was mixed with osmotic buffer (2.0 mL) pH 7.4 and pH 12 separately, and the fluorescence spectra recorded with the parameters as above. The above solution (1.0 mL) was removed and treated with 10% Triton-X-100 (20 μL) and after 30 min the fluorescence was recorded. For permeable vesicles, kinetics was carried out as described below.

Kinetics of release from fresh diluted vesicle solutions were recorded with λ*ex* 460 nm, λ*em* 510 nm, slit widths 10 nm excitation 5 nm emission for 2 h at pH 7.4 and pH 12, separately. The diluted vesicle solutions (1.0 mL) were then solubilized with 10% Triton-X-100 (20 μL), and the fluorescence was recorded as above for another 2 h.

4.1.5 Bacterial aggregation assay

The bacterial aggregation assay by using UV spectrometer followed a similar protocol as described in **Chapter 3**. Briefly, 285 μL of the overnight culture, diluted with AB media to reach an optical density of approximately 1.0, were placed in a UV cuvette and combined with 15 μL of original vesicle samples to be analyzed. The final concentration of vesicles was 0.25 mg/mL. Optical density (600 nm) was recorded at 30 °C every 30 seconds for 60 min.

4.1.6 Bioluminescence assay with MM32 strain

MM32 assays were carried out with ***protocol 2***, ***3*** and ***4*** in **Chapter 3**. *V. harveyi* MM32 grown on LB agar plate containing kanamycin (50 μg/mL) and chloramphenicol (10 μg/mL) was used to inoculate 2 mL LB from a fresh plate. The bacteria were then grown with aeration at 30 ºC overnight. AB medium was then inoculated with this preculture (5000:1) and DPD was added to a final

concentration of 22 μM. 180 μL of the inoculated medium were placed in each of the wells of a 96 well plate and combined with 20 μL of the samples to be analyzed. The vesicle samples were prepared one day before the assay, and purified through Sephadex G-50 column just before the assay. The effect of different protocol on assay results was also investigated.

4.1.7 DPD release studies

Amphiphilic diblock copolymer (5.0 mg) was completely dissolved in a volatile organic solvent (e.g. THF, Methanol or mixture, 1.0 mL). DPD solution (3.7 mM, 1.0 mL) was placed in a narrow neck flask (25 mL) with continuous stirring. Organic phase loaded with copolymer samples was added dropwise into DPD aqueous solution. The top of flask was covered with clean tissues. The mixture was kept stirring over night in cold room to remove all the organic solvent.

To remove the free DPD molecules and purify the vesicles, the crude sample was purified through a PD-10 column twice. The pure sample of DPD-loaded vesicles was collected for MM32 assay.

The MM32 assay was carried out with ***protocol 4*** in **Chapter 3**. Additionally, three types of assays were devised: 1) Different diol-concentrations of vesicles were added into media with DPD (0.10 μM); 2) Different diol-concentrations of DPD loaded vesicles were added into media with DPD (0.10 μM); 3) Different diol-concentrations of DPD loaded vesicles were added into media without DPD.

4.2 Results and discussions

4.2.1 Monomers

The preparation of amphiphilic block copolymers commenced with monomer synthesis. N-(2-ethylhexyl) methacrylamide (2-EHMAm) and N-phenylmethacrylamide (PMAm) were initially selected as hydrophobic monomers, due to the assumption that the difference of the monomer structures could lead to different membrane permeability of polymeric vesicles self-assembled from their corresponding amphiphilic copolymers. Additionally, methacrylamide monomers were of preference rather than acrylamides, for the macro-CTA hydrophilic polymers (Polymer **1** and Polymer **2** prepared in **Chapter 3**) are all methacrylamides and the methyl groups on polymer backbone might have an effect on polymeric vesicle formation. Specifically, the bilayer of polymeric vesicles should be looser due to the presence of the methyl group on the backbone and less dense bilayer packing, and therefore would give the possibility to establish channels linking the inner and outer environment.

2-EHMAm was synthesized by using similar conditions according to the reference[12] with modification. The 1:1 ratio reaction was carried out in sodium hydroxide (2 M) and acetone (1 : 1, v/v) mixture solution using 1 : 2 : 3 molar ratio of 2-EHA to acryloyl chloride to sodium hydroxide at 0 °C. The mechanism of this acylation reaction to 2-ethylhexan-1-amine or aminolysis reaction to acryloyl chloride is shown in *Figure 4-1*.

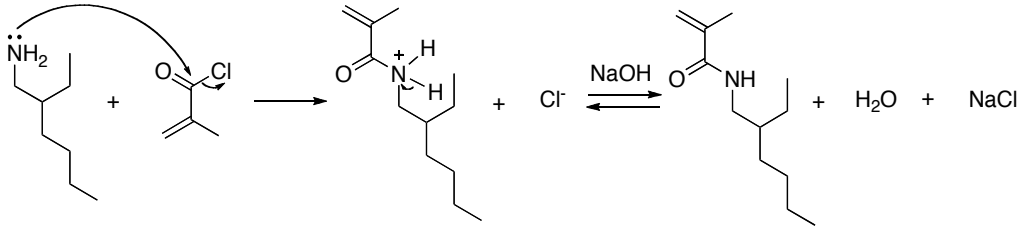

Figure 4-1. Scheme of the mechanism of synthesis of 2-EHMAm monomer

The crude product was obtained by saturating the overnight reaction mixture with sodium chloride solid and extracted with ethyl acetate three times. Emulsification was observed during extraction, and therefore the extract was settled after a while and then washed with sodium chloride solution once. Flash chromatography was performed to purify the target monomer. Since the synthesis of 2-EHMAm has not been published before, its full characterization was carried out by ^{1}H-NMR (*Figure 4-2*), ^{13}C DEPT-NMR (*Figure 4-3*), FT-IR and mass spectrum (see **Appendix**).

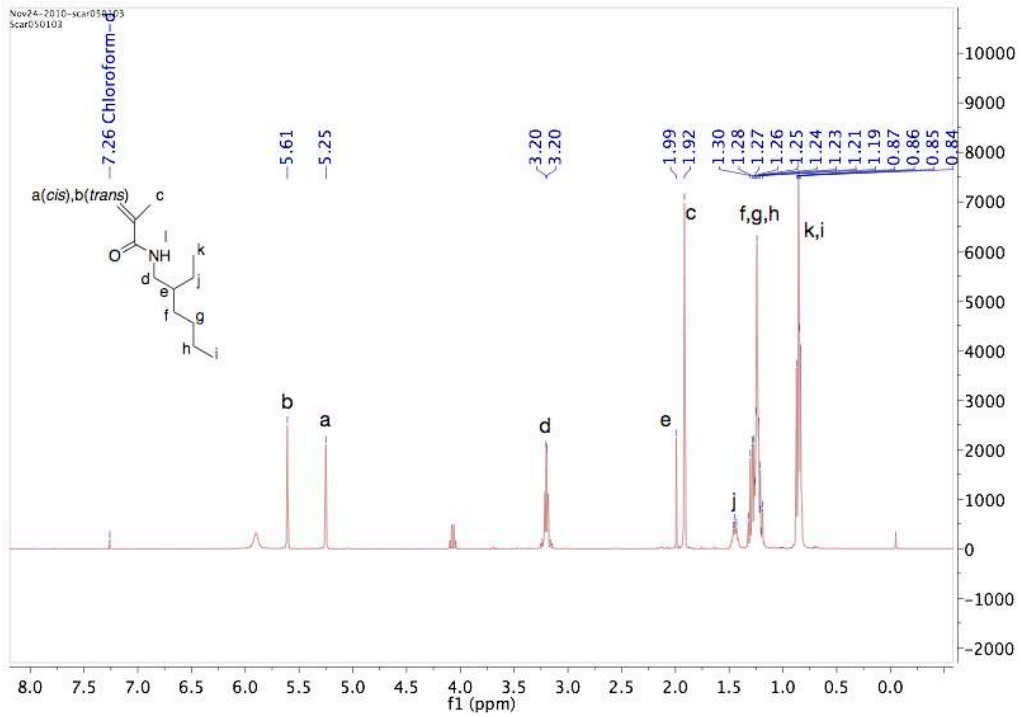

Figure 4-2 ^{1}H-NMR spectra of 2-EHMAm in d-chloroform

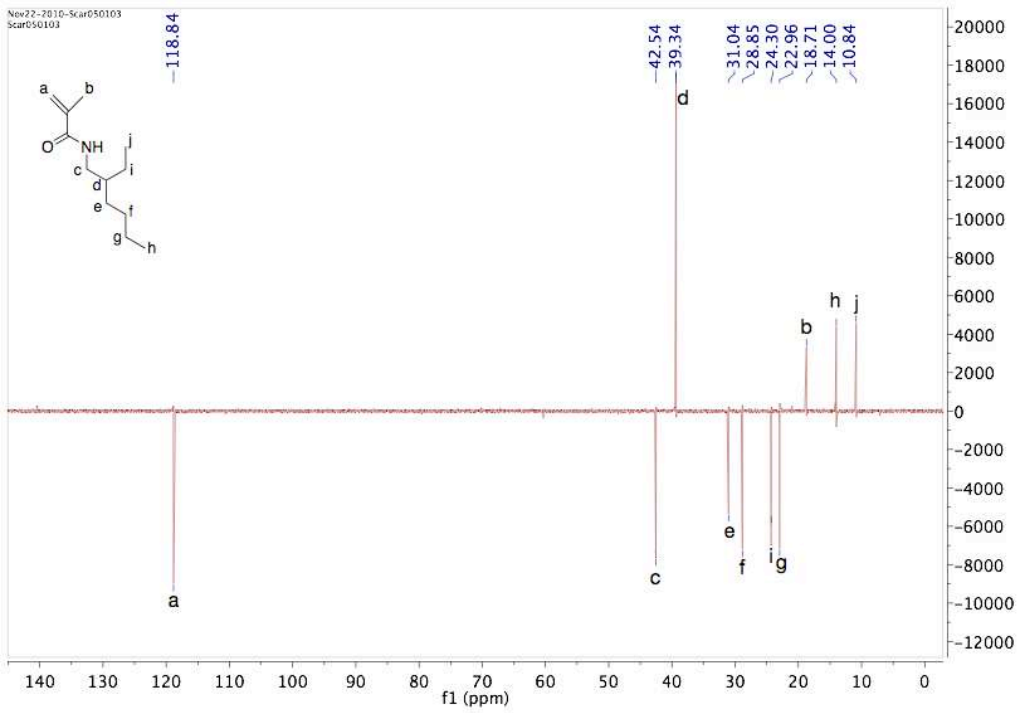

Figure 4-3 ^{13}C DEPT-NMR spectra of 2-EHMAm in d-chloroform

Monomer 2-EHMAm was then used for RAFT polymerization to grow hydrophobic blocks from macro-CTA p(L-DMAm). However, with the conditions employed, the diblock copolymer was never successfully made (see details in **4.2.2.1** about preparation of copolymers). In this case, 2-EHAm as an acrylamide monomer was considered to be an alternative and synthesized by using the same protocol. Also, in order to keep the structural coherence, N-phenylacrylamide provided by my colleague Francisco Fernandez-Trillo was used instead of its corresponding methacrylamide monomer in the subsequent polymerization studies.

In this section, as the control of the hydrophilic polymers investigated in **Chapter 3**, monomer 4-AmBA was also synthesized using a reported method[12] and was employed to form hydrophilic blocks in amphiphilic copolymers and finally applied in the bioassays. The product yield (45%) was

not as high as reported (> 70%)[1] maybe because of the inevitable loss during purification.

4.2.2 Amphiphilic block copolymers

4.2.2.1 Synthesis of p(L-DMAm)-*b*-p(2-EHAm)

The first amphiphilic block copolymer polymerized in this study was p(L-DMAm)-*b*-p(2-EHMAm) following the general RAFT polymerization protocol. In this case, p(L-DMAm) prepared in **Chapter 3** with active trithiocarbonates was used as a water-soluble macro-CTA or macro-RAFT agent. To produce the target copolymers, a series of experimental conditions were tried. Even though several batches of p(L-DMAm)-CTA were synthesized to achieve active macro-CTA for 2-EHMAm polymerization, no subsequent copolymers formed. On the other hand, the amphiphilic copolymer composed of L-DMAm and 2-EHAm (instead of EHMAm) was successfully made. P(L-DMAm)-*b*-p(2-EHAm) with a series of monomer ratios was prepared initially in order to confer different potency to both QS quenching and cell sequestrating, while at the same time maintain the desired morphological property in aqueous media.

As described in **Chapter 1** (**1.2.1**), the morphologies of nanoparticles self-assembled from amphiphilic block copolymers are theoretically a result of the inherent molecular curvature.[15] In **Eq. 1**, 'γ' represents the volume of the hydrophobic chains, 'a' is the optimal area of the head group, and 'l' means the length of the hydrophobic tail. Only when the value of 'packing parameter' of a presented molecule is between 1/2 and 1, will a polymeric vesicle be the predominant morphology existing in solution.

Equation 1

$$p = \frac{\gamma}{\alpha \cdot l}$$

Although in the theoretical 'packing parameter' equation, only the parameters of hydrophobic chains have been involved, a series of factors were found to be important for the size and shape of the aggregates empirically.[3a] Besides the environmental conditions, the key to a successfully prepared vesicle is its chemical constitution and length of each individual block. In order to synthesize p(L-DMAm)-*b*-p(2-EHAm) with different compositions, polymerization was initially performed by using the same p(L-DMAm) macro-CTA (the same degree) mixed together with 2-EHAm monomer as well as initiator in selected solvent in one pot, but the reacting mixture was taken out and therefore terminated at different reaction time points (8h 32 min for **C1a** and 20h 38min for **C1b**) (*Table 4-1*). In this case, the copolymers with different p(2-EHAm) degrees were produced. On the other hand, the kinetic experiment for this reaction has been carried out as usual, so that the copolymer products with other different compositions (data not shown) were also collected. Based on the experimental experience of the preliminary studies, amphiphilic copolymers with relatively long hydrophilic chains may tend to form micelles rather than vesicles in aqueous solution. Therefore, p(L-DMAm)-CTA was then made with low molecular weight 4204 g/mol (for **C1c**) and 3241 g/mol (for **C1d**), respectively. The feed of 2-EHAm was still 100:1 ratio to macro-CTA, and thus keeping the hydrophobic chain the same, theoretically. Even though all the conditions were the same such as solvent, initiator stock solution, oil bath (temperature) and reaction duration, the lengths

of p(2-EHAm) block were still different at the end, maybe resulting from the macro-CTA and/or degassing operation (*Table 4-1*).

A correlation between the particle morphology in water and the monomer feed as well as the weight percentage of hydrophilic block was recorded (*Table 4-1*). Copolymers of p(L-DMAm)-*b*-p(2-EHAm) with higher than 30% hydrophilic weight percentage showed broad particle-size dispersity in water as shown by DLS (*Figure 4-4*, a and b), while the same copolymer, but with L-DMAm weight percentage of around 20% gave narrow dispersities and also good correlation profiles by DLS (*Figure 4-4*, c and d). In this case, the hydrodynamic diameter of copolymer **C1c** and **C1d** were ~ 60 nm and 50 nm respectively based on the DLS data (*Table 4-4*). It was expected that particle sizes of these two copolymers would not differ much owing to the similar compositions. Additionally, all these four copolymers were negatively charged according to zeta-potential data, which was also anticipated, for the carboxyl group in p(L-DMAm) was expected to be ionized in neutral aqueous media (*Table 4-1*).

Table 4-1

Copolymer n:m[a]	$M_{hydrophilic}$[b]	$M_{hydrophobic}$[c]	$W_{hydrophilic}$ % (w/w)	Diameter (nm)	Zeta-Potential (mV)
C1a – 27 : 64	7043.18	11734.23	37.4%	-	-29.1
C1b – 27 : 66	7043.18	12161.29	36.6%	-	-29.1
C1c – 16 : 73	4204.28	13402.16	23.9%	59.7	-34.7
C1d – 12 : 84	3241.48	15475.17	17.3%	49.8	-38.3

a) n/m molar ratio of L-DMAm/2-EHAm. b) p(L-DMAm) hydrophilic block molecular weight calculated from ^{1}H-NMR. c) p(2-EHAm) hydrophobic block molecular weight calculated from ^{1}H-NMR.

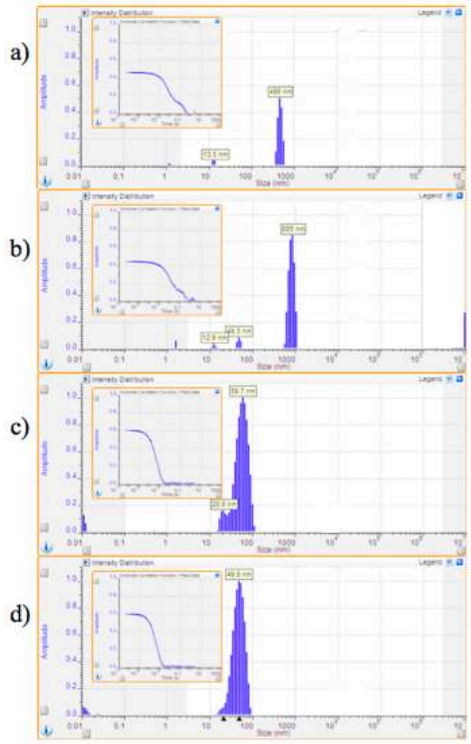

p(L-DMAm)$_n$-*b*-p(2-EHAm)$_m$

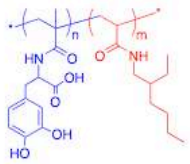

	n	*m*
C1a	27	64
C1b	27	66
C1c	16	73
C1d	12	84

Figure 4-4. DLS data for a) **C1a**, b) **C1b**, c) **C1c**, d) **C1d** in double-distilled water (2.5 mg/mL)

The non-aggregating vesicles assembled from copolymer **C1d** were investigated by cryogenic (cryo) (*Figure 4-5*, *a*) technique. The sample of cryo-TEM was prepared through suspending copolymers in dilute solution (0.25 mg/mL) and subsequently hydrating and vitrifying. Such preparative procedure caused particles' shrinking on occasions because of the inevitable dehydration of particles. According to the images (*Figure 4-5*, a and b), the average diameters of cryo-particles were mostly smaller than 60 nm, while those of stain-particles were always around 100 nm. Also the imaging of cryo-TEM always recorded ice coexisting with particles, which made it difficult to tell the particles apart. Considering all these drawbacks of cryo-TEM in this study, standard TEM techniques with staining finally employed instead, which gave more reliable particle-size evaluation and also clearer membrane

boundaries. The transparent particles overlapping with each other were observed in these imagines (*Figure 4-5*, *b* and *c*), which could demonstrate the formation of vesicles, as if the round particles were spherical micelles instead, their cores would have been solid and opaque rather than transparent.

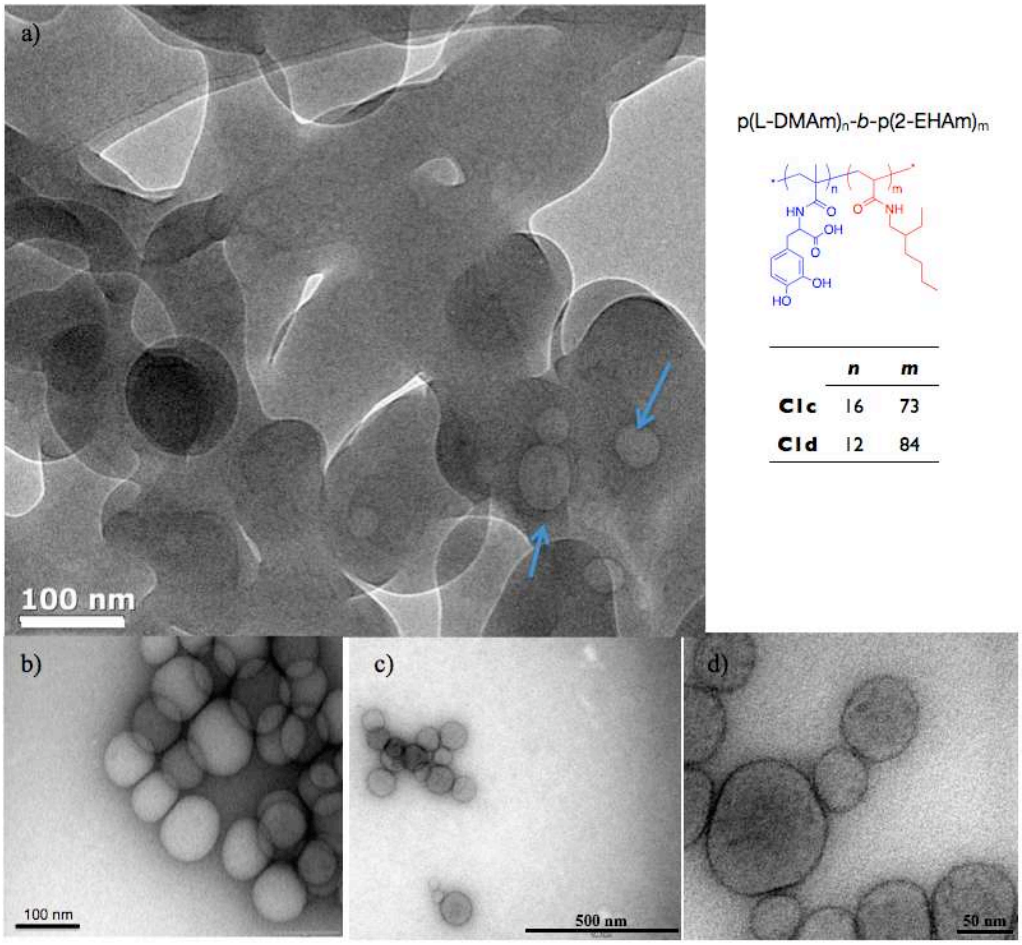

	n	m
C1c	16	73
C1d	12	84

Figure 4-5. Transmission Electron Micrograph (TEM) imaging of the copolymer a) **C1d** (cryo) b) **C1d** (stain) c) and d) **C1c** (stain) (0.25 mg/mL in H_2O)

In summary, the data from DLS and TEM characterizations revealed that aqueous suspensions of copolymer p(L-DMAm)-*b*-p(2-EHAm) with different composition probably formed mixed species of spherical micelles and vesicles

since more than two average sizes of particle groups were observed. With decreased hydrophilic weight percentage, copolymers formed vesicle-like morphology and relatively narrow dispersities. Therefore, copolymers with hydrophilic weight percentage around 20% were of more interest for subsequent study.

Alizarin Red S (AR-S) competitive binding assays were also carried out with copolymer **C1c** (*Figure 4-6*) to establish binding affinities for copolymers to phenylboronic acid (PBA). Again, as already discussed (**Chapter 3**, **3.2.4**), polymer analysis was limited by the lack of binding saturation in some of the cases, which was more significant with amphiphilic block copolymers with hydrophobic blocks. In this case, problems in the assay still existed such as low amount of material and/or low affinity, presence of new bands at 520 nm attributed to catechol structures when increasing the polymer concentrations. Therefore, no further AR-S assays were carried out.

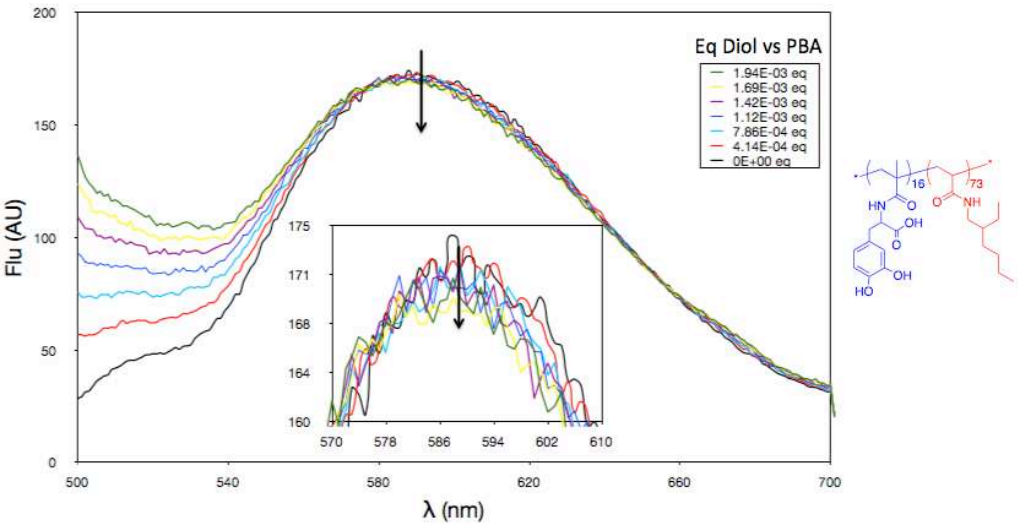

Figure 4-6. Alizarin Red S competitive binding assay was performed with copolymer **C1c**, but dose-dependent fluorescence quenching was not observed. New band of catechol structure at 520 nm appeared and was increased with the addition of copolymer **C1c**, which prevented its further analysis.

4.2.2.2 Synthesis of p(L-DMAm)-*b*-p(PAm)

The membrane properties of polymersomes investigated here were adjusted by tuning hydrophobic structures. Another hydrophobic monomer PAm was therefore selected with the expectation of giving distinct permeability for polymersomes compared to those self-assembled from p(L-DMAm)-p(2-EHAm). In this context, p(L-DMAm)-*b*-p(PAm) - copolymer **C2** was synthesized following the same reaction conditions as p(L-DMAm)-*b*-p(2-EHAm). Specifically, p(L-DMAm)-CTA used was around 3200 g/mol molecular weight (target degree of polymerization 20), while the target degree of polymerization of PAm was 100. Notably, the kinetic experiment indicated that this polymerization was very fast, so that the monomer conversion reached 94 % after only 90 min.

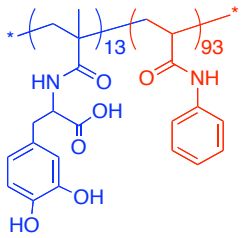

p(L-DMAm)$_{13}$-*b*-p(PAm)$_{93}$

4.2.2.3 Synthesis of p(4-AmBA)-*b*-p(PAm)

P(4-AmBA)-*b*-p(PAm) - copolymer **C3** was synthesized via similar polymerization procedures described above. In this copolymer structure, p(L-DMAm) hydrophilic block was replaced with p(4-AmBA), while p(PAm) remained as hydrophobic chain. As discussed in **Chapter 2**, a series of functional groups had been demonstrated to give various binding affinities to boron other than catechols. Therefore, copolymers p(4-AmBA)-*b*-p(PAm) composed of hydrophilic chains with carboxyl acid pendent functionalities

showing low affinities to boron were prepared to be 'control' materials for p(L-DMAm)-*b*-p(PAm).

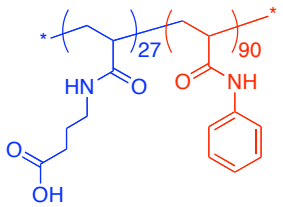

p(4-AmBA)$_{27}$-*b*-p(PAm)$_{90}$

4.2.2.4 Synthesis of p(DMAm-*c*-DMAPMAm)-*b*-p(PAm)

Having prepared copolymer vesicles with p(L-DMAm) (**4.2.3** and **4.2.4**), vesicles were formulated from p(DMAm-*c*-DMAPMAm) (polymer **1**) - another potent linear polymer targeting biological applications investigated in **Chapter 3**. A series of vesicles with variety of potency was therefore ready prior to subsequent bioassays.

First of all, the polymerization conditions to prepare p(DMAm-*c*-DMAPMAm)-CTA were modified in order to keep the CTA group active for the second block synthesis. For the alkaline conditions are known to readily quench CTA, the reaction was performed in t-BuOH and acetate buffer mixed solvent at pH 5.5. Again, the second p(PAm) blocks were successfully connected to p(DMAm-*c*-DMAPMAm) with general conditions and characterized by ^{1}H-NMR (Copolymer **C4**). However, the study of this product was at very early stage. The p(DMAm-*c*-DMAPMAm) composition was followed the previous monomer ratio (theoretical degree of polymerization 20 : 80, and final value was 14 and 86, respectively). The degree of polymerization of p(PAm) block was initially targeted to 330 and the final value was 237. The copolymers with such composition gave poor water solubility and thus were

difficult to form vesicles. To find out appropriate monomer compositions for this copolymer as well as its vesicle preparation conditions considerable extra work in future is need.

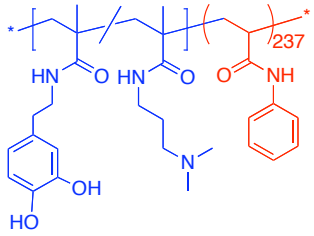

p(DMAm$_{14}$-*c*-DMAPMAm$_{86}$)-*b*-p(PAm)$_{237}$

4.2.3 Preparation of vesicles

The vesicle preparation method ultimately adopted here was the 'solvent-exchange' technique. Although at the initial study stage the 'film rehydration' technique was also considered, after several attempts it was found to be difficult in practice, at least for copolymers (**C1** and **C2**) investigated in this study. Therefore, more efforts focused on preparative conditions optimized the 'solvent-exchange' method. As introduced at the beginning of this chapter, it is key for a successful vesicle preparation to select a good volatile organic solvent for both hydrophilic and hydrophobic blocks of copolymers. It is easy to understand that the organic solvent should be good to both components, so that even and uniform nanoparticles are easily formed via dropping expanded copolymer chains into an aqueous phase. The organic solvents are also necessarily volatile and thus finally completely removed under stirring in fume hood overnight. Thus, the nanoparticles are eventually obtained in pure aqueous media. The volume ratio of 3 : 2 of THF to Methanol was found to be the best choice meeting the above requirements, and no single pure solvent could provide such good solubility for p(L-DMAm)-*b*-p(2-EHAm) and p(L-

DMAm)-*b*-p(PAm). The concentration of copolymers in organic solvents was adjusted from 10.0 mg/mL to 5.0 mg/mL, for the vesicles prepared from lower concentration solutions had more uniform morphology and more narrow dispersities (checked with DLS). The contents of vesicle buffer or aqueous phase employed were derived from those reported in the literature[14] and proved to be effective for making polymersomes. Ionic concentration and pH were therefore kept the same throughout the experiments. All the other factors such as temperature (room temperature), stirring rate and ratio for the two phases (1 : 1) were fixed for all the experiments.

A commonly used method to purify vesicles is dialysis against osmotic buffer. This method was also initially adopted for this study. However, leakage of the loaded dye was significant, which was likely due to the concentration gradient of ions between the inner and outer environments of the vesicles. Subsequently, a size-exclusion column was employed instead. This was advantageous for maintaining the dye inside and minimizing its leakage.

Vesicle morphologies were again recorded with TEM imaging. In order to evaluate particle size distribution fully, statistical analysis was used (*Table 4-2*). The diameters of at least 200 particles were randomly measured manually from the TEM images. The particle size was found to cluster into four groups. The results were also reported in histograms in order to show the particle size distribution (*Figure 4-7*). At this stage, the dispersities of preparative particles were still broad, and spherical micelles as well as polymeric vesicles probably coexisted in the mixture.

Table 4-2

Vesicle \ Diameter	0-50 nm	51-99 nm	100-150 nm	> 151 nm	Average
1a[a]	41.1 ± 9.1	74.5 ± 13.2	123.0 ± 15.1	171.4 ± 17.9	96 ± 39.2
1b[b]	40.7 ± 10.5	73.8 ± 12.7	123.3 ± 15.1	177.3 ± 23.6	105 ± 44.0
2[c]	34.8 ± 8.3	67.2 ± 11.2	122.2 ± 8.1	208.3 ± 9.6	48 ± 34.3

a) Vesicle **1a** made from copolymer **C1d** (12/84 molar ratio of L-DMAm/2-EHAm). b) Vesicle **1b** made from copolymer **C1c** (16/73 molar ratio of L-DMAm/2-EHAm). c) Vesicle **2** made from copolymer **C2** (13/93 molar ratio of L-DMAm/PAm).

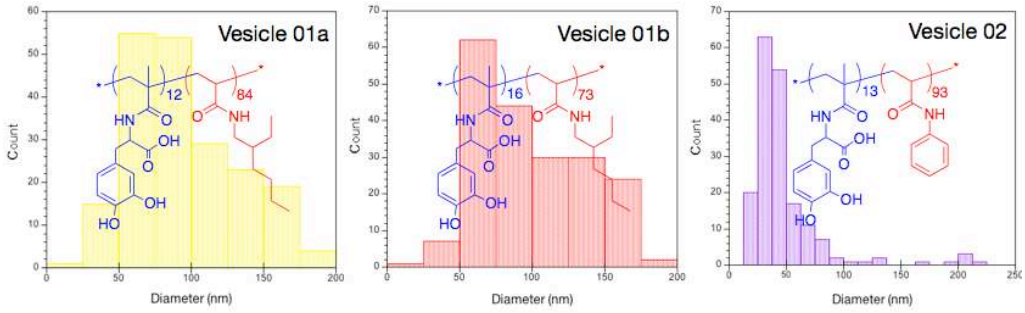

Figure 4-7. Histograms of diameter distribution of Vesicle **1a**, **1b** and **2** analyzed from TEM images

More techniques were attempted in order to better characterize vesicles and at the same time to compare particle size obtained from different techniques (*Table 4-3*). The AFM imaging was found not to be a suitable technique to characterize L-DOPA containing polymers, for DOPA-derivatives were found to adhere to AFM cantilevers as reported previously.[16] However, other techniques indicated that the particles encapsulated hydrophilic fluorescent dye. Hence, the study moved to fluorescent dye encapsulation and release experiments.

Table 4-3

Vesicle	Mean diameter (nm)			Zeta-potential
	DLS	TEM	AFM	(mV)
1a	27 ± 8.9	96 ± 39.2	-	-38.8 ± 0.9
1b	56 ± 13.7	105 ± 44.0	-	-31.7 ± 1.5
2	36 ± 10.6	48 ± 34.3	31 ± 9.6	-36.8 ± 1.6

a) Vesicle **1a** made from copolymer **C1d** (12/84 molar ratio of L-DMAm/2-EHAm). b) Vesicle **1b** made from copolymer **C1c** (16/73 molar ratio of L-DMAm/2-EHAm). c) Vesicle **2** made from copolymer **C2** (13/93 molar ratio of L-DMAm/PAm).

4.2.4 Membrane permeability

Fluorescent dye 5(6)-carboxyfluorescein was used as a reporter for testing membrane permeability. The concentrations of the dye internally trapped within vesicles were planned to be high enough to quench fluorescence.[17] After addition of Triton-X-100, the vesicles should burst and subsequently release dye into the bulk solution. Based on this strategy, both encapsulation capability and membrane permeability of resulted vesicles are examined in one experiment.

5(6)-Carboxyfluorescein was completely dissolved in vesicle-preparing buffer at pH 7.4 at an initial concentration of 50.0 mM and then encapsulated into vesicles following the vesicle preparation procedure. The free dye was removed by Sephadex G-50 column. *Figure 4-8* (*left*) shows the results of this assay for Vesicle **02** self-assembled from copolymer p(L-DMAm)$_{13}$-*b*-p(PAm)$_{93}$. The blue solid line represents sample in pH 7.4 buffer and the dashed line represents the same sample after addition of Triton. As expected, fluorescence increased when vesicles were burst and 5(6)-carboxyfluorescein was released into the bulk solution. The profile for samples in pH 12 is shown as a green solid line, while the profile following vesicle burst is shown as a green dashed line. It is necessary to note that the original 5(6)-

carboxyfluorescein concentration could not be measured directly, as it was above the sensitive range of the spectrometer. The original sample solutions (pH 7.4 in vesicle-preparing buffer) were therefore always diluted to reach a measurable fluorescence ranges. When dilution in the same fold was performed with different pH buffer, the fluorescence changed (between blue and green profiles) (*Figure 4-8*). This might be attributed to the sensitivity of the permeable membrane to the change of buffer pH. The detailed progress was recorded in the kinetic profiles (*Figure 4-8, right*). The fluorescence increase occurred within the initial 30 min after the pH of the original sample solution (pH 7.4) was adjusted to 12 (*Figure 4-8, right, green profile*). On the other hand, the pH sensitive range of 5(6)-carboxyfluorescein is from neutral to acidic conditions[18], and thus the fluorescence change before and after addition of Triton only resulted from the dye concentration increase in bulk solution (*Figure 4-8, right*).

Vesicle **1** prepared from p(L-DMAm)-*b*-p(2-EHAm) was less effective for entrapping 5(6)-carboxyfluorescein, either because it has a softer membrane and more possibilities to leak, or because it may have been the case that 5(6)-carboxyfluorescein was not a suitable dye to be encapsulated in Vesicle **1**. Hence, pyranine as a fluorescent pH indicator was used for further studies.

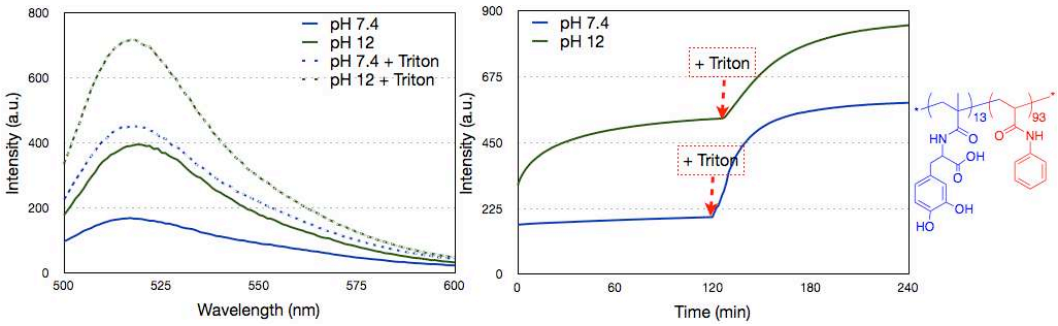

Figure 4-8. Fluorescence spectra of 5(6)-carboxyfluorescein encapsulated in Vesicle **2** at pH 7.4 and pH 12 (left), and kinetic experiments (right), before and after addition of Triton X-100

4.2.5 Membrane permeability with varying pH

According to the results showed in *Figure 4-9* (*top*), replacing 5(6)-carboxyfluorescein with pyranine as the fluorescence reporter did not significantly affect the qualitative results except the dye fluorescence emission length shifted to 510 nm. Kinetic experiment gave the possibility to compare the difference in fluorescence before and after vesicle burst under two pH-conditions. The change in fluorescence at pH 12 was remarkable compared to that at pH 7.4 owing to the pH-sensitive properties of pyranine as well as the increased dye concentration in the bulk solution following burst of the vesicle structure. Initially, the pH within vesicles was 7.4, but on vesicle burst the pyranine was exposed to the pH 12 external environment.

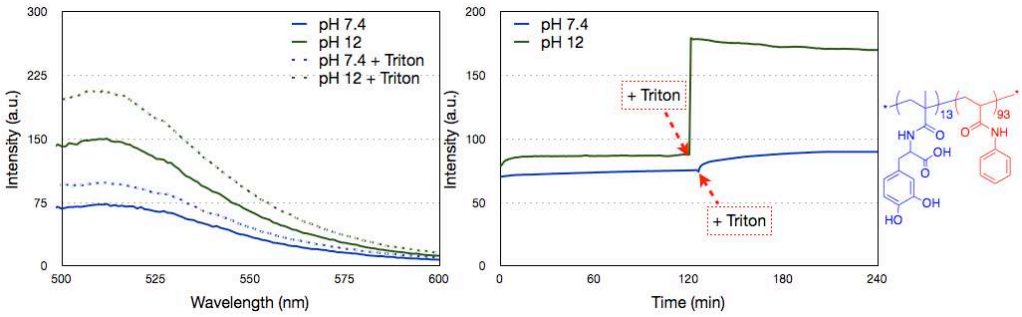

Figure 4-9. Fluorescence spectra of pyranine encapsulated in Vesicle **2** at pH 7.4 and pH 12 (left), and kinetic experiments (right), before and after addition of Triton X-100

The assay performed with Vesicle **1a** (12/84 molar ratio of L-DMAm/2-EHAm) indicated via pyranine fluorescence that encapsulation and release were successful (*Figure 4-10*). Again, the whole experimental duration was separated into two stages by the time point at which Triton was externally added. The resulting fluorescence profiles were similar as discussed for Vesicle **2**. However, there were some features observed for vesicle **1a** compared to Vesicle **2**. After diluting original sample solution, the fluorescence fluctuated in both pH conditions before the addition of triton. Also, after adding Triton the fluorescence increased fast initially but subsequently plateaued. This may have been due to the p(2-EHAm) block changing the properties of the vesicle membrane.

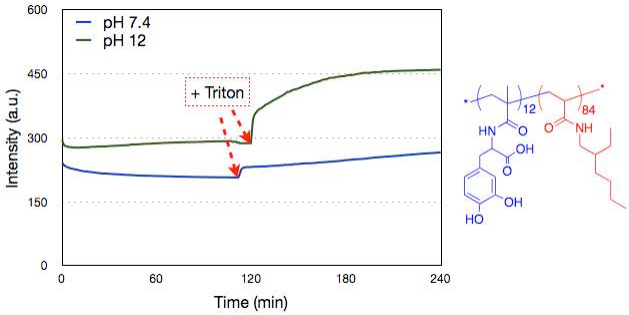

Figure 4-10. Fluorescence spectra of kinetic experiments of pyranine encapsulated in Vesicle **1a** at pH 7.4 and pH 12, before and after vesicle burst

4.2.6 Bacterial aggregation assay

The principles of the bacterial aggregation assays were described before. This assay was performed again with Vesicle **1a** and Vesicle **2** as well as Polymer **2d** - p(L-DMAm)$_{12}$ as representative for linear polymers. This is because it was demonstrated that all the three types of polymers investigated in **Chapter 3** enhanced bacterial aggregation significantly in bacterial media (*Figure 3-16*). Also, the hydrophilic blocks of Vesicle **1** and **2** were p(L-DMAm) as also the component for Polymer **2d**. The bacterial adhesion assay was performed by using the same bacterial culture as well as the same conditions to obtain comparative data to properly understand the potential capability of the vesicles to effect bacterial sequestration. Interestingly, the results (*Figure 4-11*) indicated that there was no significant difference of OD with (*blue* and *green*) and without vesicles ('*control*', *black*), but a fast decrease of bacterial OD could be observed in the presence of linear polymers (*red*). It is likely that some of the cell-binding hydrophilic functionality on the polymers would be trapped inside the particles if they were self-assembled into vesicles. This loss in binding ability may have caused the vesicles to be less effective sequestrants than the linear polymers. Alternative explanation was that, compared to linear

polymers, the contact area of vesicles and bacterial cells, both of which were ball-like round shape, allowed the formation of free spaces and therefore the inaccessibility of some binding sites of bacteria to polymersome-bound ligands.

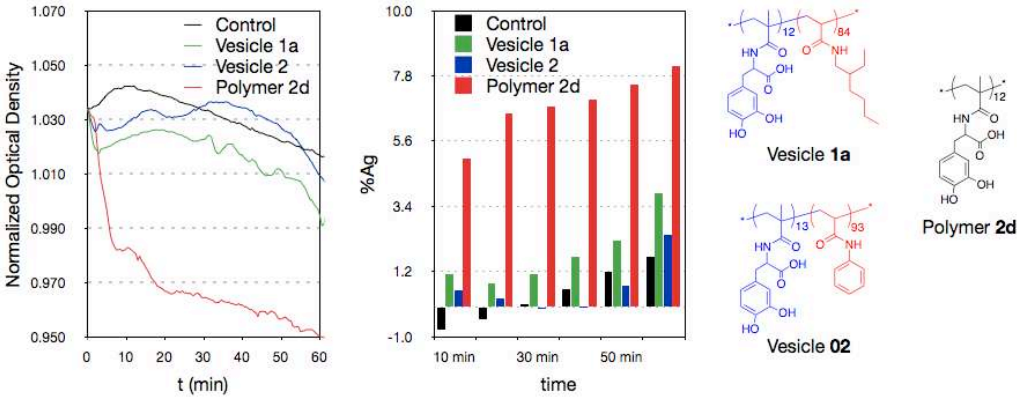

Figure 4-11. OD (600 nm) as a function of time in the absence and presence of polymers, only linear polymer (red) showed significant difference from the 'control' (black); b) %Ag as a function of time.

4.2.7 MM32 assay

In order to understand better the interaction mechanisms between investigated vesicles and bacterial cells, the bioluminescence assay was considered as the best candidate assay. This was because as already discussed in **Chapter 3** the action of investigated synthetic polymers to bacterial QS network was well characterized. For the bacterial MM32 assay with Vesicle **1a**, in order to get sufficient comparison profiles to linear polymers, each protocol (***protocol 2-4***) was employed at least once. Light production and optical density (600 nm) were recorded at 30 °C every 30 minutes for at least 6 hours in a 96-well plate, and each experiment was carried out in triplicate and the plotted curves were derived from the mean value (*Figure 4-12*). Again, the timeframe for the reported analysis was restricted to 4-10 h, for it was demonstrated that

significant differences in OD between those cultures in the presence and absence of polymers were observed with increasing time (after about 8h). *Figure 4-12* showed one example of light production curves and OD (600 nm) as a function of time for *V. harveyi* MM32 in the absence and presence of Vesicle **1a** following ***protocol 4***. This result was compared with that reported in *Figure 3-41* for Polymer **2b**. It seems that when the diol concentration of Vesicle **1a** reached 4.01×10^{-4} M, complete quenching of bioluminescence could already be observed, while in similar diol concentrations (3.6×10^{-4} M) Polymer **2b** was not as potent in reducing light production. The behavior of the vesicles also differed from that of **PVA** (*Figure 3-42*), for Vesicle **1a** not only had higher activity to decrease bioluminescence at earlier time points but also increased light production at intermediate time periods in a manner similar to the dual-action polymers described in **Chapter 3**. The block copolymers were able to aggregate bacteria as well as remove DPD, thus interfering in the cell signaling pathways by both a 'cell-binding' and a 'QS-quenching' mechanism. Again, both mechanisms should also be considered to understand interactions between vesicles and bacterial biological activities. It was demonstrated that vesicles did not aggregate bacterial cells to the same extent as analogue linear polymers. On the other hand, the diol-functionality present at vesicle surfaces could bind DPD molecules via the same functionality (p(L-DMAm)) as the linear polymers. Thus the vesicles might bind with similar affinity for boron as that of Polymer **2**, but to a lower saturation limit because 50% of diols should be on the inner wall of the vesicles. Obviously, such change simplifies the result profile of MM32 assays if we compare the two figures (*Figure 3-41* and *Figure 4-12*). For the binding activity of vesicles to boron species to be the

predominant effect, the dose-dependent reduction of bioluminescence was observed and only at low concentration of vesicles was an enhanced light production achieved. Also, the bacterial cells grew differently with a dose-dependent profile (*Figure 4-12*, *right*). It should also be noted that vesicles in the sub-nm size range could also scatter light and interfere with OD readings.

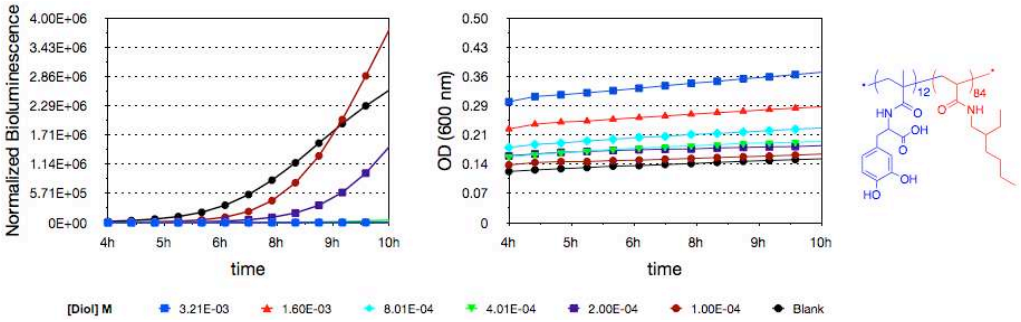

Figure 4-12. Light production curves and OD (600 nm), as a function of time for *V. harveyi* MM32 in the absence and presence of Vesicle **1a**. (***protocol 4***)

The results of repeat assays for MM32 with Vesicle **1a** following different protocols and with a variety of diol-concentrations were compared in order to have sufficient data to determine the final assay conditions, from which similar overall trends at each testing time point could be observed (*Figure 4-13*). In this case, the following assays were carried out using ***protocol 4*** and testing at least seven appropriate diol-concentrations for each vesicle (*Figure 4-13*, c), so that both the dose-dependent light reduction and the quenching trends were obtained in one experimental run. Obviously, the specific diol-concentration range for different vesicle types varied and pre-experiments were necessarily performed.

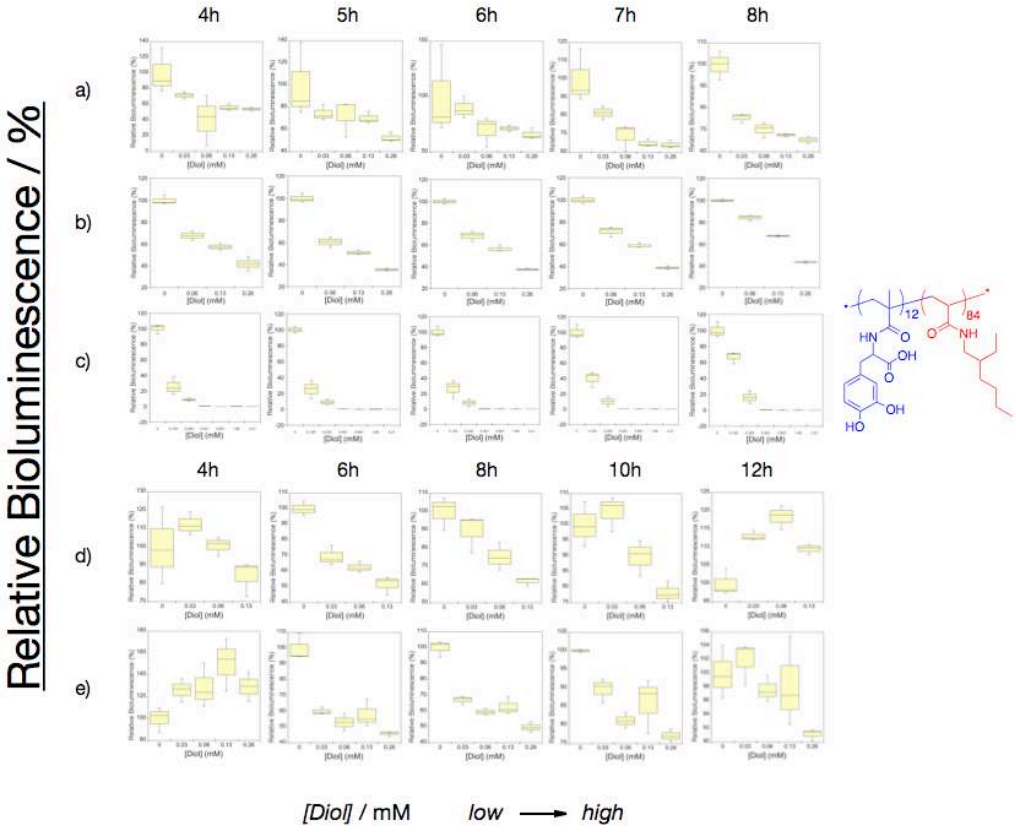

Figure 4-13. Effect of diol concentration in light production of Vesicle **1a** a) with ***protocol 2***, b) with ***protocol 4***, c) 7 concentrations of vesicles with ***protocol 4***, d) with ***protocol 3*** and e) higher concentrations of vesicles with ***protocol 3***

Following the ***protocol 4*** determined for this assay, Vesicle **1** was compared with Vesicle **2** (*Figure 4-14*). Similar results for both light production and OD (600 nm) as a function of time were observed for Vesicle **2** compared to those of Vesicle **1**. However, if the effect of diol concentration on light production is considered at certain testing times, for example at 4 h which was believed to be the onset of light production, it can be seen that Vesicle **2** quenched the bioluminescence at a lower diol-concentration (0.09 mM) (*Figure 4-14*, bottom) than that of Vesicle **1a** (0.4 mM) (*Figure 4-13*, c). Such MM32 results were in accord with those presented for the aggregation assay. Thus, according

to *Figure 4-11*, Vesicle **2** exhibited low binding affinity to bacterial cells compared to Vesicle **1a**. As these polymers and the corresponding vesicles were believed to function in both "QS-quenching" and "cell-binding" modes of action, Vesicle **2** with lower potency of cell binding was therefore anticipated to show greater QS-quenching. However, subsequent assay results discussed below suggest that the formation of vesicles rather than the linear forms in some way acts, such that the vesicle form could quench the QS network more effectively.

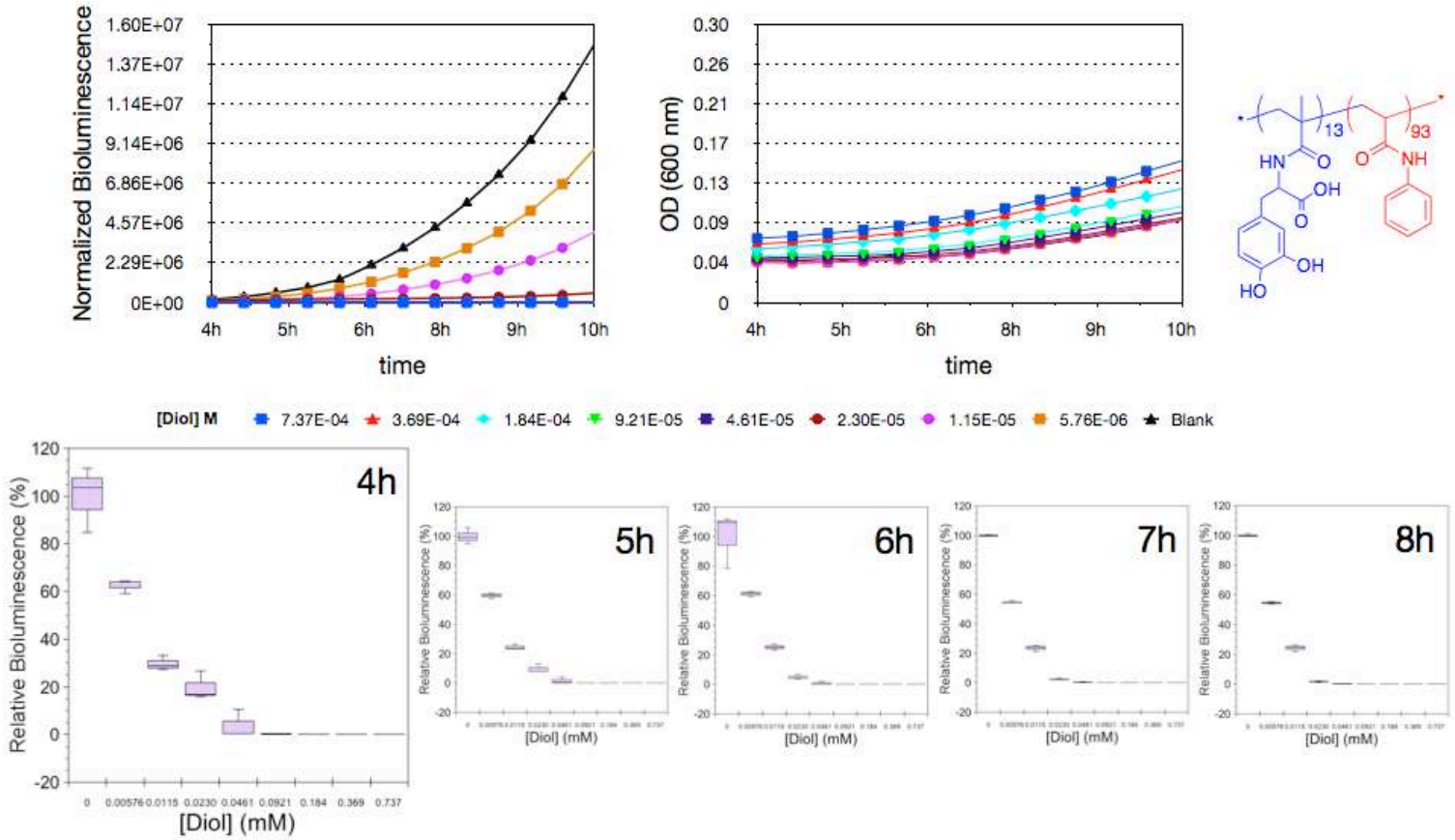

Figure 4-14. Light production curves and OD (600 nm), as a function of time for *V. harveyi* MM32 in the absence and presence of Vesicle **2**. Bottom: Effect of diol concentration in light production. (***protocol 4***)

In order to understand the mechanism better, linear Polymer **4** p(4-AmBA)$_{27}$ was introduced in this assay, due to its expected lower boron-binding affinity provided by carboxyl groups compared to catechols. The results of MM32 assay for Polymer **4** indicated that bioluminescence change as a function of time could be observed in the presence of analogous diol-concentrations of Polymer **4** (*Figure 4-15*). The trends of effect of diol concentration in light production were similar to those obtained with p(L-DMAm) homopolymers (Polymer **2**) (*Figure 3-25 and 3-26*), which suggested that Polymer **4** also had dual-functionality though with low binding affinity for both boron and bacterial cells. Therefore, we assumed that if Vesicle **3** prepared from p(4-AmBA)-*b*-p(PAm) was found to have a stronger ability to quench QS than its corresponding linear Polymer **4** or even catechol-pendent linear polymers (Polymer **1-3**) in MM32 assays, it suggested that the morphology of vesicles enhanced their binding affinity for boron, and such an effect, together with their decreased binding affinity for cells, reduced light output significantly. In fact, the experimental results demonstrated this assumption was correct (*Figure 4-16* to *Figure 4-17*). The relative bioluminescence decreased approximately 40% in the presence of Vesicle **3** (4-AmBA/PAm monomer ratio: 16 : 42, **a** and 27 : 90, **b**) with carboxyl acid concentration around 0.3 mM, while in the presence of Polymer **1b** and **2b** with similar diol-concentrations of 0.26 and 0.36 mM it did not decrease to below 60% throughout the experiment (*Figure 3-43*). This suggested that the formation of vesicles significantly enhanced polymer's binding affinity for boron and could quench bioluminescence of *V. harveyi* MM32 with relatively low concentrations compared to linear polymers investigated in **Chapter 3**.

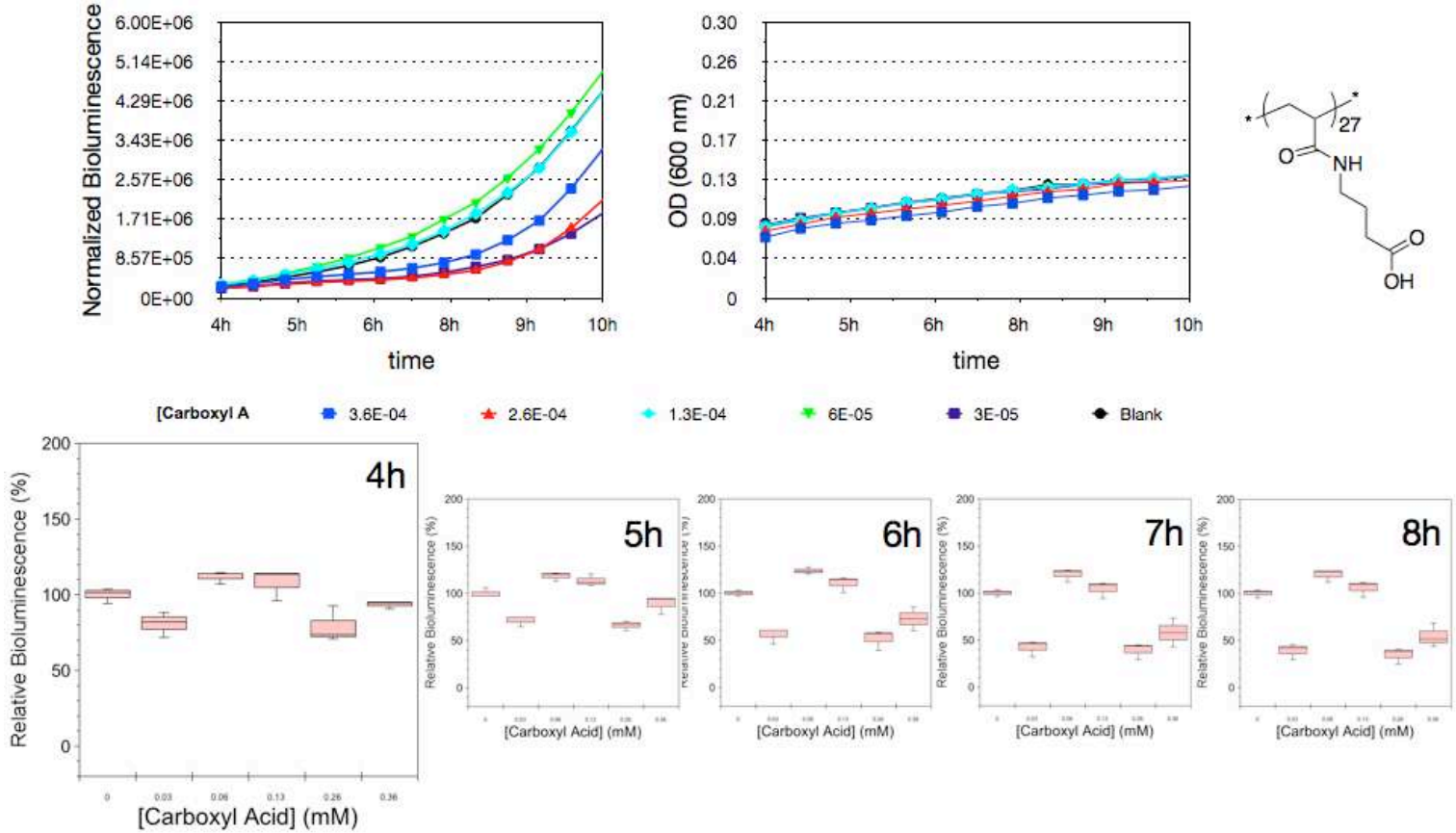

Figure 4-15. Light production curves and OD (600 nm), as a function of time for *V. harveyi* MM32 in the absence and presence of Polymer **4**. Bottom: Effect of diol concentration in light production. (***protocol 4***)

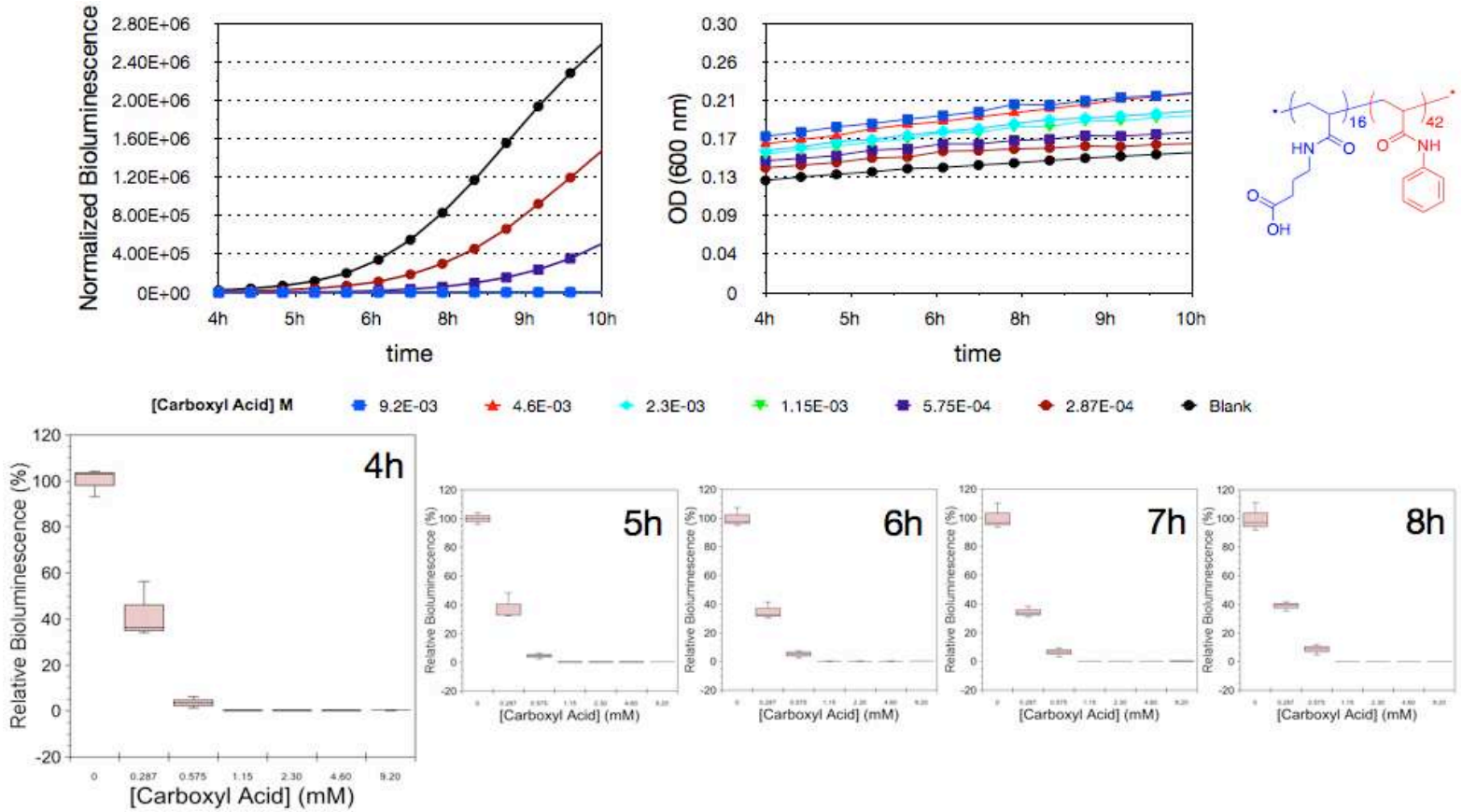

Figure 4-16. Light production curves and OD (600 nm), as a function of time for *V. harveyi* MM32 in the absence and presence of Vesicle **3a**.

Bottom: Effect of diol concentration in light production. (***protocol 4***)

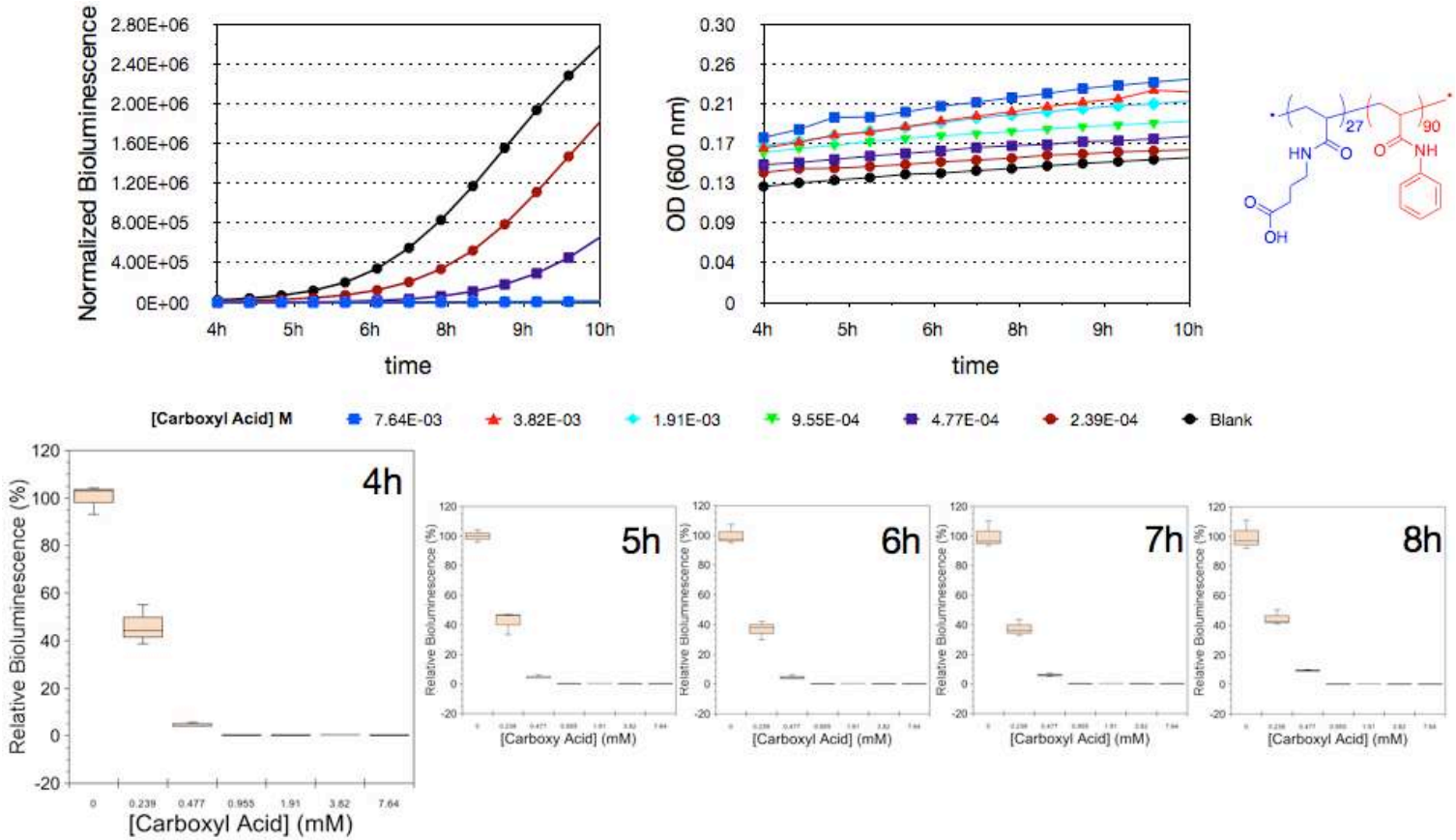

Figure 4-17. Light production curves and OD (600 nm), as a function of time for *V. harveyi* MM32 in the absence and presence of Vesicle **3b**.

Bottom: Effect of diol concentration in light production. (***protocol 4***)

Additionally commercial available lipid 1,2-dioleoyl-sn-glycero-3-phospho-rac-(1-glycerol) sodium salt (DOPG) able to form Vesicle **L1** was also of our interest due to the proposed effect of diol functionality on interfering with bacterial cell activities. As expected, the light output was completely quenched with diol concentration of 0.3 mM close to that of Vesicle **1a** (*Figure 4-18*). However, Vesicle **L2** self-assembled from 1,2-dioleoyl-sn-glycero-3-phosphocholine (DOPC) lacking of diol functionality but amine groups instead also gave comparative ability for quenching MM32 light production (*Figure 4-19*). In this case, these assays performed with a linear amine-pendent polymer Polymer **5** - p(DMAPMAm)$_{100}$ was selected as 'control' polymer (*Figure 4-20*). The amine functionality was demonstrated to contribute to aggregate bacterial cells owing to its positively charge (*Figure 3-18*) at neutral pH and also have relatively low binding affinity for boron (*Figure 3-8*). The results of MM32 assay for Polymer **5** was in accord with the above results that no reduction of light production was observed throughout the testing time, for the 'cell-binding' effect was predominant rather than 'QS-quenching'. In conclusion, all the above assay results suggest that the formation of vesicles significantly changed the effect of dual-action of linear materials (polymers and lipids) on interacting with bacterial system via increasing their affinity to boron while at the same time decreasing their affinity to cells.

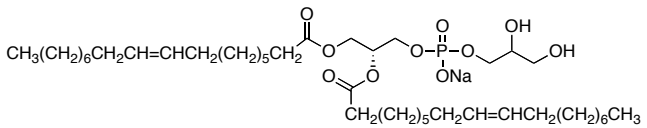

DOPG

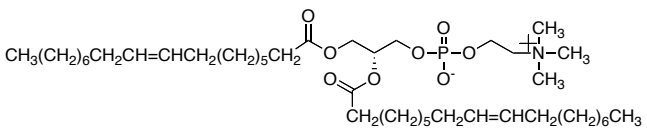

DOPC

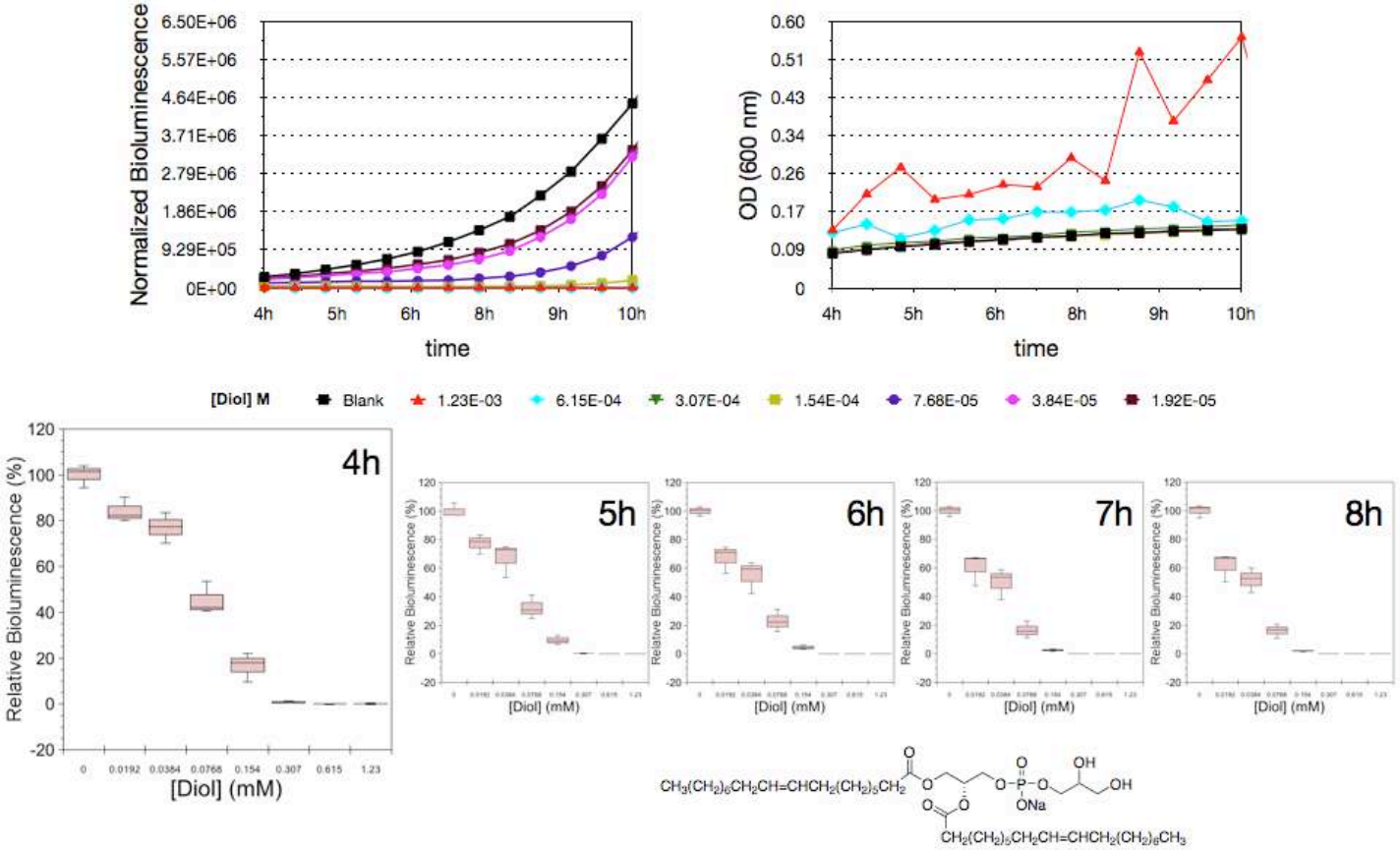

Figure 4-18. Light production curves and OD (600 nm), as a function of time for *V. harveyi* MM32 in the absence and presence of Vesicle **L1**.

Bottom: Effect of diol concentration in light production. (***protocol 4***)

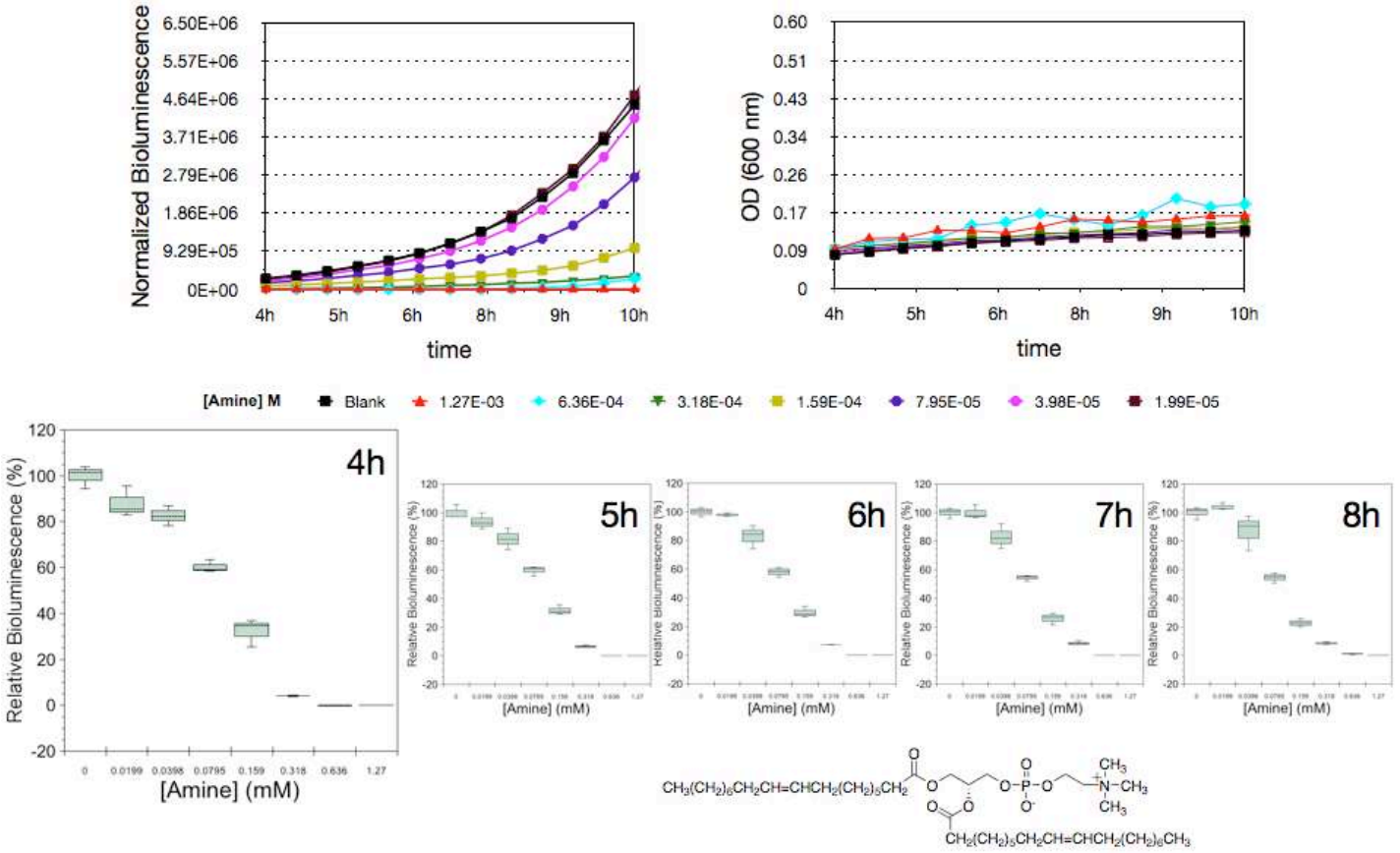

Figure 4-19. Light production curves and OD (600 nm), as a function of time for *V. harveyi* MM32 in the absence and presence of Vesicle **L2**.

Bottom: Effect of diol concentration in light production. (***protocol 4***)

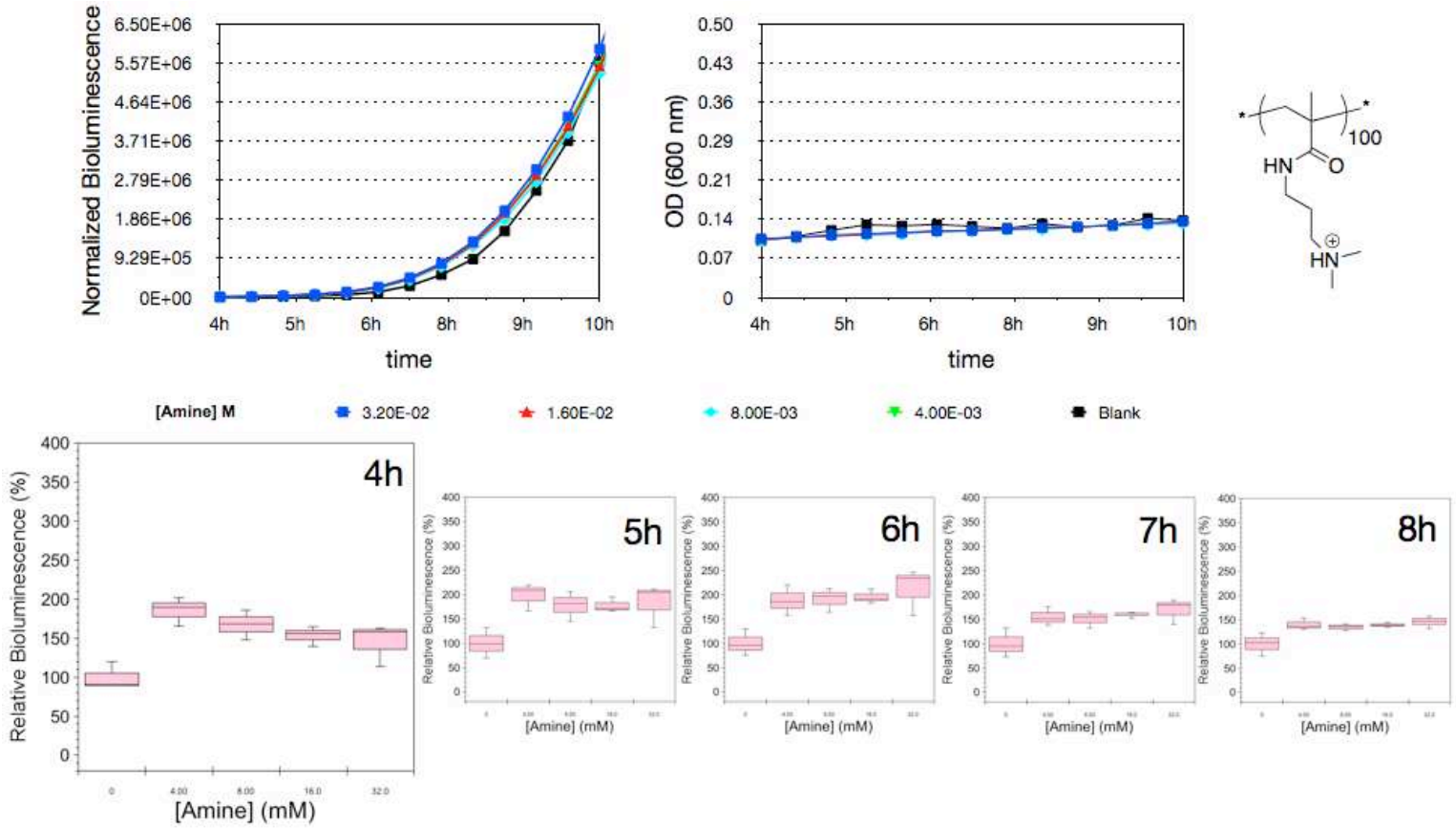

Figure 4-20. Light production curves and OD (600 nm), as a function of time for *V. harveyi* MM32 in the absence and presence of Polymer **5**. Bottom: Effect of diol concentration in light production. (***protocol 4***)

4.2.8 DPD release assay

For the second goal of this PhD project it was of interest to develop concepts in artificial cellularity and explore potential 'cross talk' between bacterial cells and polymersomes. In particular, self-assembled copolymers with surface diol functionality were designed to bind QS signals but were also considered to be capable of encapsulating and releasing QS signal precursors or metabolites. Such polymersomes could in such a case exhibit partial biomimicry of QS communication systems, such as detecting and responding/binding to bacterial signal molecules as well as binding microbial cells. In order to function as artificial protocells with QS signaling networks, the polymersomes should ideally also have their own metabolism and be able to transfer the metabolic information between polymersomes and cells. However, before incorporating a 'metabolic system', first it was necessary to investigate whether a known bacterial metabolic product could be encapsulated in the polymersomes. Therefore, the AI-2 precursor DPD was an obvious choice to be considered for inclusion into vesicle compartments and subsequent release. Although such a system is clearly an oversimplification of a protocell due to the lack of a true metabolism, it can nevertheless be considered that if the polymersomes could encapsulate and release their own signal precursor (DPD), and at the same time detect and respond to the active form of signal, ie. the product of DPD borate ester, AI-2, the first 'words' in the cross-talk experiment between protocells (Chells) and bacterial cells might be achieved (*Figure 4-21*).

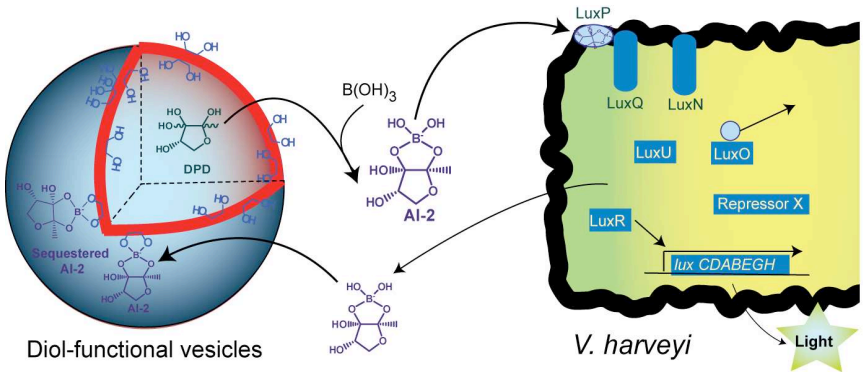

Figure 4-21. Scheme of mechanism of DPD loaded polymersomes interacting with real *V. harveyi* cells in the way of releasing DPD and reversibly binding AI-2 molecules in the media.

Initial experiments concentrated on the encapsulation process for DPD into the vesicle compartments, for there were a number of difficulties in optimizing the preparative system. Commercially available DPD is stored as a water solution at a concentration of 3.7 mM to maintain its activity. To increase the amount of DPD in the vesicles was therefore a challenge, since the highest DPD concentration without solvent evaporation was thus limited to 3.7 mM, while the optimized copolymer concentration for preparing vesicles was demonstrated to be 5.0 mg/mL. In addition, the aqueous phase for preparing the best vesicles was composed of HEPES buffer and sodium chloride solution. To retain the same buffer composition, the commercial DPD solution and stock vesicle buffer were therefore mixed with the appropriate ratio to reach the same salt concentrations as that used for making blank vesicles, however this resulted in unacceptably low incorporation of DPD. Therefore, an alternative approach by using the commercial DPD solution as the aqueous phase instead of buffers was also attempted. Following the vesicle preparation procedure, the organic solvent used to dissolve copolymers was evaporated under stirring in a

cold room to avoid DPD inactivation. The resulting solution was purified by PD-10 column twice in order to remove free DPD and in the mean time minimize the inevitable dilution of vesicles. Disposable short PD-10 columns were used to separate free DPD away from vesicle-bound DPD, which resulted in less dilution of vesicles compared to separations on Sephadex G50 columns and also reduced vesicle leakage (**4.2.4**). Samples of vesicles containing DPD were therefore purified immediately before the microbial bioluminescence assays.

The assays to evaluate DPD release from vesicles and any effects on bioluminescence were performed using three different experimental protocols.

Assay-**1**: empty/blank vesicles at different polymer concentrations were tested in the MM32 bioluminescence assay as discussed before, but with a concentration of DPD in the extra-vesicular media (i.e. assay media) of 0.1 μM.

Assay-**2**: DPD-loaded vesicles were incubated with the bacteria under the same conditions as the empty vesicles in Assay-**1**.

Assay-**3**: DPD-loaded vesicles were incubated with the bacteria in an assay buffer containing no exogenous DPD; thus the only DPD source in the assay was that released from the vesicles compared to Assay-**2**.

It should be noted that the DPD concentration (0.1 μM) in the assay media for Assay-**1** was much lower than that employed in the experiments described earlier in this thesis (20 μM). This was because preliminary results showed that the maximum bioluminescence obtained in experiments with vesicle-encapsulated DPD without exogenous DPD in the media was much smaller than that obtained in the prior experiments (i.e. those with an added DPD concentration of 20 μM). This was anticipated since prior experiments showed

that the maximum bioluminescence was related to DPD concentrations in the media (*Figure 3-21 and Figure 3-22*), although it should be noted that the data could have been skewed by surface-bound DPD on the vesicles. Therefore, by having a low amount of residual DPD in the media in Assays **1** and **2**, the hypothesis was that the bacteria would be 'primed' by the 0.1 μM DPD, but would respond much more predictably to any further release from inside the vesicles, where the 3.7mM concentration of DPD was large enough even on dilution to activate further the MM32. Specifically, it was assumed that DPD-loaded vesicles would behave differently from their non-loaded vesicle counterparts even in the presence of 0.1 μM DPD in the media.

In all the DPD release systems, the activation of MM32 light production was to be expected (*Figure 4-22* and *Figure 4-23*), however, since the vesicles were able to bind AI-2 i.e. the borate ester of DPD, but not DPD itself, a time dependent variation of bioluminescence was observed. Specifically, according to the prior results of MM32 assay, the onset of light production was 4 h with exogenous DPD in the media. However, in the absence of exogenous DPD but with DPD loaded vesicles in the media, the light onset was delayed to approximate 6 h (*Figure 4-22* and *Figure 4-23*, a). This may have been because the initial release of DPD did not cause light production because the bacteria needed some time to sense the signals and thus the MM32 cells did not produce light until AI-2 molecules accumulated to a threshold concentration. In the DPD release system, the DPD concentration increased with time, and thus the AI-2 formation rates were expected to be different compared to those with constant DPD concentrations. It was assumed that a proportion of AI-2 signal molecules could diffuse to reach the bacteria, but the majority of AI-2 might be

immediately sequestered by the vesicle diol groups. This process could continue until vesicle diol groups became saturated with bound AI-2, at which point further DPD release would activate MM32 until the threshold AI-2 concentration was reached. Alternatively, the reversible binding of the vesicle diol groups to AI-2 molecules/boron might increase their local concentration around some of the bacteria, and therefore might cause some local response.

On the other hand, according to the results (*Figure 4-22* and *Figure 4-23*, a), in the absence of externally added DPD, only Vesicle **1a** loaded with DPD caused bioluminescence, compared to control experiments where no investigated materials were added. These results were anticipated as the previous vesicle membrane permeability assays had shown that Vesicle **1a**, with p(2-EHAm) as their hydrophobic blocks, were able to release their contents in diluted solution at pH 7.4. Vesicles prepared with p(PAm) as the hydrophobic chain had relatively stable and robust membrane structures. Although the reduction of light output was observed in the presence of empty/blank Vesicle **1a** in MM32 assays (*Figure 4-13* and *Figure 4-23*, b) with exogenous DPD in the media which demonstrated the quenching ability of polymeric vesicles, the released DPD from DPD-loaded Vesicle **1a** still triggered light production (*Figure 4-22* and *Figure 4-23,* a: 7h and 8h) without externally added DPD in the media. In contrast, no light production could be observed throughout the experiment in the presence of DPD-loaded Vesicle **2** and Vesicl**e 3a** with robust membranes (*Figure 4-22* and *Figure 4-23*, a), for the amount of DPD released from them were likely not sufficient to 'switch on' QS, especially in the presence of diol functionality on the vesicle surfaces.

In the presence of externally added DPD molecules (0.1 μM) in the media, the assay results showed that bioluminescence was completely quenched in all cases with blank vesicles (*Figure 4-23*, b). These results were in accord with those obtained previously with DPD concentrations of 20 μM. However, when the DPD-loaded vesicles were tested in the same conditions, more complex data patterns were observed (*Figure 4-23*, b). It was expected that similar trends should be observed to those obtained in *Figure 4-23*, *a*, for the bioluminescence of the control was fixed to be 100 % and light production in each assay was compared to that of the control. However, the assay results varied across experimental repeats, suggesting heterogeneity in the initial bacterial cultures for these assays. Future efforts should focus on synchronizing bacterial cultures in larger cell numbers, in addition to optimizing DPD encapsulation, vesicle purification and assay conditions in bioluminescence experiments.

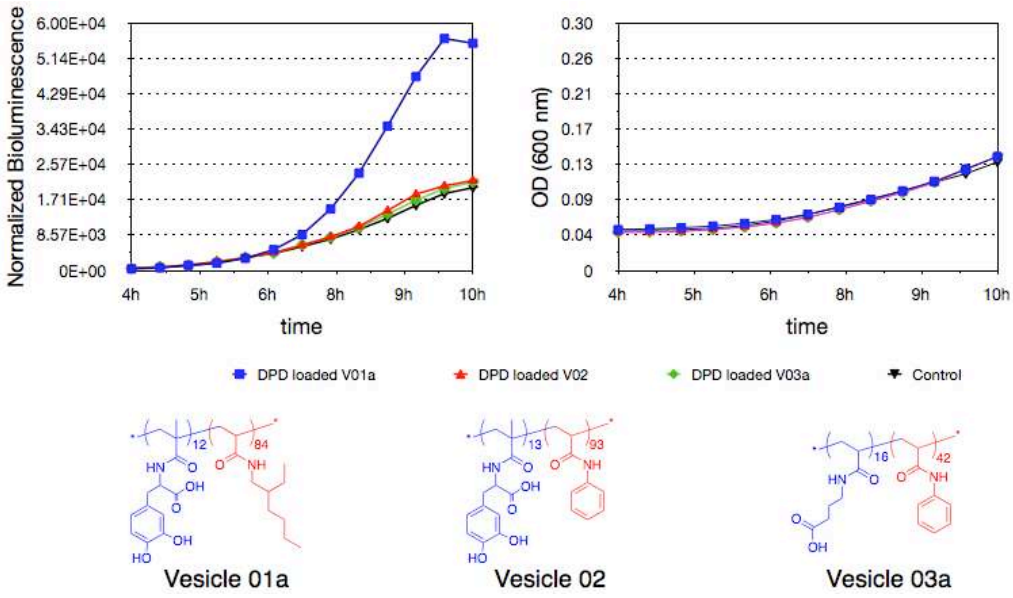

Figure 4-22. Light production curves and OD (600 nm), as a function of time for *V. harveyi* MM32 in the absence and presence of DPD loaded polymer vesicles in the media without exogenous DPD.

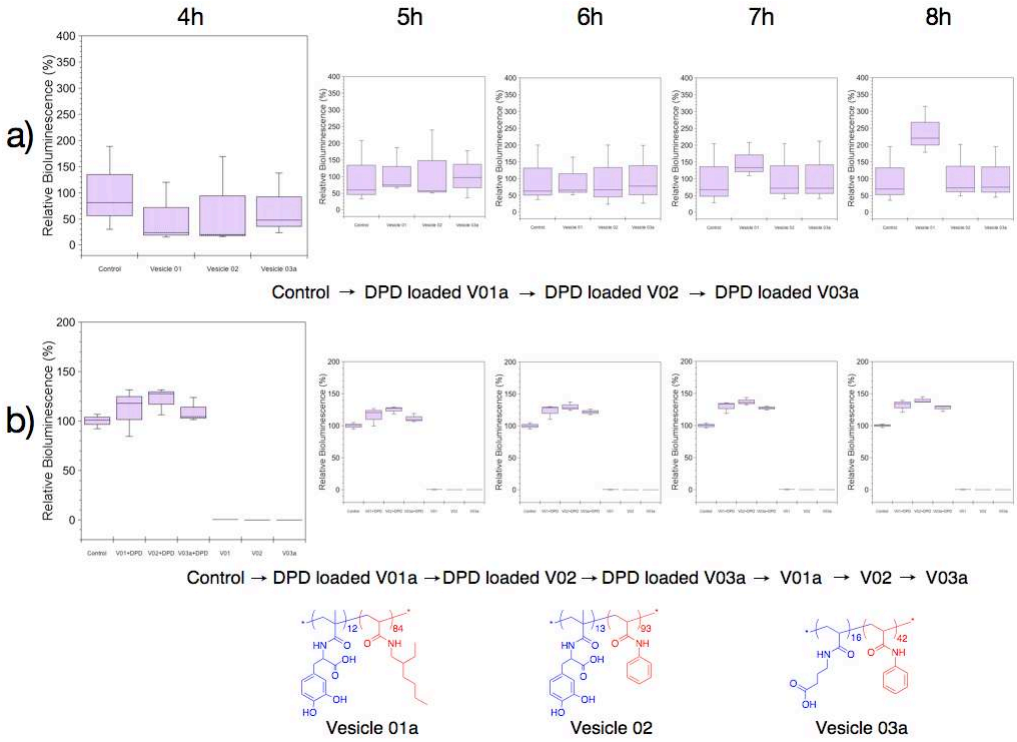

Figure 4-23. Effect of different DPD-loaded vesicles in the absence of DPD in assay media, a) and effect of different DPD-loaded vesicles, and non-loaded vesicles, in the presence of 0.1 μM DPD in assay media, b)

This DPD release assay was also attempted with the vesicles self-assembled from commercial available lipids (*Figure 4-24 and Figure 4-25*) following the same protocols as mentioned above. It was demonstrated again that empty/blank Vesicle **L1** and Vesicle **L2** were able to quench light production of MM32 bacteria in proposed media (*Figure 4-25*, b), while release of DPD from the lipid vesicles was obtained during the testing duration as reported by the increased bioluminescence *(Figure 4-24 and Figure 4-25*). In order to understand better the activity of lipid vesicles compared to the polymersomes investigated in this study, membrane permeability assays for these lipidic systems should be carried out and further DPD release assays repeated under optimized conditions.

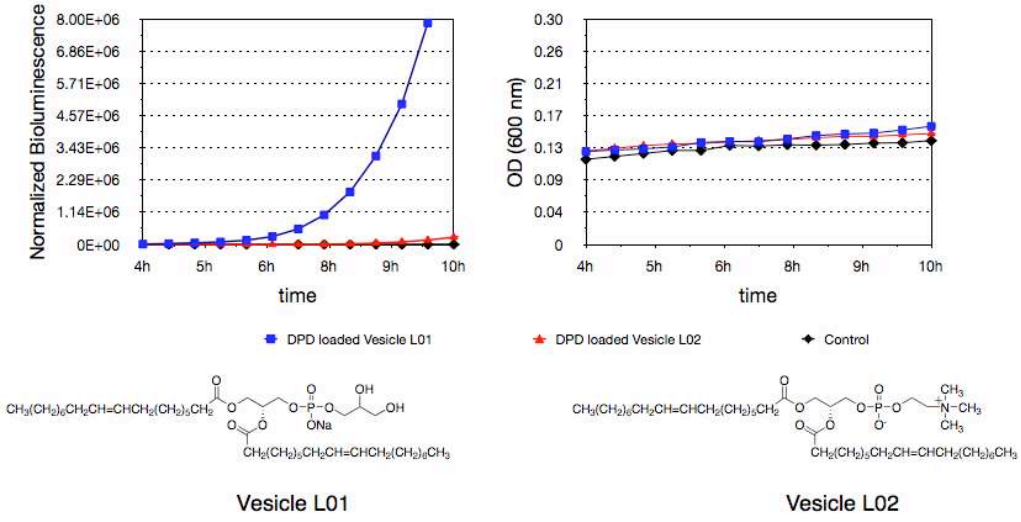

Figure 4-24. Light production curves and OD (600 nm), as a function of time for *V. harveyi* MM32 in the absence and presence of DPD loaded ligand vesicles in the media without exogenous DPD.

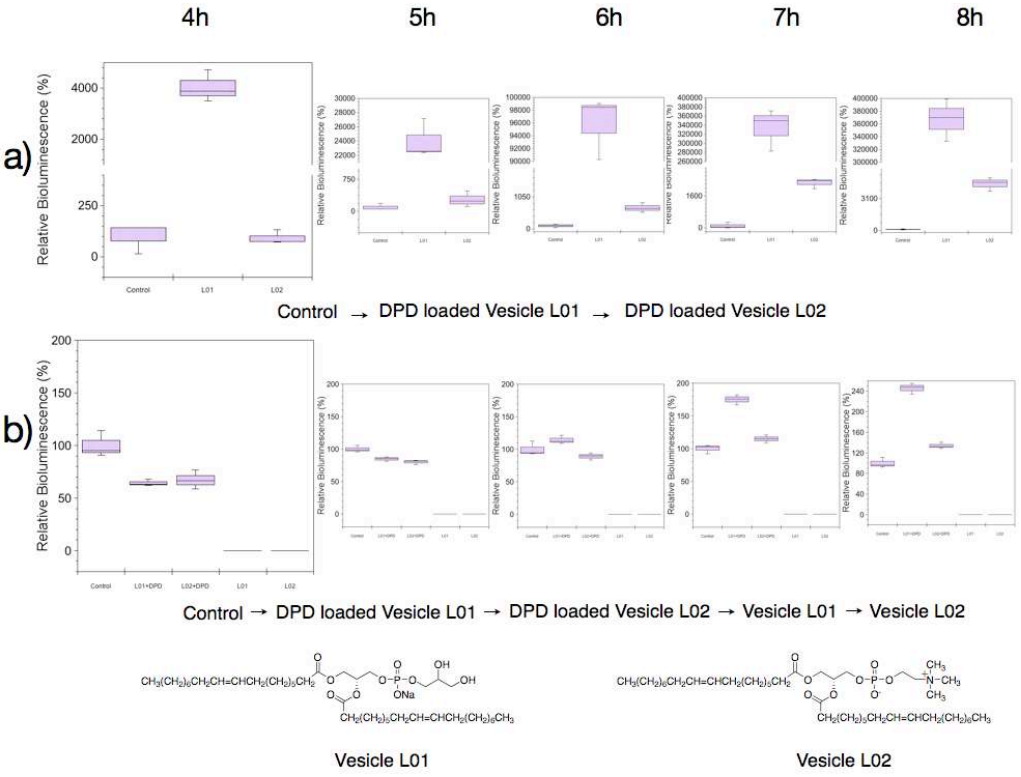

Figure 4-25. Effect of different DPD loaded lipid vesicles in the absence of DPD in assay media, a) and effect of different DPD loaded lipid vesicles as well as their blank forms in the presence of 0.1 μM DPD in assay media, b)

4.3 Conclusions

In this chapter, a series of amphiphilic block copolymers were successfully synthesized by using macro-diol-pendent polymers as chain transfer agent in RAFT polymerizations. All polymers were characterized by ^{1}H-NMR and RAFT termini removed from polymers before each biological assay. The successfully prepared polymers were self-assembled into vesicles as characterized by DLS, TEM and zeta-potential analysis. The membrane permeability of vesicles was examined by testing release of encapsulated fluorescent dyes at neutral and alkaline pH via fluorescence spectrometry. The types of hydrophobic blocks were likely to have been contributing factors in the differing membrane permeabilities and vesicle stabilities. In order to test cell sequestration activity of the polymersomes, bacterial attachment assays were performed in AB-media at pH 7.4 with both vesicles and their corresponding diol-pendent linear polymers. In this case, designed vesicles were demonstrated to induce bacterial aggregation to a lesser extent than linear polymer analogues. The binding affinities for boric acid of the reported vesicles were not accessible by the AR-S assay because of the limitations of binding saturation and light scattering from the vesicles. Therefore, the research was moved to the in-vitro assays.

In all cases, catechol-, carboxyl acid- and amine-pendent polymeric vesicles, as well as vesicles self-assembled from commercial available lipids, were demonstrated to reduce light production of *V. harveyi* bacteria in a dose-dependent manner and even with higher potency than that of linear polymers. Also, these vesicles did not damage the cells as judged by continuing growth in optical density measurements.

In order to approach an extended aim of this project to establish artificial cellularity and 'cross talk' with bacterial cells by using *V. harveyi* species MM32 as a model, DPD was selected as a QS mediator to be encapsulated in vesicle compartments. The DPD release assay gave some promising results as anticipated. However, there remain difficulties in repeating the experiments and so complete understanding of the interaction mechanisms is not possible at this stage. The light producing process was more complicated with DPD-loaded vesicles than that with polymers/blank vesicles. There was insufficient time in the thesis period to conclude the experiments to probe release rates and bioluminescence profiles, but future work should consider simulations of rate equations computationally.

In conclusion, vesicles with functionalities capable of binding QS signals have shown high potency in deactivating population bioluminescence responses, but low affinities to cell surfaces. Such vesicles are potentially useful as diagnostics and anti-microbials, while further work to control binding and release of contents from the vesicle interiors may allow their use as information carriers in synthetic biology studies.

References

[1] A. Moya, R. Gil, A. Latorre, J. Pereto, M. Pilar Garcillan-Barcia, F. de la Cruz, *Fems Microbiology Reviews* **2009**, *33*, 225-235.

[2] aM. Antonietti, S. Forster, *Advanced Materials* **2003**, *15*, 1323-1333; bM.-H. Li, P. Keller, *Soft Matter* **2009**, *5*, 927-937.

[3] aM. C. Jones, J. C. Leroux, *European Journal of Pharmaceutics and Biopharmaceutics* **1999**, *48*, 101-111; bH. W. Shen, A. Eisenberg, *Macromolecules* **2000**, *33*, 2561-2572; cG. E. Yu, A. Eisenberg, *Macromolecules* **1998**, *31*, 5546-5549.

[4] W. Y. Ayen, K. Garkhal, N. Kumar, *Molecular Pharmaceutics* **2011**, *8*, 466-478.

[5] aT. Govender, S. Stolnik, M. C. Garnett, L. Illum, S. S. Davis, *Journal of Controlled Release* **1999**, *57*, 171-185; bT. Betancourt, B. Brown, L. Brannon-Peppas, *Nanomedicine* **2007**, *2*, 219-232; cC. Sanson, C. Schatz, J.-F. Le Meins, A. Brulet, A. Soum, S. Lecommandoux, *Langmuir* **2010**, *26*, 2751-2760; dK. K. Upadhyay, J. F. Le Meins, A. Misra, P. Voisin, V. Bouchaud, E. Ibarboure, C. Schatz, S. Lecommandoux, *Biomacromolecules* **2009**, *10*, 2802-2808; eV. Lassalle, M. L. Ferreira, *Macromolecular Bioscience* **2007**, *7*, 767-783.

[6] aC. Zheng, X. Yao, L. Qiu, *Macromolecular Bioscience* **2011**, *11*, 338-343; bV. Malinova, S. Belegrinou, D. d. B. Ouboter, W. P. Meier, in *Polymer Membranes/Biomembranes* (Ed.: W. P. K. W. Meier), **2010**, *224*, 113-165.

[7] aT. M. Taylor, S. Gaysinsky, P. M. Davidson, B. D. Bruce, J. Weiss, *Food Biophysics* **2007**, *2*, 1-9; bK. Ohsawa, M. Murata, H. Ohshima, *Colloid and Polymer Science* **1986**, *264*, 1005-1009; cM. Amin, *Indian Journal of Biochemistry & Biophysics* **1980**, *17*, 380-384.

[8] aK. T. Kim, S. A. Meeuwissen, R. J. M. Nolte, J. C. M. van Hest, *Nanoscale* **2010**, *2*, 844-858; bO. Onaca, R. Enea, D. W. Hughes, W. Meier, *Macromolecular Bioscience* **2009**, *9*, 129-139; cA. Blanazs, S. P. Armes, A. J. Ryan, *Macromolecular Rapid Communications* **2009**, *30*, 267-277.

[9] aD. V. Patel, C. N. J. McGhee, *Clinical and Experimental Ophthalmology* **2007**, *35*, 71-88; bY. Ohno, H. Birn, E. I. Christensen, *Journal of the American Society of Nephrology* **2003**, *14*, 316-316; cP. Ramoino, F. Beltrame, A. Diaspro, M. Fato, *Microscopy Research and Technique* **1996**, *35*, 377-384.

[10] A. Alessandrini, P. Facci, *Measurement Science & Technology* **2005**, *16*, 65-92.

[11] N. Faucheux, R. Schweiss, K. Lutzow, C. Werner, T. Groth, *Biomaterials* **2004**, *25*, 2721-2730.

[12] aD. Roy, J. N. Cambre, B. S. Sumerlin, *Chem Commun* **2008**, 2477-2479; bD. Roy, J. N. Cambre, B. S. Sumerlin, *Chem Commun* **2009**, 2106-2108.

[13] L. Albertin, M. H. Stenzel, C. Barner-Kowollik, T. P. Davis, *Polymer* **2006**, *47*, 1011-1019.

[14] P. M. Gardner, K. Winzer, B. G. Davis, *Nat Chem* **2009**, *1*, 377-383.

[15] K. S. Soppimath, T. M. Aminabhavi, A. R. Kulkarni, W. E. Rudzinski, *Journal of Controlled Release* **2001**, *70*, 1-20.

[16] aH. Lee, N. F. Scherer, P. B. Messersmith, *Proceedings of the National Academy of Sciences of the United States of America* **2006**, *103*, 12999-13003; bP. Podsiadlo, Z. Liu, D. Paterson, P. B. Messersmith, N. A. Kotov, *Advanced Materials* **2007**, *19*, 949-955; cH. Lee, B. P. Lee, P. B. Messersmith, *Nature* **2007**, *448*, 338-342; dM. Guvendiren, P. B. Messersmith, K. R. Shull, *Biomacromolecules* **2008**, *9*, 122-128; eL. M. Hamming, X. W. Fan, P. B. Messersmith, L. C. Brinson, *Composites Science and Technology* **2008**, *68*, 2042-2048; fM. Guvendiren, D. A. Brass, P. B. Messersmith, K. R. Shull, *Journal of Adhesion* **2009**, *85*, 631-645; gB. P. Lee, P. B. Messersmith, J. N. Israelachvili, J. H. Waite, in *Annual Review of Materials Research* (Ed.: D. R. F. P. Clarke), **2011**, *41*, 99-132.

[17] B. Z. Lin, C. C. Yin, H. Hauser, *Biochimica Et Biophysica Acta* **1993**, *1147*, 237-244.

[18] aS. Mordon, V. Maunoury, J. M. Devoisselle, Y. Abbas, D. Coustaud, *Journal of Photochemistry and Photobiology B-Biology* **1992**, *13*, 307-314; bS. Mordon, J. M. Devoisselle, V. Maunoury, *Photochemistry and Photobiology* **1994**, *60*, 274-279.

Chapter 5. Conclusions and Future Work

5.1 Conclusions

Within this thesis two related concepts have been considered. The first concerns a possible new strategy for anti-infective drugs as it is known that existing antimicrobial agents including antibiotics, oxidants and biocides can act as a powerful selective force for promoting the emergence of resistant mutations in a population.[1] Although tremendous efforts have been made on prevention of resistance emergence and also management of its frequency as two pathways to treat bacterial infection,[1b] the selection pressure and resistance invoked by antimicrobial use still restrict curative effects against bacteria. The development of 'intelligent' anti-infective materials via strategies that target bacterial communication is a potential means to avoid selection pressure. Therefore, the strategies in this research were: 1) interference with the bacterial communication system Quorum Sense (QS) network, which can be linked to bacterial virulence and biofilm formation,[2] and 2) prevention of bacterial-host adhesion, to prevent colonization[3] and subsequent formation of resistant biofilms.[4] The understanding of each individual mechanism within these strategies has been developed over several decades, but at the start of this thesis no research groups had previously reported materials with potential to interfere with both routes.

Synthetic polymers were used for the interference strategy because they possess repeating structural units and their affinities with cell surface receptors can be tailored through multivalent ligand attachment. Also, the affinities of polymer-displayed receptors with both bacterial QS signals and host cell surfaces, the ability to solubilize these receptors at neutral pH through

attachment to a water soluble polymer, and the potential tuning of surface charge, morphology and self-assembly of polymers in solution were all advantageous factors for anti-infective strategies. Furthermore, the use of reversible addition-fragmentation chain transfer (RAFT) radical polymerization methods allowed fine control of macromolecular structure and architecture. This in turn enabled extension of the strategy into the synthesis of block copolymers with both hydrophilic and hydrophobic components to form polymersomes, potentially able to act both as containers for QS molecules, and sequestrants for QS signals.

These polymersomes were intended as simple protocell mimics for QS interference, as it is difficult to contain all the key characters[5] of living cells in a single synthetic cell model. Micelles or vesicles have already been used in antimicrobial strategies, as they have been shown to be more efficient in disintegrating cell walls compared with individual molecules.[6] Accordingly, the thesis investigated the protocell concept combined with dual-action ('QS quenching' and 'bacterial sequestration') with a view to generating 'dual-action' bacterial interference agents. Specifically, the polymersomes investigated here were designed to maintain the dual advantages of the linear polymers, while at the same time enhance their potency for antibacterial therapy by releasing encapsulated QS-mediators to disrupt the QS communication system. In such a way, a feedback/communication/interference loop between the real bacterial cells and the investigated polymersomes was to be established. Ultimately, the polymersomes were intended to respond to the QS signals as well as mimicking the behavior of the bacterial cell surfaces via binding (aggregation).

The project started by screening small molecules as monomer candidates with strong potency to interfere with bacterial communication. QS systems based on the active form of AI-2 signaling were chosen as these derive from furanosyl borate diester produced from 4,5-dihydroxy-2,3-pentanedione (DPD) and borate in marine environments. Representative diols were investigated as potential AI-2 scavengers, using an assay involving reversible ester formation with boric and boronic acids and Alizarin Red S (AR-S).[7] Binding affinities with diol species were examined by titration studies at pH 7.4 using the AR-S assay and evaluated using the Benesi-Hildebrand equations.[7] The relative order of binding affinities for different diols towards boron species were in accord with prior reports: linear diols < cyclic diols (sugars) < aromatic diols or catechols.[7-8] Even though DPD has a similar structure to carbohydrates, its affinity was much higher than that obtained for the other saccharides analyzed, and only the catechols gave comparable affinities. These observations were confirmed by mass spectrometry and ^{11}B-NMR spectroscopy. ^{11}B-NMR technique confirmed the presence of 1:1 and 1:2 complexes between boric acid and dopamine or 3,4-dihydroxy-L-phenylalanine methacrylamide (L-DOPA) depending on the ratio of sodium borate to catechols in solution. The competitive binding of the catechol molecules to quench the 'active' AI-2 was also observed in the ^{11}B-NMR spectrum, in which the addition of catechols completely suppressed the AI-2 signals while generating new signals assigned to catechol-boron complexes. These experiments suggested that monomers derived from dopamine and its derivative L-DOPA were the best candidates for polymeric QS control, showing a similar affinity for boron compared to DPD and the potential ability to decrease the concentration of AI-2 in solution.

Three types of polymers with diol structures to quench QS signals and functionality to mediate cell attachment were studied. First of all, a cationic statistical copolymer, poly{N-(3,4-dihydroxyphenethyl)methacrylamide -co-N-[3-(dimethylamino)propyl] methacrylamide} (p(DMAm-*c*-DMAPMAm), Polymer **1**) was prepared via RAFT polymerization. N-(3,4-dihydroxyphenethyl)methacrylamide (DMAm) was synthesized[9] to give the polymer high affinity to boron, while N-[3-(dimethylamino)propyl] methacrylamide (DMAPMAm) was designed to confer water-solubility in neutral solution and also possess a positive charge to bind strongly to negatively charged bacterial surfaces.[10] Also, L-DOPA monomer was synthesized[9] and an anionic homopolymer poly(3,4-dihydroxy-L-phenylalanine methacrylamide) (p(L-DMAm), Polymer **2**) was also produced via RAFT polymerization. For this material, L-DOPA showed similar affinities for boron but improved water solubility for its homopolymer compared to p(DMAm) in neutral pH, and was expected to attach to the bacterial surfaces less readily because of charge-charge repulsion. Subsequently, p(DMAm-*c*-DMAPMAm) and p(L-DMAm) with varying degrees of polymerization (DP) were successfully synthesized and characterized. In addition, carbohydrate-based poly(β-D-glucosyloxyethyl methacrylate) (p(GlcEMA), Polymer **3**), previously prepared in the group, was also evaluated in dual-action experiments, for its highly active bacterial sequestration ability,[11] but low affinity for boron had been demonstrated in prior AR-S assay. The binding affinities of the polymers on boronates were also established by AR-S assay and confirmed by ^{11}B-NMR spectra. In all cases, polymers exhibited higher affinities to boron species than their corresponding monomer analogues. In

order to test cell sequestration function of the polymers, bacterial attachment assays were performed in both AB-media and PBS buffer at pH 7.4. All the data suggested that the tested polymers displayed dual-action in terms of AI-2 binding and cell attachment, though to varying extents.

Assays with *Vibrio harveyi* MM32, which is bioluminescent with active QS signaling, were performed in different conditions (batch of cells, protocols and batch of DPD), showed that the trends of light output in the presence of each individual polymer were constant in all the experiments. Significantly, this range of polymers was able to maintain bacterial capture and suppression of QS signaling without damaging the cells as judged by continuing growth in optical density (OD) measurements.

Structures of dual-action polymers:

Polymer **1**

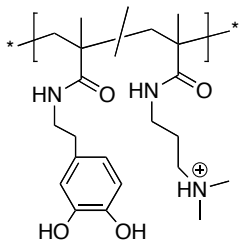

DMAm : DMAPMAm
a: 14 : 86; **b**: 29 : 71

Polymer **2**

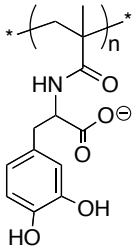

a: n = 15; **b**: n = 26

Polymer **3**

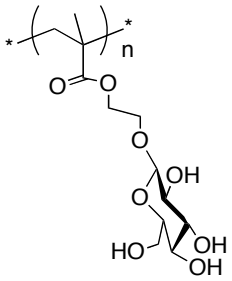

n = 16

The studies progressed to develop a more complex system in which simple cell-mimic polymersomes were evaluated in the presence of bacterial cells. A series of amphiphilic block copolymers with various DPs were successfully synthesized via RAFT polymerization process and characterized by ^{1}H-NMR. Successfully assembled polymersomes were characterized by DLS, TEM, AFM and zeta-potential analysis. However, the dispersities of the prepared

particles were broad and spherical micelles as well as polymeric vesicles probably coexisted in the mixtures. The membrane permeability of vesicles was examined by encapsulating and releasing fluorescent dyes (model dye: 5(6)-carboxyfluorescein and pyranine) at neutral and alkaline pH. The type of hydrophobic blocks was found to be important in determining membrane permeability and stability. Specifically, the dye release of polymersomes with PAm in their membrane structures was observed to be slower than those with 2-EHAm. Again, to examine cell sequestration activity of the polymersomes, bacterial attachment assays were performed in AB-media at pH 7.4 with both vesicles and their corresponding diol-pendent linear polymers. The polymersomes were demonstrated to induce less bacterial aggregation than their linear polymer counterparts.

Structures of copolymers with dual-action:

Copolymer **1**

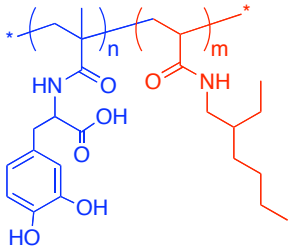

p(L-DMAm)-b-p(2-EHAm)

c: n = 16, m = 73 (Vesicle **1b**)
d: n = 12, m = 84 (Vesicle **1a**)

Copolymer **2**

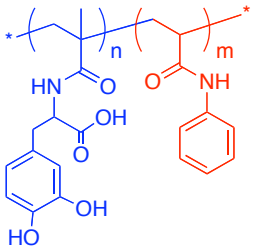

p(L-DMAm)-b-p(PAm)

n = 13, m = 93 (Vesicle **2**)

In all cases, catechol-, carboxyl acid- and amine-pendent polymeric vesicles were demonstrated to reduce light production of *V. harveyi* bacteria in a dose-dependent manner and with higher potency than that of corresponding linear polymers. In addition, vesicles self-assembled from commercially available hydroxyl-containing lipids also suppressed bioluminescence. As with the linear

polymers, no damage to bacterial cells, as judged by continuing growth in OD measurements, occurred in the bioluminescence assays.

At the last stage, in attempts to 'cross talk' with the *V. harveyi* MM32 strain, DPD was selected as a QS mediator and encapsulated in vesicle compartments. The DPD release assay indicated variations in bioluminescence but it was not possible to establish whether an equilibrium was established between DPD release, sequestration and QS interference.

In summation, polymersomes with functionality for binding QS signals with high potency but with low affinities for cell surfaces were demonstrated. Such vesicles are not only potentially powerful diagnostics and anti-microbials, but might, if optimized for controlled release, act as information carriers and synthetic cell mimics.

5.2 Future work

Although the development of polymersomes with dual-action on bacterial infective behaviors seems promising to date, the study of establishing synthetic protocells is still on its early stage. First of all, the DPD loading content (LC) (**Eq. 1**) and loading efficiency (LE) (**Eq. 2**) for investigated polymersomes and also vesicles made from commercial lipids have not been quantified in this research thesis. In **Eq. 1** and **Eq. 2**, where W_{load} represents weigh of loaded cargo, W_{carrier} is the weight of polymer/lipid and W_{feed} means weight of cargo in feed.

Equation 1

$$LC(wt\%) = \frac{W_{load}}{W_{carrier}} \times 100\%$$

Equation 2

$$LE(\%) = \frac{W_{load}}{W_{feed}} \times 100\%$$

Obviously, this is one of the key issues to solve in the future. However, there are some difficulties in evaluating LC and LE of investigated polymersomes encapsulating with DPD molecules. DPD exists with tautomeric forms and binds boron to form boronate ester in solution. So, it is difficult to conjugate DPD with chromophores which give a readout way to evaluate the amount of DPD inside the polymersomes. Therefore, some efforts need to be made on investigation of the synthesis of chromophore labeled DPD molecules. An alternative approach might use model dyes instead of DPD itself in encapsulation and release experiments, which would be a roughly evaluation. However, according to some preliminary results (data not shown in this thesis) that LC and LE of p(L-DMAm)-p(PAm) polymersomes with pyranine were very low, it is necessary to improve the copolymer structures based on the specific membrane properties needed. Optimizing the RAFT polymerization conditions (CTA, solvents, temperature and pH environment) and vesicle preparation techniques might allow improvements in particle size, encapsulation efficiency and in vitro release.[12]

Future work in the area of cell mimicry might envisage artificial metabolisms, in which synthetic polymersomes act as microreactors to generate metabolites (e.g. QS products) that could be released across the bilayer membrane to the external environment in a controlled manner. Collaborators in the Davis group at Oxford have shown that DPD derivatives can be produced by the formose reaction within vesicles made from commercial available lipids. When these are released from the compartments light output is induced from *V. harveyi*.[13] Functional polymersomes with the ability to enclose the formose reaction and

release the sugar products in a controlled manner are an ongoing investigation. These might not only contribute to antibacterial therapeutic studies, but also be a large step towards construction of a wholly synthetic biologic entity.

References

[1] aC. Wongsrichanalai, A. L. Pickard, W. H. Wernsdorfer, S. R. Meshnick, *Lancet Infect Dis* **2002**, *2*, 209-218; bP. A. zur Wiesch, R. Kouyos, J. Engelstadter, R. R. Regoes, S. Bonhoeffer, *Lancet Infect Dis* **2011**, *11*, 236-247.

[2] aM. B. Miller, B. L. Bassler, *Annu Rev Microbiol* **2001**, *55*, 165-199; bK. R. Hardie, K. Heurlier, *Nat Rev Microbiol* **2008**, *6*, 635-643.

[3] P. Cossart, P. J. Sansonetti, *Science* **2004**, *304*, 242-248.

[4] K. Hori, S. Matsumoto, *Biochem Eng J* **2010**, *48*, 424-434.

[5] P. Walde, *Bioessays* **2010**, *32*, 296-303.

[6] aL. Liu, K. Xu, H. Wang, J. P. K. Tan, W. Fan, S. S. Venkatraman, L. Li, Y.-Y. Yang, *Nature Nanotechnology* **2009**, *4*, 457-463; bF. Nederberg, Y. Zhang, J. P. K. Tan, K. Xu, H. Wang, C. Yang, S. Gao, X. D. Guo, K. Fukushima, L. Li, J. L. Hedrick, Y.-Y. Yang, *Nature Chemistry* **2011**, *3*, 409-414.

[7] G. Springsteen, B. H. Wang, *Tetrahedron* **2002**, *58*, 5291-5300.

[8] J. P. Lorand, J. O. Edwards, *J Org Chem* **1959**, *24*, 769-774.

[9] aH. Lee, B. P. Lee, P. B. Messersmith, *Nature* **2007**, *448*, 338-342; bP. Glass, H. Chung, N. R. Washburn, M. Sitti, *Langmuir* **2009**, *25*, 6607-6612.

[10] G. P. Treweek, J. J. Morgan, *J Colloid Interf Sci* **1977**, *60*, 258-273.

[11] aC. Alexander, G. Pasparakis, A. Cockayne, *Journal of the American Chemical Society* **2007**, *129*, 11014-11015; bC. Alexander, G. Pasparakis, *Angewandte Chemie-International Edition* **2008**, *47*, 4847-4850.

[12] S. L. Gosangari, K. L. Watkin, *Pharm. Dev. Technol.* **2012**, *17*, 103-109.

[13] P. M. Gardner, K. Winzer, B. G. Davis, *Nat Chem* **2009**, *1*, 377-383.

Appendix

Materials

All solvents and reagents were of analytical or HPLC grade and purchased from Sigma or Fisher Scientific without further purification unless otherwise stated. We thank Bonnie Bassler (Department of Molecular Biology, Princeton University) for the gift of *Vibrio harveyi* strain MM32.

Supplier and purity detail of chemicals

- Acetonitrile - Sigma Aldrich
- Acryloyl chloride (96%) - Alfa Aesar
- Alizarin Red S (AR-S, indicator) - Riedel-deHaën
- Amberlite IRA743 free base - Sigma Aldrich
- Ammonium hydroxide (28% NH_3 in H_2O) - Sigma Aldrich
- Azobisisobutyronitrile (2,2'-azobis(2-methylpropionitrile), AIBN, 98%) - Sigma Aldrich
- Benzyl 2-hydroxyethyl carbonotrithioate (CTA **2** in **Chapter 3**) - synthesized by Francisco Fernandez-Trillo, School of Pharmacy, the University of Nottingham
- Carbon disulfide (anhydrous, ≥ 99%) - Sigma Aldrich
- Casamino acids - Acros Organics
- Cesium carbonate (≥ 99%) - Fluka
- Dopamine hydrochloride (99%) - Alfa Aesar
- Dulbecco phosphate buffer saline (PBS, 10X without Ca^{2+} and Mg^{2+}) - Lonza
- Glycerol (for molecular biology, ≥ 99%) - Sigma Aldrich

- Hydrochloric acid (ACS reagent, 37%) - Sigma Aldrich
- L-arginine (reagent grade, ≥ 98% (TLC), powder) - Sigma Aldrich
- LB media with kanamycin (antibiotic, 30 g/mL) - prepared by Nigel Halliday, School of Molecular Medical Science, Centre for Biomolecular Sciences, the University of Nottingham
- Magnesium sulfate (anhydrous, ≥99.5%) - Sigma Aldrich
- Methacrylic anhydride - Sigma Aldrich
- Methacryloyl chloride (≥97%) - Fluka
- Nitric acid (70%) - Sigma Aldrich
- N-[3-(dimethylamino)propyl]-methacrylamide (99%) - Sigma Aldrich
- Phenylboronic acid (≥ 97%) - Fluka
- Poly(β-D-glucosyloxyethyl methacrylate) (p(GlcEMA)) - synthesized by George Pasparakis, School of Pharmacy, the University of Nottingham
- Phloroglucinol (99%, anhydrous) - Acros Organics
- Poly(N-phenylacrylamide) - synthesized by Francisco Fernandez-Trillo, School of Pharmacy, the University of Nottingham
- Poly(vinyl alcohol) (PVA, 87-89% hydrolyzed, Mw 13000-23000) - Sigma Aldrich
- Potassium hydroxide (Na < 0.002%, ≥ 86%) - Fluka
- Potassium phosphate tribasic (≥ 98%) - Sigma Aldrich
- Pyranine - Sigma Aldrich
- Sephadex G50 - (dry bead diameter: 20-80 μm, bed volum 9-11 mL/g) - Sigma Aldrich
- Silica 60Å (particle size 35-70 micron, chromatography grade) - Fisher Scientific

- Sodium bicarbonate (for molecular biology, 99.7%-100.3%) - Sigma Aldrich
- Sodium borate - Sigma Aldrich
- Sodium carbonate (≥99.0%, anhydrous) - Sigma Aldrich
- Sodium chloride - Fisher Scientific
- Sodium hydroxide (≥98%) - Sigma Aldrich
- Sodium phosphate monobasic (≥ 99%) - Sigma Aldrich
- Spectra/Por dialysis membrane (MWCO: 1000, 6000-8000) - Spectrum Laboratories, Inc.
- (*S*)-4,5-dihydroxy-2,3-pentadione-(DPD) - Ommscientific or synthesized by Paul M. Gardner, Department of Chemistry, University of Oxford, Chemistry Research Laboratory
- Triton X-100, toctylhenoxypolyethoxyethanol - Sigma Aldrich
- V-501 (recrystallized from MeOH) - Fluka
- 1,2-dioleoyl-sn-glycero-3-phosphocholine (DOPC) - Fisher Scientific
- 1,2-dioleoyl-sn-glycero-3-phospho-rac-(1-glycerol) sodium salt (DOPG) - Fisher Scientific
- 2-amino-1,3-propanediol (98%) - Alfa Aesar
- 2-bromoisobutyric acid - Alfa Aesar
- 2-(decylthiocarbonothioylthio)-2-methylpropanoic acid (CTA **3** in **Chapter 3**) - synthesized by Francisco Fernandez-Trillo, School of Pharmacy, the University of Nottingham
- 2-ethylhexan-1-amine - Alfa Aesar

- 2-(ethylthiocarbonothioylthio)-2-methylpropanoic acid (CTA **5** in **Chpater 3**) - synthesized by Francisco Fernandez-Trillo, School of Pharmacy, the University of Nottingham
- 2-mercaptoethanol (≥ 99.0%) - Sigma Aldrich
- 2-methyl-1,3-propandiol (99%) - Sigma Aldrich
- 3,4-dihydroxyhydrozimtsäure (98%) - Sigma Aldrich
- 3,4-dihydroxy-L-phenylalanine (≥ 98%) - Alfa Aesar
- 3-methoxy-1,2-propandiol (98%) - Sigma Aldrich
- 4-aminobutanoic acid (≥ 99%) - Acros Organics
- 4-cyano-4-(phenylcarbonothioylthio)pentanoic acid (CTP, CTA **4** in **Chapter 3**) - synthesized by Francisco Fernandez-Trillo, School of Pharmacy, the University of Nottingham
- 4-(2-hydroxyethyl) piperazine-1-ethanesulfonic acid (HEPES) (≥99.5%) - Sigma Aldrich
- 5(6)-carboxyfluorescein - Sigma Aldrich

Instrumentation

NMR Spectroscopy

^{1}H and ^{13}C Nuclear magnetic resonance (NMR) spectra were recorded on a Bruker 400 MHz (^{1}H) and 100 MHz (^{13}C) spectrometers in DMSO-d_6, D_2O, chloroform-d or methanol-d. Chemical shifts are reported in ppm (δ units) relative to TMS.

Mass Spectroscopy

Mass spectra (MS) (TOF-ESI) were recorded on a Waters 2795 separation module/micromass LCT platform, under positive scan mode (monomer characterization) or negative scan mode (binding analysis), with direct injection of the purified compounds.

Infrared Spectroscopy (IR)

IR spectrum of 3,4-dihydroxy-L-phenylamanine methacrylamide (L-DOPA methacrylamide, L-DMAm in **Chapter 3**) was recorded on KBr pellets on a Perkin Elmer Paragon 1000 FT-IR instrument.

N-(2-Ethylhexyl) methacrylamide (2-EHMAm) (in **Chapter 4**) was dissolved in chloroform and spread on NaCl discs to remove the solvent. IR spectrum of the dry sample was recorded on a Perkin Elmer Paragon 1000 FT-IR instrument.

Gel Permeation Chromatography (GPC)

Aqueous GPC was performed on a Polymer Labs GPC50 Plus fitted with differential refractometer (RI), capillary viscometer (DP) and dual angle laser light-scattering (15° and 90°) detectors. The eluent was Dulbecco's PBS without Ca^{2+} and Mg^{2+}, at 30 °C and a flow rate of 1 mL/min. The instrument was fitted with a Polymer Labs aquagel-OH guard column (50 × 7.5 mm, 8 μm) followed by a pair of PL aquagel-OH columns (30 and 40, 300 × 7.5 mm, 8 μm). Calibration for detector response and inter-detector delays was achieved using a single, narrow PEO standard (Polymer Labs, Mp 128 kDa, [η] 1.2968 dL/g) using a dn/dc value of 0.133 g/mL.

UV/Vis Spectroscopy

UV/Vis spectroscopy was performed using a Bechman Coultier DU-800 UV spectrophotometer equipped with a temperature control.

Specifically, aggregation experiments were performed in a Bechman DU 640 UV spectrophotometer.

Fluorescence Spectroscopy

Fluorescence spectra were recorded on a Cary Eclipse fluorimeter equipped with a Peltier apparatus for temperature control.

Dynamic Light Scattering (DLS)

Dynamic Light Scattering (DLS) was measured using a Viscotec Model 802 instrument equipped with an internal laser (825–832 nm) with a maximum radiation power of 60 mW. At least ten measurements of each sample were taken. The mean and standard deviation were calculated. Data processing was performed with the software program OmniSize2.

Transmission Electron Microscopy (TEM)

TEM samples were examined using a transmission electron microscope (TEM) (JEOL JEM 1010 electron microscope, Japan) with ITEM Olympus software. The accelerating voltage was 100.0 kV and magnification was x10K to x50K.

Negative-stained TEM samples were prepared as following procedure.

1. Suspend (coated) grid over edge of petri dish using forceps with locking ring, coated side up.
2. Add one drop of concentrated particulate suspension to the grid.

3. Remove most of the suspension by wicking with filter-paper after 3mins.
4. Add one drop of uranyl acetate (UA, 0.2-4.0% aqueous solution pH 4~5) to the grid coated with a formvar carbon film.
5. Dry grid by wicking with filter-paper after 1 min.
6. Slide fresh filter-paper between jaws of forceps to push dried grip (sample-side up) onto a clean dry part of the filter paper in the bottom of a petri-dish.
7. Let the grid dry for at least 15mins (we do overnight) before imaging on the TEM.

Atomic Force Microscopy (AFM)

AFM topography images and particle analysis of block copolymer vesicles were obtained in liquid at room temperature using a Multimode 8 Scanning Probe Microscopy station, operating in PeakForce Tapping™ mode. Images were acquired using an E-scanner, at scan rates between 1-2 Hz. $MgCl_2$ (10 mM) solution was incubated with the freshly cleaved mica for 10 min, and then the mica was washed with distilled water several times and blown dry completely with nitrogen at room temperature.

The samples used in AFM studies were prepared with the concentration of 1 mg/mL in HEPES buffer (10 mM HEPES, 10mM NaCl, pH 7.4, filtered by 0.2 μm syringe filter).

The experiments were designed to assess the morphology and the size of block copolymer vesicles. The diameters of the block copolymer structures were determined by grain analysis. Image data were analysed using NanoScope Analysis software (Version 1.20 - Bruker).

Zeta Potential

Zeta potential measurements of polymeric vesicles were performed by laser Doppler anemometry using a Malvern Zetasizer 2000 equipped with a 10 mW He-Ne laser operating at a wavelength of 633 nm. Measurements were performed at 25 ± 0.10 °C, on samples appropriately diluted with H_2O. The mean value and standard deviation for each sample was calculated from at least three measurements.

Tecan Microplate Reader

Bioluminescence assays were performed using a Tecan Infinite 200 microplate reader.

Optical Microscopy

A Nikon optical microscope equipped with a camera connected to a personal computer was used for optical microscopy studies.

Chromatography Fraction Collector

An Amersham BioScience RediFrac chromatography fraction collector with a Pharmacia LKB Uvicord SII and a Pharmacia LKB Pump P-1 was used to remove boron from media for MM32 assay.

Freeze Drier

Water was removed by immersing reagent tubes containing the samples in liquid nitrogen, once frozen the samples were placed on an Edwards Modulyo

freeze drier equipped with an Edwards high vacuum pump and the water removed.

Rotary Evaporator

Solvent was evaporated under reduced pressure on a Buchi Rotavapor R-200 equipped with a B490 heating bath.

Chapter 2

One example of calculation of binding affinity for PBA-Dopamine

a. Determination of binding constant (K_{a1}) of AR with PBA

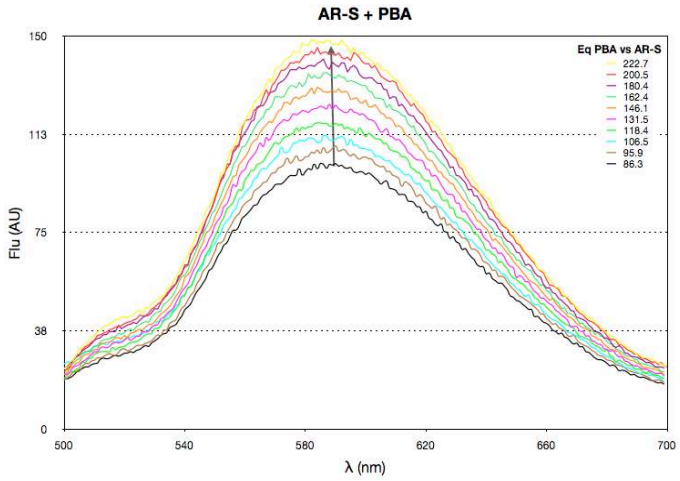

Figure A-1. Fluorescence profile of **AR** and phenylboronic acid (**PBA**) $[\mathbf{AR}]_0$ = 0.009 mM, $[\mathbf{PBA}]_0$ = 2 mM. $[\mathbf{PO_4^-}]$ = 100 mM

Table A-1 Row data analysis

	A	B	C	D	E	F	G	H
	PBA mM	I (572)	I (592)	I ($Av_{573-614}$)	ΔI (572)	ΔI (592)	ΔI ($Av_{573-614}$)	eq per AR
9	2.000	138.5773	148.4355	142.3242	45.1307	48.1032	45.2885	222.7171
8	1.800	136.9506	141.7629	139.0949	43.5039	41.4306	42.0592	200.4454
7	1.620	131.8352	138.1750	134.9886	38.3885	37.8427	37.9529	180.4009
6	1.458	126.7838	135.1427	130.0652	33.3372	34.8105	33.0296	162.3608
5	1.312	121.2769	129.8374	124.7907	27.8303	29.5051	27.7550	146.1247
4	1.181	116.0158	122.2126	118.7287	22.5691	21.8803	21.6930	131.5122
3	1.063	108.7451	115.8925	112.6737	15.2984	15.5602	15.6380	118.3610
2	0.957	104.4109	111.2752	107.2686	10.9643	10.9429	10.2329	106.5249
1	0.861	99.5566	106.0199	102.7327	6.1100	5.6876	5.6970	95.8724
0	0.775	93.4466	100.3323	97.0357	0.0000	0.0000	0.0000	86.2852

Equation 1.

$$\Delta I = I - I_0$$

Equation 2.

$$eq(perAR) = \frac{[Boron]}{[AR]}$$

Table A-2 Analyzed data

	A	B	C	D
	1/[Boron] (M)	1/ΔI (572)	1/ΔI (592)	1/ΔI (Av573-614)
9	500.0000	0.0222	0.0208	0.0221
8	555.5556	0.0230	0.0241	0.0238
7	617.2840	0.0260	0.0264	0.0263
6	685.8711	0.0300	0.0287	0.0303
5	762.0790	0.0359	0.0339	0.0360
4	846.7544	0.0443	0.0457	0.0461
3	940.8382	0.0654	0.0643	0.0639
2	1045.3758	0.0912	0.0914	0.0977
1	1161.5287	0.1637	0.1758	0.1755
0	1290.5874	0.0000	0.0000	0.0000

Equation 3.

$$\frac{1}{\Delta I} = \frac{1}{\Delta k \cdot p_0 \cdot [AR]_0 \cdot K_{a1}} \cdot \frac{1}{[Boron]} + \frac{1}{\Delta k \cdot p_0 \cdot [AR]_0}$$

$$y = \frac{1}{\Delta I};\ x = \frac{1}{[Boron]};$$

$$a = \frac{1}{\Delta k \cdot p_0 \cdot [AR]_0};\ \frac{1}{\Delta k \cdot p_0 \cdot [AR]_0 \cdot K_{a1}} = a \cdot \frac{1}{K_{a1}}$$

$$y = a \cdot \frac{1}{K_{a1}} \cdot x + a$$

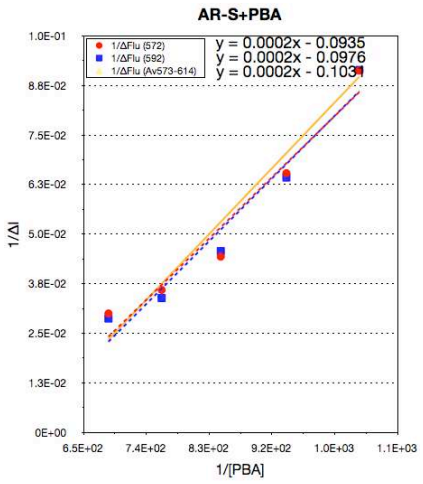

Figure A-2. The corresponding fitting plots of **AR** and phenylboronic acid (**PBA**) $[\mathbf{AR}]_0$ = 0.009 mM, $[\mathbf{PBA}]_0$ = 2 mM, $[\mathbf{PO_4^-}]$ = 100 mM $\mathbf{K_{a1}}$ **(PBA)** = 477.8 ± 10.3 M^{-1}

b. Determination of binding constant (K_a) of Dopamine with PBA

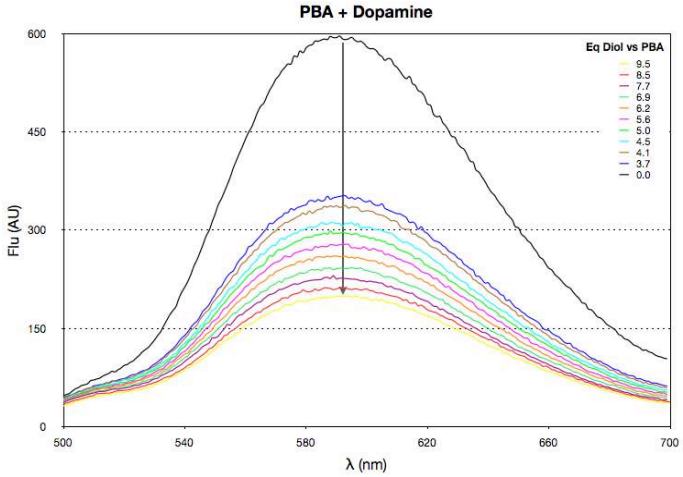

Figure A-3. Fluorescence profile of **PBA** and Dopamine Hydrochloride (**Dopamine**) titration $[\mathbf{AR}]_0$ = 0.12 mM, $[\mathbf{PBA}]_0$ = 1 mM, $[\mathbf{Dopamine}]_0$ = 9.5 mM, $[\mathbf{PO_4^-}]$ = 200 mM

Table A-3 Row data analysis

Diol mM	I (572)	I (592)	I ($Av_{573-614}$)	ΔI (572)	ΔI (592)	ΔI ($Av_{573-614}$)
9.49167	181.9394	198.3201	192.6344	353.7722	398.0732	381.2248
8.54250	195.8346	212.7969	205.1471	339.8770	383.5964	368.7121
7.68825	209.1834	226.4885	219.8799	326.5282	369.9047	353.9793
6.91943	222.0738	241.6397	234.4157	313.6378	354.7535	339.4435
6.22748	238.4105	259.2784	252.0162	297.3011	337.1149	321.8429
5.60474	252.1991	277.4991	268.3772	283.5126	318.8942	305.4820
5.04426	270.2956	295.1168	285.8995	265.4160	301.2764	287.9597
4.53984	284.1180	310.2656	300.7638	251.5937	286.1276	273.0954
4.08585	304.3359	334.4363	324.6095	231.3757	261.9569	249.2497
3.67727	318.2632	351.3763	339.1521	217.4484	245.0170	234.7071
0.00000	535.7116	596.3932	573.8591	0.0000	0.0000	0.0000

Table A-4 Analyzed data

	Average 573-614						
M Diol	I	[AR-PBA] mM	[AR] mM	Q	P	**Q**	**[Dopamine]$_0$/P**
0.0095	192.6344	4.028E-05	7.972E-05	1.9790	-0.0002	**1.9790**	**-45.2931**
0.0085	205.1471	4.290E-05	7.710E-05	1.7973	-0.0003	**1.7973**	**-28.7289**
0.0077	219.8799	4.598E-05	7.402E-05	1.6099	-0.0005	**1.6099**	**-19.6367**
0.0069	234.4157	4.902E-05	7.098E-05	1.4480	-0.0006	**1.4480**	**-14.6692**
0.0062	252.0162	5.270E-05	6.730E-05	1.2771	-0.0009	**1.2771**	**-10.9773**
0.0056	268.3772	5.612E-05	6.388E-05	1.1383	-0.0011	**1.1383**	**-8.7154**
0.0050	285.8995	5.978E-05	6.022E-05	1.0072	-0.0014	**1.0072**	**-6.9934**
0.0045	300.7638	6.289E-05	5.711E-05	0.9080	-0.0016	**0.9080**	**-5.8905**
0.0041	324.6095	6.788E-05	5.212E-05	0.7678	-0.0021	**0.7678**	**-4.5600**
0.0037	339.1521	7.092E-05	4.908E-05	0.6920	-0.0024	**0.6920**	**-3.9308**
0.0000	573.8591	1.200E-04	0.000E+00	0.0000	0.0000	**0.0000**	**0.0000**

	592 nm						
M Diol	I	[AR-PBA] mM	[AR] mM	Q	P	**Q**	**[Dopamine]$_0$/P**
0.0095	198.3201	3.990E-05	8.010E-05	2.0072	-0.0002	**2.0072**	**-49.2448**
0.0085	212.7969	4.282E-05	7.718E-05	1.8026	-0.0003	**1.8026**	**-29.0714**
0.0077	226.4885	4.557E-05	7.443E-05	1.6332	-0.0005	**1.6332**	**-20.5263**
0.0069	241.6397	4.862E-05	7.138E-05	1.4681	-0.0006	**1.4681**	**-15.1914**
0.0062	259.2784	5.217E-05	6.783E-05	1.3002	-0.0008	**1.3002**	**-11.4097**
0.0056	277.4991	5.584E-05	6.416E-05	1.1492	-0.0011	**1.1492**	**-8.8751**
0.0050	295.1168	5.938E-05	6.062E-05	1.0209	-0.0013	**1.0209**	**-7.1577**
0.0045	310.2656	6.243E-05	5.757E-05	0.9222	-0.0016	**0.9222**	**-6.0393**
0.0041	334.4363	6.729E-05	5.271E-05	0.7833	-0.0020	**0.7833**	**-4.6952**
0.0037	351.3763	7.070E-05	4.930E-05	0.6973	-0.0024	**0.6973**	**-3.9727**
0.0000	596.3932	1.200E-04	0.000E+00	0.0000	0.0000	**0.0000**	**0.0000**

	572 nm						
M Diol	I	[AR-PBA] mM	[AR] mM	Q	P	**Q**	**[Dopamine]$_0$/P**
0.0095	181.9394	4.075E-05	7.925E-05	1.9445	-0.0002	**1.9445**	**-41.1226**
0.0085	195.8346	4.387E-05	7.613E-05	1.7355	-0.0004	**1.7355**	**-25.1646**
0.0077	209.1834	4.686E-05	7.314E-05	1.5610	-0.0005	**1.5610**	**-17.9332**
0.0069	222.0738	4.974E-05	7.026E-05	1.4123	-0.0007	**1.4123**	**-13.7920**
0.0062	238.4105	5.340E-05	6.660E-05	1.2470	-0.0009	**1.2470**	**-10.4413**
0.0056	252.1991	5.649E-05	6.351E-05	1.1242	-0.0011	**1.1242**	**-8.5133**
0.0050	270.2956	6.055E-05	5.945E-05	0.9819	-0.0014	**0.9819**	**-6.6980**
0.0045	284.1180	6.364E-05	5.636E-05	0.8855	-0.0017	**0.8855**	**-5.6606**
0.0041	304.3359	6.817E-05	5.183E-05	0.7603	-0.0021	**0.7603**	**-4.4944**
0.0037	318.2632	7.129E-05	4.871E-05	0.6832	-0.0025	**0.6832**	**-3.8613**
0.0000	535.7116	1.200E-04	0.000E+00	0.0000	0.0000	**0.0000**	**0.0000**

Equation 4.

$$Q = \frac{[AR]}{[AR^{-}PBA]}$$

Equation 5.

$$P = [PBA]_0 - \frac{1}{Q \cdot K_{a1}} - \frac{[AR]_0}{Q+1}$$

Equation 6.

$$\frac{[Dopa\min e]_0}{P} = \frac{K_{a1}}{K_a} Q + 1$$

$$[AR^{-}PBA] = [AR]_0 \cdot \Delta I$$

$$[AR] = [AR]_0 - [AR^{-}PBA]$$

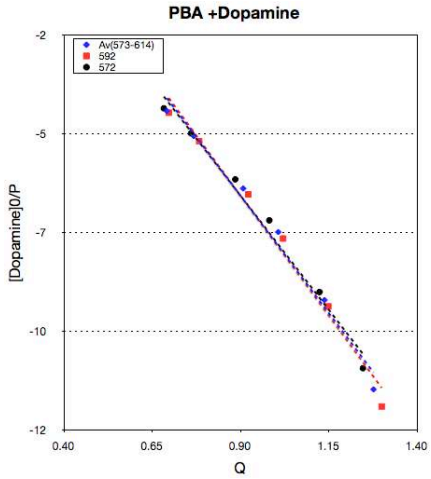

Figure A-4. The corresponding fitting plot of **PBA** and Dopamine Hydrochloride (**Dopamine**) $[\mathbf{AR}]_0$ = 0.12 mM, $[\mathbf{PBA}]_0$ = 1 mM, $[\mathbf{Dopamine}]_0$ = 9.5 mM, $[\mathbf{PO_4^-}]$ = 200 mM; $\mathbf{K_a}$ = 36.4 ± 0.9 M^{-1}

Monomer: N-(3,4-dihydroxyphenethyl)methacrylamide (DMAm)

Proton NMR

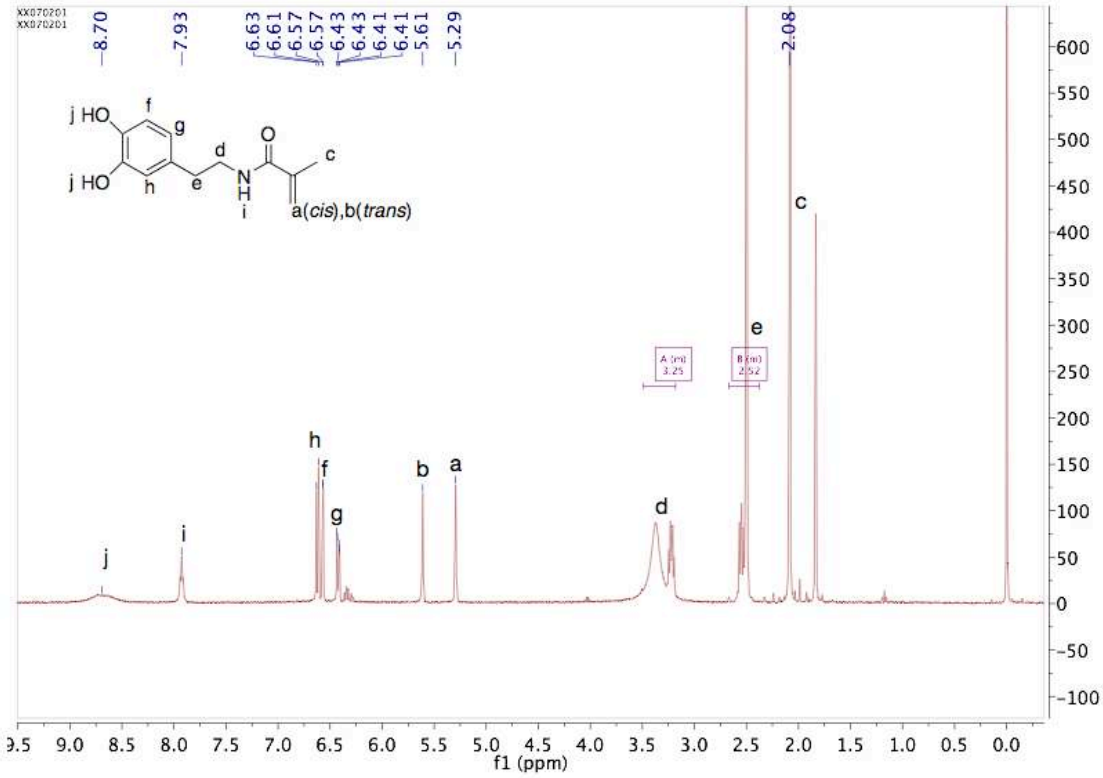

Monomer: 3,4-dihydroxy-L-phenylamanine methacrylamide (L-DOPA metacrylamide, L-DMAm)

FT-IR

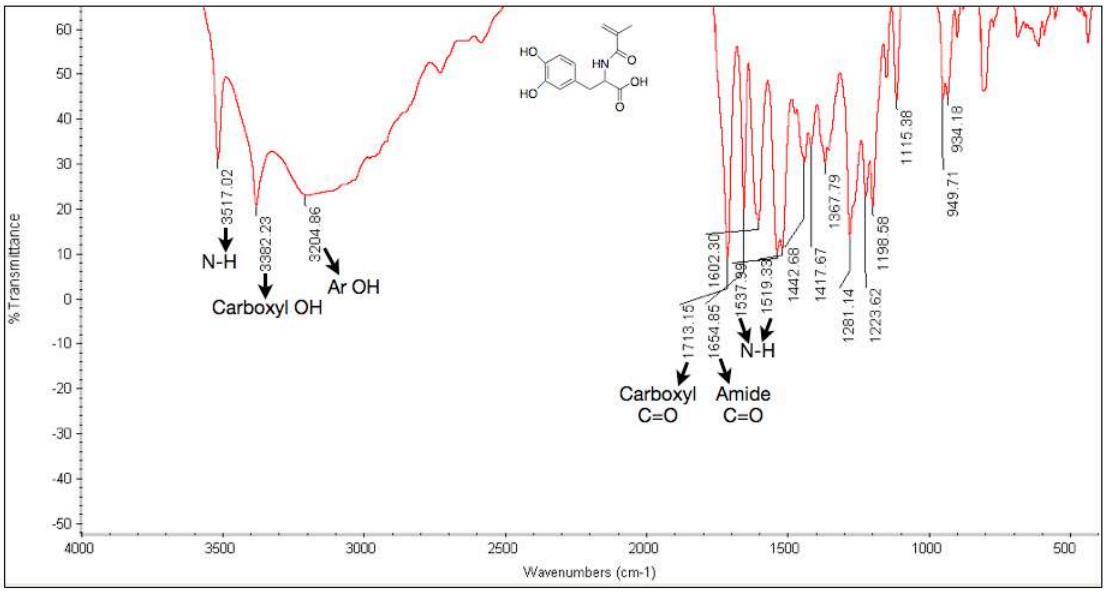

Mass spectrum

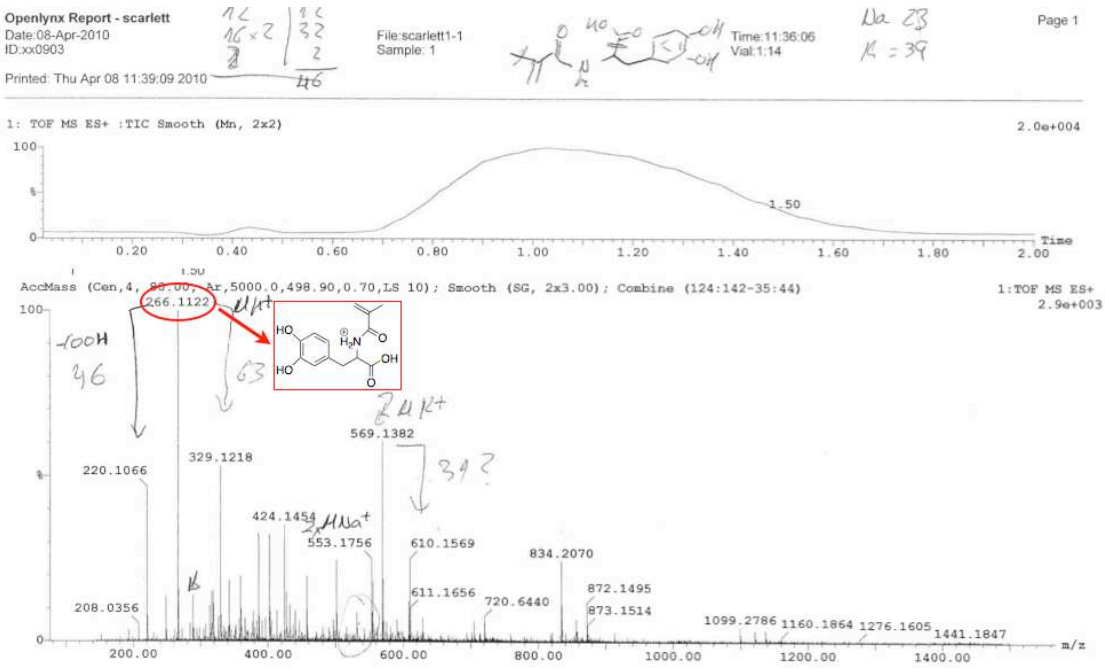

Chapter 3

CTA - 1: 2-((2-hydroxyethylthio)carbonothioylthio)-2-methylpropanoic acid

Proton NMR

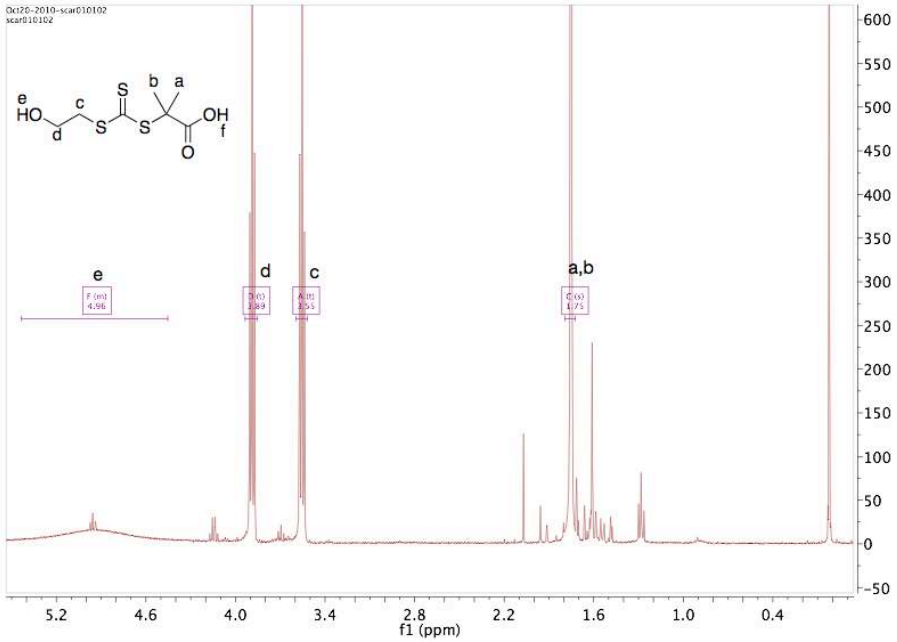

Polymer: p(DMAm$_{14}$-*c*-DMAPMAm$_{86}$) - Polymer 1a

Proton NMR

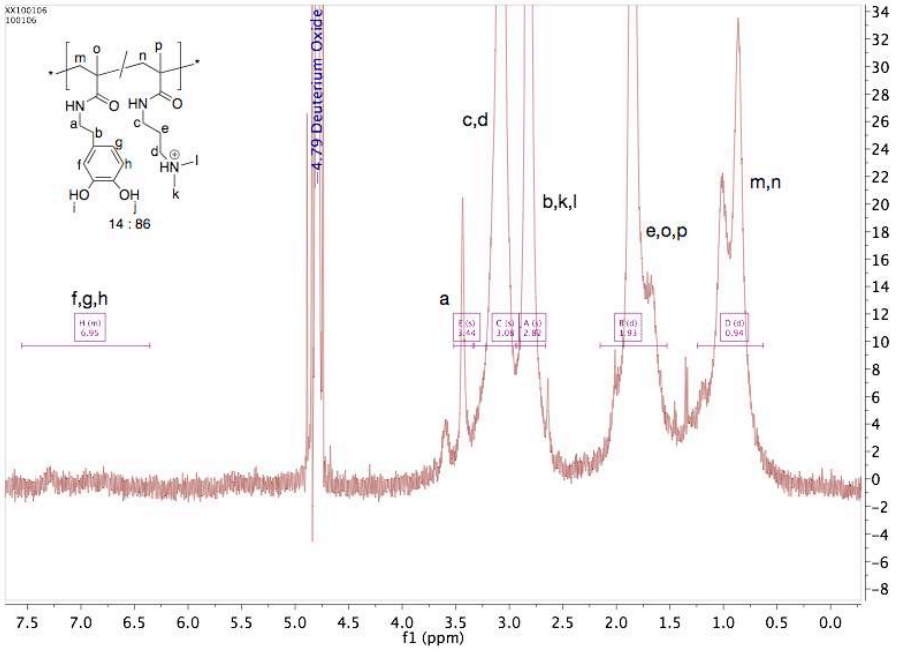

GPC (aqueous solution)

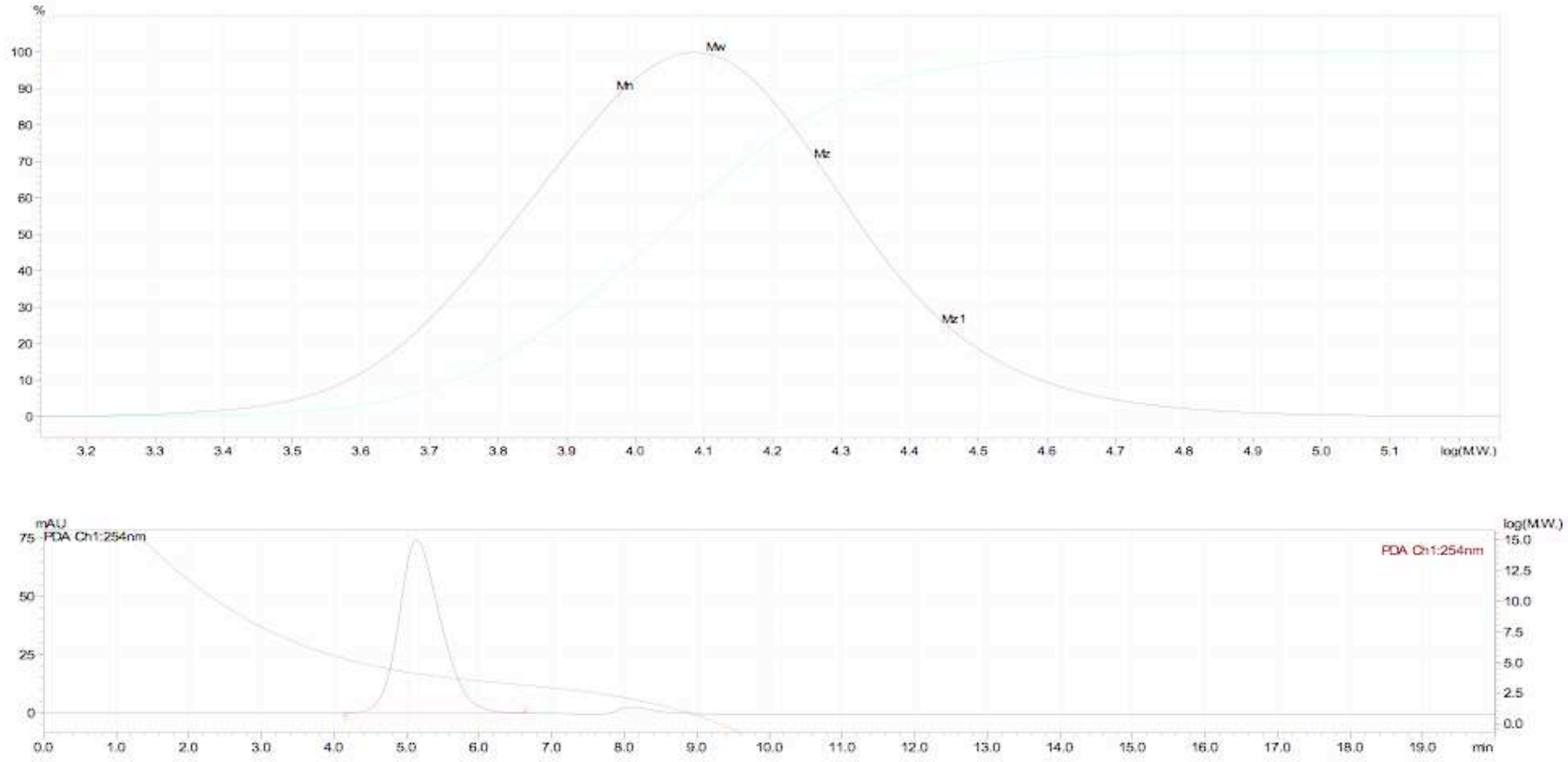

Polymer: p(L-DMAm)$_{15}$ - Polymer 2a

Proton NMR

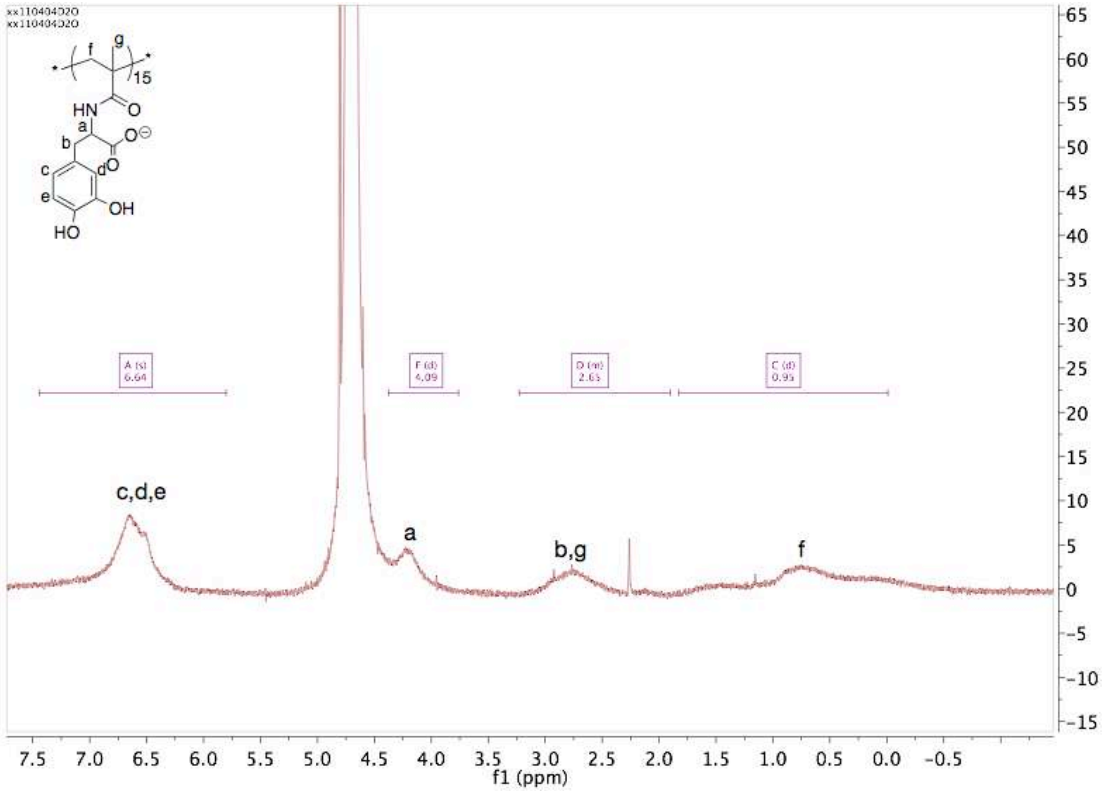

Chapter 4

Monomer: N-(2-ethylhexyl) methacrylamide (2-EHMAm)

FT-IR

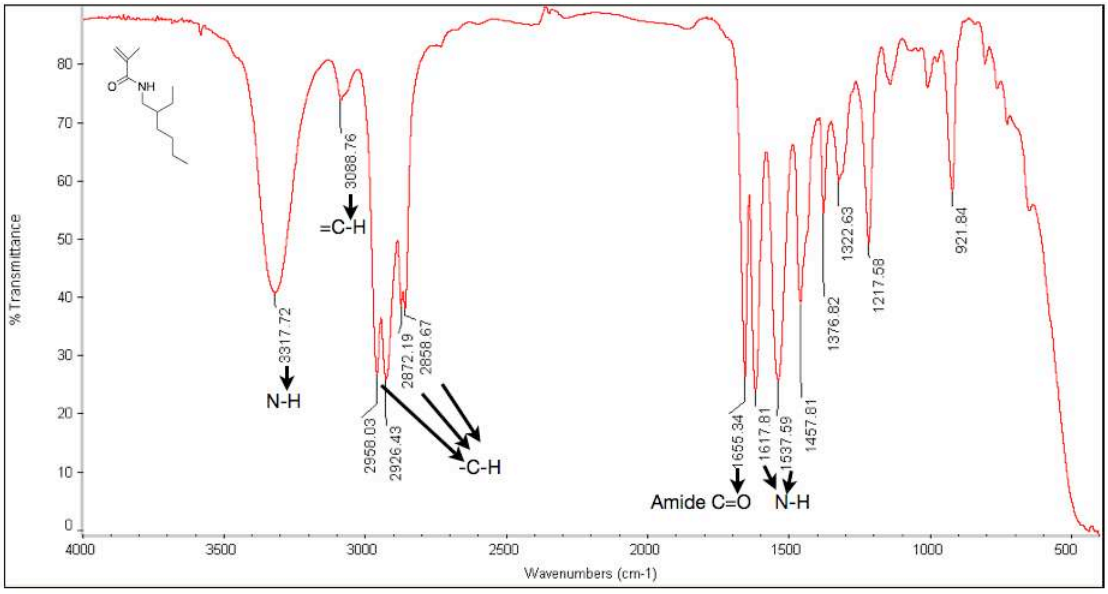

Mass spectrum

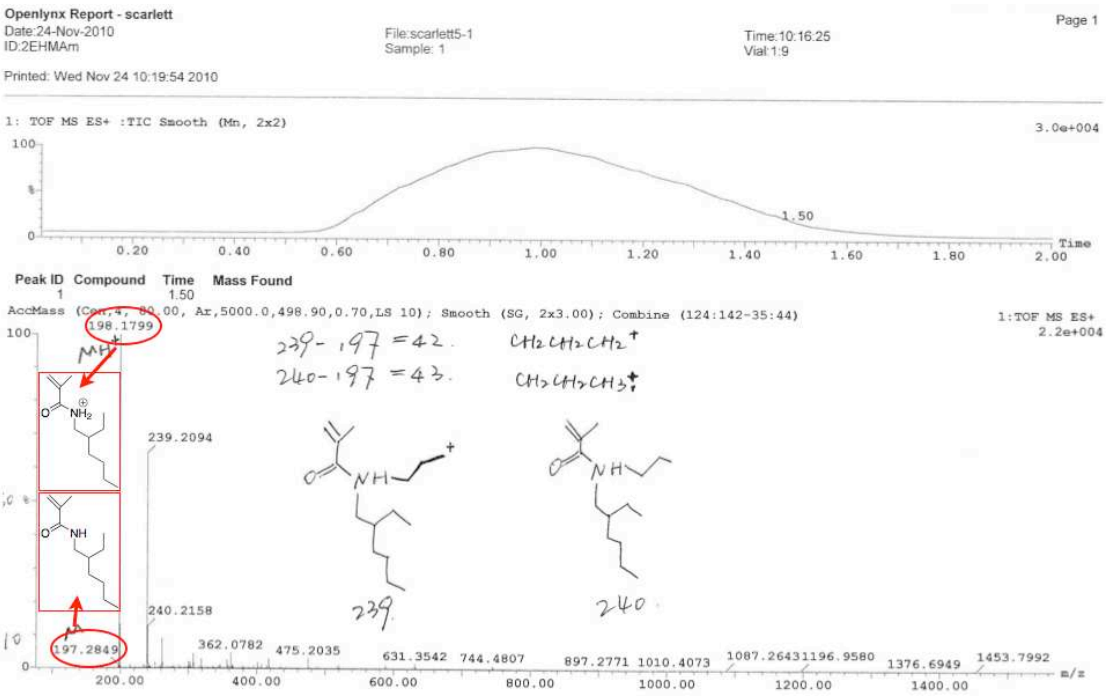

Monomer: N-(2-ethylhexyl) acrylamide (2-EHAm)

Proton NMR

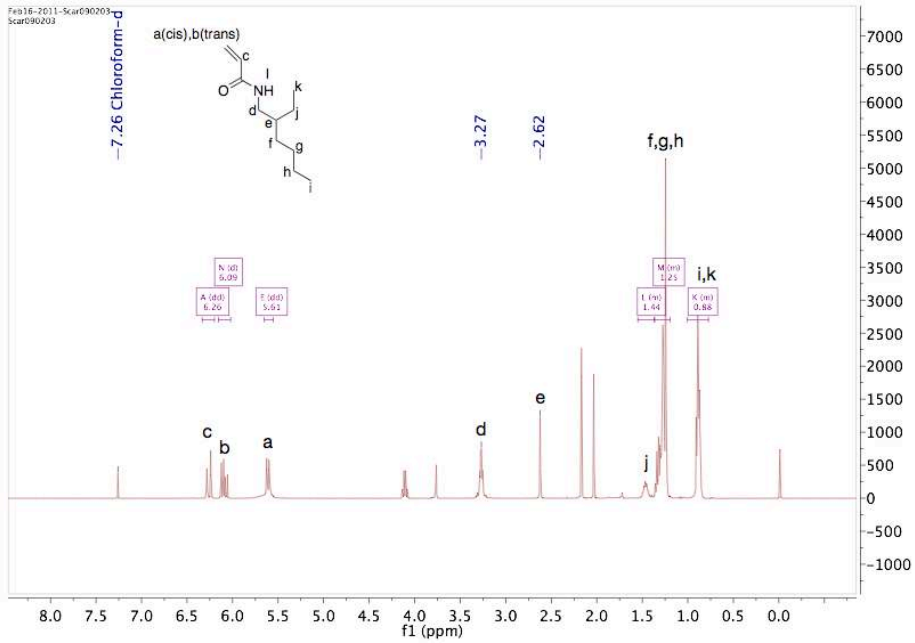

Monomer: 4-acrylamidobutanoic acid (4-AmBA)

Proton NMR

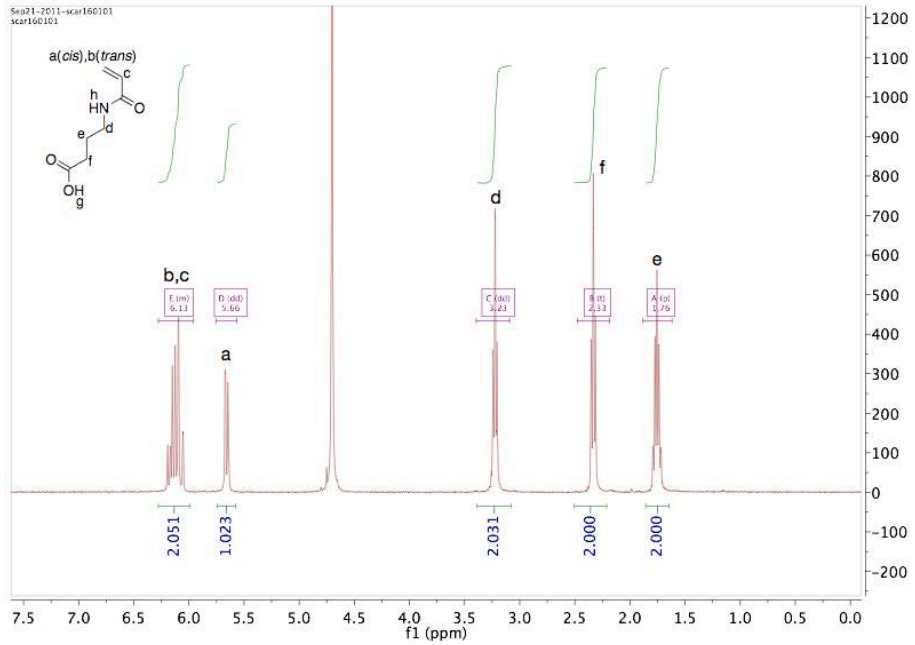

Copolymer: p(L-DMAm)$_{16}$-*b*-p(EHAm)$_{73}$ - Copolymer C1c

Proton NMR

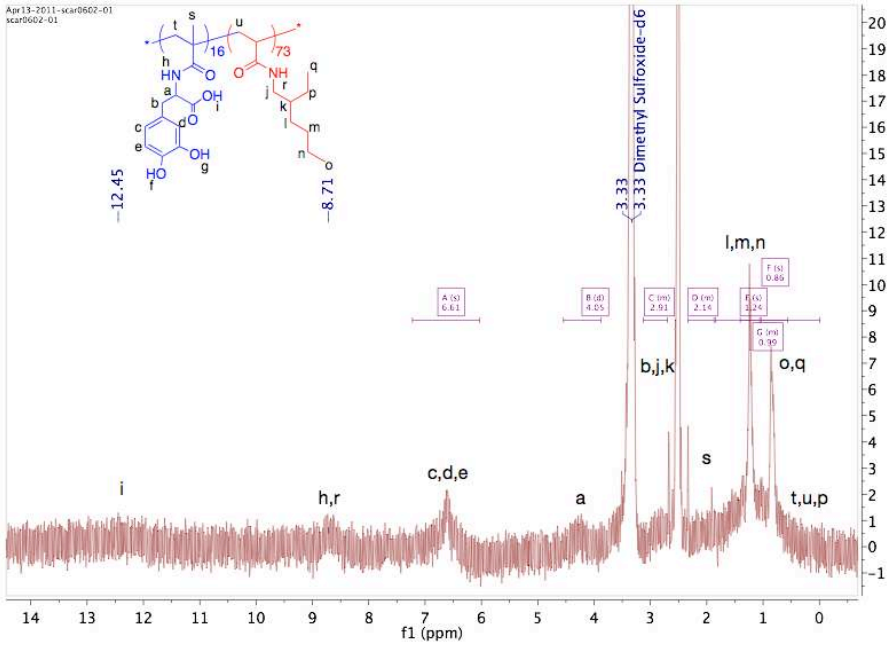

Polymer: p(L-DMAm)$_{13}$-*b*-p(PAm)$_{93}$ - Copolymer C2

Proton NMR

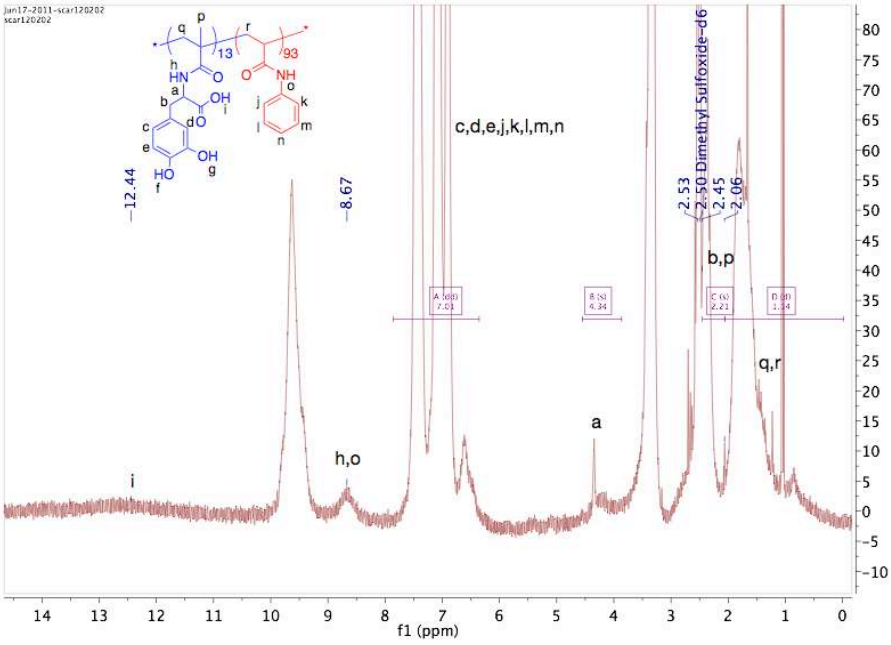

Polymer: p(4-AmBA) - Polymer 4

Proton NMR

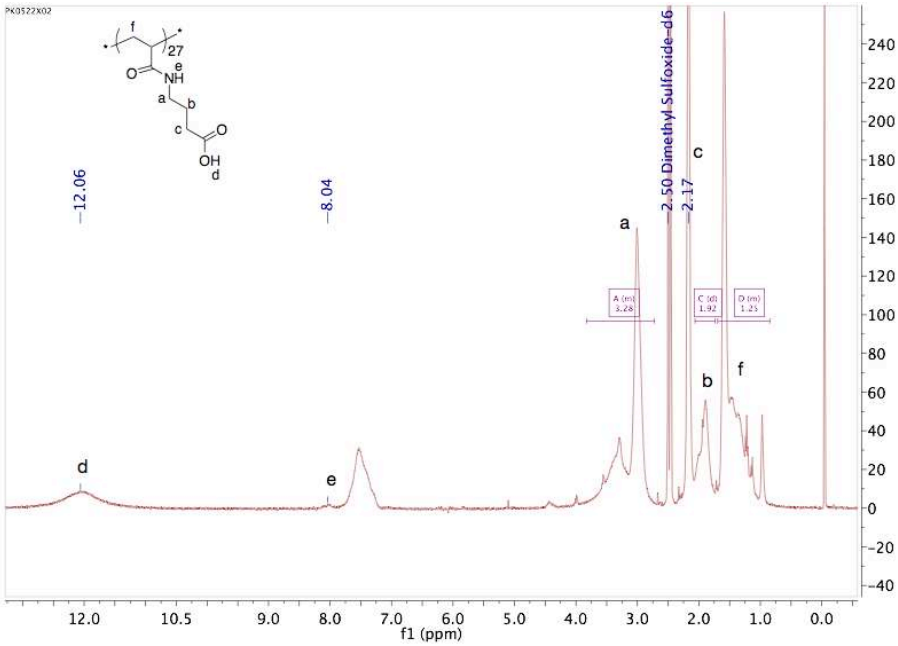

Polymer: p(4-AmBA)$_{27}$-*b*-p(PAm)$_{90}$ - Copolymer C3

Proton NMR

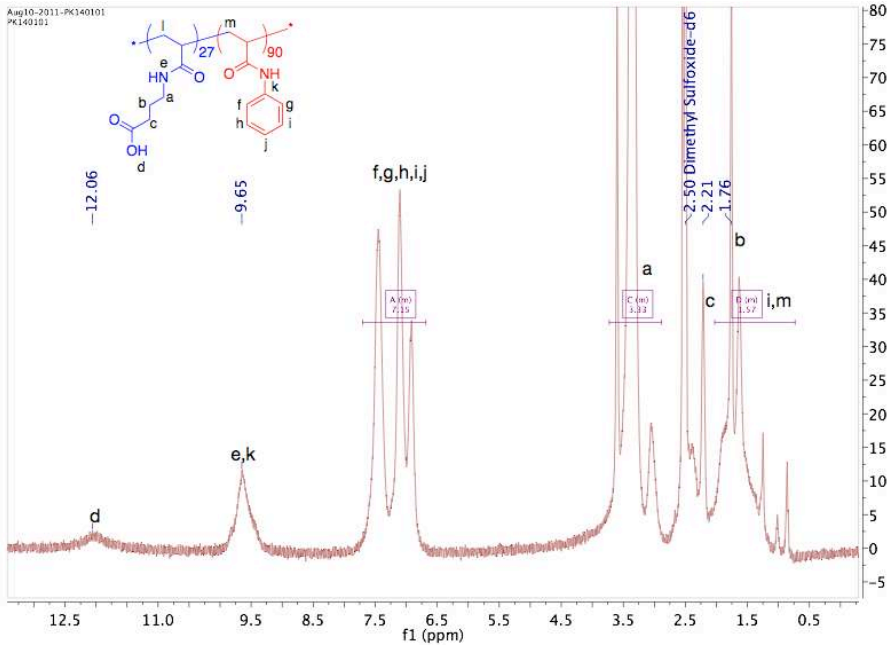

Polymer: p(DMAm$_{14}$-*c*-DMAPMAm$_{86}$)-*b*-p(PAm)$_{237}$ - Copolymer C4

Proton NMR